UNIVERSITY OF Southampton

University of Southampton Research Repository

Copyright © and Moral Rights for this thesis and, where applicable, any accompanying data are retained by the author and/or other copyright owners. A copy can be downloaded for personal non-commercial research or study, without prior permission or charge. This thesis and the accompanying data cannot be reproduced or quoted extensively from without first obtaining permission in writing from the copyright holder/s. The content of the thesis and accompanying research data (where applicable) must not be changed in any way or sold commercially in any format or medium without the formal permission of the copyright holder/s.

When referring to this thesis and any accompanying data, full bibliographic details must be given, e.g.

Thesis: James David Ingram (2017) "The Identification of Inhibitors of Nerve Growth Factor and Brain-Derived Neurotrophic Factor", University of Southampton, School of Chemistry, PhD Thesis, page ##.

**University of Southampton**

Faculty of Natural and Environmental Sciences

School of Chemistry

# The Identification of Inhibitors of Nerve Growth Factor and Brain-Derived Neurotrophic Factor

by

James David Ingram

Thesis for the degree of

Doctor of Philosophy

September 2017

# Acknowledgements

I would like to thank Ali Tavassoli, David Pryde and Peter Cox for their assistance and guidance. I am very grateful to Pfizer Neusentis and the Engineering and Physical Sciences Research Council who have funded this research. A great debt of thanks is due to Katrin Deinhardt and Prutha Patel for their extensive help with the mammalian cell data.

Thanks also to the Tavassoli research group, particularly Fiona Rowan for her instruction in protein expression and purification, Andy Ball for his advice on peptide synthesis and especially Eliot Osher for keeping things upbeat!

I would especially like to thank my friends and family for their continued help and support, particularly my parents for their continuous encouragement. Paramount thanks are due to Lauren Henderson, to whom I owe a very great deal.

# Abstract

Chronic pain affects up to 43% of the UK population, with 12% reporting moderate to severely limiting chronic pain.[1-2] This incidence rate rises with age, with 62% of over 75s being diagnosed.[1] The current standard of care for chronic pain almost exclusively involves COX-1, COX-2 or μ-opioid receptor inhibitors and considerable research has been conducted in this area. Despite this, the current state of pharmacological treatments is seen by patients as decidedly lacking, with the prevailing opinion being one of concern for efficacy, side effects and addiction.[2]

Recent drug advances suggest a promising new area for development may be found in inhibiting neurotrophins or their receptors: both animal modelling and clinical trials show that significant reduction of pain sensation (nociception) may be found in the inhibition of these proteins. This is supported by Pfizer's Tanezumab, which recently (June 2017) received FDA fast-track approval status for the treatment of chronic pain in patients with osteoarthritis and chronic lower back pain. This monoclonal antibody binds to nerve growth factor (βNGF) to prevent it binding to its receptor, and has been shown to dramatically reduce nociception. Despite this, Tanezumab shows room for improvement: a meta-analysis of trials involving Tanezumab for treatment of osteoarthritis of the knee revealed significant discontinuations due to adverse effects.[3] A Phase III trial for osteoarthritic hip pain (while successful) also showed an increase in the required number of hip replacements for those taking the drug.[4] Further development is therefore sought, and this research documents the initial hit discovery and development of a number of neurotrophin inhibitors.

Initially this was sought through the development of a high throughput screening platform using a reverse two-hybrid system, however this proved unsuccessful. Phage display was therefore employed and successfully identified a number of peptides which bound to either βNGF or another promising neurotrophin target, mBDNF. This adherence was then tested for its target specificity, and an ELISA screen developed to assess agonist/antagonist activity. Peptides were then synthesised and further assays were attempted to ascertain binding data. Finally, the biological activity of the lead peptides was tested against TrkB/PC12 cells in western blot and morphology assays.

In conclusion, this research identified several antagonists and antagonists of the neurotrophin-receptor interaction for βNGF and mBDNF.

# Table of Contents

Acknowledgements ..... v

Abstract ..... vii

Table of Contents ..... ix

List of Figures ..... xv

List of Tables ..... xxv

List of Schemes ..... xxvii

Declaration of Authorship ..... xxix

Definitions and Abbreviations ..... xxxi

Amino Acid Abbreviations ..... xxxii

1. Chapter 1: Introduction to βNGF and mBDNF ..... 1

1.1 The Importance of Novel Pain Therapies ..... 1

1.2 mBDNF Inhibition as a Novel Cancer Therapy ..... 6

1.3 βNGF and mBDNF as Targets for Inhibition ..... 7

1.3.1 Brain-Derived Neurotrophic Factor ..... 9

1.3.2 Nerve Growth Factor ..... 13

1.3.3 Existing Agonists and Antagonists ..... 15

1.4 Targeting Neurotrophin PPIs ..... 19

1.5 Project Aims ..... 20

1.6 Project Overview ..... 20

2. Chapter 2: Exploring mBDNF Inhibition Through RTHS ..... 21

2.1 Discussion of Techniques ..... 21

2.2 Introduction to Reverse Two-Hybrid Systems ..... 21

2.3 Results and Discussion ..... 28

2.3.1 RTHS 1: 434-mBDNF ..... 28

2.3.2 RTHS 2-4: 434-Truncated mBDNF ..... 36

2.3.3 RTHS 5: C-Terminal mBDNF-FL-434 ..... 43

2.3.4 RTHS 6: C-Terminal mBDNF-FL-434D ..... 48

2.4 Chapter 2 Conclusions ..... 52

3. Chapter 3: Identifying Inhibitors of βNGF and mBDNF Through Phage Display ..... 57

3.1 Introduction to Phage Display ..... 57

3.1.1 Results and Discussion: Phage Display Screening and Verification ..... 61

3.1.1.1 βNGF and mBDNF Phage Display Pans 1-3 ..... 64

3.1.1.2 Pan 3 Phage Binding ELISA ..... 66
3.1.1.3 βNGF and mBDNF Phage Display Pans 4-5 ..... 72
3.1.1.4 Pan 5 Phage Binding ELISA ..... 75
3.2 Chapter 3 Conclusions ..... 82
4. Chapter 4: Screening Identified Peptides for Neurotrophin-Trk PPI Modulatory Activity ..... 85
4.1 Discussion of Suitable Techniques for Investigating PPIs ..... 85
4.2 Two-Component Inhibitory ELISA Development ..... 85
4.2.1 Expression and Purification of Tagged TrkA-D5 & TrkB-D5 ..... 87
4.2.2 Expression and Purification of βNGF & mBDNF ..... 97
4.2.2.1 *E. coli* Disulfide Bridge Formation ..... 97
4.2.2.2 βNGF and mBDNF expression ..... 101
4.2.3 ELISA Development & Testing ..... 110
4.2.3.1 Two-Component ELISA Design ..... 110
4.2.3.2 Two-Component Inhibitory ELISA of the Peptide Library ..... 114
4.2.4 Lead Peptide Titred ELISA ..... 119
4.3 Chapter 4 Conclusions ..... 122
5. Chapter 5: Development of Approaches to Determine the Modulatory Effect of Identified Binders ..... 124
5.1 Lead Peptide Solid Phase Peptide Synthesis ..... 124
5.2 tide Binding Characterisation by Microscale Thermophoresis ..... 130
5.2.1 Introduction to Microscale Thermophoresis ..... 130
5.2.2 Microscale Thermophoresis Overview and Results ..... 132
5.3 *In Vitro* Peptide Testing ..... 133
5.3.1 Lead Peptide Activation/Inhibition Western Blot Assays ..... 134
5.3.2 Morphology Assays ..... 142
5.4 Chapter 5 Conclusions ..... 146
6. Chapter 6: Thesis Overview, Conclusions and Future Work ..... 148
6.1 Thesis Introduction ..... 148
6.2 Overview and Conclusions ..... 148
6.3 Future Work ..... 150
7. Chapter 7: Experimental ..... 155
7.1 Materials and Equipment ..... 155
7.2 Preparation of Materials ..... 156
7.2.1 Agarose Gel ..... 156
7.2.2 Antibiotic Stock Solutions ..... 156
7.2.3 Antibody Blocking Buffer ..... 157

7.2.4 Auto-induction Media ..... 157
7.2.5 Biotin Streptavidin Elution Buffer ..... 157
7.2.6 Blocking Buffer ..... 157
7.2.7 Coomassie Destain Solution ..... 157
7.2.8 Coomassie Stain ..... 157
7.2.9 Glutathione (Oxidised) ..... 157
7.2.10 Glutathione (Reduced) ..... 157
7.2.11 HEPES Buffered Saline ..... 158
7.2.12 HisTrap Column Binding Buffer ..... 158
7.2.13 HisTrap Column Elution Buffer ..... 158
7.2.14 HisTrap Lysis Buffer ..... 158
7.2.15 Inclusion Body Lysis Buffer ..... 158
7.2.16 Inclusion Body Wash Buffer ..... 158
7.2.17 Inclusion Body Extraction Buffer ..... 158
7.2.18 Inclusion Body Folding Buffer A ..... 159
7.2.19 Inclusion Body Folding Buffer B ..... 159
7.2.20 Intein Extraction Buffer ..... 159
7.2.21 Iodide Buffer ..... 159
7.2.22 IPTG/Xgal Stock ..... 159
7.2.23 Laemmli Buffer ..... 159
7.2.24 Laemmli Buffer (Non-Denaturing) ..... 159
7.2.25 LB Agar/IPTG/Xgal/Tet Plates ..... 160
7.2.26 LB Agar Tet Plates ..... 160
7.2.27 Lysogeny Broth ..... 160
7.2.28 Lysogeny Broth (for ER2738) ..... 160
7.2.29 Lysogeny Broth Agar Plates ..... 160
7.2.30 Minimal Media Salt Stock ..... 160
7.2.31 PEG/NaCl Phage Storage Solution ..... 161
7.2.32 Phosphate Buffered Saline (PBS) ..... 161
7.2.33 PBST ..... 161
7.2.34 pH Phage Elution Buffer ..... 161
7.2.35 pH Phage Elution Neutralisation Buffer ..... 161
7.2.36 Plating Buffer ..... 161
7.2.37 Protein Storage Buffer ..... 161
7.2.38 SDS Running Buffer ..... 161
7.2.39 Sodium Iodide Buffer ..... 162
7.2.40 Streptavidin Stock Solution ..... 162
7.2.41 Super Optimal Broth with Catabolite Repression (SOC) Media ..... 162

7.2.42 TAE Buffer ..... 162
7.2.43 TBFI Buffer ..... 162
7.2.44 TBFII Buffer ..... 162
7.2.45 Terrific Broth (TB) ..... 163
7.2.46 Top Agar ..... 163
7.2.47 Tris Buffered Saline (TBS) ..... 163
7.3 General Procedures ..... 163
7.3.1 Bacterial Manipulation ..... 163
7.3.1.1 Storing Bacterial Stock ..... 163
7.3.1.2 Growing Bacterial Culture ..... 163
7.3.1.3 Plasmid Mini-Prep ..... 163
7.3.1.4 Competent Cell Preparation and Usage ..... 164
7.3.1.5 Repressor Efficacy and Toxicity Drop Spotting ..... 166
7.3.2 DNA Manipulation ..... 167
7.3.2.1 PCR ..... 167
7.3.2.2 Spin Column Purification ..... 170
7.3.2.3 Gel Purification ..... 170
7.3.2.4 Restriction Endonuclease Digestion ..... 170
7.3.2.5 Ligation ..... 170
7.3.3 Protein Manipulation ..... 171
7.3.3.1 Circular Dichroism ..... 171
7.3.3.2 MST ..... 171
7.3.3.3 Peptide ELISAs ..... 171
7.3.3.4 Protein Unfolding and Refolding ..... 172
7.3.3.5 Protein Expression - Small Scale Test ..... 173
7.3.3.6 Protein Expression - Mid-Large Scale ..... 174
7.3.3.7 Protein Imaging ..... 175
7.3.3.8 Protein Purification – HisTrap Affinity Chromatography ..... 176
7.3.3.9 Protein Purification – Size Exclusion Chromatography ..... 176
7.3.3.10 Thermal Shift ..... 177
7.3.4 Phage Protocols ..... 177
7.3.4.1 Measuring Phage Concentration ..... 177
7.3.4.2 Storage of Phage Solutions ..... 178
7.3.4.3 Phage Display Surface Panning Procedure ..... 178
7.3.4.4 Phage ELISA Binding Assay with Direct Target Coating ..... 181
7.3.5 Solid-Phase Peptide Synthesis ..... 182
7.3.5.1 General SPPS Protocol, Disulfide Cyclisation and Purification ..... 182
7.3.5.2 Kaiser Test ..... 184
7.3.5.3 Analytical HPLC ..... 185
7.3.5.4 Lead Peptide Synthesis ..... 185

7.3.6 Cloning ..... 196
7.3.6.1 Reverse Two-Hybrid Systems ..... 196
7.3.6.2 Expression Plasmids ..... 200
8. Chapter 8: Appendices ..... 205
8.1 Bacterial Strains and Plasmids ..... 205
8.2 Primer Table ..... 206
8.3 Protein Sequences Table ..... 207
9. Chapter 9: References ..... 209

# List of Figures

**Figure 1: The impact of chronic pain on the daily life of those affected.**[2] ..... 3

**Figure 2: The attitudes of chronic pain patients about pain treatments.** Respondents either agreed somewhat or completely with the statements read out by interviewers.[2] 4

**Figure 3: Paracrine, autocrine and target-derived modes of neurotrophin presentation.** 7

**Figure 4: Crystal structures of neurotrophins.** βNGF homodimer (RSCB protein data bank (PDB) entry: 1WWW),[49] mBDNF (blue) and NT4/5 heterodimer (magenta, PDB entry 1B8M)[50] NT4/5 homodimer (magenta, PDB entry 1B98),[51] and NT3 homodimer (PDB entry 3BUK)[52]..... 8

**Figure 5: Crystal structures of other "neurotrophins".** GDNF monomer (green, PDB entry: 3FUB),[59] ARTN homodimer (blue, PDB entry 2ASK)[60] and CNTF homodimer (magenta, PDB entry 1CNT).[61] ..... 9

**Figure 6: Diagram of translated BDNF and post-translational modification variants.** Numbers show amino acid residue number. .....10

**Figure 7: Neurotrophin receptor selectivity and receptor domain structure.**[62, 67] ..10

**Figure 8: Simplified schematic of mBDNF and proBDNF activity in neurons.** .....12

**Figure 9: Diagram of translated βNGF and post-translational modification variants.** 13

**Figure 10: Simplified schematic of βNGF and ProNGF activity in neurons.**.....14

**Figure 11: Flowchart of RTHS activity.** A: an RTHS host when the fusion proteins are not expressed or where they fail to dimerise. B: when the fusion proteins are express and dimerise, the cell dies as it cannot express the survival genes. C: the identification of a hit inhibitor: the fusion protein dimerization is inhibited, so survival gene expression isn't inhibited: the cell lives, so it can be isolated and the hit elucidated.....22

**Figure 12: Overview of the strategy used to identify PPI inhibitors using RTHSs.** A) Section using bacteria to express peptides and proteins. B) Section using synthesised peptides. ..... 23

**Figure 13: Homodimeric 434 (residues 2-63) binding $O_R3$[126] (PDB 1PER).** ..... 25

**Figure 14: Demonstration of how RTHS link a PPI with an externally visible phenotype in SNS118.**[120] ..... 26

**Figure 15: Graphical representation of the six fusion proteins developed in this chapter.** 28

**Figure 16: Plasmid map of pTHCP16(434-mBDNF).** ..... 28

**Figure 17: CRIM plasmid integration of pAH68(434-mBDNF) at $Att_{HK022}$ into the chromosome of SNS118.**[135] $Int_{HK022}$ joins the right half of attP (blue) with the left half of attB (blue) and vice versa (green with green)..... 30

**Figure 18: Plasmid map of CRIM plasmids pAH68(434-mBDNF) and helper plasmid pAH69.** 31

**Figure 19: Assessing pAH68(434-mBDNF) CRIM plasmid integration into SNS118.** A) mixed primer PCR of potential SNS118 pAH68 434-mBDNF colonies, B) split-primer PCR of Figure 19A lanes 6-7. ..... 32

**Figure 20: Explanation of the drop spotting assay readout.** ..... 33

**Figure 21: Assessing 434-mBDNF RTHS toxicity (A) and repressor activity (B) by drop spotting.** Blue curve shows the direction of bacterial culture dilution. Positive control: SNS118_int.pAH68(434-CtBP), negative control: SNS118. 35

**Figure 22: Crystal structures of the two components in 434-TrmBDNF chimeric proteins.** A) mBDNF (green) NT4/5 (blue) heterodimer (PDB 1B8M).[51] Arrow shows the N-termini. Lines show positions of truncation. B) Dimeric 434 (residues 2-63) binding OR3[126] (PDB 1PER), arrows indicate the C-termini, however the 434 used in this project uses residues 2-106). ..... 36

**Figure 23: Assessing non-integrated 434-TrmBDNF RTHS toxicity (A) and repressor activity (B) in SNS118 by drop spotting.** Blue curve shows the direction of bacterial culture dilution. Positive control: SNS118_int.pAH68(434-CtBP), negative control: SNS118.....37

**Figure 24: Assessing 434-TrmBDNF CRIM plasmid integration by mixed primer PCR.** 824 and 289 bp: Single integration, 740 bp: No integration, 373 bp: Multiple integration.....38

**Figure 25: Assessing 434-TrmBDNF-30 and 434-TrmBDNF-44 CRIM plasmid integration in SNS118 by split-primer PCR.** P1/P4: 740 bp: No integration, P1/P2: 289 bp: Single integration, P3/P4: 824 bp: Single integration, P2/P3: 373 bp: Multiple integration. .....39

**Figure 26: Assessing 434-TrmBDNF-38 CRIM plasmid integration in SNS118 by split-primer PCR.** P1/P4: 740 bp: No integration, P1/P2: 289 bp: Single integration, P3/P4: 824 bp: Single integration, P2/P3: 373 bp: Multiple integration. 40

**Figure 27 Assessing 434-TrmBDNF-30 and 434-TrmBDNF-44 RTHS toxicity (A) and repressor activity (B) by drop spotting.** Blue curve shows the direction of bacterial culture dilution. Positive control: SNS118_int.pAH68(434-CtBP), negative control: SNS118.....41

**Figure 28 Assessing 434-TrmBDNF-38 RTHS toxicity (A) and repressor activity (B) by drop spotting.** Blue curve shows the direction of bacterial culture dilution. Positive control: SNS118_int.pAH68(434-CtBP), negative control: SNS118. 42

**Figure 29A: Crystal structures of the two components in mBDNF-FL-434 chimeric protein.** A) mBDNF (green) NT4/5 heterodimer (blue)[50] (PDB 1B8M). Arrow shows the C-termini. B) Dimeric 434 coupling with $O_R3$[126] (PDB 1PER), arrows showing the N-termini. .....44

Figure 30: Assessing mBDNF-FL-434 CRIM plasmid integration in SNS118 by mixed-primer PCR. 824 and 289 bp: Single integration, 740 bp: No integration, 373 bp: Multiple integration. .....44

**Figure 31: Assessing mBDNF-FL-434 CRIM plasmid integration in SNS118 by split-primer PCR.** P1/P4: 740 bp: No integration, P1/P2: 289 bp: Single integration, P3/P4: 824 bp: Single integration, P2/P3: 373 bp: Multiple integration. 45

**Figure 32 Assessing mBDNF-FL-434 RTHS toxicity (A) and repressor activity (B) by drop spotting.** Blue curve shows the direction of bacterial culture dilution. Positive control: SNS118_int.pAH68(434-CtBP), negative control: SNS118. 46

**Figure 33A: Theoretical model of dimeric wild type (residues 1-209) 434, coupling with $O_R3$ (PDB 1RPD)** B: amino acid residues 2-101 used so far in this project. Blue: residues 2-69 necessary for binding the ORI site, purple: residues 70-101 retained as a "linker" in previous N-terminal fusion proteins, teal/green: remainder of the wild-type 434 protein. ..... 47

**Figure 34: Assessing mBDNF-FL-434D CRIM plasmid integration in SNS118 by mixed-primer PCR.** 824 and 289 bp: Single integration, 740 bp: No integration, 373 bp: Multiple integration. ..... 49

**Figure 35: Assessing mBDNF-FL-434D CRIM plasmid integration in SNS118 by split-primer PCR.** P1/P4: 740 bp: No integration, P1/P2: 289 bp: Single integration, P3/P4: 824 bp: Single integration, P2/P3: 373 bp: Multiple integration. 50

**Figure 36: Assessing mBDNF-FL-434D RTHS toxicity (A) and repressor activity (B) by drop spotting.** Blue curve shows the direction of bacterial culture dilution. Positive control: SNS118_int.pAH68(434-CtBP), negative control: SNS118. 51

**Figure 37: Structure of mBDNF (green) NT4/5 (blue) heterodimer[51] (PDB 1B8M).** 52

**Figure 38: Graphical representation of the six fusion proteins investigated in this chapter; none of which functioned in SNS118 as a successful repressor.** 53

**Figure 39: mBDNF (green) NT4/5 (blue) heterodimer (PDB 1B8M[51]) highlighting the three non-consecutive intramolecular disulfide bridges per mBDNF monomer (C142-C209, C187-C238, C197-C240).** .....54

**Figure 40: Overview flowchart of the process of identifying and verifying PPI inhibitors using phage display.** A) Section using phages to produce peptides with an attached genetic tag. B) Section using synthesised peptides and peptide analogues. 58

**Figure 41: The structure of an M13 filamentous phage.** Included to indicate the position of pIII and pVIII, and explain the copy number: 5 vs. ~2000.....59

**Figure 42: The iterative phage display panning process.** .....60

**Figure 43: Phage target specificity assay to check for artefact binding.** .....67

**Figure 44: Thermal shift of βNGF in a variety of buffers.**.....68

**Figure 45: Phage binding ELISA for varying βNGF concentrations.** Mean ± SD n=2, normalised to untreated mean. .....69

**Figure 46: Selectivity of phage binding to neurotrophin treated or untreated well.** Mean ± SD, n=2, normalised to the untreated mean. .....71

**Figure 47: Graph of pan 5 phage ELISA against mBDNF and βNGF, normalised to untreated mean and ranked by average binding to βNGF and mBDNF.** Mean ± SD, n=2. .....76

**Figure 48: Graph of pan 5 phage ELISA at 1x10[11] pfu/mL against mBDNF and βNGF, normalised to non-target binding and ranked by average binding to βNGF and mBDNF.** Mean ± SD, n=2. .....77

**Figure 49: Graph of phage ELISA at 1x10[11] pfu/mL against mBDNF, βNGF HIF-2α PasB, normalised to no-target mean.** Mean ± SD, n=2. .....78

**Figure 50: Titred ELISA of some Pan 5 phage against βNGF and HIF-2α PasB.** n=2. 79

**Figure 51: ELISA of Pan 5 phage against βNGF, HIF-2α PasB or no target, normalised to the mean of the no-target control.** n=2. .....80

**Figure 52: Crystal structure of βNGF bound by domain 5 of TrkA.** RSCB entry 1WWW.[49] 85

**Figure 53: Overview of the intended two-component ELISA testing for antagonist or agonist peptides.** A: positive control, B: antagonist peptide (reduced colour change), C: agonist peptide (increased colour change), D: non-competing peptide (same as positive control). ..... 86

**Figure 54: Crystal structure of TrkB-D5 bound to NT4/5. RSCB PDB entry 1HCF.[170]** 87

**Figure 55: SDS PAGE of a small-scale test expression of A: TrkA-D5 and B: TrkB-D5 in SHuffle T7 Express E. coli.** ..... 89

**Figure 56: SDS PAGE of a mid-scale test of TrkA-D5 and TrkB-D5 expression in SHuffle T7 Express, using a HisTrap nickel affinity column to purify.** 90

**Figure 57: SDS PAGE of a 3 L TrkB-D5 expression and purification from SHuffle T7 Express cells.** ..... 91

**Figure 58: SDS PAGE of a small-scale test expression of A. TrkA-D5 and B. Anti-$His_6$ western blot.** TrkB-D5 in BL21 DE3 E. coli, superimposed with an anti-$His_6$ western blot of a duplicate gel. TrkA-D5: 16.3 kDa, TrkB-D5: 16.0 kDa. 92

**Figure 59: SDS PAGE of the expression, unfolding, refolding and purification of A: TrkA-D5 and B: TrkB-D5.** ..... 94

**Figure 60: Crystal structure of TrkA-D5, highlighting the predominantly antiparallel β-sheet secondary structure.** RCSB PDB entry 1WWW.[49] ..... 95

**Figure 61A: CD spectra of polypeptides and proteins with some representative secondary structure.[181] Figure 61B: CD spectra of TrkA-D5, indicating mainly anti-parallel β-sheet secondary structure.** ..... 95

**Figure 62: Neurotrophin binding ELISAs of the second synthesis of TrkA-D5 and TrkB-D5.** Mean ± SD, n=2. ..... 97

**Figure 63: Dimeric βNGF (PDB 1WWW[49]), highlighting the six intramolecular disulfide bridges per dimer of neurotrophin (C136-C201 C179-C229 and C189-C231).** 98

**Figure 64: Eukaryotic non-consecutive disulfide bridge formation in the endoplasmic reticulum.** 99

**Figure 65: Prokaryotic non-consecutive disulfide bridge formation in the periplasm.** 100

**Figure 66: SDS PAGE of a small-scale test expression of A: βNGF-$His_6$ and B: OmpA-βNGF-$His_6$in SHuffle T7 Express E. coli.** .....102

**Figure 67: SDS PAGE of a mid-scale test expression of A: mBDNF-$His_6$ and B: OmpA-mBDNF-$His_6$ in SHuffle T7 Express E. coli.** Non-denaturing Laemmli buffer was used to preserve polymeric state.....103

**Figure 68: SDS PAGE of a mid-scale test expression of A. βNGF-$His_6$ and B. OmpA-βNGF-$His_6$ in SHuffle T7 Express E. coli, superimposed with an anti-$His_6$ western blot of a duplicate gel.**.....104

**Figure 69: SDS PAGE of a small-scale test expression of A. mBDNF-$His_6$ and B. OmpA-mBDNF-$His_6$ in SHuffle T7 Express E. coli, superimposed with an anti-$His_6$ western blot of a duplicate gel.**.....106

**Figure 70: SDS PAGE of a 5 L large-scale bioreactor expression of OmpA-mBDNF-$His_6$ in SHuffle T7 Express, induced with 400 µM IPTG.** Samples were purified by HisTrap FF nickel affinity columns and s75 size-exclusion chromatography. .....107

**Figure 71: Overview of Lac operon used in auto-induction media.**.....108

**Figure 72: Time course SDS PAGE, anti-$His_6$ western blot and overlay from a 1 L expression of OmpA-mBDNF-$His_6$ in auto-induction media.**.....109

**Figure 73: Two component ELISA of TrkA-D5 binding βNGF, normalised to a +βNGF -TrkA-D5 negative control.** n=2. .....111

**Figure 74: Two component ELISA of TrkB-D5 binding mBDNF, normalised to a +mBDNF –TrkB-D5 negative control.** n=2. ..... 112

**Figure 75: ELISA to assess the selectivity of expressed, refolded and purified TrkA-D5 and TrkB-D5.** Mean ± SD, n=2 ..... 113

**Figure 76: Two-component inhibition ELISA of βNGF and TrkA-D5 binding.** Normalised to a –βNGF +TrkA-D5 negative control and a +βNGF +TrkA-D5 positive control: positive values therefore indicate PPI agonism and negative values PPI antagonism. Ranked by average relative absorbance. Mean ± SD, n=2. 116

**Figure 77: Two-component inhibition ELISA of mBDNF and TrkB-D5 binding.** Normalised to a –mBDNF +TrkB-D5 negative control and a +mBDNF +TrkB-D5 positive control: positive values therefore indicate PPI agonism and negative values PPI antagonism. Ranked by average relative absorbance. Mean ± SD, n=2. ..... 117

**Figure 78: Titred peptide ELISAs of lead βNGF peptides A. JI.5.12, B. JI.5.58, C. JI.5.14 and D. JI.5.55.** Normalised to a +βNGF –TrkA-D5 negative control. Mean ± SD, n=2..... 119

**Figure 79: Titred peptide ELISAs of lead mBDNF peptides A. JI.5.23, B. JI.5.37, C. JI.5.43, D. JI.5.44 and E. JI.5.52.** Normalised to a + mBDNF – TrkB-D5 negative control. Mean ± SD, n=2..... 121

**Figure 80: Structures of peptides selected by phage display as βNGF agonists or antagonists.** 127

**Figure 81: Structures of peptides selected by phage display as mBDNF antagonists.** 128

**Figure 82: Structures of peptides selected by βNGF and mBDNF phage display which display interesting properties.** ..... 128

**Figure 83A: Schematic of MST device. Figure 83B: Fluorescence readout stages during an MST experiment. Figure 83C: Fluorescence readout across a range of binding partner concentrations.** ..... 131

**Figure 84: Crystal structure of βNGF bound by TrkA-D5, highlighting the N-termini, lysine and arginine residues of βNGF. RSCB entry 1WWW.**[49]..132

**Figure 85: SDS PAGE western blot of the βNGF antagonist in vitro assay.**.....135

**Figure 86: SDS PAGE western blot of the βNGF agonist in vitro assay.** .....136

**Figure 87: Western blot densitometry measurements of βNGF antagonist in vitro assays.** 137

**Figure 88: Western blot densitometry measurements of βNGF agonist in vitro assays.** 138

**Figure 89: SDS PAGE western blot of the mBDNF antagonist in vitro assay.**.....139

**Figure 90: SDS PAGE western blot of the mBDNF agonist in vitro assay.**.....139

**Figure 91: Western blot densitometry measurements of mBDNF antagonist in vitro assays.** 140

**Figure 92: Western blot densitometry measurements of mBDNF agonist in vitro assays.** 141

**Figure 93: βNGF morphology assays of A: antagonist and B: agonist activity.** Mean ± SD, n=3 with 100 measurements per condition per repeat.....143

**Figure 94: mBDNF morphology assays of A: antagonist and B: agonist activity.** Mean ± SD, n=2 with 100 measurements per condition per repeat.....144

**Figure 95: mBDNF morphology assays of A: antagonist and B: agonist activity.** n=1 with 100 measurements per condition.....145

**Figure 96: Linear and hairpin disulfide cyclised JI.5.1**.....185

**Figure 97: Linear and hairpin disulfide cyclised JI.5.12**.....186

**Figure 98: Linear and hairpin disulfide cyclised JI.5.13**.....187

**Figure 99: Linear and hairpin disulfide cyclised JI.5.14**.....188

**Figure 100: Linear and hairpin disulfide cyclised JI.5.23**.....189

**Figure 101: Linear and hairpin disulfide cyclised JI.5.37** ..... 190

**Figure 102: Linear and hairpin disulfide cyclised JI.5.43** ..... 191

**Figure 103: Linear and hairpin disulfide cyclised JI.5.44** ..... 192

**Figure 104: Linear and hairpin disulfide cyclised JI.5.52** ..... 193

**Figure 105: Linear and hairpin disulfide cyclised JI.5.55** ..... 194

**Figure 106: Linear and hairpin disulfide cyclised JI.5.58.** ..... 195

# List of Tables

**Table 1: Respondent's opinion of the cause(s) of their chronic pain.** n=4292.[2] ..... 2

**Table 2: A selection of Trk and neurotrophin agonists and antagonists with their known effects.** 16

**Table 3: N-terminal pIII randomised peptide motifs sequenced from streptavidin binding phage.** Sequences sorted by Clustal Omega similarity ranking.[161 162] 63

**Table 4: Phage display library diversity of the variable motif in a NEB Ph.D. C7C library (lot 8).** 64

**Table 5: Pan 3 N-terminal pIII peptide motifs sequenced from βNGF and mBDNF binding phage.** 65

**Table 6: Thermal shift assay summary of βNGF melting points in various buffers.** 68

**Table 7: Pan 5 N-terminal pIII peptide motifs sequenced from βNGF and mBDNF binding phage.** # indicates number of duplicates observed.....73

**Table 8: $ACX_7CG_3S$ groups identified by ClustalO sequence similarity ranking.[161-162]** 74

**Table 9: Observed incidence of amino acids in hit phage variable region, compared with that of the initial unbiased library** .....75

**Table 10: Results from this chapter, ranked by inferred binding affinity in the assay of Figure 51** 84

**Table 11: Collated characterisation data from SPPS of lead peptides** .....129

**Table 12: Collated qualitative results of modulatory ELISA and in vitro assays** .147

**Table 13: Lead peptide activity** 153

**Table 14: Antibiotic concentrations.** .....156

**Table 15: Formula for bisacrylamide gels for SDS PAGE**.....175

**Table 16: Formula for stacking gel bisacrylamide gels for SDS PAGE**.....175

**Table 17: RP-HPLC Biotage program used in general SPPS of linear peptides.** . 183

**Table 18: RP-HPLC program used in general SPPS of hairpin peptides.**.....184

**Table 19: Analytical RP-HPLC program used the analysis of linear peptides.**....185

**Table 20: E. coli cell lines used in this research.** .....205

**Table 21: Table of ssDNA primers used in this research.**.....206

**Table 22: Protein sequences created for this research.**.....207

# List of Schemes

**Scheme 1: TMB colourimetric assay reaction.**[165] .....70

**Scheme 2A: Fmoc deprotection, Scheme 2B: DIC and HOBt preparatory reaction Scheme 2C: amide coupling reaction** .....125

**Scheme 3: Kaiser test reaction mechanism.** A: thermal decay (~120 ˚C), b: imine formation and condensation, c: imine rearrangement, d: imine hydrolysis, e: Ruhemann's Purple formation by nucleophilic attack with the newly formed amine with a second molecule of indantrione. .....126

**Scheme 4: Second generation alkene/alkane disulfide bridge analogues.** Scheme 4A: JI.5.23. Scheme 4B: synthesis of a JI.5.23 alkene or alkane analogue using allyl glycine. 1: Grubb's second generation catalyst in DCM. 2: $H_2$, Pd/C in MeOH. 152

# Declaration of Authorship

I, James David Ingram, declare that the thesis entitled *The Identification of Inhibitors of Nerve Growth Factor and Brain-Derived Neurotrophic Factor* and the work presented in it are my own and has been generated by me as the result of my own original research:

I confirm that:

1. This work was done wholly or mainly while in candidature for a research degree at this University;
2. Where I have consulted the published work of others, this is always clearly attributed;
3. Where I have quoted from the work of others, the source is always given. With the exception of such quotations, this thesis is entirely my own work;
4. I have acknowledged all main sources of help;
5. Where the thesis is based on work done by myself jointly with others, I have made clear exactly what was done by others and what I have contributed myself;
6. None of this work has been published before submission

Date: 26th April 2017

Signed:

James David Ingram

# Definitions and Abbreviations

| | |
|---|---|
| 3-AT | 3-aminotriazole |
| 434 | Bacteriophage 434 repressor protein CI residues 1-101 |
| 434D | 434 Bacteriophage 434 repressor protein CI residues 2-69 |
| ACN | Acetonitrile |
| AIM | Auto-induction media |
| Amp | Ampicillin |
| ARTN | Artemin |
| attB | bacterial phage attachment site |
| attP | phage attachment site |
| Boc | Tert-butyloxycarbonyl |
| β-ME | β-mercaptoethanol |
| βNGF | Nerve growth factor |
| bp | Base pairs |
| BSA | Bovine serum albumin |
| cAMP | Cyclic adenosine monophosphate |
| Camp | Carbenicillin |
| CBD | Chitin binding domain |
| CD | Circular dichroism |
| Chlor | Chloramphenicol |
| CI | Confidence interval |
| CRIM | Conditional-replication, integration, and modular |
| CNTF | Ciliary neurotrophic factor |
| CNS | Central nervous system |
| CtBP | C-terminal binding protein |
| DCM | Dichloromethane |
| DD | Death domain |
| DIC | *N,N'*-Diisopropylcarbodiimide |
| DMF | Dimethylformamide |
| DMSO | Dimethylsulfoxide |
| DNA | Deoxyribonucleic acid |
| DTT | Dithiothreitol |
| *E. coli* | *Escherichia coli* |
| EDTA | Ethylenediaminetetraacetic acid |
| ELISA | Enzyme-linked immunosorbent assay |
| Fmoc | Fluorenyl-methyloxycarbonyl |
| FP | Fluorescence polarisation |
| FPLC | Fast protein liquid chromatography |
| FL | Flexible linker |
| FP | fluorescence polarisation/anisotropy |
| FRET | Fluorescence resonance energy transfer |
| GDNF | Glial-cell line derived neurotrophic factor |
| Hif | Hypoxia inducible factor |
| $His_6$ | Polyhistidine tag |
| HOBt | Hydroyxbenzotriazole |
| HRP | Horseradish peroxidase |
| $IC_{50}$ | Half-maximal inhibitory concentration |
| Int | Phage integrase |
| IPTG | Isopropyl β- D-1-thiogalactopyranoside |
| IR | Infrared |
| ITC | Isothermal titration calorimetry |
| Kan | Kanamycin |
| LB | Lysogeny broth |
| LRR | Leucine-rich repeat |
| LTD | Long-term depression |
| LTP | Long-term potentiation |
| mBDNF | Mature brain-derived neurotrophic factor |
| MCS | Multiple cloning site |
| MOI | Multiplicity of infection |
| MS | Mass spectroscopy |
| MST | Microscale thermophoresis |
| NCR | Non-coding region |
| NMDAR | N-methyl-D-aspartate receptor |
| NRS | Numeric rating scheme |
| NRTN | Neurturin |

| | |
|---|---|
| NT3 | Neurotrophin 3 |
| NT4/5 | Neurotrophin 4/5 |
| Ori | Origin of replication |
| $p75^{NTR}$ | Low-affinity neurotrophin receptor |
| attP | phage attachment site |
| PBS | Phosphate buffered saline |
| PCR | Polymerase chain reaction |
| PDB | Protein Data Bank |
| PDI | Protein deisomerase |
| PEG | Polyethylene glycol |
| Pfu | Plaque forming units (unit of phage concentration) |
| POI | Protein of interest |
| PPI | Protein-protein interaction |
| PromBDNF | mBDNF following pre-domain removal, prior to pro-domain removal |
| PSPN | Persephin |
| PTM | Post-translational modification |
| REN | Restriction endonuclease |
| RA | Rheumatoid arthritis |
| RCSB | Research Collaboratory for Structural Bioinformatics |
| RP-HPLC | Reverse-phase high performance liquid chromatography |
| RTHS | Reverse two-hybrid system |
| RTP | Room temperature and pressure |
| SAR | Structure-activity relationship |
| SDS PAGE | Sodium dodecyl sulfate polyacrylamide gel electrophoresis |
| SDM | Site directed mutagenesis |
| SEC | Size-exclusion chromatography |
| SOC | Super-optimal with catabolite repression |
| SPPS | Solid-phase peptide synthesis |
| SPR | Surface plasmon resonance |
| Spec | Spectinomycin |
| TAE | Tris-acetate-EDTA |
| TB | Terrific broth |
| TBF | Transformation buffer |
| TCS | Thrombin cleavage site |
| Tet | Tetracycline |
| TFA | Trifluoroacetic acid |
| THS | Two-hybrid system |
| TIS | Triisopropylsilane |
| TK | Tyrosine kinase domain |
| TMB | 3,3',5,5'-tetramethylbenzidine |
| TrmBDNF | Truncated mBDNF |
| Trk | Tropomyosin receptor kinase |

## Amino Acid Abbreviations

| | | | | | | | | |
|---|---|---|---|---|---|---|---|---|
| Ala | A | Alanine | Gly | G | Glycine | Pro | P | Proline |
| Arg | R | Arginine | His | H | Histidine | Ser | S | Serine |
| Asn | N | Asparagine | Ile | I | Isoleucine | Thr | T | Threonine |
| Asp | D | Aspartic Acid | Leu | L | Leucine | Try | W | Tryptophan |
| Cys | C | Cysteine | Lys | K | Lysine | Tyr | Y | Tyrosine |
| Gln | Q | Glutamine | Met | M | Methionine | Val | V | Valine |
| Glu | E | Glutamic Acid | Phe | F | Phenylalanine | | | |

# Chapter 1: Introduction to βNGF and mBDNF

## 1.1 The Importance of Novel Pain Therapies

Pain is an unpleasant sensory and emotional experience; an evolutionary response used to prevent further injury and promote healing. While sources of pain vary, pain is classified as either acute (lasting less than 12 weeks) or chronic (lasting more than 12 weeks). Chronic pain can be particularly debilitating: significantly affect a person's quality of life, general health and psychological state. It can cause those affected to experience depression, job loss or the inability to work at all.[2] While pain clearly serves an evolutionary purpose, errors occurring in nociception (the sensing of pain) which causes chronic pain can find our current pharmacopeial arsenal to be lacking: this section hopes to set out the causes and prevalence of chronic pain, current treatments and the need for novel therapies.

While chronic pain may be caused by a long-term recurring injury, commonly it is due to an aberrant signalling or a lesion in the somatosensory nervous system. Pain originating from the nervous system and not an external stimulus is known as neuropathic pain. This may be either centralised or peripheral. Neuropathic pain may present as allodynia (a pain sensation to a stimulus which normally doesn't provoke a response), hyperalgesia (increased response to a normally painful stimuli), sensory gain or loss. Conditions which may cause central neuropathic pain include stroke, spinal cord injury or multiple sclerosis. Peripheral neuropathic pain may be caused by neuropathic cancer pain (e.g. chemotherapy induced neuropathy, invasion into or compression of neural structures, or tumour antigens causing an autoimmune response) diabetic neuropathy or post-surgery chronic neuropathic pain.

Regarding the epidemiology of chronic pain in the UK and the care burden on the NHS that this entails, several meta-analyses of studies have been performed: these place the prevalence of chronic pain to be 43% of the population, or 12% for moderately to severely limiting chronic pain (95% CI).[1-2] This equates to 28 million or 8 million people respectively and the prevalence rises with increasing age: 62% of the population aged over 75 experience chronic pain.[1] If incidence rates remain, the burden of care on society will increase as our population continues to age. In addition to the financial strain this places on the National Health Service (NHS), this also creates an economic burden on society due to reduced productivity and days missed: the productivity cost of chronic back pain in the UK (prevalence ~10%) is estimated to be circa £5-11 billion annually, on top of costing the

NHS circa £1 billion in direct care costs.[5-6] Other sources of chronic pain similarly affect productivity, for instance over a five year study of early onset rheumatoid arthritis (RA), 29% of the patient population stopped working because of the disease.[7] The causes of chronic pain are shown in Table 1.

***Table 1: Respondent's opinion of the cause(s) of their chronic pain.*** *n=4292.*[2]

| Cause of Chronic Pain | Respondents | Cause of Chronic Pain | Respondents |
|---|---|---|---|
| Arthritis/osteoarthritis | 34% | Fracture/deterioration of the spine | 6% |
| Herniated/deteriorating discs | 15% | Nerve damage | 4% |
| Traumatic injury | 12% | Cartilage damage | 4% |
| Rheumatoid arthritis | 8% | Whiplash | 4% |
| Migraine headaches | 7% | Surgery | 3% |

Regarding the effects of chronic pain, the largest European survey of chronic pain examined the prevalence, impact on daily life and treatment used by those affected.[2] It used an initial telephone interview to reach 46,394 people affected by chronic pain (who rated their pain ≥5 on a 10-point Numeric Rating Scale (NRS) where 1 = no pain and 10 = worst pain imaginable) across 16 countries. This was followed by in-depth interviews with 4839 participants (~300 per country). This study uncovered the severe impact that chronic pain had on the lives of those affected: 19% (n=4336) stated that chronic pain had cost them a job, 13% (n=4272) had changed jobs because of their chronic pain. 61% stated that their chronic pain affected whether they could work outside the home and 21% (n=4808) stated their pain had led to a depression diagnosis. Other ways in which chronic pain affected the lives of those who suffer it are shown in Figure 1.

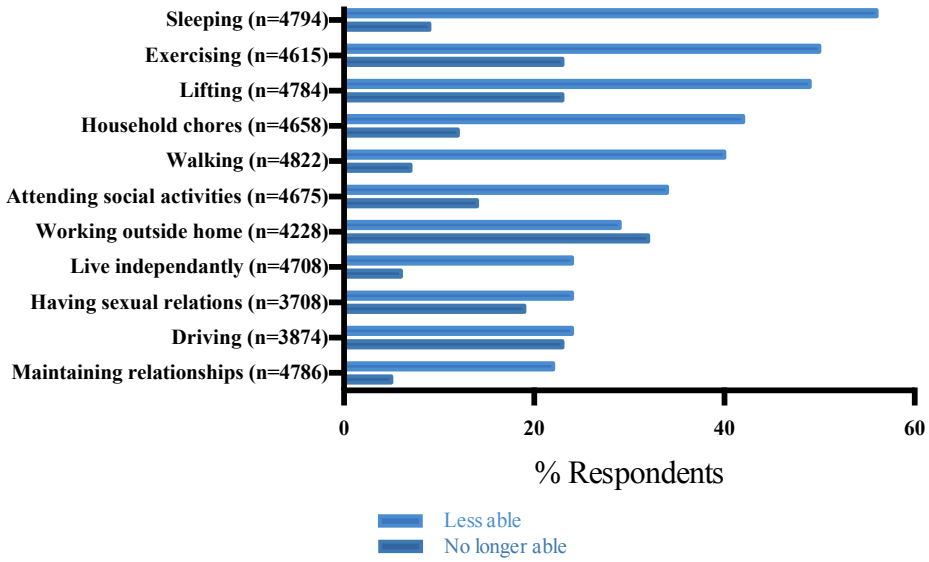



***Figure 1: The impact of chronic pain on the daily life of those affected.[2]***

Despite this impact on their lives, the study found that 31% of those affected by chronic pain go untreated. While the most popular reason for this was due to managing pain on their own (33% of that 31%) or pain not being bad enough (13%), other responses included that there was nothing more to be done (12%), that they "just live with the pain" (11%), that the side effects of treatment led them to abandoning it (11%) or that the treatment wasn't effective in managing their pain, so they abandoned it (5%). This 39% of the 31% who go untreated suggests a need for new treatment or therapies: that these people should not have to accept their fate and so greatly impact their daily life (Figure 1). This need for better treatments is compounded by the drug history of those treating their pain: while 52% were currently taking prescription medication to treat their pain, 26% had lapsed: 64% of this was thankfully due to lack of need for prescription strength medication, but 34% were due to side effects, low efficacy or worries about addiction.[2]

In fact, the study found that 40% of those diagnosed with chronic pain were not satisfied by the efficacy of the treatment they were receiving. The general attitude towards their pain treatments was one of concern or mistrust, as shown in Figure 2: the most popular statement being concern about side effects, and the third most popular being a desire for greater efficacy.

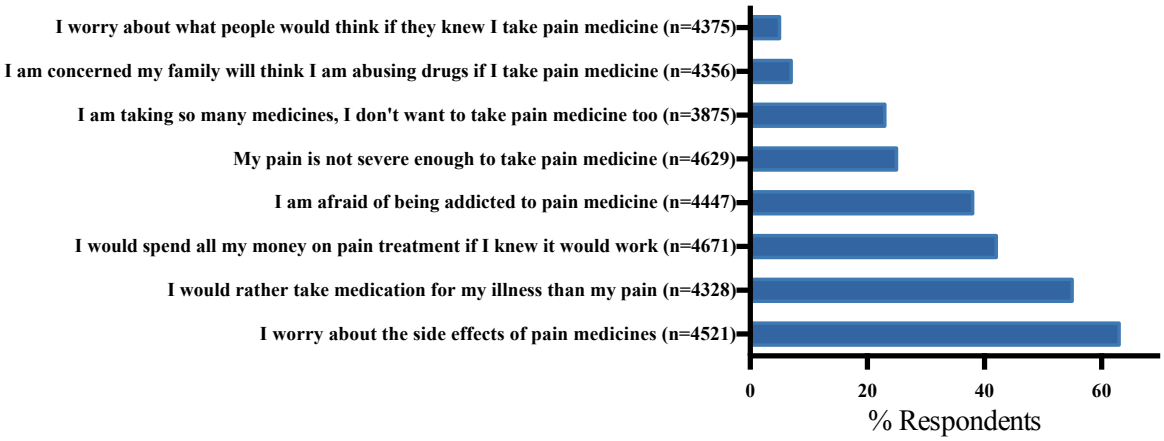



***Figure 2: The attitudes of chronic pain patients about pain treatments.*** *Respondents either agreed somewhat or completely with the statements read out by interviewers.*[2]

Concluding this section, chronic pain affects 43% of the UK population, with 12% experiencing chronic pain which is moderately to severely limiting.[1] The attitudes of those affected by chronic pain is one of worry: of the side effects, their lack of efficacy and their addictive properties.[2] Examining the drugs taken by these patients, half were taking non-prescription analgesics: 55% used over the counter (OTC) non-steroidal anti-inflammatory drugs (NSAIDs), 43% used paracetamol, 13% used weak opioids (mainly codeine or dihydrocodeine mixed with paracetamol). Two thirds used prescription medicines: 44% used NSAIDs, 23% used weak opioids (as above), 18% used stronger paracetamol, 6% used COX-2 inhibitors and 5% used strong opioids.

There is clearly a need for more effective analgesics with lower side effects. Because of the extensive research that has been conducted on inhibiting classic targets such as the μ-opioid receptor, COX-1 or COX-2, it's arguable that new targets should be approached in an attempt to develop drugs with better profiles. The following research tables the neurotrophins nerve growth factor (βNGF) and brain-derived neurotrophic factor (mBDNF) as such targets: inhibiting these autocrine/paracrines from interacting with their receptors tyrosine receptor kinase (Trk) A and TrkB may be used as novel pain therapies. The rationale for antagonising the βNGF-TrkA interaction to produce an analgesic effect is supported by the following: a missense mutation of TrkA occurs in patients with congenital insensitivity to pain with anhidrosis (CIPA). This autosomal recessive condition prevents the expression of functional TrkA, and is characterised by a complete lack of nociception.[8] This lack of pain (though not sensation) is so strong that self-mutilation

frequently occurs: patients commonly remove parts of their tongue, teeth and fingertips. Other symptoms are neuropathic arthropathy and ulcers.[9-10]

In addition to CIPA, the rationale for inhibiting the βNGF-TrkA and mBDNF-TrkB interactions is supported by the fact that these interactions modulate pain sensation:[11] upregulation of βNGF/TrkA and mBDNF/TrkB occurs following trauma,[12] and that administration of βNGF or mBDNF induces a pain-state,[13] causing nociception and hyperalgesia in both human and animal models,[12, 14-15] whereas treatment with anti-mBDNF antibodies reduce inflammation-induced hyperalgesia and allodynia.[16] A TrkA, TrkB and TrkC blockade in mice with femoral fractures halved pain-related behaviours without significant sedation, weight gain or inhibiting fracture healing.[17] Due to this extensive rat and mouse modelling, it is thought that preventing mBDNF signalling represents a novel method for treating neuropathic pain.[13-15]

While both βNGF and mBDNF inhibitors have been identified (see Section 1.3.3), no candidate has been developed through to the clinic as a treatment for pain, primarily due to lack of efficacy or toxicity. The nearest approved treatment in the area is Lestaurinib (a TrkA, TrkB, TrkC and Fms-Related Tyrosine Kinase 3 antagonist) approved for use as a treatment of acute myeloid leukaemia (for an explanation of the links between βNGF-TrkA and mBDNF-TrkB and cancer, see Section 1.2). The closest anti-neurotrophin treatment is Pfizer's anti-NGF monoclonal antibody Tanezumab, which has successfully undergone several Phase III trials and has been granted FDA Fast Track designation in June 2017 for the treatment of chronic pain in patients with osteoarthritis and chronic lower back pain.[4, 18-19] As shown in Section 1.3.3, all identified neurotrophin inhibitors have so far relied on either small molecule inhibitors or large protein antibodies and epimers. This presents the question as to whether more efficacious neurotrophin inhibitors exist between these chemical spaces, above Lipinski's rules[20] but smaller than antibody therapy may provide the properties required.

As stated, Lestaurinib antagonises neurotrophin receptors TrkA, TrkB, TrkC and Fms-Related Tyrosine Kinase 3 as a cancer treatment. These interactions have a number of links with various cancers and while this project is primarily involved with initial hit discovery of novel pain therapies, such inhibitors may also prove useful as cancer treatments. What follows is an overview of these connections, further validating investigating novel inhibitors in this area.

## 1.2 mBDNF Inhibition as a Novel Cancer Therapy

Not only is mBDNF-TrkB activity linked with nociception, it plays a strong role in neuronal activity-based survival and synaptic plasticity: mBDNF activity promotes neuronal survival, its absence promotes neuronal death, and changes the strength of synaptic junctions. When an afferent neurone activates a downstream efferent neurone it not only releases neurotransmitter into the synaptic cleft (in the case of nociception, glutamate[21]), it also releases a number of regulatory proteins including mBDNF and βNGF. These diffuse across to the efferent neurone and interact with their respective membrane-bound receptors, triggering signalling cascades. These, as part of mBDNF's activity-based survival activity promote the cell to ignore apoptosis signals and change the cells morphology: growing more neurites, longer axons and larger synaptic boutons. These morphological changes in the presence or absence of mBDNF play a major role in memory and learning.[22-23] In fact, Huntington's disease has been linked with dysregulation of mBDNF: Huntington's disease is caused by a mutation in the HTT gene, which encodes the protein huntingtin: in Huntington's disease the mutant huntingtin is non-functional and aggregates, however one of the few known functions of huntingtin is transcriptional upregulation of mBDNF. It is unclear how much of the symptoms of Huntington's are due to the downregulation of mBDNF expression.[24] Interestingly however, βNGF (but not mBDNF) overexpression prevents hippocampal impairment by β-amyloid plaques, a key part of Alzheimer's pathology.[25]

The neuronal activity-based survival has a caveat however: certain cancers use this autocrine/paracrine pathway to ignore apoptosis signalling.[26-29] In this case, inhibiting mBDNF-TrkB activity has been shown to increase apoptosis and severely impact cancer proliferation.[28-29] This pathway is not just limited to tissues which normally express mBDNF either: none is usually expressed in breast tissue, yet some breast cancers have been found to be using mBDNF autocrine activity to self-stimulate, ignoring apoptosis signals.[30] Inhibition of mBDNF in these cases (through knockdown, siRNA or antibody treatment) has been shown to decrease cancer growth and proliferation.[31-32] As such, antagonising the mBDNF-TrkB interaction may provide a novel cancer therapy. Additionally, as mBDNF and βNGF are not widely expressed (outside of foetal development and the central nervous system (CNS)), should such an inhibitor fail to enter the blood-brain barrier, treatments selective to this interaction would be limited to the aberrant tissues expressing them.

## 1.3 βNGF and mBDNF as Targets for Inhibition

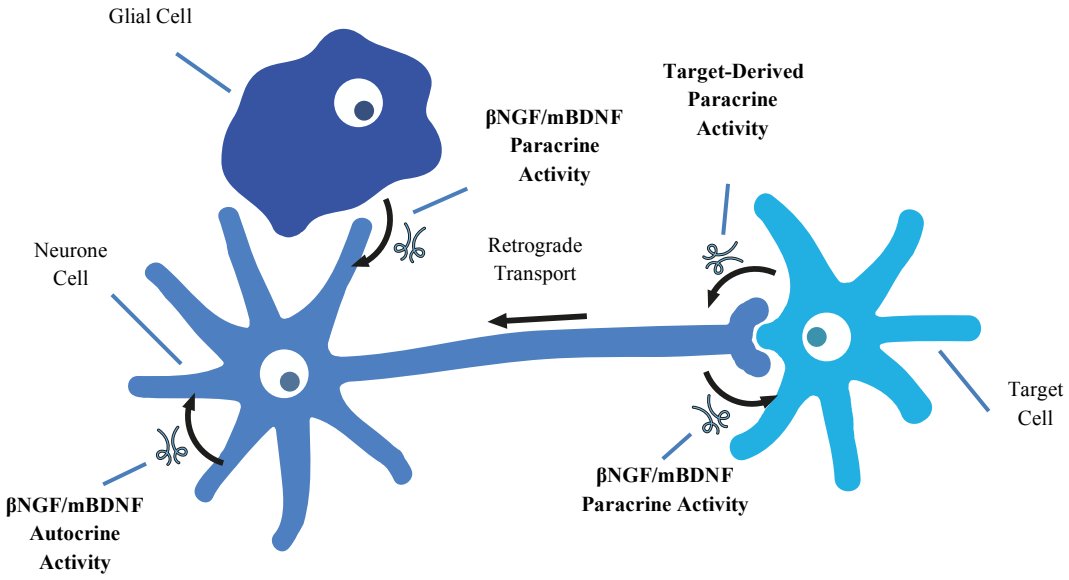



***Figure 3: Paracrine, autocrine and target-derived modes of neurotrophin presentation.***

βNGF and mBDNF are members of the neurotrophin family. As shown in Figure 3, their biological function is to act as messengers (autocrines and paracrines) between nerve cells. They are released into the intracellular space where they bind with membrane-bound receptors on either the target cell (paracrine activity) or on the releasing cell (autocrine activity). The membrane-bound neurotrophin receptor then undergoes invagination and the activated receptor is transported back to the nucleus, triggering a number of signalling cascades. As stated, the downstream phenotypes from neurotrophin activity include promoting nerve cell survival, ignoring apoptosis signals, neurite growth, and increased sensitivity to pain. βNGF and mBDNF inhibition is therefore a promising therapeutic area, as aberrant neurotrophin and neurotrophin receptor expression, splice variants and polymorphs are implicit in chronic pain,[11, 13-15, 17] central and peripheral nervous system trauma;[33] various cancers (e.g. glioma,[26] medulloblastoma[27] or choriocarcinoma[28-29]), Alzheimer's,[34-36] Down's syndrome,[37-38] epilepsy,[39-40] Huntington's,[24, 41] Parkinson's,[42-43] anxiety[44-45] and eating disorders.[46] It is thought that the manipulation of neurotrophins and neurotrophin receptor activity provides an interesting and novel area for treating pain and cancer.[17, 47-48]

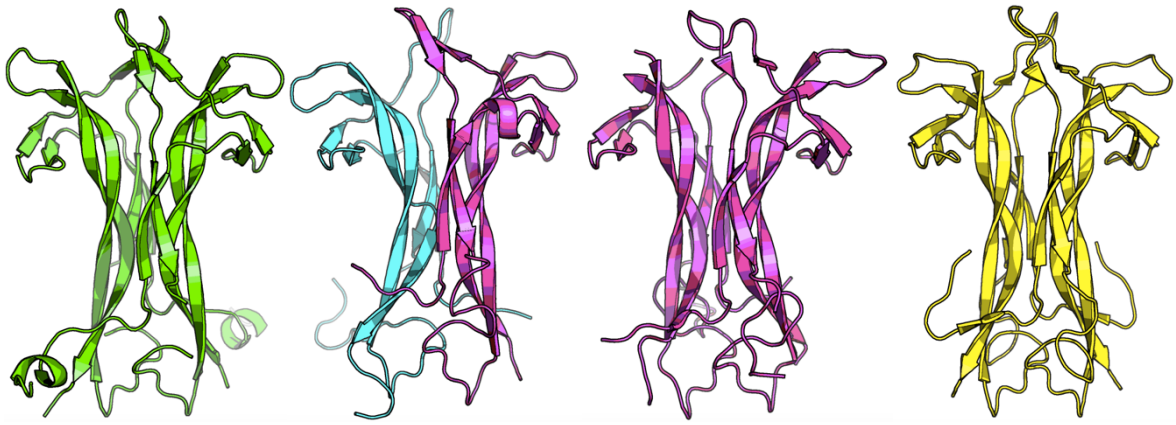


***Figure 4: Crystal structures of neurotrophins.*** *βNGF homodimer (RSCB protein data bank (PDB) entry: 1WWW),[49] mBDNF (blue) and NT4/5 heterodimer (magenta, PDB entry 1B8M)[50] NT4/5 homodimer (magenta, PDB entry 1B98),[51] and NT3 homodimer (PDB entry 3BUK)[52]*

In addition to βNGF and mBDNF, the main neurotrophin family consists of neurotrophin 3 (NT3) and neurotrophin 4/5 (NT4/5 was originally named NT5 as was initially unclear whether it was a homolog of *Xenopus* NT-4. NT-4/5 was adopted despite this being verified). βNGF,[53] mBDNF,[54] NT3[54] and NT4/5[55] are paralogs: genes related by chromosomal duplication, which evolve different functions. As shown in Figure 4, these four proteins have high structural similarity due to significantly high sequence similarity. While heterodimers are possible between these main neurotrophins and such heterodimers display similar activity to their homodimers[56] they preferentially homodimerise. As yet, no publically available mBDNF homodimer crystal structure exists, hence using the 1B8M heterodimer in Figure 4. All four main neurotrophins cause similar but distinct phenotypes (neuronal differentiation and activity-based survival).

Although they use different membrane bound receptors, causing distinct signalling cascades and similar but different phenotypes, a number of other proteins in the "neurotrophin" family exist, including the GDNF family: glial cell line-derived neurotrophic factor (GDNF), neurturin (NRTN), artemin (ARTN) and persephin (PSPN);[57] and ciliary neurotrophic factor (CNTF).[58] As shown in Figure 5 these are structurally highly dissimilar both from each other and the main neurotrophin family (Figure 4). As they are dissimilar (and therefore less of a potential problem for inhibitor selectivity) and have different activity outside of the remit of this research, they will not be covered further, and as such, hereafter "neurotrophins" refers to βNGF, mBDNF, NT3 and NT4.

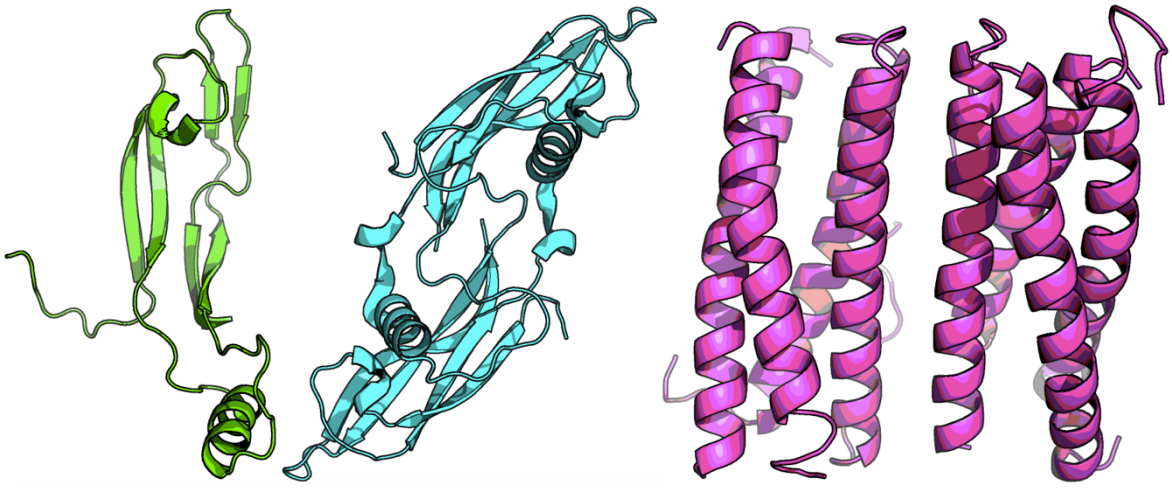


***Figure 5: Crystal structures of other "neurotrophins".*** *GDNF monomer (green, PDB entry: 3FUB),[59] ARTN homodimer (blue, PDB entry 2ASK)[60] and CNTF homodimer (magenta, PDB entry 1CNT).[61]*

This project initially focused on the selective inhibition of mBDNF, however midway through the project this was expanded to include investigation of βNGF. What follows is an overview of their activity:

### 1.3.1 Brain-Derived Neurotrophic Factor

As stated, mBDNF has the broadest activity of the neurotrophins and regulates neuronal survival and differentiation; activity-dependent plasticity processes such as long-term potentiation (LTP), long-term depression (LTD), learning, and memory.[62] Note: LTP and LTD refer to neuronal morphological changes which respectively improve or decline synaptic transmission (e.g. enlarged boutons) or the respective lowering or raising of the potential difference change required to fire a target cell's excitation, causing more or less downstream firing for the same input.

As shown in Figure 6, when BDNF is expressed it has a signalling domain, a pro-protein domain and the mature protein domain. Once translated, pre-proBDNF homodimerises and the signalling domains dictate transport to the Golgi apparatus. Here, the signalling domains are cleaved in a post-translational modification (PTM).[63] The removal of the pro-domain may happen at two points in the lifecycle of BDNF and is critical to the observed downstream phenotype: proBDNF causes distinct counteractivity from mBDNF, resulting in activity-based death as opposed to activity-based survival.

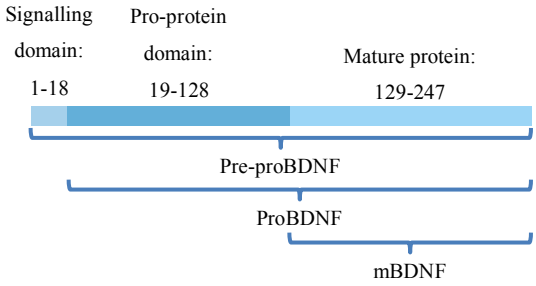



***Figure 6: Diagram of translated BDNF and post-translational modification variants.*** *Numbers show amino acid residue number.*

It is in the Golgi apparatus that the mBDNF pro-domain *may* be cleaved by SKI-1/S1P convertase or furin to produce mature neurotrophin.[64-65] ProBDNF and mBDNF are then packaged for extracellular release at the *trans*-Golgi network into either small (50-100 nm) constitutive vesicles or regulated large (100-300 nm) dense-core vesicles. The small vesicles are continuously released into the synaptic cleft, providing a constant low concentration of these proteins. The large dense-core vesicles are only released into the synaptic cleft upon neuronal excitation, providing a high concentration of proBDNF or mBDNF based on neuronal usage. The regulated pathway therefore ensures that frequently excited neurons secrete more mBDNF, having a greater survival and LTP effect. Once in the synaptic cleft, residual pro-mBDNF may be proteolytically activated by plasmin, however this is controlled by the amount of high-frequency neurotransmission.[66]

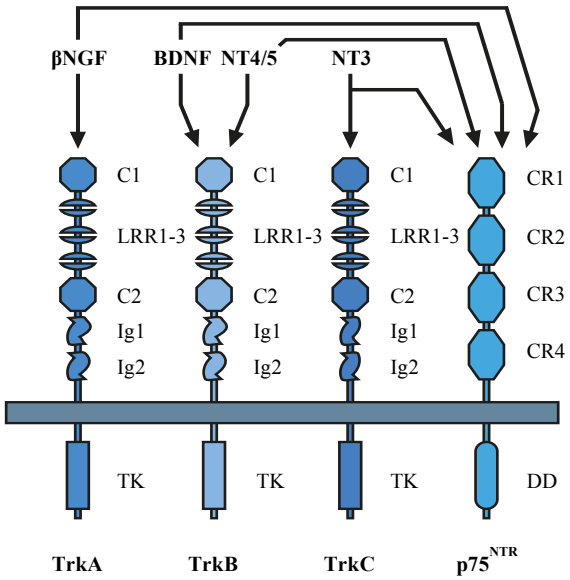



**Figure 7: Neurotrophin receptor selectivity and receptor domain structure.[62, 67]**

As stated, βNGF and mBDNF bind to TrkA and TrkB respectively. The selectivity of the neurotrophin family shown in Figure 7, including the low-affinity neurotrophin receptor ($p75^{NTR}$) activity shown by all family members.

As shown in Figure 7, all Trk receptors consist of two cysteine-rich domains (C1 and C2) flanking a leucine rich repeat (LRR1-3), two IgG-like domains (Ig1 and Ig2), a juxtamembrane domain and a tyrosine kinase domain (TK). This structure is particularly relevant to Section 4.2, when the Ig2 domain is used in an agonist/antagonist ELISA screen.

$p75^{NTR}$ consists of four cysteine rich domains (CR1-4), a juxtamembrane domain and a death domain (DD). Additionally, pro-neurotrophins display different binding Trk and $p75^{NTR}$ activity and affinity; typically pro-neurotrophins bind strongly to $p75^{NTR}$ and weakly to the Trk their mature version binds to.

ProBDNF and mBDNF activation of $p75^{NTR}$ or TrkB leads to invagination: the inversion of an area of the cell membrane to create a pocket which becomes an endosome inside the cell, with the DD or TK domain of $p75^{NTR}$ or TrkB on the outer (intracellular) surface of the endosome. Typically these endosomes are then transported back to the nucleus.

Upon activation, $p75^{NTR}$ recruits various signalling adaptors and so triggers several signalling cascades (Figure 8). The cascades it initiates are neurotrophin dependant e.g. ProNGF-$p75^{NTR}$ activity is capable of inducing the NADE cascade resulting in apoptosis, but proBDNF-$p75^{NTR}$, proNT3-$p75^{NTR}$ and proNT4/5-$p75^{NTR}$ activity cannot.[68]

Pro-neurotrophins and mature neurotrophins also trigger distinct $p75^{NTR}$ activity: the neurotrophin pro-domain recruits sortilin,[69-70] allowing high-affinity trimerisation with $p75^{NTR}$, which then activate several pathways involved in apoptosis[70-72] or long-term depression (LTD):[72-73] destabilising neurites and forming smaller boutons. This runs entirely counter to mBDNF activity, and is therefore used as a negative feedback loop. Lacking the pro-domain, mature neurotrophins are unable to form this trimer.[71]

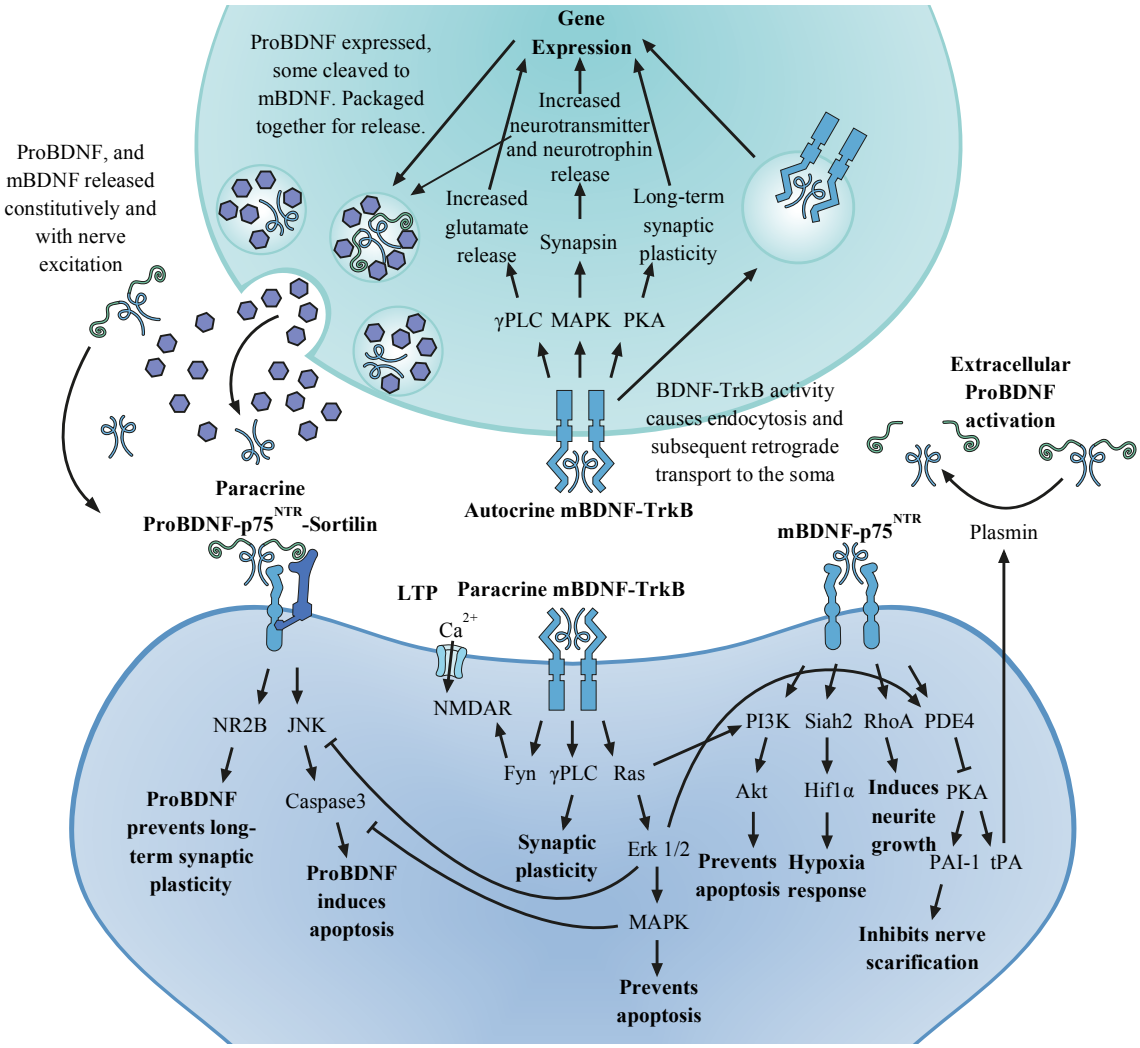



***Figure 8: Simplified schematic of mBDNF and proBDNF activity in neurons.***

mBDNF-p75$^{NTR}$ activity however causes signalling cascades involved in cell survival (Ras-MAPK[74]) (PI3K[75]), hypoxia response (Siah2[76-77]) and neurite growth (RhoA[78]) – more dendrites, longer axons and a higher baseline polarity requiring less excitation to cause efferent nerve firing (LTP). mBDNF-p75$^{NTR}$ activity also inhibits pathways involved in nerve scarification after injury by decreasing the amount of cyclic adenosine monophosphate in cells.[79] mBDNF-TrkB activity promotes cell survival (Ras[74, 80]) (Erk[81-82]) and increases long-term potentiation (LTP) – more neurites,[22, 83] larger boutons,[23] increased glutamate release[84] and/or greater AMDAR synthesis and surface expression.[85] mBDNF-TrkB activity also triggers the N-methyl-*D*-aspartate receptor (NMDAR) fast-feedback loop; mBDNF-TrkB phosphorylates tyrosine-protein kinase Fyn, which activates the NMDAR ion channel. This causes the influx of positive ions into the cell, triggering mBDNF secretion.[86] Finally, several of the cascades triggered by mBDNF-TrkB activity inhibit pathways involved in apoptosis and nerve scarification/pro-mBDNF (MapK-Caspase3,[74] Erk-JNK,[71] Erk-PDE4[79]). Because of the anti-apoptotic, pro-survival and

feedback activity loop activity, mBDNF-TrkB activity is involved in certain cancer states.[19, 20] Aberrant $p75^{NTR}$ activity is also implicated in aggressive metastatic cancer activity.[26-27] Splice variants for TrkB and TrkC exist which lack the kinase domain and are therefore functionally inert. Because activation of TRK receptors causes endocytosis of both the Trk and the neurotrophin, these are thought to act as dominant negatives and reduce Trk activity by reducing the effective local concentrations of neurotrophins and neurotrophin receptors.[87]

### 1.3.2 Nerve Growth Factor

Upregulation of βNGF/TrkA has been shown to occur at sites of injury in pain disease in human and animal models, and administration of βNGF induces pain in both humans and nonclinical species. Potent, selective small molecule inhibitors of TrkA may provide a novel approach to pain management.

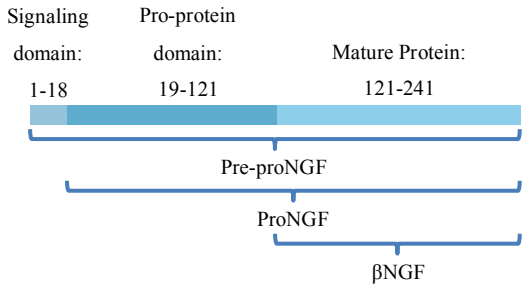



***Figure 9: Diagram of translated βNGF and post-translational modification variants.***

As they are paralogs, βNGF and mBDNF have a significant number of similarities: both are expressed with a signalling domain, pro-domain and a mature domain (Figure 9); both have a similar quaternary homodimeric structure (Figure 4), both are packaged into constitutional and constitutive and regulated vesicles for extracellular release; both have a pro-protein with activity contrary to the mature protein, finally both bind to $p75^{NTR}$ and a specific tyrosine kinase domain. Despite these similarities, as previously stated they do activate some distinct signalling cascades:

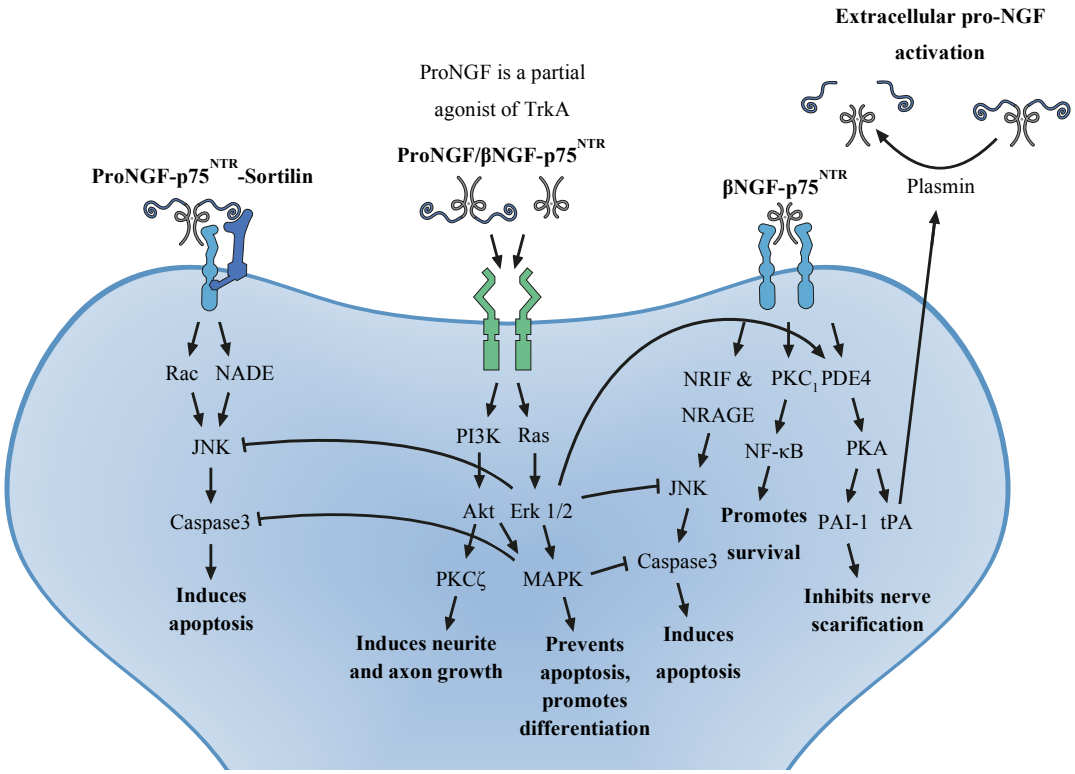



***Figure 10: Simplified schematic of βNGF and ProNGF activity in neurons.***

While the βNGF and ProNGF signalling cascades shown in Figure 10 are simplified, the key pathways are indicated: it shares a number of pathways with mBDNF/proBDNF but diverges in a number of ways: ProNGF-p75$^{NTR}$ induces the NADE cascade resulting in apoptosis,[88] however this pathway is also activated by βNGF-p75$^{NTR}$ activity via NRIF and NRAGE involvement.[68] This βNGF-p75$^{NTR}$ pro-apoptotic activity is tightly regulated and has been found to be dependent on the presence of a number of DNA repair enzymes, such as Ku70[89] and Ku86, these have proved to be important interactions during invasive cancer growth.[90] Similar to mBDNF and TrkA, βNGF-TrkA activates the MAPK pathway via Ras and Erk 1/2; and the P13K/Akt pathway to produce anti-apoptotic phenotypes and neurite outgrowth.[91-92] Interestingly ProNGF has proved to be a partial agonist of TrkA, however it has a significantly slow off-rate: this inhibits full activation by βNGF, contributing to the pro-apoptotic nature of ProNGF.[93] Like other members of the tumour necrosis factor, p75$^{NTR}$ is capable of promoting the activation and nuclear translocation of NF-κB, however a number of adaptor proteins (e.g. RIP2) can bind to the death domain of p75$^{NTR}$ and convert a death signal into an anti-apoptotic one.[94] As with mBDNF and ProBDNF signalling, the resulting βNGF and ProNGF phenotype is highly dependent on the concentration of downstream proteins, especially the concentrations of p75$^{NTR}$ and TrkA or TrkB.[95]

### 1.3.3 Existing Agonists and Antagonists

Significant efforts have been made to identify and develop agonists and antagonists of mBDNF, βNGF, TrkA and TrkB. This section details the identification and testing of several in this area, including the one pan-tyrosine receptor kinase antagonist (Lestaurinib) to be approved as a treatment for acute myeloid leukaemia, and one βNGF-sequestering treatment which looks likely for prompt approval for chronic pain (Tanezumab).

The selective inhibition or activation of these targets have proved to be a challenge: this is primarily due to the limited extracellular exposure of the neurotrophins, the limited stability of neurotrophins (mBDNF plasma half-life: <1 min, βNGF plasma half-life: 7.2 min[96]), the difficulties of protein-protein interaction (PPI) inhibition and studying the induced-fit dimerisation of the membrane-bound neurotrophin receptors.[48] Additionally, the high structural similarity of mBDNF, βNGF, NT3 and NT4 makes selective inhibition difficult. Selectivity in neurotrophin inhibition is important as they each activate distinct signalling cascades – non-selective inhibition increases toxicity concerns due to a broader range of effects. What follows are an overview of the anti-NGF treatments which have reached clinical trials (at present no mBDNF antagonist has reached clinical trials[97]):

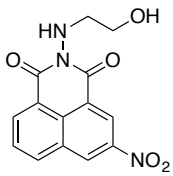
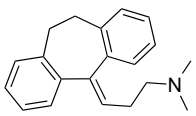
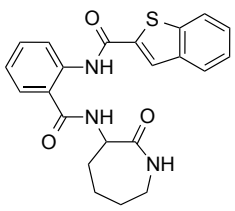
The most successful anti-neurotrophin therapy for chronic pain to date is Pfizer's Tanezumab, which was granted FDA Fast Track designation in June 2017 for the treatment of osteoarthritis and chronic lower back pain. An investigational humanised monoclonal antibody, Tanezumab selectively binds βNGF. If approved, will be the first in a new class of non-opioidal chronic pain medications. It is currently undergoing several Phase III trials involving ~7000 patients and the results should be announced in 2018.[4, 18-19] It is not without controversy however, as a phase III trial for osteoarthritic hip pain while successful in the primary end goals showed an increase in the required number of hip replacements.[4] This was attributed to the absence of protective pain stimuli, resulting in an overuse of the affected joints. Other βNGF sequestering antibody treatments (Amgen's Fulranumab, Regeneron's Fasinumab) have entered Phase II and Phase III trials, however they have been abandoned due to lack of sufficient efficacy.[98-100]

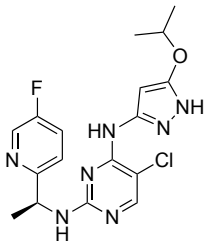
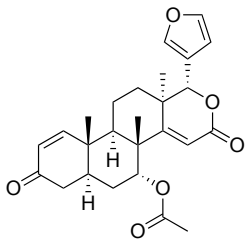
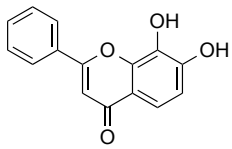
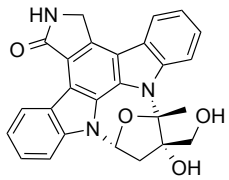
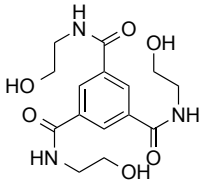
Another frontrunner in this area is AMG819, which entered (and failed) Phase I trials. A "peptibody" consisting of an βNGF-binding domain fused with an Fc-domain to increase avidity, AMG819 showed sub nM activity. The βNGF-binding domain was identified by major coat protein filamentous phage display and in rat models it was shown to have

reasonable efficacy in hypersensitivity and allodynia models.[101] First in man Phase 1 trials revealed a reasonable plasma half-life of 3.5 days, but as with all peptide based drugs there was a possibility of an immunological response. Unfortunately, 37% of phase 1 subjects developed detectable anti-AMG819 IgG antibodies after a single injection, indicating a T-cell response. Computational analysis suggested that 14 amino acids of the 20-mer peptide identified by phage display were a potential promiscuous immunogenic epitope, which was confirmed by a memory T-cell response. Development of AMG819 was then ceased as the immunological response was too strong, which can cause serious problems.[102]

As stated, significant research has been conducted in this area, identifying a number of compounds which inhibit βNGF-TrkA or mBDNF-TrkB activity. As with all drug development, the vast majority of hits and leads fail to reach clinical trials. Table 2 indicates a number of agonists and antagonists in this area, detailing the in vitro and in vivo testing performed on them:

***Table 2: A selection of Trk and neurotrophin agonists and antagonists with their known effects.***

| Name and Structure | Identification Method | Target, Observed Phenotype/Usage |
|---|---|---|
| **ALE-0540**  | High-throughput screen of a commercial library, $^{125}$I-NGF binding to PC12 cells | NGF antagonist<br>Anti-allodynic in rat models of neuropathic pain. Discontinued due to lack of specificity. [103] |
| **Amitryptylene**  | High-throughput screen of a commercial library, fluorescent cell-based assay of anti-apoptosis compounds | TrkA/TrkB agonist:<br>Promotes neuronal regeneration and prevented acid-induced neuronal cell death in mice.[104] |
| **ANA-12**  | Computer modelling of BDNF/TrkB specificity patch and docking-based virtual screening | TrkB antagonist:<br>Anxiolytic and antidepressant activity in mice. [44] |

| Name and Structure | Identification Method | Target, Observed Phenotype/Usage |
|---|---|---|
| **AZ-23**  | High-throughput screen of an internal compound collection by *in vitro* TrkA kinase assay | TrkB antagonist:<br>Prevents neuroblastoma growth in rats.[105-106] |
| **Cyclotraxin-B**<br>Disulfide bridged<br>$H_2N$**C**NPMGYTKEGC**C**O OH | Proteolysis of mBDNF into fragments, screening on CHO cells expressing TrkB | TrkB antagonist:<br>Reversal of cold allodynia[107], anxiolytic[108] in mice. |
| **Deoxygedunin**  | High-throughput screen of a commercial library, anti-apoptotic BDNF/TrkB T48 cell-based assay | TrkB agonist:<br>Prevents vestibular ganglion degradation in mice, prevents rat neuron cell death. Anti-depressant and learning enhancement effects in mice.[23] |
| **Dihydroxy-flavone**  | High-throughput screen of a commercial library, anti-apoptotic BDNF/TrkB T48 and T62 cell-based assay | TrkB agonist:<br>Increased synaptic plasticity in the hippocampus of aged rats (improved learning), increased fear memory retention in rats. [22] |
| **Lestaurinib**  | High-throughput screen of tyrosine kinase inhibitors, BaF3/ITD cells cell-based assay | TrkA, TrkB, TrkC and Fms-Related Tyrosine Kinase 3 antagonist:<br>Approved as a treatment of acute myeloid leukaemia, with clinical trials underway for treatment of advanced multiple myeloma, prostate cancer and recurrent or refractory high-risk neuroblastoma.[109-110] |
| **LM22A-4**  | mBDNF Loop II mimic identified by anti-apoptotic BDNF/TrkB E16 hippocampal neurons cell-based assay | TrkB agonist:<br>Reduces motor impairment and neuropathology in mouse models of Huntington's disease.[111] Prevents neuronal degeneration.[112] Initiates periodontal regeneration in vivo[113] |

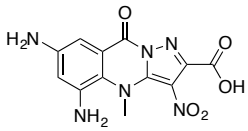
| Name and Structure | Identification Method | Target, Observed Phenotype/Usage |
|---|---|---|
| **MNAC13** (PDB 1SEQ)[114]  | Mice were immunised with cells expressing TrkA, hybridoma were formed from splenocytes, antibodies were screened by assessing $^{125}$I-NGF binding to TrkA-BA LB/C 3T3 cells | TrkA antagonist:<br>Anti-TrkA monoclonal mouse antibody, induces analgesia in mouse models of inflammatory and neuropathic pain. Synergistic with low-dose opioids.[115] Attempts to humanise the antibody failed. |
| **PQC083**  | Molecular modelling and *in silico* docking to βNGF and mBDNF | βNGF and mBDNF antagonist:<br>Second generation Y1036, showing markedly higher potency.[117] although neither PQC083 or Y1036 have undergone animal testing, they are included here as small-molecule neurotrophin binders: similar to the research undertaken in this project. |

Table 2 indicates that currently only three main methods have been used to identify agonists or antagonists of the βNGF/TrkA or mBDNF/TrkB interactions: predominantly commercial or internal library screening using whole-cell assays, antibody development by mouse immunisation of whole cells, and *in silico* docking of computer models.

Whole-cell assay screening of commercial libraries are notoriously low-throughput, due to the complexity of the processes involved. As they are complex systems, there may also be considerable noise produced as compounds interact with other cellular components; this may be advantageous however as it may interact obliquely with the intended target, identifying new targets in existing pathways. Compound library screening is also only as good as the structural diversity of the library: libraries limit potential inhibitors to the chemical space covered by the library. If the space is small (i.e. a lack of diversity), there's a decreased chance of identifying a hit, and the hits identified may be of dubious value if the library contains pan-assay interference compounds. As an example of the libraries used in previous research, both amitryptylene and deoxygedunin were identified from the same 2000 member library, the Spectrum Collection.[23, 104] 2000 members is a relatively small library screen.

Antibody development is promising as it allows for highly specific antibodies to be developed, however the process of humanising them (to reduce the immunogenic response when used in man) is not always successful, as shown in MNAC13. Antibody drugs also have a number of setbacks; sensitivity to mutation (typically not a concern here as both

βNGF and mBDNF are highly conserved, however cancers may rapidly mutate to adapt and overcome selection pressures), problematic scale-up and commercial considerations.

Finally, *in silico* screening offers a number of advantages in terms of accessible chemical space and structural diversity in that a compound may be rationally designed to bind to specific motifs on the target. The caveat however is that such structures may be difficult to synthesise, and solubility and selectivity of hits may be an issue. It is also strongly reliant on a representative structure of the target molecule and software that permits variability, such as an induced-fit model. Currently no structures of the mBDNF homodimer is publically available, nor are structures representing βNGF/TrkA or mBDNF/TrkB interactions; this considerably complicates using *in silico* screening to identify quality inhibitors or these interactions.

Table 2 also highlights that due to the varied roles of βNGF, mBDNF, TrkA, TrkB and $p75^{NTR}$ and the fact that different tissues express different concentrations of receptor and downstream cascades, inhibiting any of these proteins can lead to several different outcomes.[118-119] These include anxiolytic and antidepressant activity, a reduction of allodynia (i.e. pain suppression), and cancer growth suppression. Inspecting the effects of agonists suggests the possible side effects of inhibition, increased neuronal cell death, depression, decreased memory retention and learning difficulties.

## 1.4 Targeting Neurotrophin PPIs

When considering the inhibition of neurotrophin PPIs, several interactions may be targeted: their transcription, golgi-body packaging and folding, homodimerisation, the vesicle-packing process, their release into the synaptic cleft, their interaction with their respective receptors or the receptor activity. Two particularly attractive interactions are their homodimerisation and the recognition and activation of their receptors, primarily due to the target specificity and mimicry of CIPA. It is also advantageous to target an extracellular interaction as it removes the necessity of crossing the cell-membrane. As shown in Table 2, significant research has been conducted into inhibiting neurotrophin-receptor binding by binding inhibitors to the receptors, or the inhibition of tyrosine kinase activity. The inhibition of neurotrophin dimerization is relatively unknown. The initial purpose of this project was therefore to identify novel homodimerisation inhibitors, however this scope was later expanded to inhibitors which bound to neurotrophins to prevent them interacting with their receptors.

## 1.5 Project Aims

There is a definite need for new analgesics with improved efficacy and side effects. The aim of this project was therefore to identify novel inhibitors of neurotrophins. This was to be achieved by high-throughput screening of genetically encoded libraries. Hits were to be synthesised and inhibition verified by i*n vitro* assays. Analogues (including an alanine scan) were to be synthesised and assayed as a first-attempt at assessing structure-activity relationships. Finally, cell-based assays were to be used to assess activity.

## 1.6 Project Overview

This project concerns the identification of a number of agonists and antagonists of nerve growth factor and brain-derived neurotrophic factor—two promising targets to treat chronic pain with the added benefit that inhibitors may show anti-cancer properties.

Chapter 2 covers several attempts to use reverse two-hybrid methodology to create a library screening platform to identify mBDNF inhibitors. Challenges here were ascribed to the difficulties involved in expression of mBDNF in *E. coli*.

In Chapter 3, phage display was used against both βNGF and mBDNF to screen a large library of peptides for their ability to bind to these targets, identifying a number of hit peptides. Phage binding was then tested for target specificity to βNGF and mBDNF over background binding, which also permitted the ranking of hit phage for binding strength.

Chapter 4 concerned the development of a novel assay to assess the βNGF/TrkA and mBDNF/TrkB modulatory activity of the peptides identified by phage display. This required the optimisation of the expression and purification of a number of fusion proteins, and successfully identified a number of agonist and antagonist lead peptides.

In Chapter 5, microscale thermophoresis was attempted, to characterise the binding and inhibitory properties of the lead peptides using direct- and competitive binding assays. Mammalian cell-based western blot and morphology assays were then used to verify lead peptide biological activity.

# Chapter 2: Exploring mBDNF Inhibition Through RTHS

## 2.1 Discussion of Techniques

Using genetically-encoded libraries severely limits the number of molecular skeletons available compared to small-molecule libraries, but genetic libraries can contain far more structures than commercially available screening libraries. This is primarily due to the use of randomisation processes during creation: selective genes encoding the library are randomised, which when expressed generate a peptide library. Using the canonical amino acid library, seven randomised positions equals 20 x20 x20 x20 x20 x20 x20 possible structures: 1,280,000,000 library members.

Library members can be further expanded by extending the canonical library to include unnatural amino acids using techniques such as Flexizyme. This can also be used to expand library skeleton diversity. This technique requires considerable genetic forethought however: it relies on the reprogramming of a STOP codon, and as such any instance in the bacterial chromosome needs to be replaced.

Genetic libraries may be rapidly screened using high-throughput techniques; these include intracellular translation techniques such as reverse two-hybrid systems, phage display, and RNA display; and extracellular translation techniques using *in vitro* transcription and translation; usually chip-based fluorescence resonance energy transfer assays or fluorescence polarisation assays. Isothermal titration calorimetry (ITC), surface plasmon resonance (SPR) may also be used, but again require considerable mechanisation for sizeable library screening.

One key advantage of the first two techniques is that significant library sizes can be screened without mechanisation; a key advantage with the equipment available. The other techniques permit larger library screening and the use of more varied libraries, as well as the use of proteins and genes which may be toxic to the cells used for translation.

## 2.2 Introduction to Reverse Two-Hybrid Systems

A reverse two-hybrid system (RTHS) links the disruption of a specific PPI with an externally observable phenotype, e.g. cell death. Should an inhibitor of that PPI be introduced, the phenotype is no longer observed: the cell lives. When combined with a library of molecules, RTHSs can be used for selecting library members which disrupt that

PPI.[120] This chapter involves attempting to create an RTHS where mBDNF dimerisation leads to cell death.

An overview of how RTHSs function is shown in Figure 11:

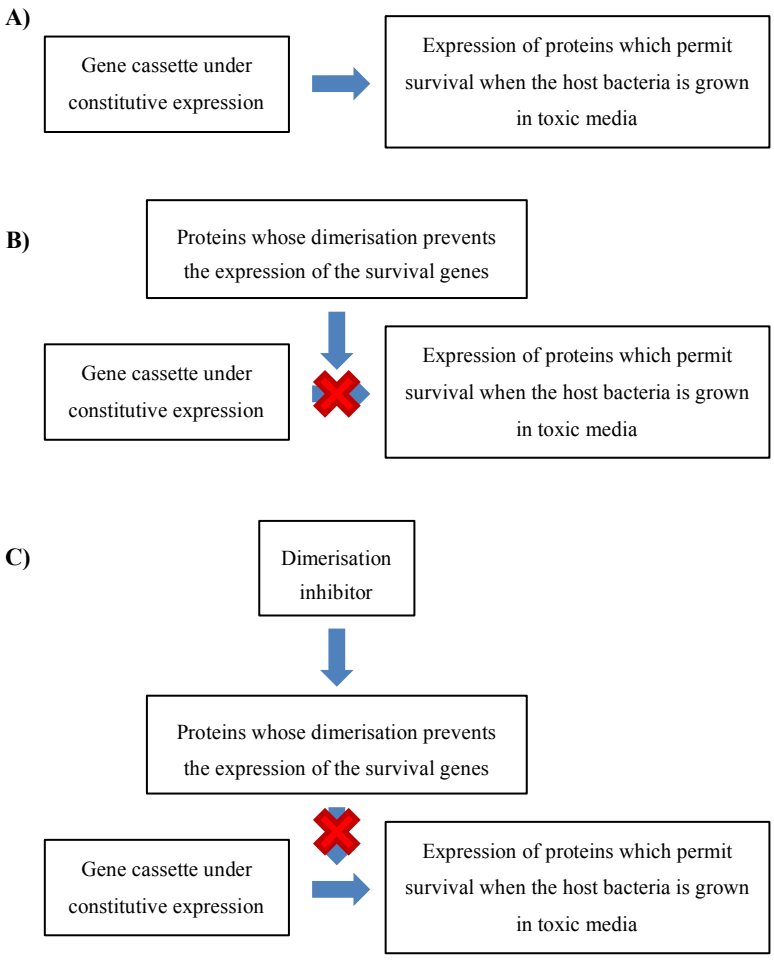



***Figure 11: Flowchart of RTHS activity.*** *A: an RTHS host when the fusion proteins are not expressed or where they fail to dimerise. B: when the fusion proteins are express and dimerise, the cell dies as it cannot express the survival genes. C: the identification of a hit inhibitor: the fusion protein dimerization is inhibited, so survival gene expression isn't inhibited: the cell lives, so it can be isolated and the hit elucidated.*

How this can be implemented as a strategy to identify PPI inhibitors (and thus, the aim of this project) is shown in **Figure 12**:

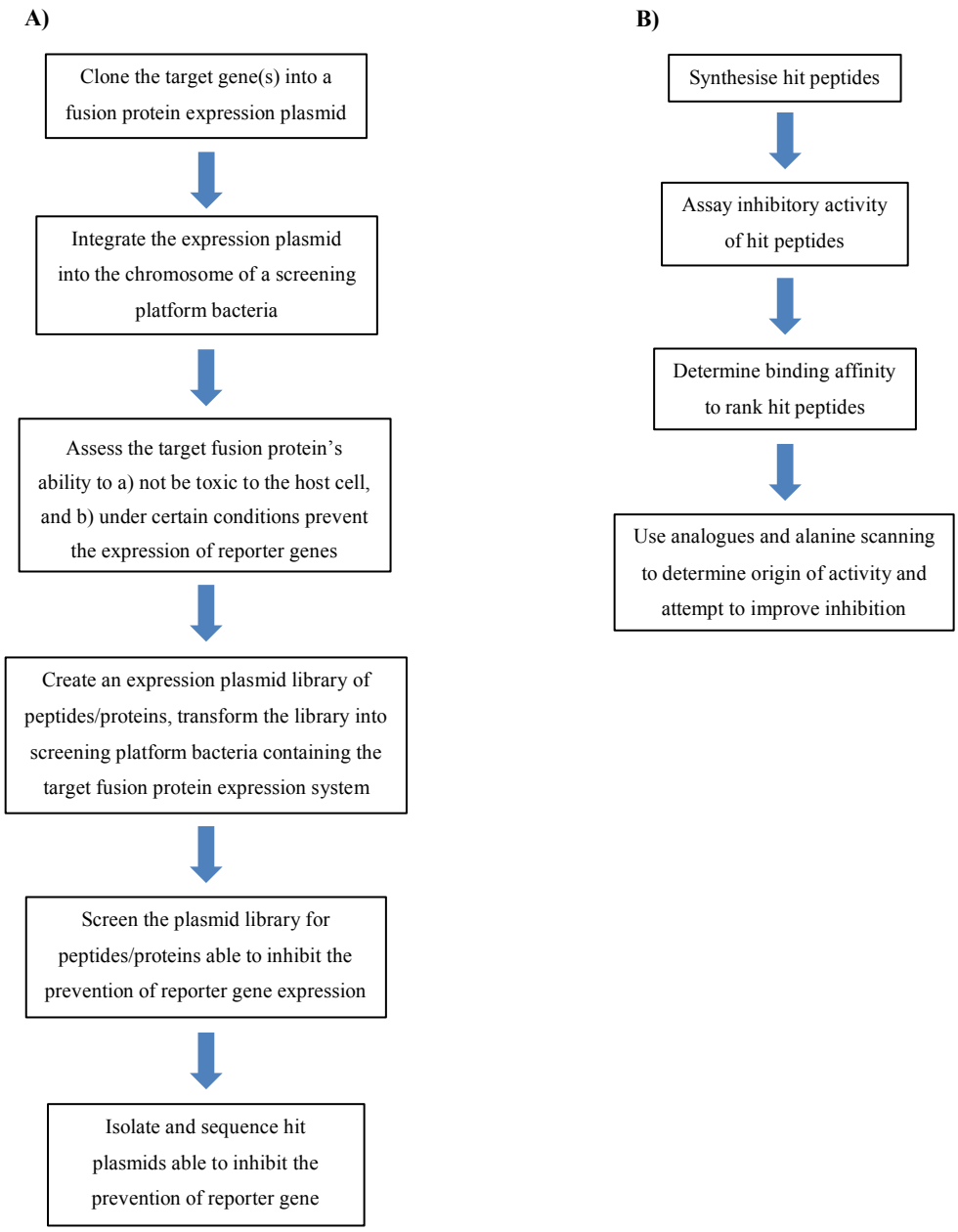



***Figure 12: Overview of the strategy used to identify PPI inhibitors using RTHSs.*** *A) Section using bacteria to express peptides and proteins. B) Section using synthesised peptides.*

RTHS have a number of distinct advantages over the above assays: the ability to screen libraries with high throughput quickly and cheaply; screening libraries—particularly genetically encoded libraries—can be significantly larger than libraries tested by most high throughput screens (the functional upper limit with RTHSs are ~1x10$^8$ members), the libraries may be tuned to mimic specific "hot loops"[121] (short, conformationally restrained loops which make key intermolecular interactions at PPI interfaces), and finally the screening of proteins intracellularly providing a closer mimic to *in vitro* environments.

This last point is important: the aim of this project was to identify neurotrophin inhibitors such that the inhibitors could be used as a basis for novel drug development. As such, it is important that such inhibition functions in a physiological environment: it is of no use if inhibition requires a pH, temperature or other factor which is not present *in vitro*. Screening for inhibition in these conditions therefore assures that this is not the case.

Using an RTHS as a screening platform has a number of caveats however: the proteins under investigation must readily express in the host cell, and in their native conformation for the hits to have any fidelity; the number of available library scaffolds for screening is limited, and the hits are identified purely by inhibition, not specifically or by monomer-monomer inhibition.

RTHSs are an inventive step along from two-hybrid systems (THS), a method first used in yeast to investigate PPIs: linking the interaction of two proteins to the transcription of reporter genes (in this case, LacZ).[122] Yeast two-hybrid systems were successfully used to identify and characterise Bcl2 homodimerisation using truncated variants, and Bcl2 heterodimerisation with Bcl-X-L, Mcl-1, Bax and Bcl-X-S.[123] Yeast however is ill-suited to high throughput screening: growth is significantly slower than bacteria, and transformation efficiency dramatically lower. THS were therefore developed for bacteria; investigating the role of amino acid side chains in the dimerisation of lysine zippers. In this study, homodimerisation allowed the enclosing cell to survive in selective media.[124]

In RTHSs a PPI is integral to the repression of the expression of downstream reporter genes vital to the survival of the host bacteria when grown on selective media. The repressor function is created by fusing the proteins of interest from the PPI to DNA binding domains such that the DNA binding domains cannot form a functional repressor without the PPI of interest. In the RTHSs described herein, the DNA binding domains used are based on the N-terminal domains of the cI or 434 protein. 434 consists of two domains, and is part of a bacteriophage regulatory protein used by λ-phage to switch from the lysogenic stage to the lytic stage of their lifecycle.[125] the N-terminal domain of 434 binds to the $O_R3$ operator, formed of a specific palindromic DNA motif as shown in Figure 13. The C-terminal domain permits homodimerisation and is integral to repressor function. Bacterial RTHS using N-terminal 434 replace the C-terminal domain with the relevant protein of interest, thereby the PPI in question becomes vital to repressor function.

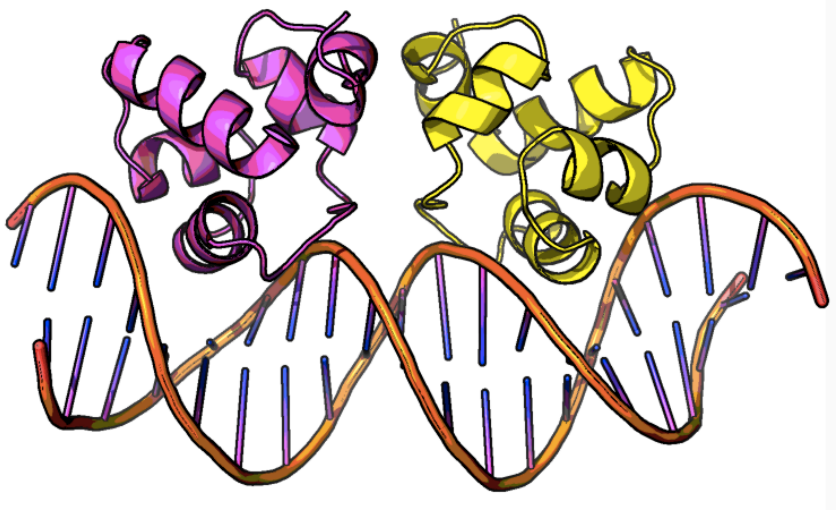


***Figure 13: Homodimeric 434 (residues 2-63) binding $O_R3^{126}$ (PDB 1PER).***

The above technology was used to develop an *E. coli*-based high-throughput screening platform whereby a t7 promoter (allowing constitutive expression), two $O_R3$ operators and a gene cassette of survival reporter genes was cloned into the chromosome of a BW27786 *E, coli* to form *SNS118*. When the host cells are grown on selective media repression of the operators causes cell death (Figure 14.2). If a library of inhibitors is distributed amongst a culture of bacteria (usually through transforming an encoding plasmid with approximately one library member per cell), inhibitors of the repressor permit the cell to express the reporter gene cassette and survive (Figure 14.4). This makes for easy sampling and hit elucidation by sequencing the encoding plasmid. This system has been successfully used to identify a number of inhibitors to a wide range of PPIs.[120, 127-128]

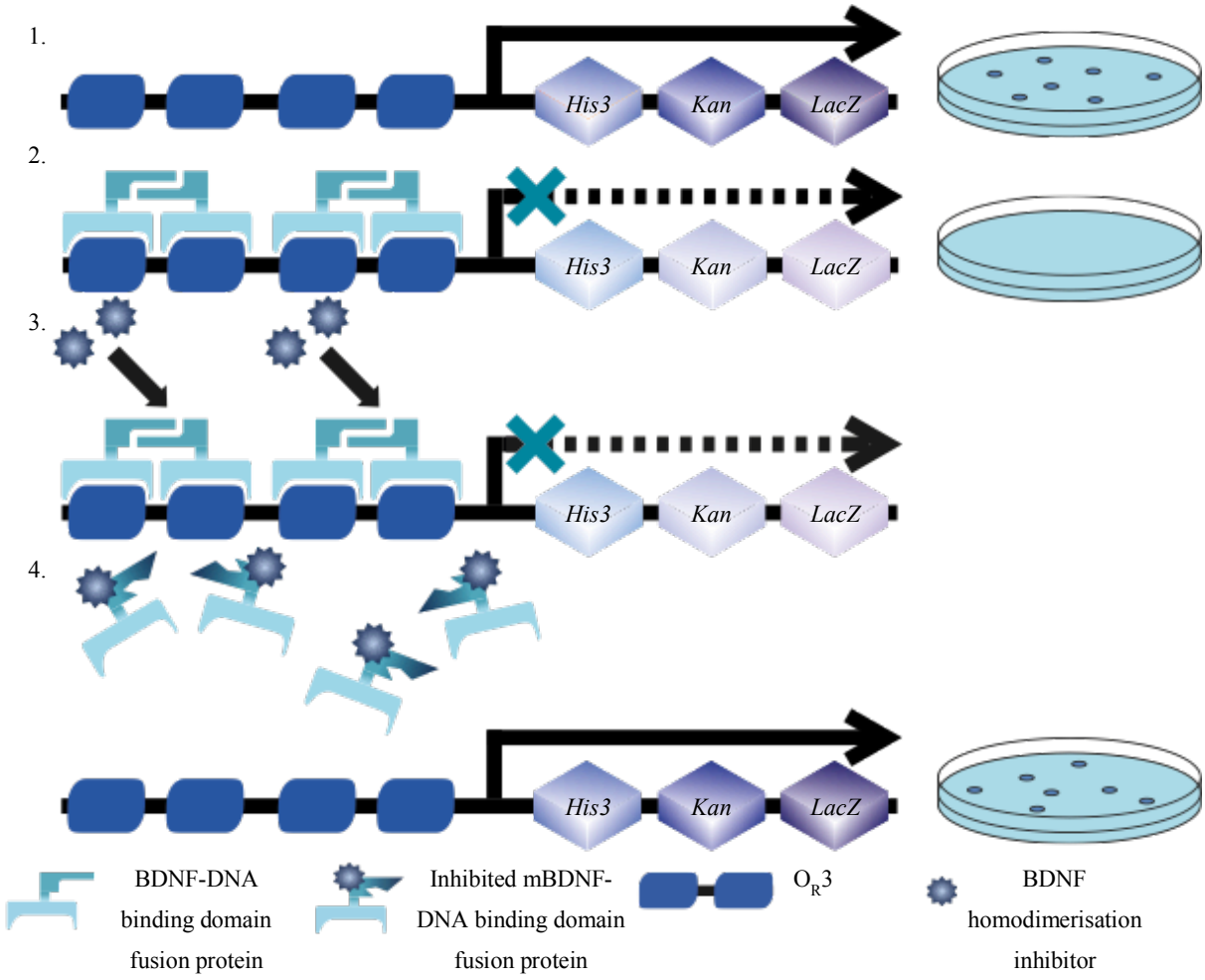



***Figure 14: Demonstration of how RTHS link a PPI with an externally visible phenotype in SNS118.***[120]

*Figure 14.1: fusion protein not expressed or non-functional (e.g. no IPTG in growth media, no dimerisation) permits effective reporter gene expression, allowing growth on selective media (including Kan or histidine). Assuming successful repressor function, Figure 14.2: induction of fusion protein expression (by addition of IPTG to growth media) causes effective repression of reporter genes, therefore cells do not grow. Figure 14.3: addition of an inhibitor to fusion protein homodimerisation causes Figure 14.4: fusion protein expression is induced but incapable of repressing reporter gene expression. Cells therefore continue to grow and can be isolated to allow identification of the inhibitor.*

This chapter therefore covers various attempts to create mBDNF-based RTHS, fusing mBDNF with the 434 N-terminal domain (hereafter "434"). The intention was that expression of these fusion proteins in SNS118 should cause dimerisation along the mBDNF homodimer interface, the 434 domains bind $O_R3$ and therefore suppress the

expression of downstream reporter genes *His3*, *Kan* and *LacZ*. The activity of these genes is as follows:

*His3*: imidazole glycerol phosphate dehydratase, enabling the biosynthesis of histidine.[129] Residues 165-355 of *SNS118*'s HisB gene (which has the same function as His3) have been deleted,[120] making *SNS118* reliant on either external histidine or an expressed *His3* gene to survive.

*Kan*: aminoglycoside-3'-phosphotransferase, which enables resistance to the antibiotic kanamycin (Kan).[130] Growth on media containing Kan when this gene isn't expressed causes cell death.

*LacZ*: β-galactosidase,[131] allowing quantification of reporter gene expression by 2-nitrophenyl β-*D*-galactopyranoside assay.[132]

The purpose of having two genes which affect bacterial survival is twofold: it decreases the efficacy of false positives, say where an "inhibitor" affects the activity of aminoglycoside-3'-phosphotransferase instead of inhibiting the RTHS, and it allows the tuning of the selectivity media during screening.

This last point is because different PPIs will have different strengths of interaction: a strong PPI will form a better repressor than a weak PPI as the two proteins will spend more time associated with each other. As such, the host cell death/survival activity can be tuned by varying the amount of IPTG in the selectivity media, e.g. an increased concentration for a weak PPIs, however high concentrations of IPTG inhibit bacterial growth. An alternative with weak PPIs is to decrease the concentration of kanamycin or 3-amino triazole (3-AT) in the growth media (and vice versa), which would have the same effect. 3-AT is a histidine biosynthesis inhibitor, increasing bacterial sensitivity to His3 expression. By varying the selectivity conditions (the concentration of IPTG, kanamycin and/or 3-AT), a RTHS assay can be tuned to best suit the PPI of interest.

Survival of *SNS118* cells expressing fusion proteins which repress of reporter gene expression is therefore impaired by incubating in media containing Kan and lacking histidine. What follows is a number of attempts to develop mBDNF-based fusion proteins, highlighting the shortfalls this technique has in certain circumstances.

## 2.3 Results and Discussion

To identify compounds capable of inhibiting mBDNF dimerisation, various mBDNF based DNA-binding domain fusion proteins were developed and tested for their ability to form a functional repressor of reporter gene expression. If successful they could be used as a high throughput screening platform for a library of potential inhibitors. An overview of the fusion proteins developed during this chapter is given in Figure 15:

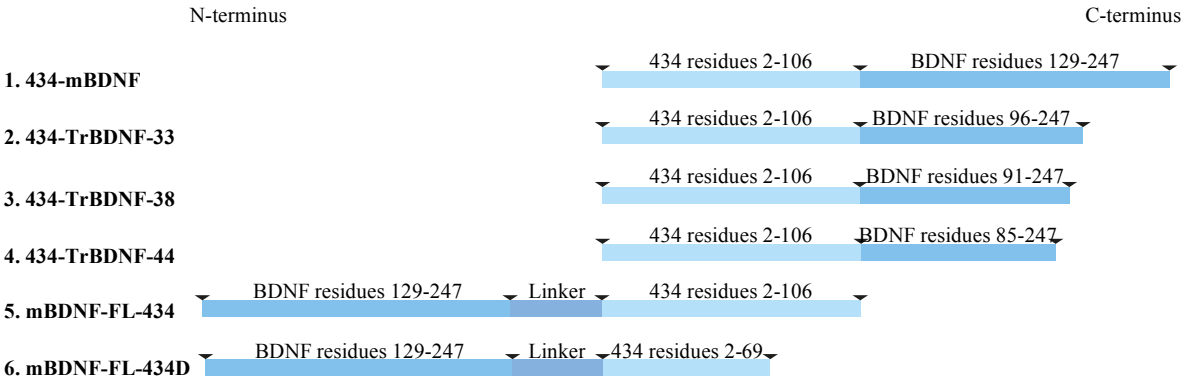



***Figure 15: Graphical representation of the six fusion proteins developed in this chapter.***

### 2.3.1 RTHS 1: 434-mBDNF

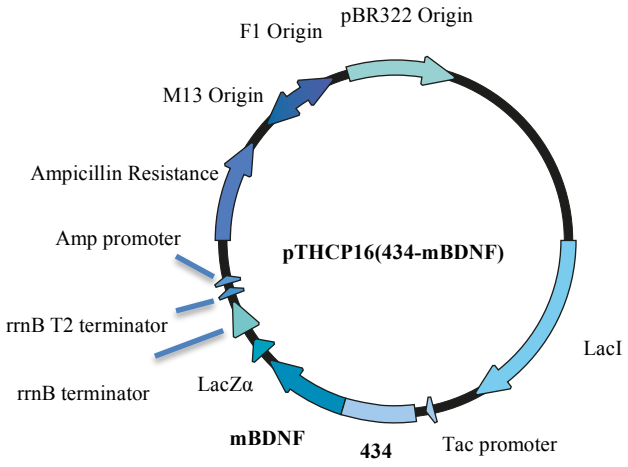



***Figure 16: Plasmid map of pTHCP16(434-mBDNF).***

The codons for mBDNF (residues 129-247)[54] were optimised for expression in K12 *E. coli* strains[133] and purchased as a delivery plasmid pEX-A2(mBDNF). This was transformed into *DH5α* (a commonly used cloning strain of K12-based *E. coli*) and cultured. Plasmids were harvested and the mBDNF gene isolated and cloned into plasmid pTHCP16[120] (a

plasmid containing the codons for 434 residues 2-106) using the *Bam*HI and *Sac*I restriction sites. This encoded mBDNF to be translated as chimeric with the C terminus of 434 and the construct downstream of the IPTG-inducible tac promoter.[134] 434-mBDNF was then sequence verified using the M13-49 primer (for all primer sequences, see Chapter 8: Appendices). Unless otherwise stated, sequences herein were verified using Eurofins MWG Operon Mix2Seq Kits, using a sample of purified plasmid.

To avoid plasmid artefacts (*e.g.* variable copy number/expression rates, reduced second plasmid transformation efficiency, recombinant plasmid instability), it is beneficial for the plasmid encoding the fusion protein to be irreversibly singly integrated into the chromosome of *SNS118*.[135]

To achieve this, a conditional-replication, integration, and modular (CRIM) plasmid-host system was used. This system uses phage integrase proteins (Int) to cause site-specific integration of plasmids containing phage attachment sites (attP) and chromosomes containing bacterial attachment sites (attB).[135] The CRIM plasmid used in this research was pAH68: it contains an attP site, and the chromosome of SNS118 contains a corresponding attB. When an SNS118 bacteria contains pAH68 and the correct Int protein ($Int_{HK022}$) is expressed, the plasmid is integrated into the bacterial chromosome. As this process is enzymatic, the reaction is reversible: it is therefore necessary to ensure that $Int_{HK022}$ is only present in SNS118 temporarily.

To achieve this, neither SNS118 nor pAH68 encodes $Int_{HK022}$; it is encoded on the helper plasmid pAH69. The necessary short expression of $Int_{HK022}$ and subsequent removal of pAH69 (to make the process irreversible) is controlled thermally: pAH68 is transformed into SNS118 containing pAH69, and the bacterial cultures are immediately cultured at 42 ˚C. This causes both a short expression of $Int_{HK022}$ and the removal of pAH69: expression of $Int_{HK022}$ on pAH69 is temperature dependant due to an upstream cI857 operator, which is suppressed by temperature-sensitive cI857 repressor (also encoded on pAH69). Culturing at 42 ˚C therefore prevents the cI857 repressor from binding to the cI857 operator, permitting the expression of $Int_{HK022}$. Replication of pAH69 is inhibited at this temperature as the plasmid origin of replication (OriR101) requires a thermally unstable protein (repA) for activity.[136] As such, when a cell undergoes mitosis, only one daughter cell receives the copy of pAH69. A second division results in only one in four cells, etc.

As a result, culturing SNS118 cells which contain pAH68, pAH69 at 42 ˚C results in SNS118 integrated with pAH68. Non-integrated pAH68 cannot replicate in SNS118 due to a γ origin of replication, which requires the expression of Π protein (not present in *SNS118*, pAH68 or pAH69). As such, it "matures" out of the culture by the same process as pAH69.

Finally, to isolate SNS118 cells containing integrated pAH68 over SNS118 cells with no pAH68, following an initial culture in LB media, cells were cultured on media containing the antibiotic Carbenicillin: the resistance for which is encoded on pAH68.

While the intention is for single integration, multiple integration is also possible, as shown in Figure 17. No integration, single or multiple integration of pAH68 into SNS118 can be qualitatively assessed by mixed primer PCR using primers P1, P2, P3 and P4, producing distinctive nucleotides of the length shown in Figure 17.

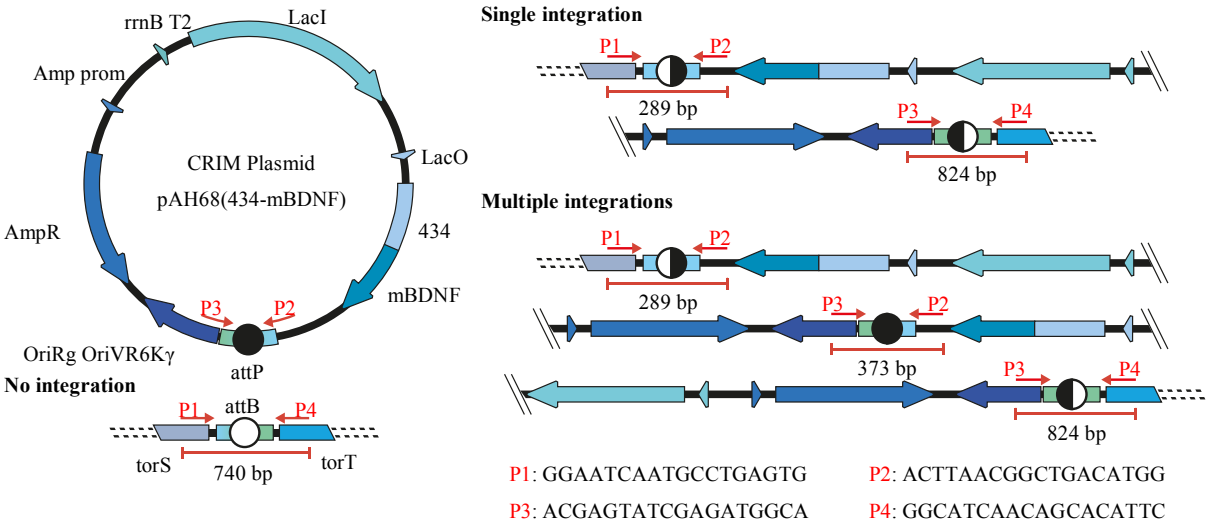



***Figure 17: CRIM plasmid integration of pAH68(434-mBDNF) at $Att_{HK022}$ into the chromosome of SNS118.***[135] *$Int_{HK022}$ joins the right half of attP (blue) with the left half of attB (blue) and vice versa (green with green).*

434-mBDNF was amplified out of pTHCP16(434-mBDNF) by polymerase chain reaction (PCR) and cloned into the CRIM plasmid pAH68[135] using the *Nde*I and *Sac*I restriction sites and sequence verified. For growth and amplification of pAH68, cloning was conducted in *DH5α-pir+* cells, which constitutively express Π protein necessary for pAH68 replication. To be singly integrated into the bacterial chromosome, pAH68(434-mBDNF) was transformed into *SNS118* cells containing helper plasmid

pAH69, expressing $Int_{HK022}$. $Int_{HK022}$ catalyses the integration of pAH68 at its $attP_{HK022}$ site, into the $attB_{HK022}$ site in the chromosome of *SNS118*.

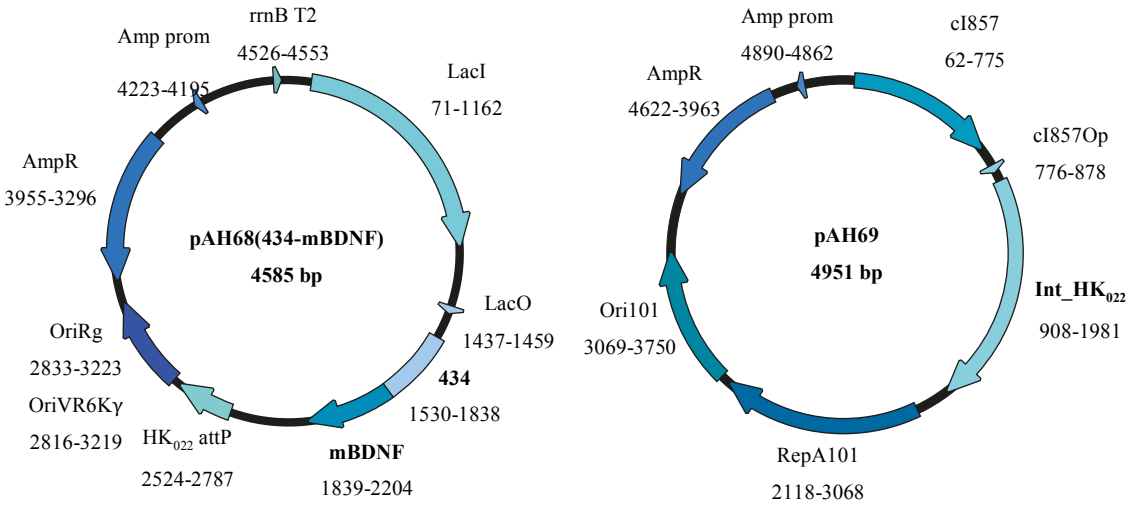



***Figure 18: Plasmid map of CRIM plasmids pAH68(434-mBDNF) and helper plasmid pAH69.***

Mixed primer PCR and split primer PCR were used to confirm integration of pAH68 into attB of SNS118. These use PCR to amplify sections of DNA at the integration sites. As shown in Figure 16 the presence and length of the amplified section implies its identity. This allow the identification of colonies where pAH68 has been integrated into the chromosome. Mixed primer PCR uses an equal mix of primers P1, P2, P3, and P4, split primer PCR uses primer pairs P1/P4, P1/P2, P3/P4 and P3/P2. Colonies with no integration of pAH68 produce one band at 740 bp (P1/P4), single integration produces two bands, 289 bp (P1/P2) and 824 bp (P3/P4); multiple integration produces three bands, 289 bp (P1/P2), 373 bp (P3/P2) and 824 bp (P3/P4).[135]

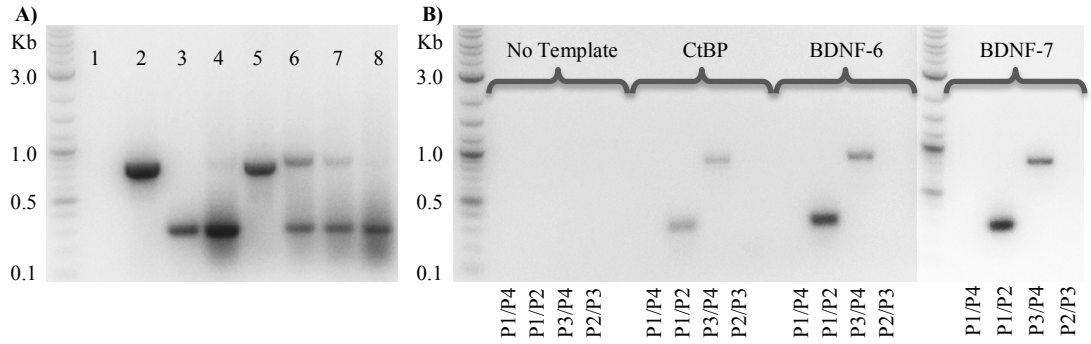



***Figure 19: Assessing pAH68(434-mBDNF) CRIM plasmid integration into SNS118.*** *A) mixed primer PCR of potential SNS118 pAH68 434-mBDNF colonies, B) split-primer PCR of Figure 19A lanes 6-7.*

*Figure 19A1: no template negative control, A2: SNS118 negative control, A3, SNS118 integrated with pAH68(CtBP) positive control,[138] A4-8: possible SNS118 integrated with pAH68(mBDNF).*

Figure 19A 6 and 7 both show single integration, and were used in split-primer PCR. Figure 19B shows that both mBDNF-6 and mBDNF-7 are singly integrated as they match the positive control of CtBP.

Following integration of pAH68 434-mBDNF into the chromosome of *SNS118*, the toxicity and repressor efficacy of 434-mBDNF must be assessed: 434-mBDNF must not be toxic to *E. coli*, but must cause shutdown (reduction in growth) due to Kan and His sensitivity. To assess toxicity, six ten-fold dilutions of *SNS118*_int.pAH68(434-mBDNF)-6 and -7 culture were dropped onto Lysogeny Broth (LB) agar containing increasing concentrations of IPTG (0-150 μM) (Figure 21A). This causes an IPTG dose-dependant expression of 434-mBDNF in the absence of Kan or His selection pressure: if increasing IPTG concentrations cause cell death then the fusion protein under investigation is toxic to *E. coli* and therefore cannot be used as a RTHS to screen libraries.

An explanation of how to interpret drop spotting images is shown in Figure 20:

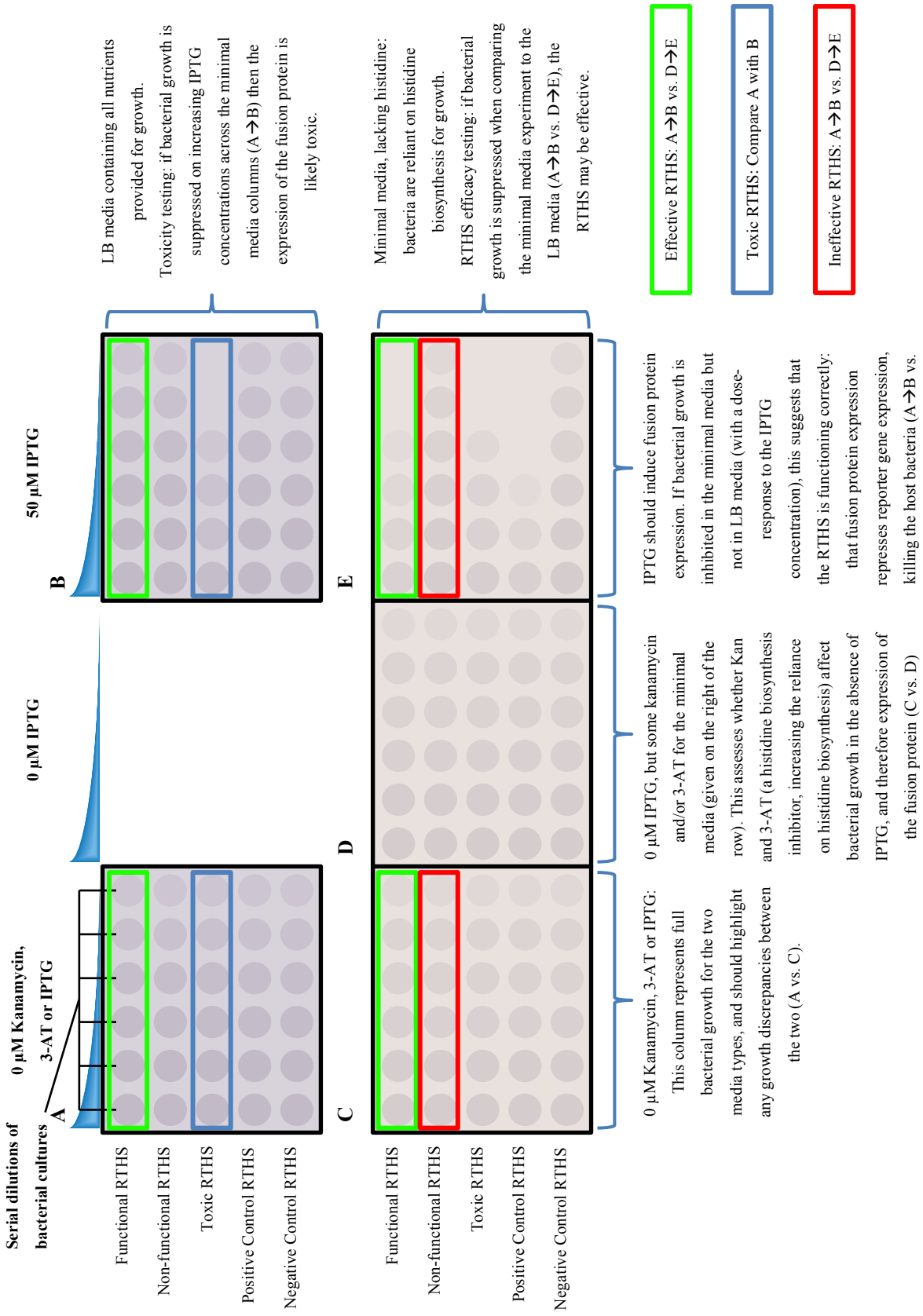



***Figure 20: Explanation of the drop spotting assay readout.***

To assess repressor formation, six ten-fold dilutions were also dropped onto minimal media containing two concentration of Kan (2.5/5 μg/mL) and 3-AT (2.5/5 mM); and increasing concentrations of IPTG (0-150 μM) (Figure 21B and C). An effective repressor would cause shutdown, markedly more than to a *SNS118* negative control which, lacking the pAH68 and therefore any repressor, should not shutdown at all.

Figure 21A indicates that 434-mBDNF is not toxic, however Figure 21B and C show no shutdown vs. *SNS118* (negative control). This indicates that 434-mBDNF is incapable of forming a functional repressor and creating Kan and His sensitivity. Figure 21B and Figure 21C were repeated (Figure 21D and Figure 21E) with additional negative controls (different lineage of *SNS118* and SNS126), however lack of repression was similarly observed. Some growth repression in all cell lines (including the *SNS118* negative control) is in evidence at high IPTG concentrations, probably due to IPTG delaying log-stage growth.[139] Figure 21 therefore indicates that 434-mBDNF cannot be used as a RTHS to screen libraries, as it does not repress expression of *Kan* and *His3* genes.

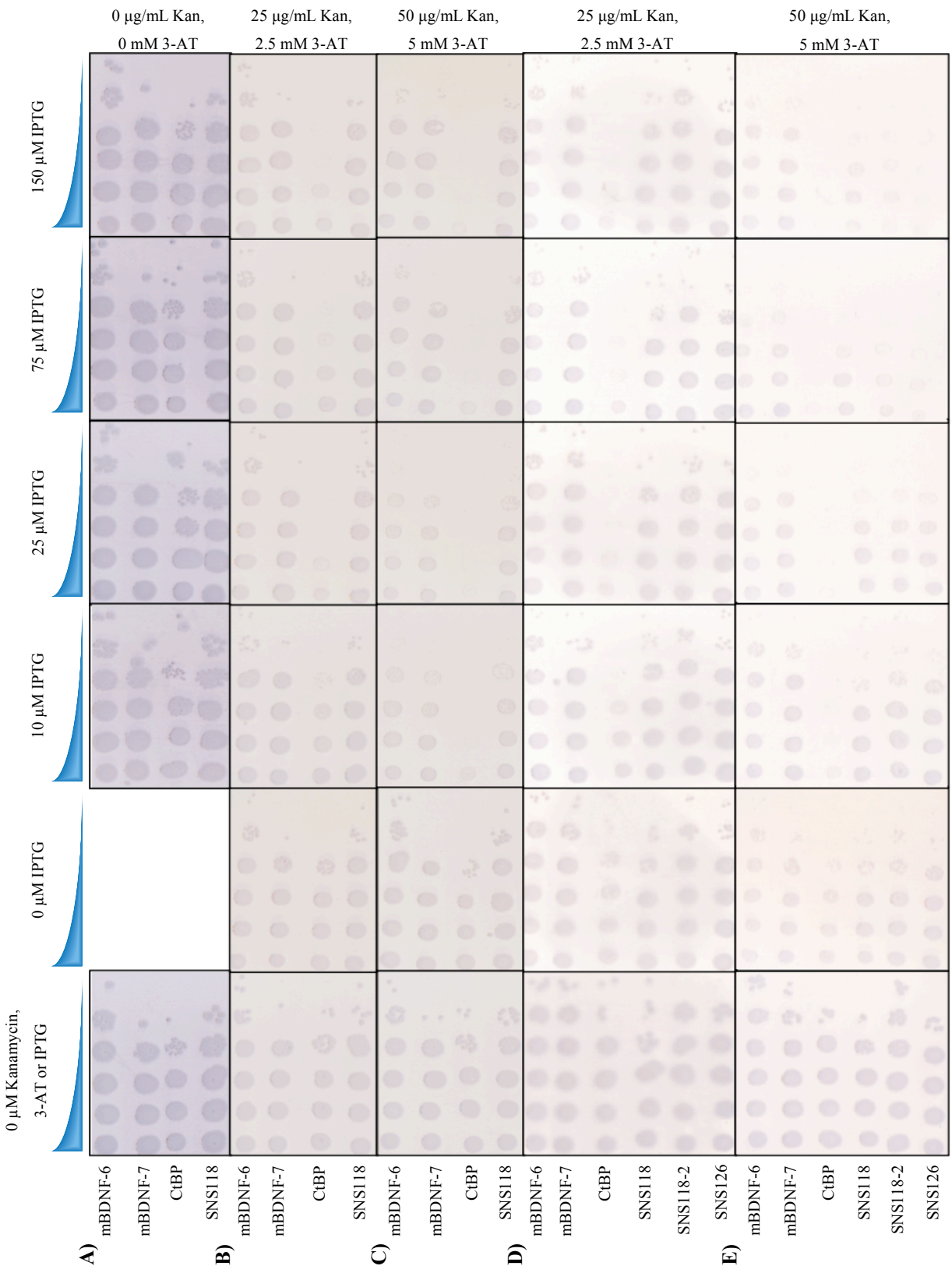



***Figure 21: Assessing 434-mBDNF RTHS toxicity (A) and repressor activity (B) by drop spotting.*** *Blue curve shows the direction of bacterial culture dilution. Positive control: SNS118_int.pAH68(434-CtBP), negative control: SNS118.*

### 2.3.2 RTHS 2-4: 434-Truncated mBDNF

Forming a functional repressor requires the mBDNF and 434 domains of 434-mBDNF to be expressing and folding correctly inside the host bacterium to achieve the correct proximity and orientation for dimerisation. The arrows of Figure 22 indicate where mBDNF is attached to 434. As the 434 domains have to be in close proximity to bind to DNA, this fusion protein may not be able to form a successful repressor: the N-termini of the mBDNF homodimer are on opposite faces of the protein. Versions of mBDNF were therefore created with removed sections, in an effort to change the orientation of the 434 on the resulting fusion protein. These were designated truncated mBDNF (TrmBDNF) , starting at amino acid positions 30, 38 and 44 of mBDNF (lines, Figure 22A).

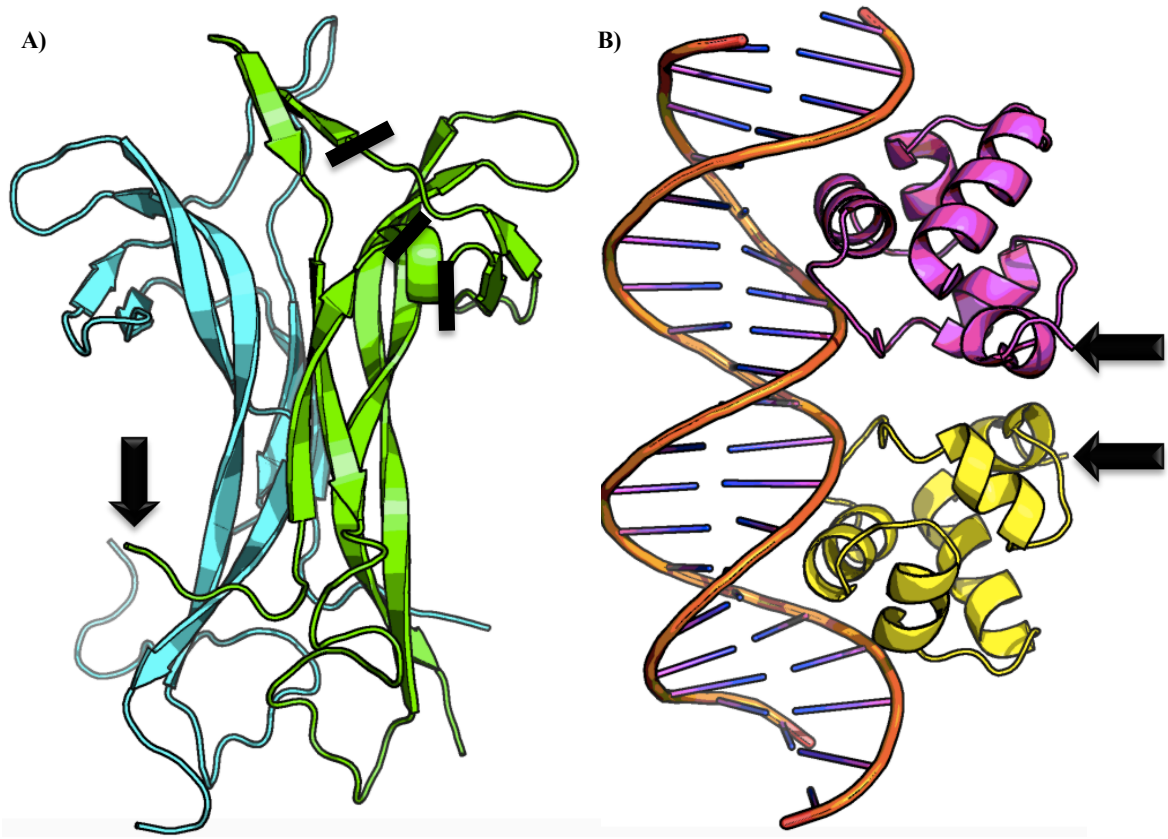



***Figure 22: Crystal structures of the two components in 434-TrmBDNF chimeric proteins.*** *A) mBDNF (green) NT4/5 (blue) heterodimer (PDB 1B8M).*[51] *Arrow shows the N-termini. Lines show positions of truncation. B) Dimeric 434 (residues 2-63) binding OR3*[126] *(PDB 1PER), arrows indicate the C-termini, however the 434 used in this project uses residues 2-106).*

TrmBDNF-30, -38 and -44 were amplified by PCR from pTHCP16(434-mBDNF) with selective primers with digestion sites and overhangs. These were then cloned back into

pTHCP16 using the *Bam*HI and *Sac*I restriction sites and sequence verified. pTHCP16(434-TrmBDNF-30) and pTHCP16(434-TrmBDNF-44) were transformed into *SNS118* and assessed for toxicity and repressor activity. Figure 23A indicates that 434-TrmBDNF-30 and -44 are nontoxic, Figure 23B suggests both form effective repressors, especially pTHCP16(434-TrmBDNF-30. This is the ideal pattern for a successful mBDNF RTHS, however the truncated mBDNF variants must be integrated into the bacterial chromosome for the reasons outlined above.

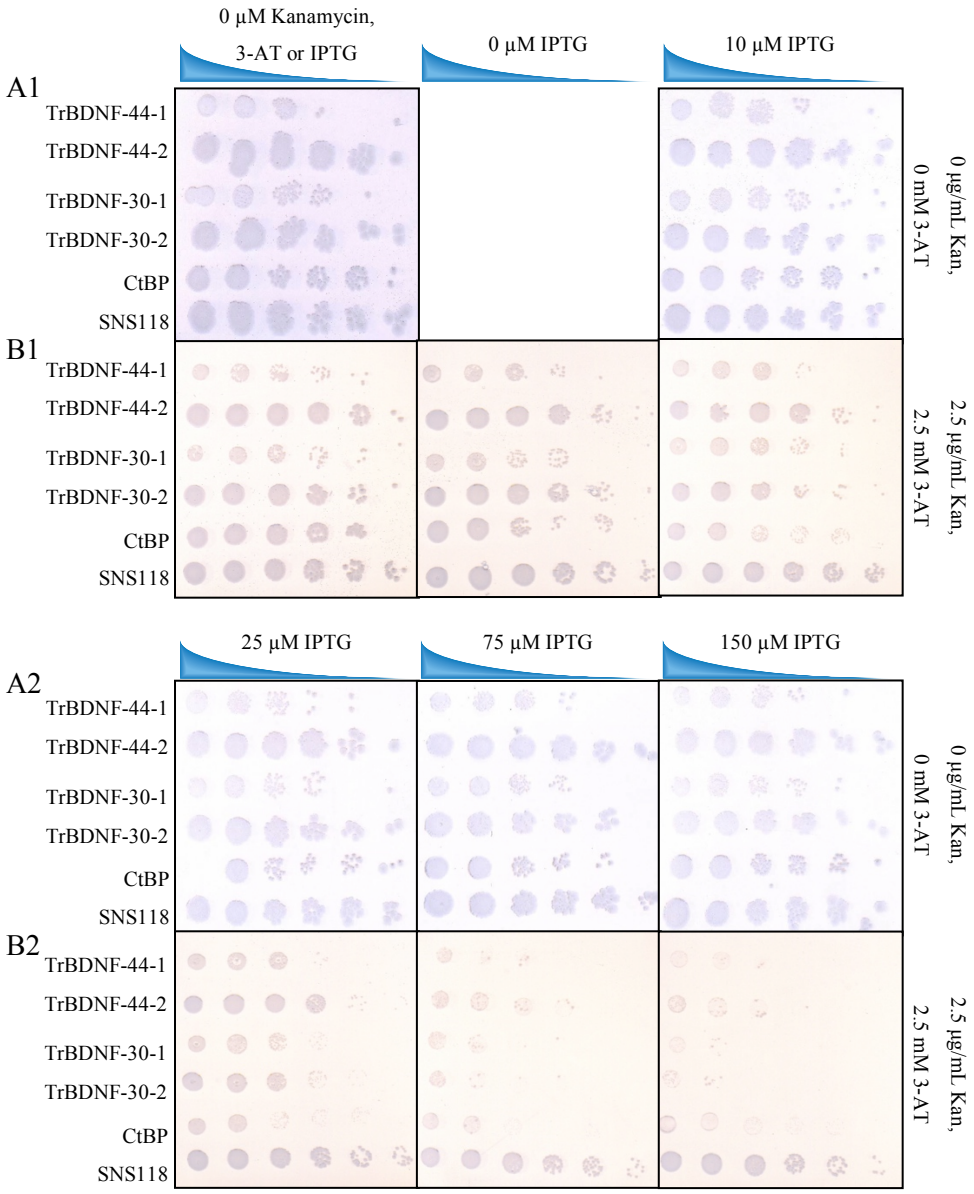



***Figure 23: Assessing non-integrated 434-TrmBDNF RTHS toxicity (A) and repressor activity (B) in SNS118 by drop spotting.*** *Blue curve shows the direction of bacterial culture dilution. Positive control: SNS118_int.pAH68(434-CtBP), negative control: SNS118.*

434-TrmBDNF-30, 434-TrmBDNF-38 and 434-TrmBDNF-44 were amplified out of the relevant pTHCP16 plasmid by PCR, cloned into pAH68 using the *Nde*I and *Sac*I restriction sites; and sequence verified. CRIM plasmids pAH68(434-TrmBDNF-30), pAH68(434-TrmBDNF-38) and pAH68(434-TrmBDNF-44) were then integrated into the $HK_{022}$ attB in *SNS118*, confirmed by mixed and split primer PCR (Figure 24).

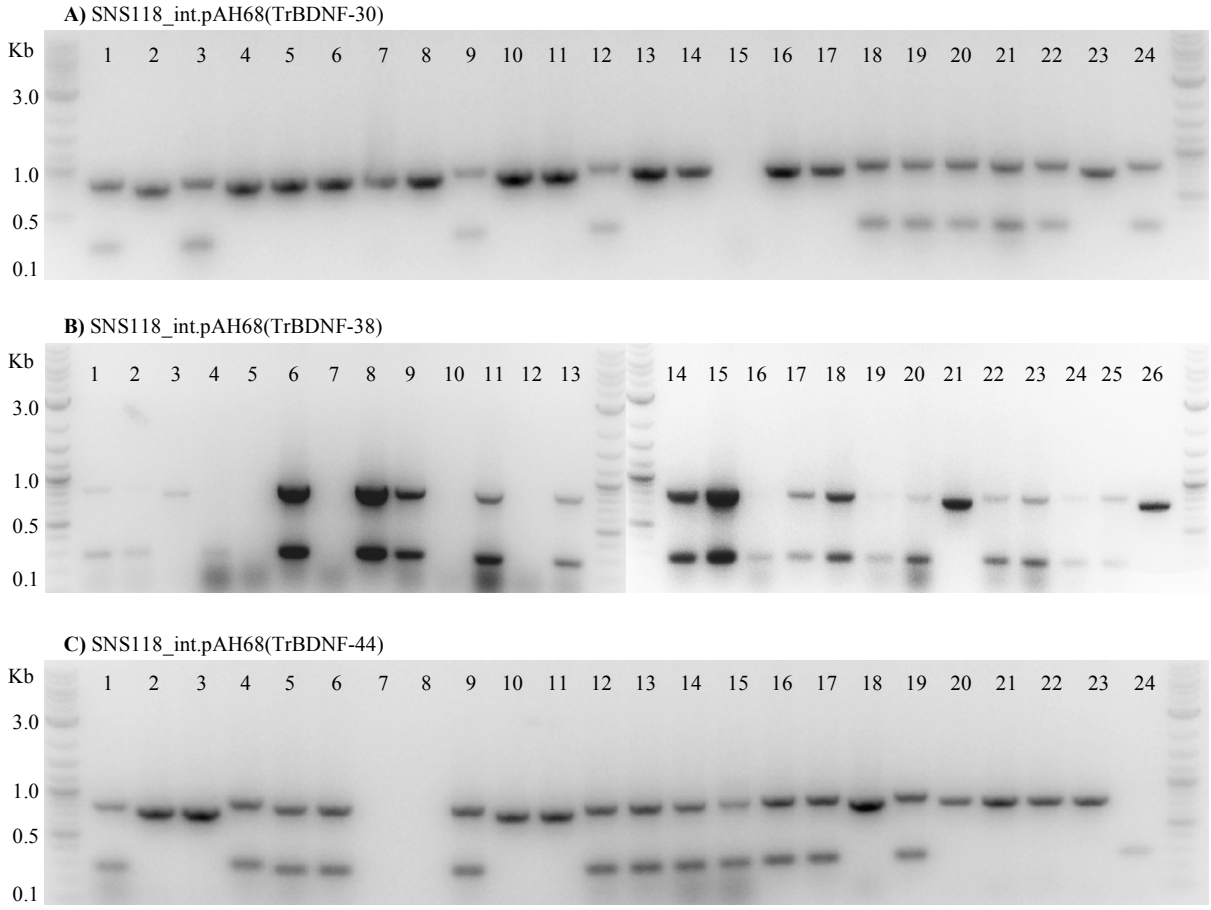



***Figure 24: Assessing 434-TrmBDNF CRIM plasmid integration by mixed primer PCR.*** *824 and 289 bp: Single integration, 740 bp: No integration, 373 bp: Multiple integration.*

*Figure 24A) 1-22: SNS118_int.pAH68(434-TrmBDNF-30) 23: SNS118 24: SNS118_int.pAH68(434-CtBP). lanes 1, 3, 9, 12 and 18-22 represent successful single integrations.*

*Figure 24B) 1-24: SNS118_int.pAH68(434-TrmBDNF-38) 25: SNS118 26: SNS118_int.pAH68(434-CtBP). Lanes 1, 6, 8, 9, 11, 13, 14, 15, 17-20, 22, 23, and 24 represent successful integrations.*

*Figure 24C) 1-22: SNS118_int.pAH68(434-TrmBDNF-44) 23: SNS118 24: SNS118_int.pAH68(434-CtBP). Lanes 1, 4, 5, 6, 9, 12-17 and 19 suggest successful integration, however the positive control (lane 24) only shows one faint band. This may be due to very small sampling versus other lanes (the camera brightness is set to the darkest band, therefore fainter bands are lost).*

Colonies for *Figure 24A* lanes 1, 3, 9, 20, 21 and 22 were cultured and stored as *SNS118*_int.pAH68(434-TrmBDNF-30) variants. Colonies for *Figure 24B* lanes 13, 14, 17, 18, 23 and 24 were cultured and stored as *SNS118*_int.pAH68(434-TrmBDNF-38) variants. Colonies for *Figure 24C* lanes 4, 5, 9, 16, 17 and 19 were cultured and stored as *SNS118*_int.pAH68(434-TrmBDNF-44) variants. All 18 of these stocks were tested with split-primer PCR (Figure 25 and Figure 26).

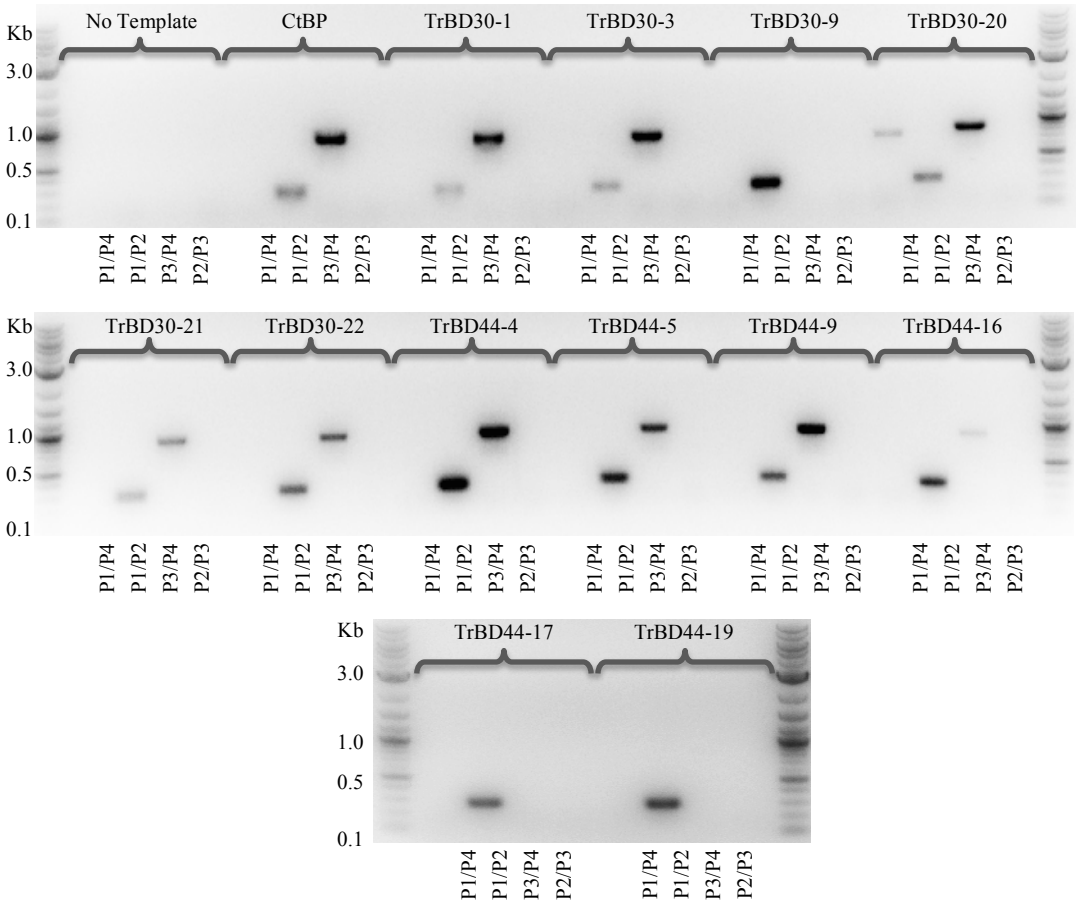



***Figure 25: Assessing 434-TrmBDNF-30 and 434-TrmBDNF-44 CRIM plasmid integration in SNS118 by split-primer PCR.*** *P1/P4: 740 bp: No integration, P1/P2: 289 bp: Single integration, P3/P4: 824 bp: Single integration, P2/P3: 373 bp: Multiple integration.*

Figure 25 indicates that TrmBDNF-30-1, -3, -21 and -22; TrmBDNF-44-4, -5, -9 and -16 have integrated successfully. TrmBDNF-30-20 produced bands for P1/P4, P1/P2 and P3/P4 which suggests that there are two species present. TrmBDNF-44-17 and -19 are showing a band for P1/P2, which suggests integration.

*SNS118*_int.pAH68(434-TrmBDNF-30)-1, -3 and -22; and *SNS118*_int.pAH68(434-TrmBDNF-44)-4, -5 and -9 were used in toxicity and effective repressor drop-spot testing.

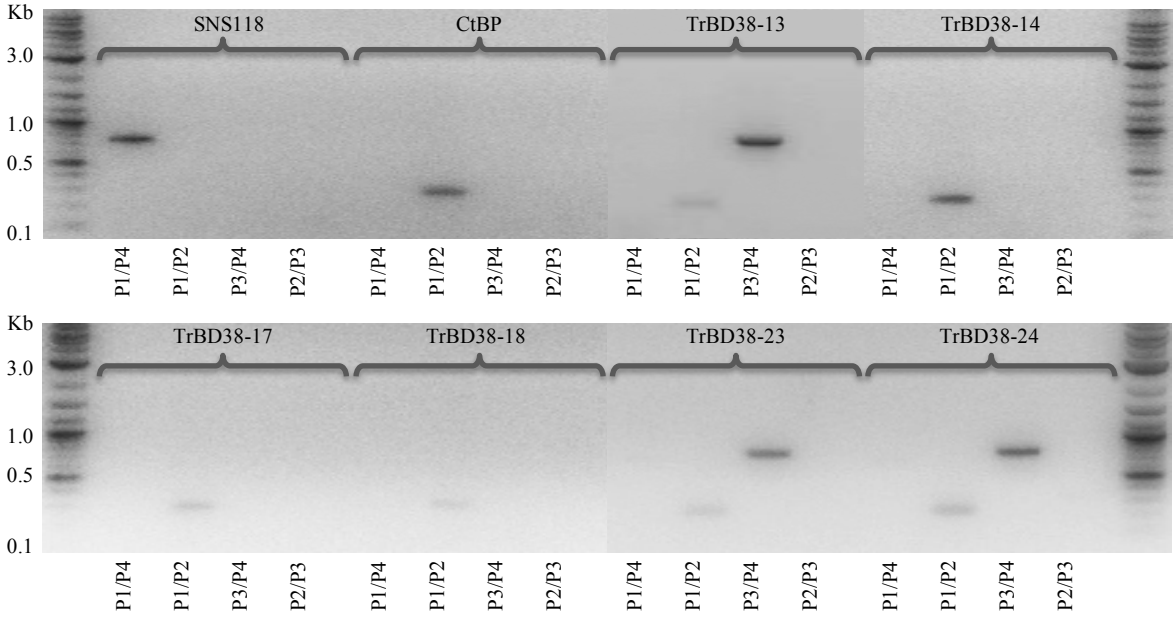



***Figure 26: Assessing 434-TrmBDNF-38 CRIM plasmid integration in SNS118 by split-primer PCR.*** *P1/P4: 740 bp: No integration, P1/P2: 289 bp: Single integration, P3/P4: 824 bp: Single integration, P2/P3: 373 bp: Multiple integration.*

Figure 26 indicates that all TrBD38 integrants have integrated, despite not displaying p3/p4 bands. Although this suggests a pipetting error has occurred, this was replicated in triplicate and the only P3/P4 bands observed are shown. This may be due to small bacterial sample size – if cultures are allowed to settle before PCR, or insufficient mixing. As TrBD38-23 and -24 indicate full integration, all six TrmBDNF-38 variants were used in toxicity and effective repressor drop spot testing:

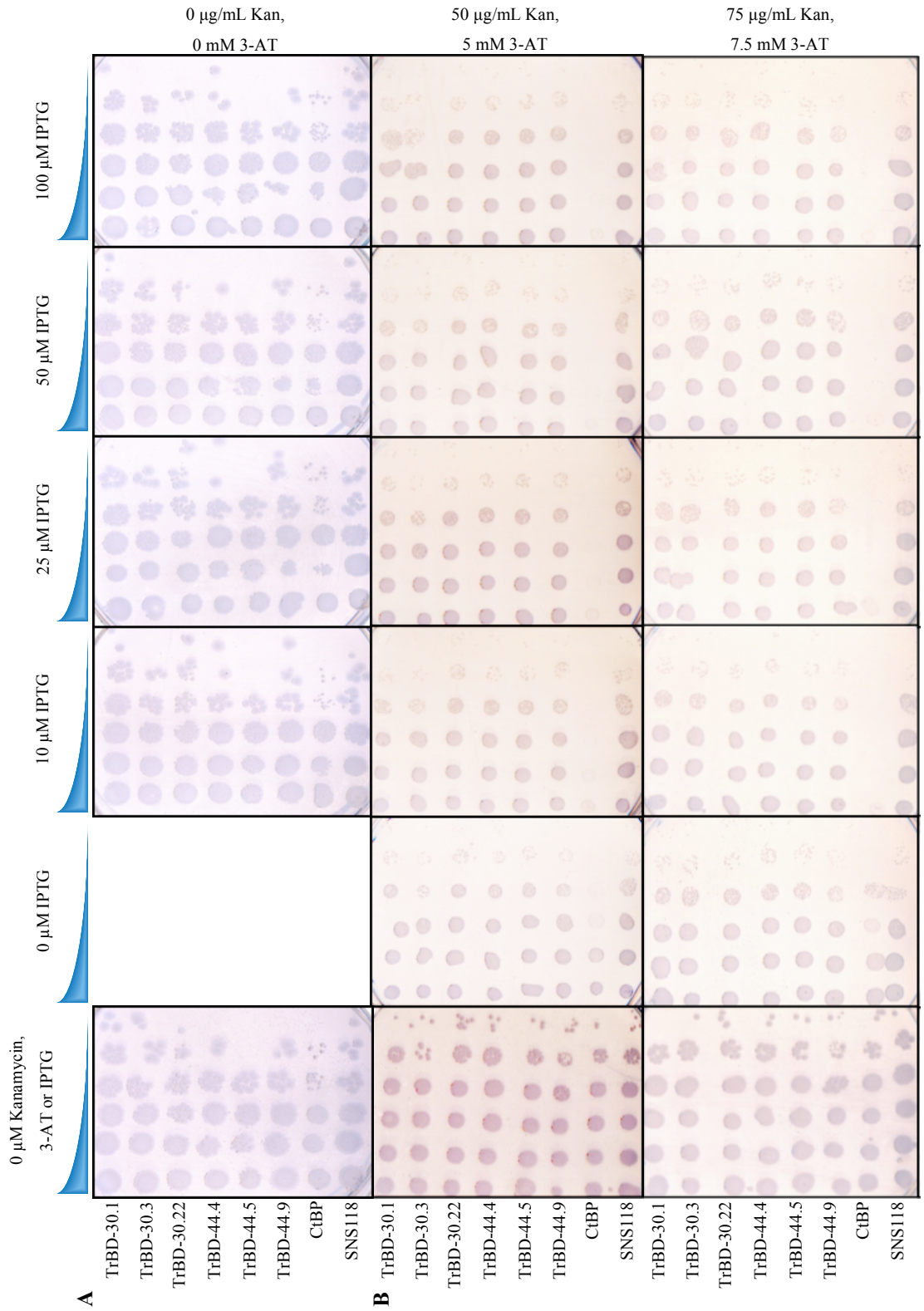



***Figure 27 Assessing 434-TrmBDNF-30 and 434-TrmBDNF-44 RTHS toxicity (A) and repressor activity (B) by drop spotting.*** *Blue curve shows the direction of bacterial culture dilution. Positive control: SNS118_int.pAH68(434-CtBP), negative control: SNS118.*

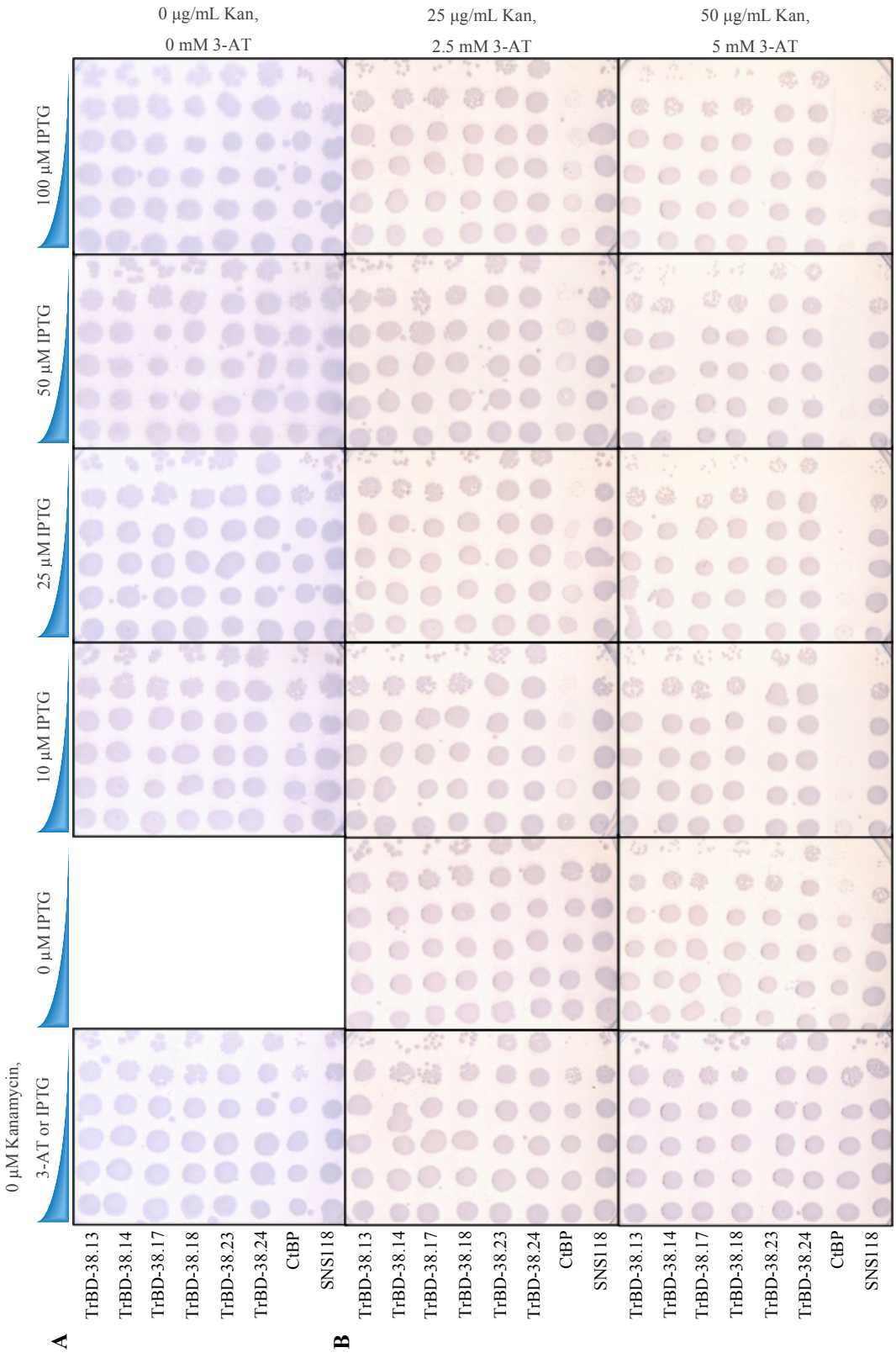



***Figure 28 Assessing 434-TrmBDNF-38 RTHS toxicity (A) and repressor activity (B) by drop spotting.*** *Blue curve shows the direction of bacterial culture dilution. Positive control: SNS118_int.pAH68(434-CtBP), negative control: SNS118.*

To assess toxicity, six-point ten-fold dilutions of *SNS118*_int.pAH68(434-TrmBDNF-30)-1, -3 and -22; and *SNS118*_int.pAH68(434-TrmBDNF-44)-4, -5 and -9 were dropped onto LB agar containing increasing concentrations of IPTG (0-150 μM) (Figure 27A and Figure 28A), indicating that none of the integrants are toxic to *E. coli*. This was then repeated on minimal media containing Kan (2.5/5/7.5 μg/mL) and 3-AT (2.5/5/7.5 mM) to assess effective repression of the RTHS cassette (Figure 27B and Figure 28B).

Figure 27 indicates that neither 434-TrmBDNF-30 or 434-TrmBDNF-44 form an effective repressor when singly integrated, and therefore cannot be used in an RTHS to assess mBDNF dimerisation. This was repeated in triplicate, validating results.

The disparity between Figure 23B and Figure 27B may be due to copy number – there are ~50 copies per cell of pTHCP16 in Figure 23B, compared to one copy per cell in Figure 27B. This would result in a greater expression rate for the same amount of IPTG induction. It may be that at high fusion protein concentration this forms an effective repressor, or conversely that high expression affects functional growth: if the fusion proteins expressed at such a rate misfolds and form large occlusion bodies, which could kill the bacteria. The disparity between minimal and LB media may be due to the added stress of Kan on the cells.

Six-point ten-fold dilutions of *SNS118*_int.pAH68(434-TrmBDNF-38)-13, 14, 17, 18, 23 and 24 were dropped onto LB agar containing increasing concentrations of IPTG (0-150 μM) (Figure 28A), indicating that none of the integrants are toxic to *E. coli*. This was then repeated on minimal media containing Kan (2.5/5 μg/mL) and 3-AT (2.5/5 mM) to assess effective repression of the RTHS cassette (Figure 28B) suggesting that 434-TrmBDNF-38 does not form an effective repressor of $O_R3$ and cannot be used in an RTHS to assess mBDNF dimerisation.

### 2.3.3 RTHS 5: C-Terminal mBDNF-FL-434

All prior bacterial RTHS systems developed by the above methods used N-terminal fusion proteins (e.g. 434-Hif-1$\beta^{140}$); no C-terminal versions have been created. Due to the proximity of the C-termini on the same face of mBDNF (Figure 29), it was hypothesised that fusing the C-termini to the N-termini of 434 could improve the orientation of the homodimer, allowing a functional repressor to form. Initially, 434 was amplified out of pTHCP16(434-mBDNF) by PCR using selective primers, adding a multiple cloning site

(MCS) to the 5′ termini and changing the 3′ termini digestion site. This was cloned back into pTHCP16 using the *Nde*I and *Sac*I restriction sites yet could not be isolated from re-ligated pTHCP16. This may be due to *Nde*I having a short sticky end of only "AT", and using a short insert: both of which reduce ligation efficiency. Instead, a gene block of mBDNF, a flexible linker (FL, ~50 Å 19 amino acid sequence, FL3[141]) and 434 ("mBDNF-FL-434") was purchased, amplified by PCR and cloned directly into pAH68 using the *Nde*I and *Sac*I restriction sites, then sequence verified.

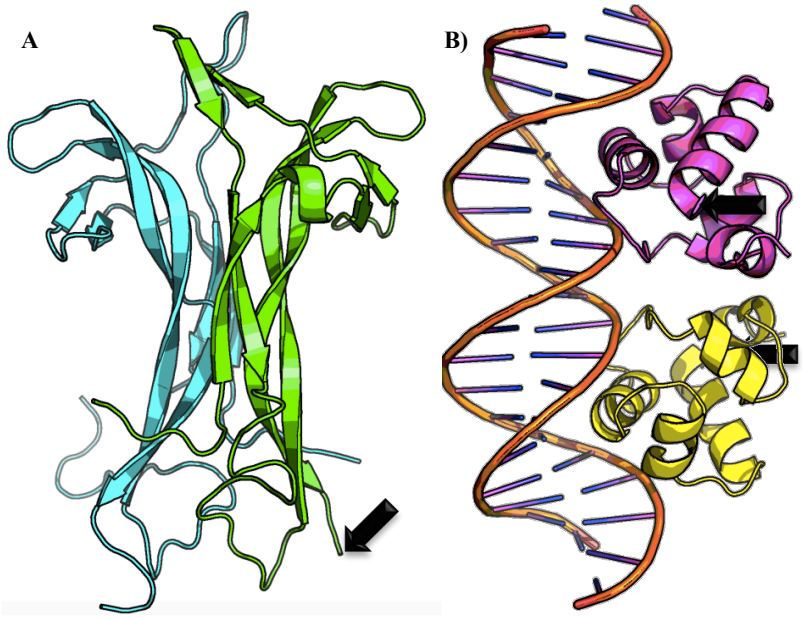



***Figure 29A: Crystal structures of the two components in mBDNF-FL-434 chimeric protein.*** *A) mBDNF (green) NT4/5 heterodimer (blue)[50] (PDB 1B8M). Arrow shows the C-termini. B) Dimeric 434 coupling with $O_R3$[126] (PDB 1PER), arrows showing the N-termini.*

pAH68(mBDNF-FL-434) was integrated into the $HK_{022}$ attB in *SNS118*, confirmed by mixed and split primer PCR:

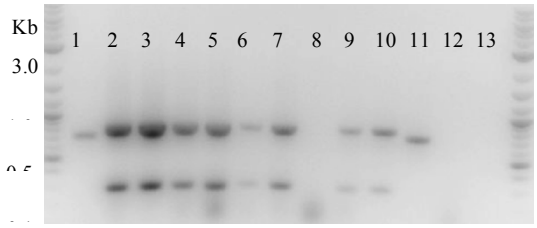



*Figure 30: Assessing mBDNF-FL-434 CRIM plasmid integration in SNS118 by mixed-primer PCR. 824 and 289 bp: Single integration, 740 bp: No integration, 373 bp: Multiple integration.*

*Figure 30 Lane 1: negative control SNS118_pAH69, lanes 2-13 pAH68(mBDNF-FL-434) integrants.*

Lanes 2-7, 9 and 10 of Figure 30A represent single integrations. Colonies for lanes 2, 4, 6, 7, 9 and 10 were cultured and used in split primer PCR to confirm integration:

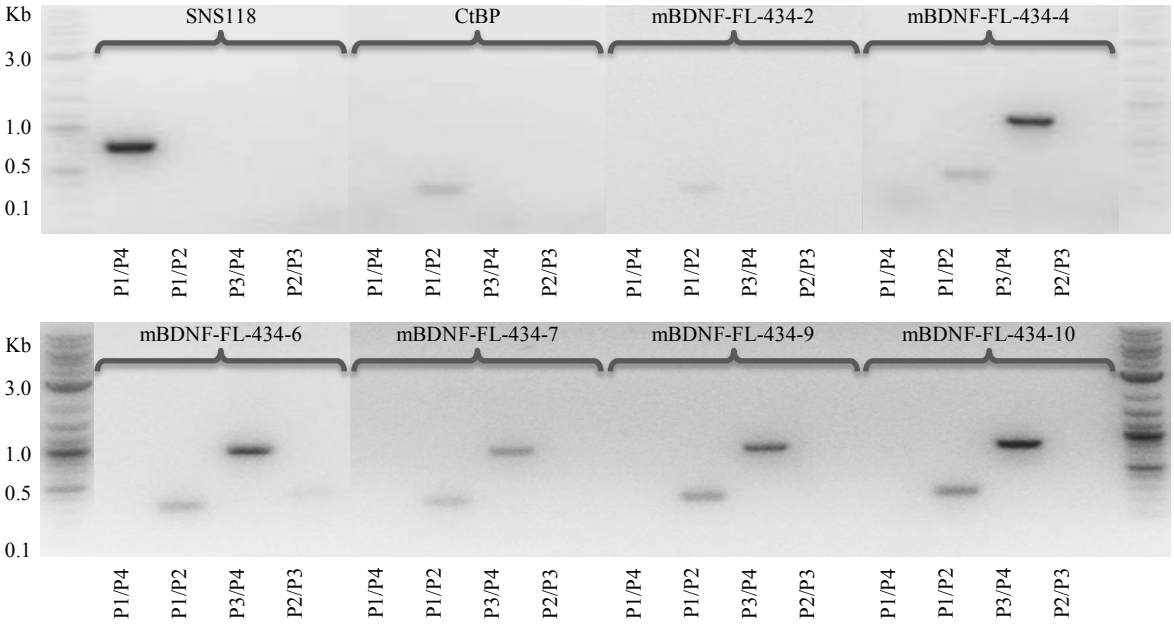



***Figure 31: Assessing mBDNF-FL-434 CRIM plasmid integration in SNS118 by split-primer PCR.*** *P1/P4: 740 bp: No integration, P1/P2: 289 bp: Single integration, P3/P4: 824 bp: Single integration, P2/P3: 373 bp: Multiple integration.*

This shows a similarly mixed amplification profile, particularly with the CtBP positive control. As pAH68(mBDNF-FL-434)-4 – 6, -7 -9 and -10 show correct bands, all six mBDNF-FL-434 variants underwent toxicity and effective repressor testing.

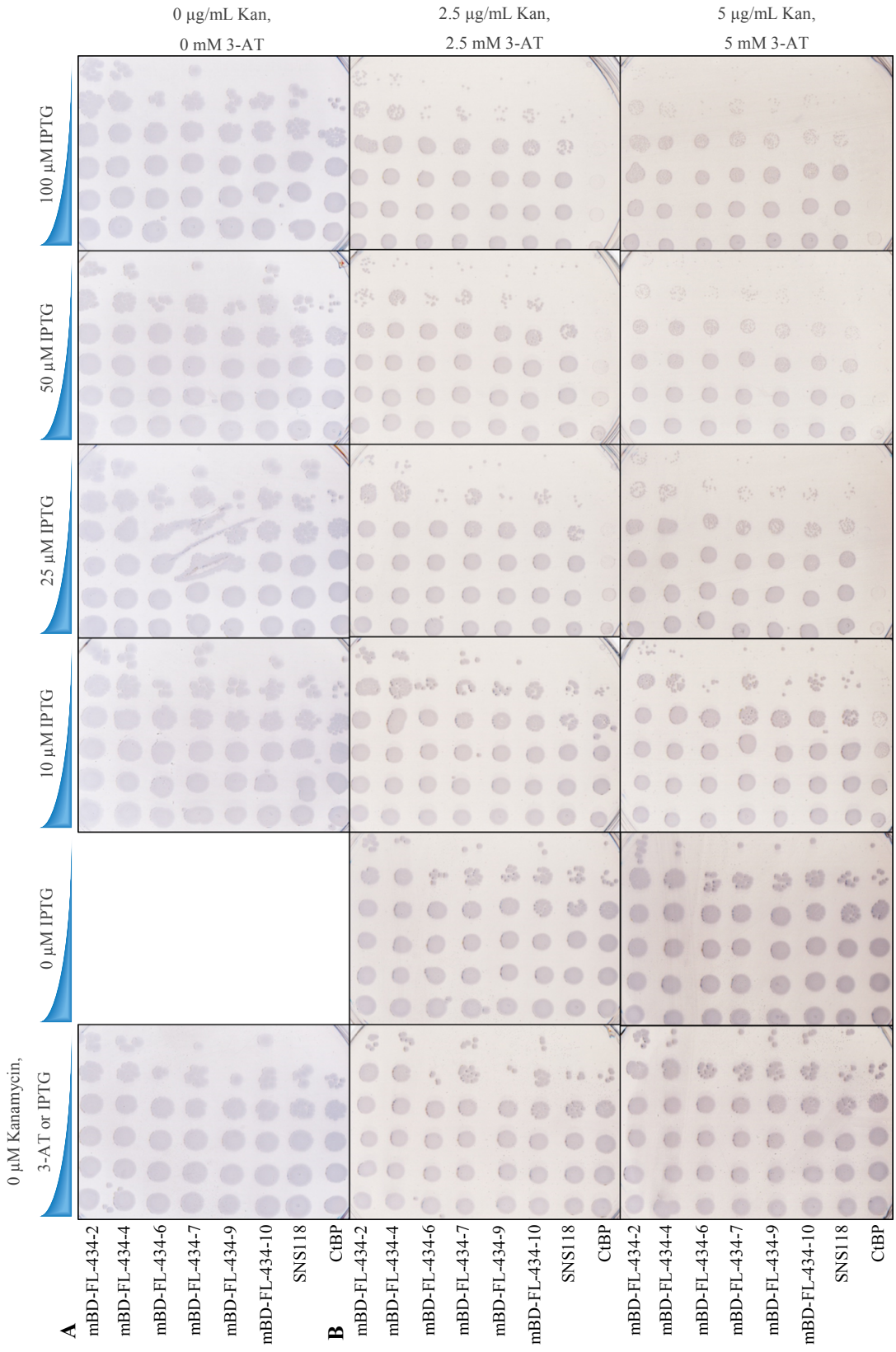



***Figure 32 Assessing mBDNF-FL-434 RTHS toxicity (A) and repressor activity (B) by drop spotting.*** *Blue curve shows the direction of bacterial culture dilution. Positive control: SNS118_int.pAH68(434-CtBP), negative control: SNS118.*

Figure 32A indicates that no *SNS118*_int.pAH68(mBDNF-FL-434) variant is toxic to the growth of *E. coli* in the presence of increasing concentrations of IPTG. Figure 32B however indicates that mBDNF-FL-434 is incapable of repressing growth in increasing concentrations of IPTG in media containing Kan and 3-AT. Therefore mBDNF-FL-434 cannot be used as an RTHS to assess dimerisation inhibitors of mBDNF.

It was hypothesised that the lack of repressor activity was be due to the "434" used so far in the project being more than the DNA binding domain:

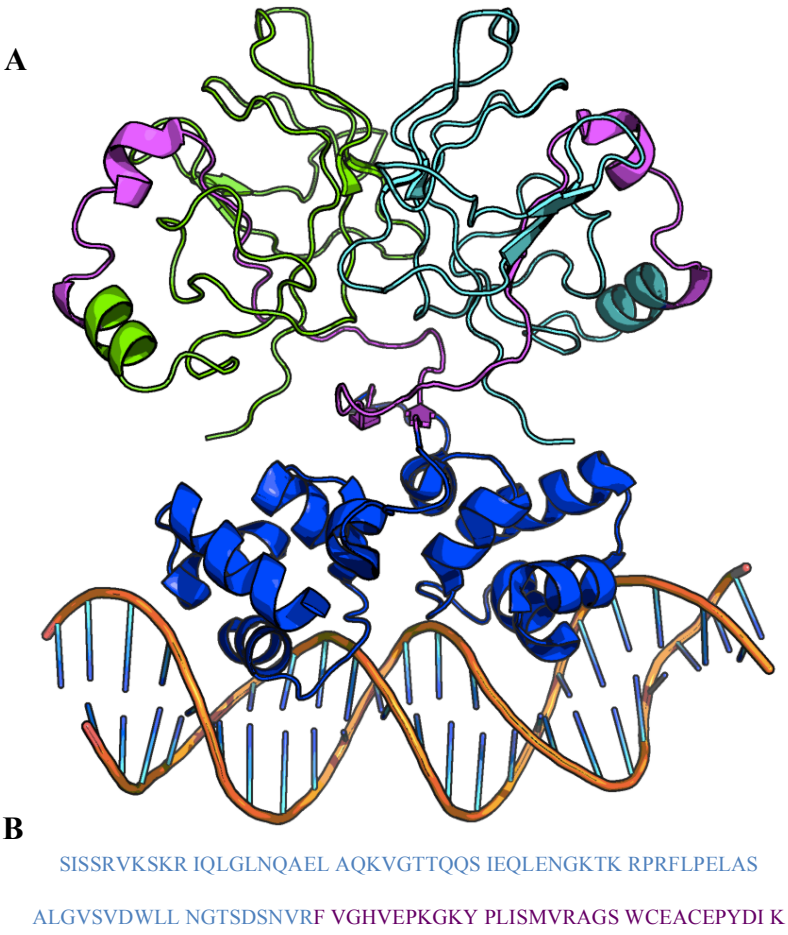



***Figure 33A: Theoretical model of dimeric wild type (residues 1-209) 434, coupling with $O_R3$ (PDB 1RPD)*** *B: amino acid residues 2-101 used so far in this project. Blue: residues 2-69 necessary for binding the ORI site, purple: residues 70-101 retained as a "linker" in previous N-terminal fusion proteins, teal/green: remainder of the wild-type 434 protein.*

Wild-type 434 cI (Figure 33) consists of a DNA binding domain, a disordered linker containing a recA digestion site and a dimerisation domain.[142] In previous RTHS based on this system, residues 2-101 were used: 2-69 as the DNA binding domain, with residues 70-

101 acting as a disordered linker between the DNA binding domain and the protein investigated in the RTHS. As shown in Figure 33, this disordered linker is not solvent exposed and is instead buried in the dimerisation domain. A typical flexible linker is highly flexible and solvent exposed, inspecting the primary amino acid sequence of 434 residues 70-101 shows a high degree of hydrophobicity and aromaticity: when expressed, these residues will have a high proclivity for burying themselves away from the surface of a protein and could therefore interfere with the correct folding of a fusion protein. For example, the flexible linker used in the following section ("FL") was LGGGGSGGGGSGGGGSAAA.[141] A modified C-terminal mBDNF based RTHS was therefore created:

### 2.3.4 RTHS 6: C-Terminal mBDNF-FL-434D

Creating an RTHS using only residues 2-69 of cI 434 (hereafter "434D") required considerable recombineering: the original concept was to amplify 434D out of pAH68(mBDNF-FL-434) by PCR and clone it back into pAH68(mBDNF-FL-) using the *BamHI* and *SacI* restriction sites. This revealed the presence of a second BamHI site well outside the cloning region, not present in the recorded sequence for the plasmid.

Sequencing upstream of the LacI revealed a completely different sequence to what was expected, suggesting that the ancestry of this plasmid was not what was expected. The same plasmid had been used by others in the group (e.g. E. Osher, unpublished) to create working RTHSs and is therefore functional, however it was decided for fidelity to clone this final RTHS into a completely sequenced version of pAH68 from the CGSC, Yale (catalogue number: 70955). This blank pAH68 lacked LacI, the MCS for the RTHS, or the non-coding regions (NCR) surrounding the RTHS such as the Shine-Dalgarno ribosome binding sequence. These would be taken from a sequence-verified pTHCP16.

To achieve this, mBDNF-FL-434 was amplified out of pAH68(mBDNF-FL-434) and cloned into pTHCP16. This was sequenced, revealing a K→R mutation in mBDNF, introduced by the low-fidelity polymerase used: Promega GoTaq G2 (catalogue number: M7845). This was corrected by KOD polymerase site directed mutagenesis (SDM) and sequence verified. 434D was amplified out of the mBDNF-FL-434 gene block using PCR and cloned into pTHCP16(mBDNF-FL-) using the *BamHI* and *SacI* restriction sites. Cloning from pTHCP16 to pAH68 required the use of *MscI*, which is methylation sensitive. To permit digestion, pTHCP16(mBDNF-FL-434D) was transformed into

GM2929 cells to prevent methylation of the DNA, and LacI-NCR-mBDNF-FL-434D was isolated using the *SacI-HF* and *MscI* restriction sites. This was then cloned into the fully sequence verified pAH68 using the *SmaI* and *SacI* restriction sites using blunt-end ligation, creating pAH68(mBDNF-FL-434D) which was sequence verified.

Three colonies were picked from the previous step and while being sequence verified they were integrated and checked by mixed and split PCR. All proved the correct sequence, and so were taken through for repressor efficacy testing:

pAH68(mBDNF-FL-434D) was integrated into the $HK_{022}$ attB site of *SNS118*, confirmed by mixed and split primer PCR:

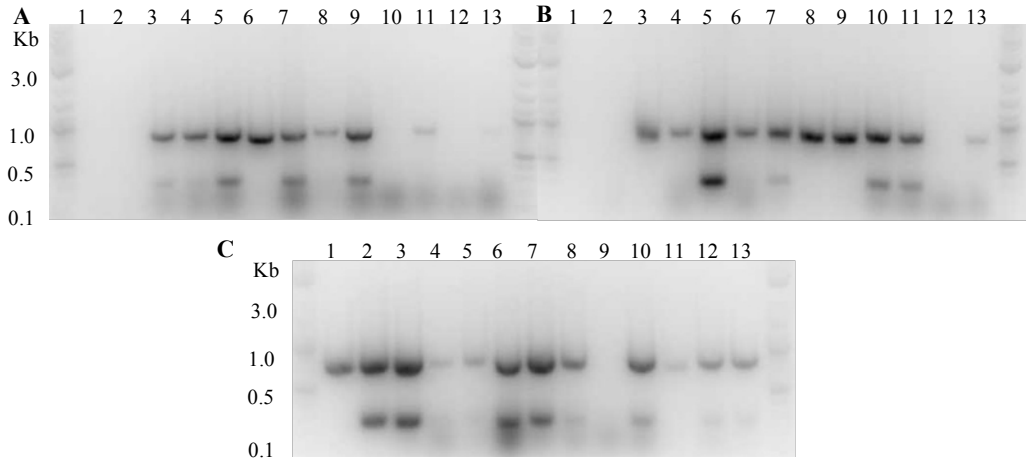



***Figure 34: Assessing mBDNF-FL-434D CRIM plasmid integration in SNS118 by mixed-primer PCR.*** *824 and 289 bp: Single integration, 740 bp: No integration, 373 bp: Multiple integration.*

*Figure 34A: Lane 1: no template negative control, Lanes 2-13 pAH68(mBDNF-FL-434D).1 integrants.*

Lanes 3-5, 7, 9, 11 and arguably 13 represent integrated pAH68(mBDNF-FL-434D), therefore colonies for lanes 3, 4, 5, 7 and 9 were cultured and used in split primer PCR to confirm integration. Figure 34B: colonies 5, 7, 10 and 11 represent integrated pAH68(mBDNF-FL-434D).2, therefore they were all cultured and used in split primer PCR to confirm integration. Figure 34C: colonies 2-4 6-8, 10, 12 and 13 represent integrated pAH68(mBDNF-FL-434D).3, therefore colonies representing lanes 2, 3, 6-8 and 10 were cultured and used in split primer PCR to confirm integration:

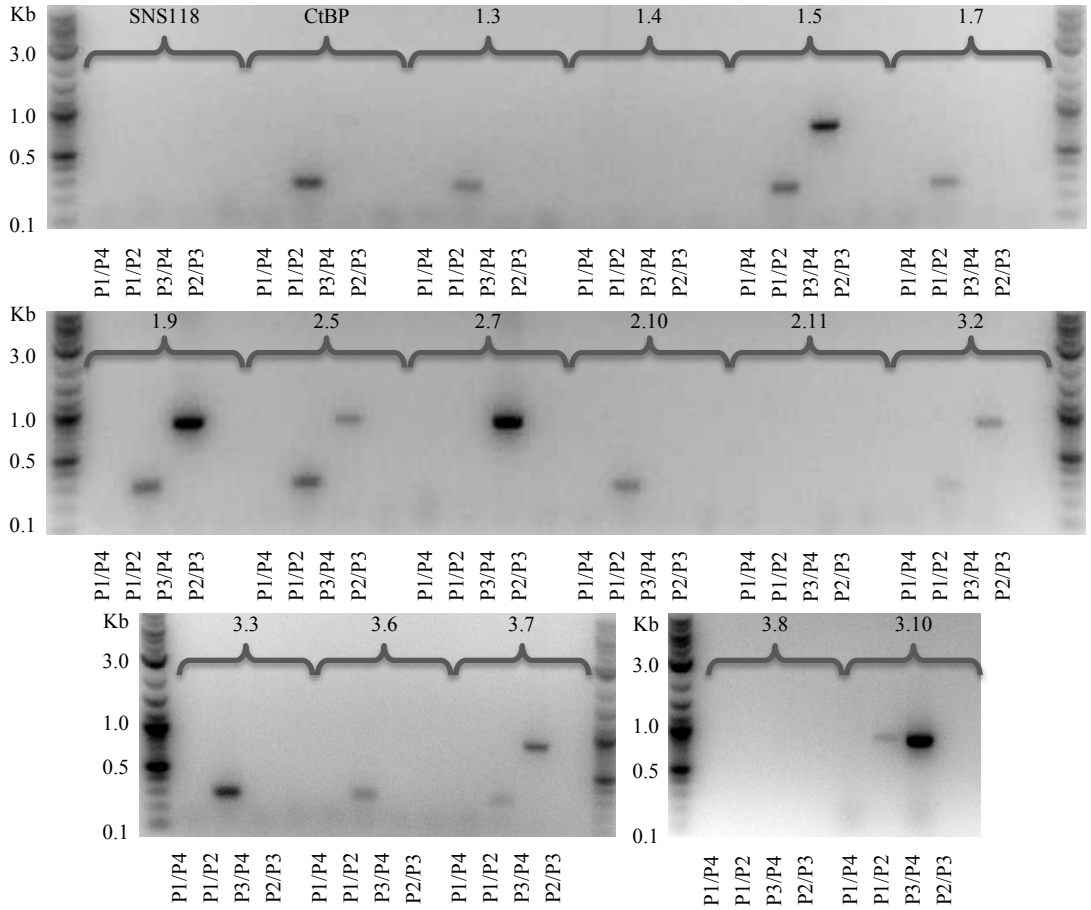



***Figure 35: Assessing mBDNF-FL-434D CRIM plasmid integration in SNS118 by split-primer PCR.*** *P1/P4: 740 bp: No integration, P1/P2: 289 bp: Single integration, P3/P4: 824 bp: Single integration, P2/P3: 373 bp: Multiple integration.*

Despite being repeated twice each, more consistent gels could not be produced. The lack of a P3/P4 band in some may be due the GoTaq G2 polymerase's lytic activity on primers destroying one/both of a primer pair, despite preparation on ice. The polymerase activity could be solved by the use of HotStart GoTaq, this uses a thermally sensitive antibody to prevent unintentional activity below a temperature threshold. Alternatively, the lack of a complete PCR profile may be a sampling error – if the cultures had settled before sampling there will be very few cells in the PCR mix. Nonetheless, Colony 1.5, 1.9, 2.5, 3.2 and 3.7 demonstrate the correct PCR profile, and therefore they and 2.7 were taken forward for repressor efficacy drop spot testing.

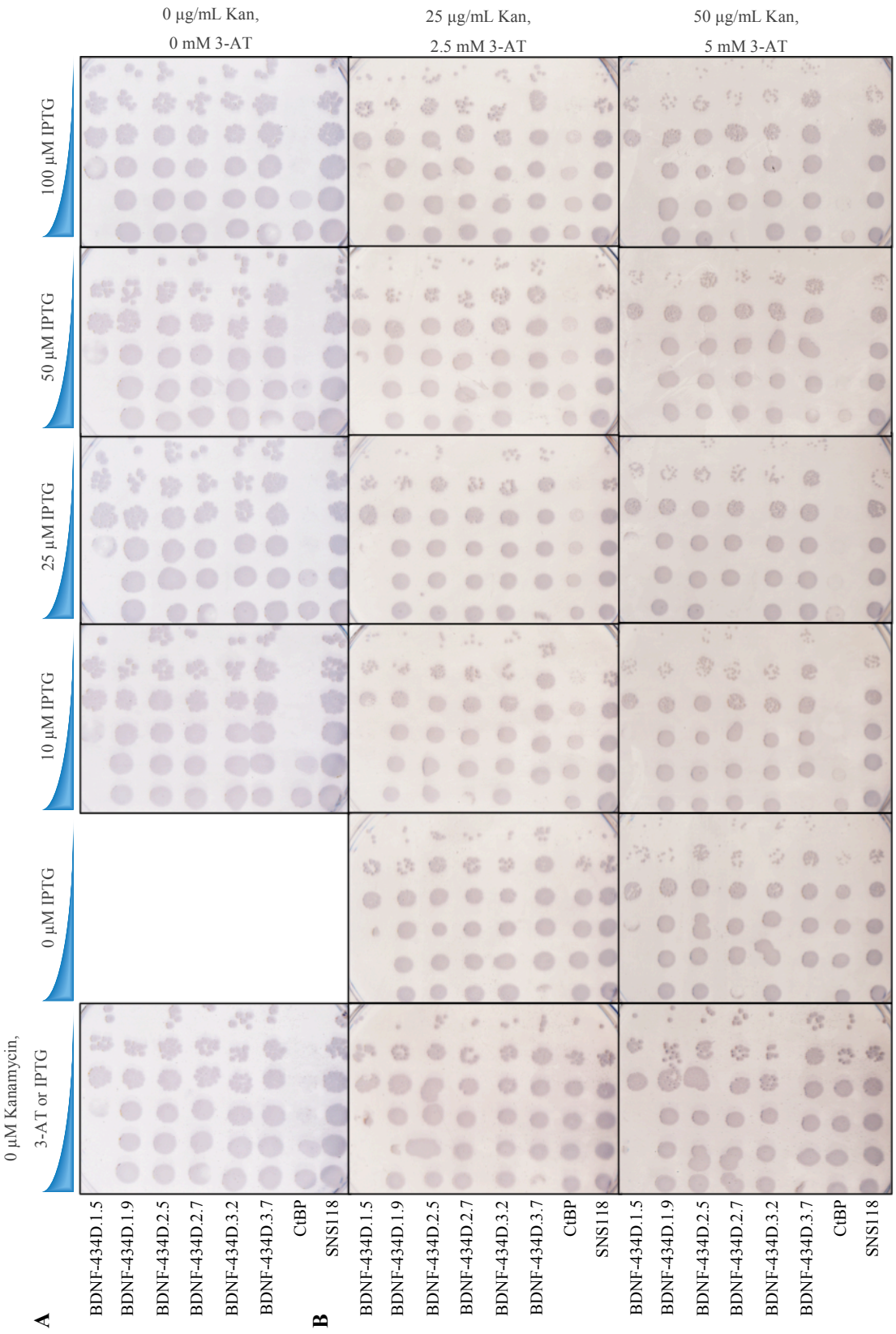



***Figure 36: Assessing mBDNF-FL-434D RTHS toxicity (A) and repressor activity (B) by drop spotting.*** *Blue curve shows the direction of bacterial culture dilution. Positive control: SNS118_int.pAH68(434-CtBP), negative control: SNS118.*

Figure 36A indicates that no *SNS118*_int.pAH68(mBDNF-FL-434D) variant is toxic to the growth of *E. coli* in the presence of increasing concentrations of IPTG. Figure 32B however indicates that no mBDNF-FL-434D variant is incapable of repressing growth in increasing concentrations of IPTG in media containing Kan and 3-AT. Therefore mBDNF-FL-434D cannot be used as an RTHS to assess dimerisation inhibitors of mBDNF.

## 2.4 Chapter 2 Conclusions

The majority of this project thus far was spent creating and testing different varieties of mBDNF RTHS, which proved ineffective at preventing growth of *SNS118* under increasing IPTG concentrations in the presence of Kan and 3-AT, indicative of an inability of the fusion protein to dimerise and bind as an effective repressor of the $O_R3$ operator. This may be due to various reasons, as described below.

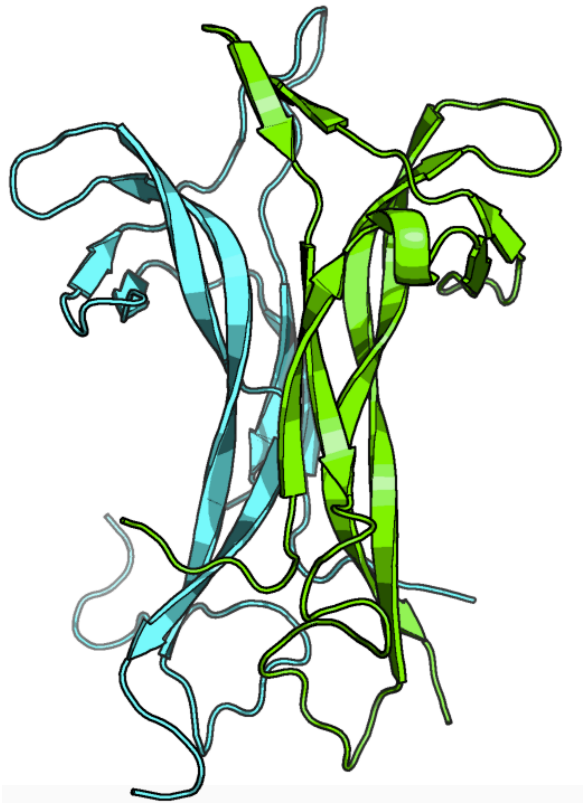


***Figure 37: Structure of mBDNF (green) NT4/5 (blue) heterodimer[51] (PDB 1B8M).***

Initially the classic (with regards to previous SNS118 RTHSs) N-terminally fused 434-mBDNF protein was explored, yet no shut down in host cell growth was observed upon induction of chimeric protein expression. Examination of the predicted structure of the mBDNF interaction indicated that the N-termini are not in close proximity – they lie on

opposite faces midway down the molecule. In an attempt to alter the proximity and orientation of the mBDNF N-termini, several truncated N-terminal fusion proteins versions were created. Finally, when 434-TrmBDNF-30, 434-TrmBDNF-38 and 434-TrmBDNF-44 proved similarly ineffective at suppression of *SNS118* growth, novel C-terminal fusion proteins were explored. mBDNF-FL-434 was developed with a flexible linker joining mBDNF to 434. mBDNF-FL-434 likewise proved impotent at quelling *SNS118* growth under increasing IPTG concentrations in the presence of Kan and 3-AT, potentially due to residues 70-101 of 434 providing steric hindrance to dimerisation or disrupting correct folding. Finally, a C-terminal mBDNF 434 fusion protein using only residues 2-69 of 434 was created (mBDNF-FL-434D), but was similarly ineffective at repressing SNS118 growth in media treated with Kan and 3AT. An overview of the attempted mBDNF-based RTHSs is shown in Figure 39.

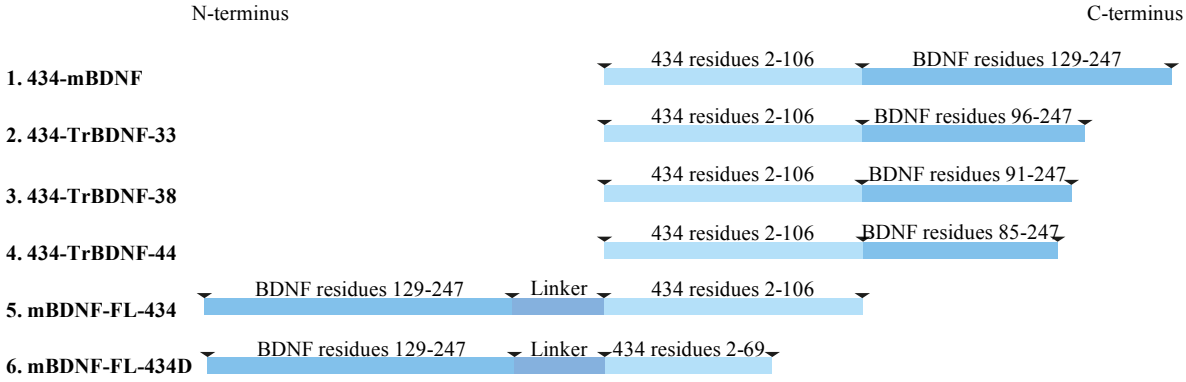



***Figure 38: Graphical representation of the six fusion proteins investigated in this chapter; none of which functioned in SNS118 as a successful repressor.***

Up to this point it was hypothesised that the mBDNF fusion proteins were sufficiently expressing but were incapable of either forming a homodimer, or if a homodimer was formed, that it was incapable of binding to the gene cassette. In hindsight, whether soluble protein was being expressed should have been explored by SDS-PAGE, however all crystal structures of neurotrophins present in the literature were from protein derived from *E. coli* expression, therefore it was assumed that mBDNF expressed without major issue. In later chapters, significant attempts were made to express mBDNF in *E. coli,* wherein the complexities of neurotrophin expression in *E. coli* became apparent.

By also investigating the expression of βNGF, the literature revealed that neurotrophins require several ancillary proteins (DsbA, DsbB, DsbC and DsbD) to express beyond

baseline levels.[143] When expressed without those proteins, the neurotrophin misfolds and is present in the insoluble fraction. Considering these ancillary proteins are critical to the formation and isomerisation of disulfide bonds in the periplasm of *E. coli* (for more details, see Section 4.2.2.1), misfolding is likely due to the six non-consecutive disulfide bridges present per dimer of neurotrophin (see Figure 39), causing misfolding and inactivity.

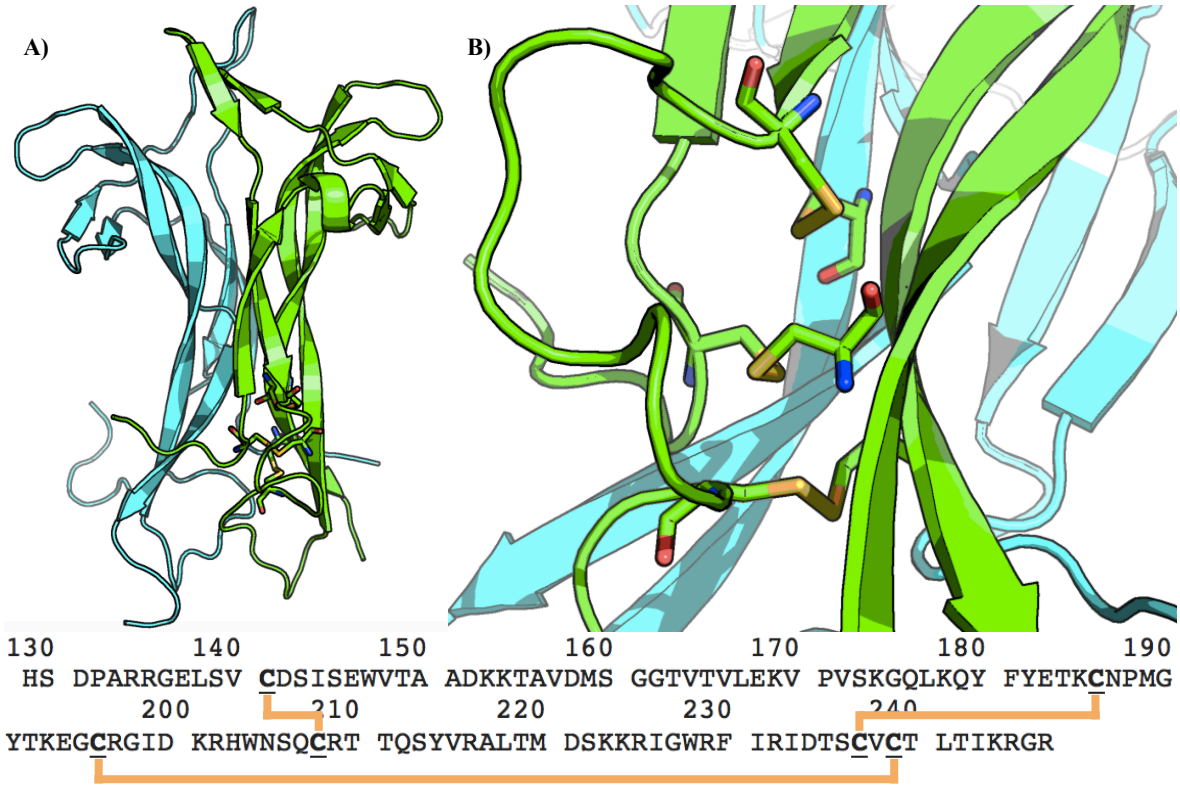



***Figure 39: mBDNF (green) NT4/5 (blue) heterodimer (PDB 1B8M[51]) highlighting the three non-consecutive intramolecular disulfide bridges per mBDNF monomer (C142-C209, C187-C238, C197-C240).***

With the number of Cys residues present in mBDNF, the chance of intermolecular disulphide bridges being formed during misfolding is increased. If the mBDNF fusion proteins had a purification tag or could be isolated in some way (e.g. antibody-coated beads), then a number of techniques outside of non-denaturing SDS PAGE could have been used to assess the polymeric state. For instance, ultracentrifugation would permit the measurement of percentages of monomer, dimer and aggregate.

Developing a new RTHS for proteins containing multiple non-consecutive disulfide bridges was considered, co-expressing the necessary ancillary proteins. Considering however that protein translation occurs in the cytoplasm and disulfide bridge formation in *E. coli* occurs in the periplasm, the genetic cassette for the RTHS is in the chromosome (in

the cytoplasm): there is no method to transport proteins back to the cytoplasm from the periplasm.

It was felt than an alternative method of library screening should be applied to mBDNF. To maximise success, the project was expanded to include screening against βNGF. Bacteriophage (phage) display screening was chosen as an effective method to identify peptides capable of binding to βNGF and mBDNF.

# Chapter 3: Identifying Inhibitors of βNGF and mBDNF Through Phage Display

## 3.1 Introduction to Phage Display

Having investigated the use of mBDNF fusion proteins to create RTHS as methods of identifying mBDNF inhibitors, no mBDNF-DNA fusion protein could be identified which successfully prevents reporter gene expression in the *SNS118* system. Alternative routes to mBDNF inhibition were therefore pursued: bacteriophage (phage) display was employed as a method for identifying small peptide loops capable of binding neurotrophins. In an effort to ensure success, inhibition targets were increased to include βNGF as well as mBDNF.

Phage display is a high throughput library screening technique used to identify peptide sequences able to bind to a specific target. The phage (a virus which parasitises or preys on bacteria) is modified to express a selectively randomised variable peptide on the surface of one coat protein, and the virion is merely a carrier used to link the peptide sequence to a genetic tag (the viral genome). As a technique, phage display has been widely used to identify peptides specific to the vasculature of osteosarcomas over regular vasculature (allowing the specific localisation of therapeutics),[146] amyloid precursor protein (as a potential Alzheimer's therapy),[147] paclitaxel (identifying the binding of paclitaxel to Bcl-2)[148] and the cell surface receptors of termite protozoa (allowing paratransgenesis for pest control).[149] Significant recent research has been directed towards discovering mimotopes (protein mimics of epitopes) which illicit immunological response – an interesting route towards new vaccines and diagnostic tests without the use of attenuated or live bacteria.[150-156]

The overall process of using phage display to identify peptide-peptide interaction inhibitors is shown in Figure 40. This may be divided into two sections: screens and assays of phages, and screens and assays of peptides identified by the first section. Initially an unbiased library is screened, isolating phages with an ability to bind to a target. These phages are then amplified and the screen repeated in an attempt to isolate phages with the strongest binding characteristics. Hit phages are then assayed for their ability to bind to the target over non-targets, in an effort to eliminate non-specific binding phage. Successful phages are then sequenced to identify the specific variable peptide with the binding

activity. These hit peptides are then synthesised as either free or tagged peptides and assayed for agonistic or antagonistic activity to identify lead peptides. The binding activity of these lead peptides is then assayed to identify peptides with the best profile, and analogues are made to: identify the sub-sequence in the peptide from which the activity derives, identify the target binding site, and increase the binding activity.

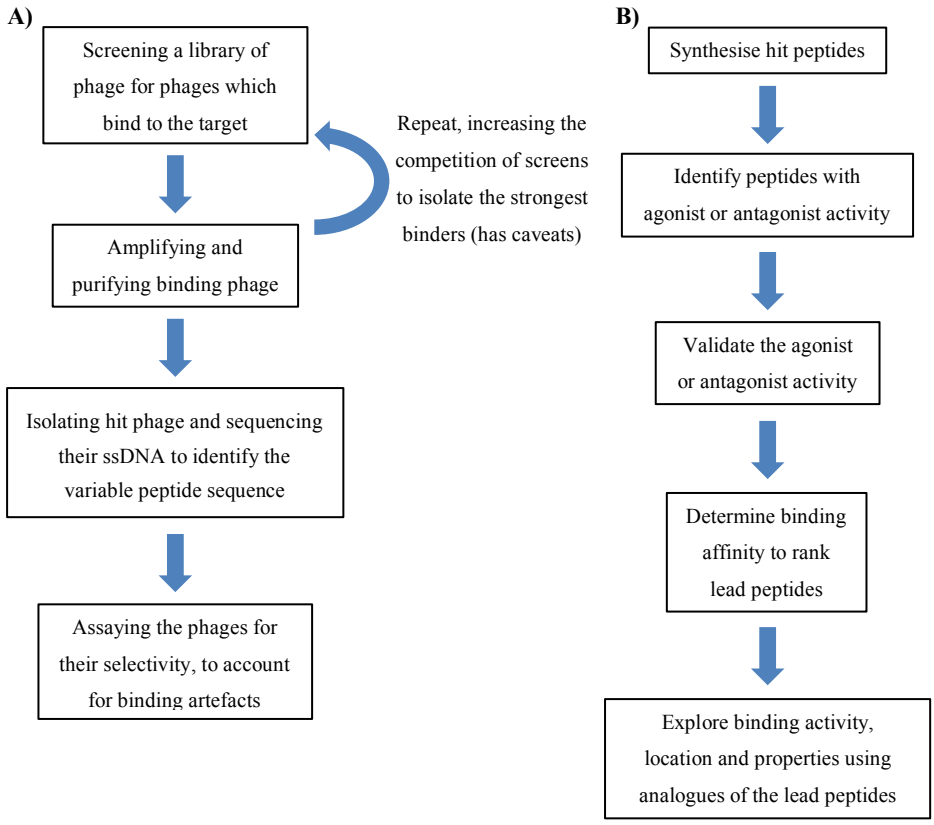



***Figure 40: Overview flowchart of the process of identifying and verifying PPI inhibitors using phage display.*** *A) Section using phages to produce peptides with an attached genetic tag. B) Section using synthesised peptides and peptide analogues.*

Phage display libraries consist of a variable motif added to a viral coat protein. This is usually added by using site-specific mutagenesis with degenerate primers, and theoretically each phage expresses a different variable motif. This has been used to create libraries of phages of up to $1x10^{12}$ members. To conduct a phage display screen, the target of interest is bound to a surface (e.g. petri dishes, affinity bead capture *etc.*) and exposed to the library of phage. Phages expressing modified coat proteins capable of adhering to the target are retained, whilst non-binders are removed by washing ("panning"). Hit phage are then eluted by lowering pH or with an excess of a known competitor, then phages are amplified by culturing with susceptible bacteria and purifying the sample. Panning is then repeated several times under more stringent conditions (e.g. presence of a surfactant) to remove

binders with weaker affinity and increase the fidelity of hits. Sequencing the phage genome (which encodes the additional short variable peptide) is used to rapidly elucidate hits.

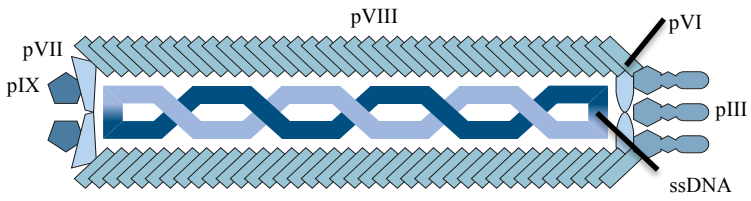



***Figure 41: The structure of an M13 filamentous phage.*** *Included to indicate the position of pIII and pVIII, and explain the copy number: 5 vs. ~2000.*

Several methods of phage display exist; using different species of phage or creating semi-randomised fusion proteins out of different viral coat-proteins. One of the most well used, versatile and containable (in a mixed microbiology lab) is that of F-specific filamentous phage display; usually using M13 phage.

Containment was important as the following research was conducted in a lab using *E. coli* for a myriad of projects. In contrast, T1 phage (a different species) are airborne lytic phage which are very hard to remove from bacteria/plasmids and require advanced laminar flow cabinets unavailable for the author's use.

In M13 based phage display, coat protein pIII or pVIII are modified with an N-terminal variable peptide. As each virion contains only five copies of pIII and several thousand copies of pVIII, pIII libraries screen for affinity, instead of avidity. As M13 phage only parasitises *E. coli* containing an F or fertility factor plasmid (hence F-specific filamentous phage), they are also easy to contain in labs which use *E. coli* for other research.

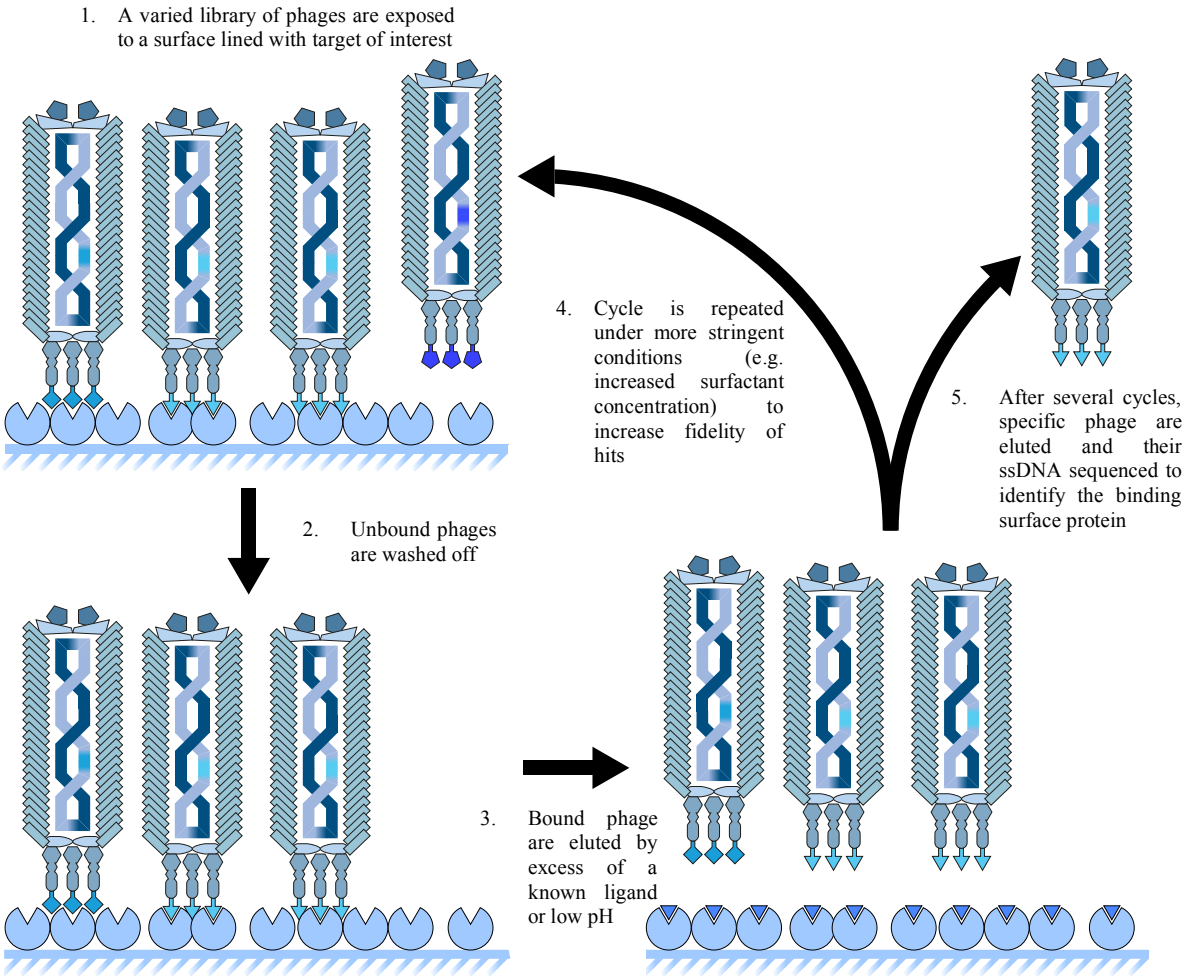



***Figure 42: The iterative phage display panning process.***

A commercially available phage library was used in this research: NEB produce three M13 pIII libraries: two linear libraries with seven or twelve randomised amino acids (i.e. $X_7$[149-151] and $X_{12}$[148, 152-154]), and a constrained library containing seven randomised amino acids flanked by a disulphide bridge (i.e. $CX_7C$[146-147, 153, 155-157]). Each library is designed for specific roles: $X_7$ is used to identify small pockets on a target, $X_{12}$ is used to identify larger binding surfaces when the $X_7$ library fails, and $CX_7C$ creates a constrained loop which mimics more fixed structures such as antibodies or hot loops. Constraining the library lowers the chance of it containing a hit, as each library member has fewer possible 3D conformations available to it. Alternatively, constraining the ring lowers the entropic cost of binding due to prearrangement. This improves the overall free energy of binding, which can result in hits which may have higher binding affinity.[158-159] As such, the $CX_7C$ was chosen to identify peptides which bind to mBDNF and βNGF. The $CX_7C$ library adds the motif $ACX_7CG_3S$ to the N-termini of phage coat protein pIII (the alanine allows efficient splicing from a leader sequence, $G_3S$ is a flexible linker to pIII).

The library may be screened under a number of conditions, such as in solution or on a surface. Both solution and surface-based panning rely on a method of isolating the target (and any phages bound to it) from solution. Given that reliable sources of commercially available mBDNF and βNGF are untagged (e.g. lacking a polyhistidine tag which would bind to nickel-affinity chromatography plates or beads), this limits the methods of isolation to non-specific binding on highly aromatic polystyrene beads or plates, or through the use of anti-mBDNF and anti-βNGF antibodies.

Concerning both solution- and surface-based panning, two main options present: adding the phages to the targets in solution then isolating the targets with antibodies, or coating surfaces or beads with the target and then adding the phage library for screening. The strengths of the former are that with the target in solution, all target orientations are available, and it minimises the avidity effect: retaining weakly-binding phage (which each have five copies of the variable domain) on a surface with several targets (i.e. making five different PPIs to create a chelate effect). However, if phages obscure the surface of the target used by the antibody to isolate the target, no target will be retained. Conversely, the surface techniques either create a number of orientations (non-specific binding) or one orientation (antibody binding). As a result of this, and under the advisement of NEB manual E8120, the surface panning technique was chosen using high-binding polystyrene plates.

### 3.1.1 Results and Discussion: Phage Display Screening and Verification

Phage display is used to identify peptide loops capable of binding to a surface. Without due controls, this may result in false positives where identified peptides bind to the plastic support (e.g. 96 well polystyrene plate or affinity beads), or to any ancillary proteins present (e.g. BSA present to aid peptide folding) rather than the target protein. A control phage display screen against a target which pulls down a known sequence is therefore advisable to ensure the validity of hits. Streptavidin binds strongly to the amino acid sequence HPQ:[160] a phage display screen against streptavidin should identify peptides which contain this motif.

A streptavidin phage display control screen was successfully performed using the Ph.D™-C7C Phage Display Library (Catalogue number: E8121L), using the supplied M13KE phage and following an adapted variant of the surface panning procedure in NEB

manual E8120. For a full explanation, see Section 7.3.4.3. Briefly, one round of surface panning consisted of adding 100 μL of 1.5 mg/mL streptavidin solution to one well of 96-well polystyrene plate and refrigerating overnight with agitation. The plate was then blocked with a solution of BSA and 0.1 μg/mL streptavidin (to bind any biotin in the BSA), before a hundredfold representation of the $CX_7C$ library was added. Phage are measured by plaque forming units (pfu): the number of mature virions in a sample. Therefore, $1x10^{11}$ pfu were added to the plate for this $1x10^9$ member library. The plate was then repeatedly washed with phosphate buffered saline (PBS) treated with a surfactant (Tween-20, 0.1% v/v) to remove non-binding phage. Bound phages were then eluted with 0.1 mM biotin in PBS. These phages were then amplified by addition to a culture of ER2738 *E. coli* bearing an F-plasmid and grown in an orbital incubator (4 h, 37 ˚C). The amplified phages were then harvested by centrifugation and precipitation (20% PEG/2.5 M NaCl). Panning was repeated twice more, using an increased Tween-20 concentration of 0.5%, before a final phage isolation of hopefully streptavidin-selective phage.

To verify whether these phages are streptavidin-selective, following the third pan, phages were isolated and sequenced: briefly, cultures of ER2738 were infected with phages at a multiplicity of infection (MOI) <<1 and immediately mixed with “top agar” (LB agar with half the normal amount of agar). This was then spread on LB agar plates containing IPTG, Xgal and tetracycline.

The IPTG was used to induce expression of LacZα from the library phage’s ssDNA and LacZβ from the ER2738 chromosome. These were recombineered into phage’s genome to provide a colorimetric reaction to distinguish library phage from wild phage: the LacZα and LacZβ dimerises and cleaves the colourless Xgal into galactose and 5-bromo-4-chloro-3-hydroxyindole. 5-bromo-4-chloro-3-hydroxyindole then dimerises and is oxidised to form 5,5'-dibromo-4,4'-dichloro-indigo, which is intensely blue. Wild phages do not encode LacZα and therefore appear as translucent plaques in the resulting lawn of ER2738. Each blue plaque should therefore represent a single library phage infecting a bacterium due to the very low MOI to which the ER2738 were infected. The phage then multiplied and all subsequent phage in that plaque should be identical.

Plaques were then picked to isolate individual phage clones and amplified individually by culture with fresh ER2738 followed by isolation and purification. Phage genomes were then sequenced by stripping ssDNA from the viral coat proteins using high salt buffers and a brief ethanol precipitation. The salt (NaI) interferes with intermolecular interactions and

causes viral coat proteins to dissociate, the brief ethanol treatment causes the ssDNA to precipitate, which is then isolated by centrifugation. Purified ssDNA was sequenced by automated dideoxy sequencing using the supplied -96 gIII sequencing primer.

Conducting the streptavidin screen proved its necessity: as polystyrene plate type wasn't specified in NEB manual E8120, initially Greiner Cellstar® plates (catalogue number: 655083) were used due to their abundance in the lab. These are treated for tissue culture adherence and following phage display screening, every phage sequenced bore the peptide motif ACGMMVPHRCGGGGS, which presumably binds very strongly to this surface treatment. Upon switching to Greiner Microlon® high binding polystyrene plates (catalogue number: 655061), the control screen was successful: 20 phages were sequenced, 13 included the HPQ motif, 1 contained the HPM motif (which is also known to bind to streptavidin), 4 did not contain a known streptavidin binder, and two were wild phage (identified through sequencing): unavoidable when phage display is conducted on a bench top not a laminar flow cupboard, in a lab without overnight ozone/ultraviolet treatment. The sequences of the variable motifs are as follows:

***Table 3: N-terminal pIII randomised peptide motifs sequenced from streptavidin binding phage.*** *Sequences sorted by Clustal Omega similarity ranking.*[161 162]

| **Code** | $X_7$ Region | **Code** | $X_7$ Region | **Code** | $X_7$ Region | **Code** | $X_7$ Region |
|---|---|---|---|---|---|---|---|
| JI.S.1 | GTFDHPM | JI.S.6 | GSFNHPQ | JI.S.11 | GIFVHPQ | JI.S.16 | SLAPHGD |
| JI.S.2 | GSFTHPQ | JI.S.7 | GSFNHPQ | JI.S.12 | GSYVHPQ | JI.S.17 | FNSGYWV |
| JI.S.3 | GSFTHPQ | JI.S.8 | GSFAHPQ | JI.S.13 | GSYVHPQ | JI.S.18 | PDMCVSC |
| JI.S.4 | GSFTHPQ | JI.S.9 | GSFAHPQ | JI.S.14 | GSYVHPQ | | |
| JI.S.5 | GSFNHPQ | JI.S.10 | GIFVHPQ | JI.S.15 | PKGDENT | | |

It may be that library is biased towards HPQ motifs (streptavidin *is* the control recommended by NEB) and a further screen against another target would provide additional verification, however, to demonstrate sufficient library diversity, NEB provide deep sequencing of their libraries (Table 4).

***Table 4: Phage display library diversity of the variable motif in a NEB Ph.D. C7C library (lot 8).***

| Amino Acid | Codons | Expected Frequency | Observed Frequency | Amino Acid | Codons | Expected Frequency | Observed Frequency |
|---|---|---|---|---|---|---|---|
| Arg | CGK, AGG | 9.4% | 5.59%[1] | Asp | GAT | 3.1% | 3.95% |
| Leu | CTK, TTG | 9.4% | 8.53% | Cys | TGT | 3.1% | 0.59%[1] |
| Ser | TCK, AGT | 9.4% | 10.44% | Glu | GAG | 3.1% | 3.45% |
| Ala | GCK | 6.2% | 5.28% | His | CAT | 3.1% | 4.98% |
| Gly | GGK | 6.2% | 4.22% | Ile | ATT | 3.1% | 3.16% |
| Pro | CCK | 6.2% | 6.97% | Lys | AAG | 3.1% | 5.13% |
| Thr | ACK | 6.2% | 9.45% | Met | ATG | 3.1% | 4.27% |
| Gln | CAG, TAG[2] | 6.2% | 5.31% | Phe | TTT | 3.1% | 1.94% |
| Val | GTK | 6.2% | 4.18% | Trp | TGG | 3.1% | 2.18% |
| Asn | AAT | 3.1% | 6.75% | Tyr | TAT | 3.1% | 3.64% |

*Table 4[1]: Arginine and cysteine are underrepresented in the randomised sequence, as they interfere with secretion of pIII and phage infectivity.*

*Table 4[2]: The ER2738 E. coli used to express this library contains the amber codon suppressor mutation glnV, therefore TAG encodes glutamine instead of the amber stop codon.*

That the control screen successfully pulled down HPQ motifs and the library is sufficiently diverse signifies that correct phage display technique has been achieved. Subsequent βNGF or mBDNF screens should pull down relevant phage.

#### 3.1.1.1 βNGF and mBDNF Phage Display Pans 1-3

Four phage display screens were performed concurrently against human βNGF and human mBDNF (Peprotech, catalogue numbers 450-01 and 450-02), following the above protocol but with 100 µL of 30 µg/mL neurotrophin per well and no target added in the blocking step. Binding phage were eluted with a low pH buffer (pH 2.2) rather than biotin.

Two screens were performed as described by the above protocol (target screens), however two screens were performed following a variant method which was intended to bias the library against either βNGF of mBDNF, such that the resulting peptides would be specific between the two (anti-target screens). In the case of the anti-BDNF βNGF screen

(attempting to identify phages which bound preferentially to βNGF over mBDNF), well 1 was treated with mBDNF and the library was added and incubated. During this time, any mBDNF-binding phage should have been sequestered from solution. The remaining unbound library was aspirated away and used in a well-treated with βNGF for a standard panning method. The inverse was used for the anti-βNGF BDNF screen.

After the third round of panning, twenty phages were isolated and sequenced from each screen. The sequences of their variable motifs are as follows:

***Table 5: Pan 3 N-terminal pIII peptide motifs sequenced from βNGF and mBDNF binding phage.***

| βNGF Screen | | mBDNF Screen | | anti-BDNF βNGF Screen | | anti-βNGF mBDNF Screen | |
|---|---|---|---|---|---|---|---|
| Code | X7 Region | Code | X7 Region | Code | X7 Region | Code | X7 Region |
| JI.3.1 | FTSMFWN | JI.3.21 | LYMAHPQ | JI.3.41 | WQARIMN | JI.3.61 | KDLNQMR |
| JI.3.2 | GSSTYYF | JI.3.22 | MRNLTHM | JI.3.42 | TYPVMAW | JI.3.62 | KSYDSWA |
| JI.3.3 | NAGHLSQ | JI.3.23 | DRDMTPD | JI.3.43 | YTYFPWP | JI.3.63 | KLATHIS |
| JI.3.4 | PPWYWSF | JI.3.24 | FLSTLFE | JI.3.44 | WNIHWWT | JI.3.64 | MTWTLHH |
| JI.3.5 | SPLNRLY | JI.3.25 | WMPWYHT | JI.3.45 | VPSKPGL | JI.3.65 | VFAWPFN |
| JI.3.6 | PRMSHMY | JI.3.26 | WLGWHYW | JI.3.46 | WWDPDHN | JI.3.66 | EEVKPRL |
| JI.3.7 | VTLMRSE | JI.3.27 | YWPLWYH | JI.3.47 | MWTGQTT | JI.3.68 | YSGHLEV |
| JI.3.8 | QWPQMPQ | JI.3.28 | WSLWNHI | JI.3.49 | YAGLLKY | JI.3.69 | YIRETFE |
| JI.3.9 | NASYFWQ | JI.3.29 | ISSVVVS | JI.3.50 | HNKNSLK | JI.3.70 | YHWWLHA |
| JI.3.10 | NKQWTAR | JI.3.30 | SWLHWWQ | JI.3.51 | HFEWFME | JI.3.71 | TTPQLNK |
| JI.3.11 | HSLNHLS | JI.3.31 | WLNRNSN | JI.3.52 | YAGPWYT | JI.3.72 | MIWGTDD |
| JI.3.12 | LQRYLHS | JI.3.32 | PWFFYQG | JI.3.53 | TPMGPNL | JI.3.73 | YSRNLNY |
| JI.3.13 | VKLWTQQ | JI.3.34 | MMHWDWA | JI.3.54 | HWWEAVL | JI.3.74 | QAYHKRV |
| JI.3.14 | HETPTPA | JI.3.35 | WLGWHYW | JI.3.55 | WSGLDWL | JI.3.75 | TNWATLD |
| JI.3.15 | NWLRSTS | JI.3.36 | YTGTGMQ | JI.3.56 | GHKTSLS | JI.3.76 | YSFRSTE |
| JI.3.16 | WMPWWGS | JI.3.37 | QNNMTQT | JI.3.57 | RLNTTSY | JI.3.77 | NNQFWTW |
| JI.3.17 | LKTQLGK | JI.3.38 | HNHSVAV | JI.3.58 | QNFKYMI | JI.3.78 | RMTAPSS |
| JI.3.18 | IGTSVPN | JI.3.39 | WLPWDRS | JI.3.60 | LSWSFLW | JI.3.79 | NRPGVER |
| JI.3.19 | GLQEGPR | JI.3.40 | TWWLPFP | | | JI.3.80 | GTLHWNK |
| JI.3.20 | QMKTPHM | | | | | | |

Sequencing failed for four phages (5%). This may be due to the fragility of the ssDNA or spontaneous mutations, and was not repeated due to the reasons outlined below:

Ideally these four screens would each identify common, repeated motifs with variations. Such hits would indicate that the most common sequence was the most successful peptide for that screen, and variants are other permitted sequences. A lack of common, repeated motifs indicates that panning had not yet identified the strongest binding peptide motifs: there may have been insufficient competition between phages, and/or too many target binding sites per well. It may be that non-specific binding phage were surviving the panning cycles, however this goes against the positive streptavidin control screen. In fact, only one sequence (mBDNF: WLGWHYW) is repeated at all, and the high tryptophan content suggests that it is a classic plastic binder.[163] Further panning using more stringent conditions (i.e. increasing the competition between phages and decreasing the number of phage binding sites) was therefore necessary to identify the best binders. Prior to further screens however, the phages identified by pan 3 were assessed for specificity of target over support. If the latter was evident then the phages identified should be disregarded and other means for phage display would have been attempted (e.g. solution based panning using resin supports).

#### 3.1.1.2 Pan 3 Phage Binding ELISA

To test whether the identified phage was selective for βNGF or mBDNF over the solid support and ancillary proteins, a colourimetric ELISA was developed. This involved creating duplicate wells on a high-binding plate, whose only difference was the presence or absence of βNGF or mBDNF. An Anti-M13 monoclonal antibody is then used to ascertain whether phage have been retained, an overview of this technique is shown in Figure 43.

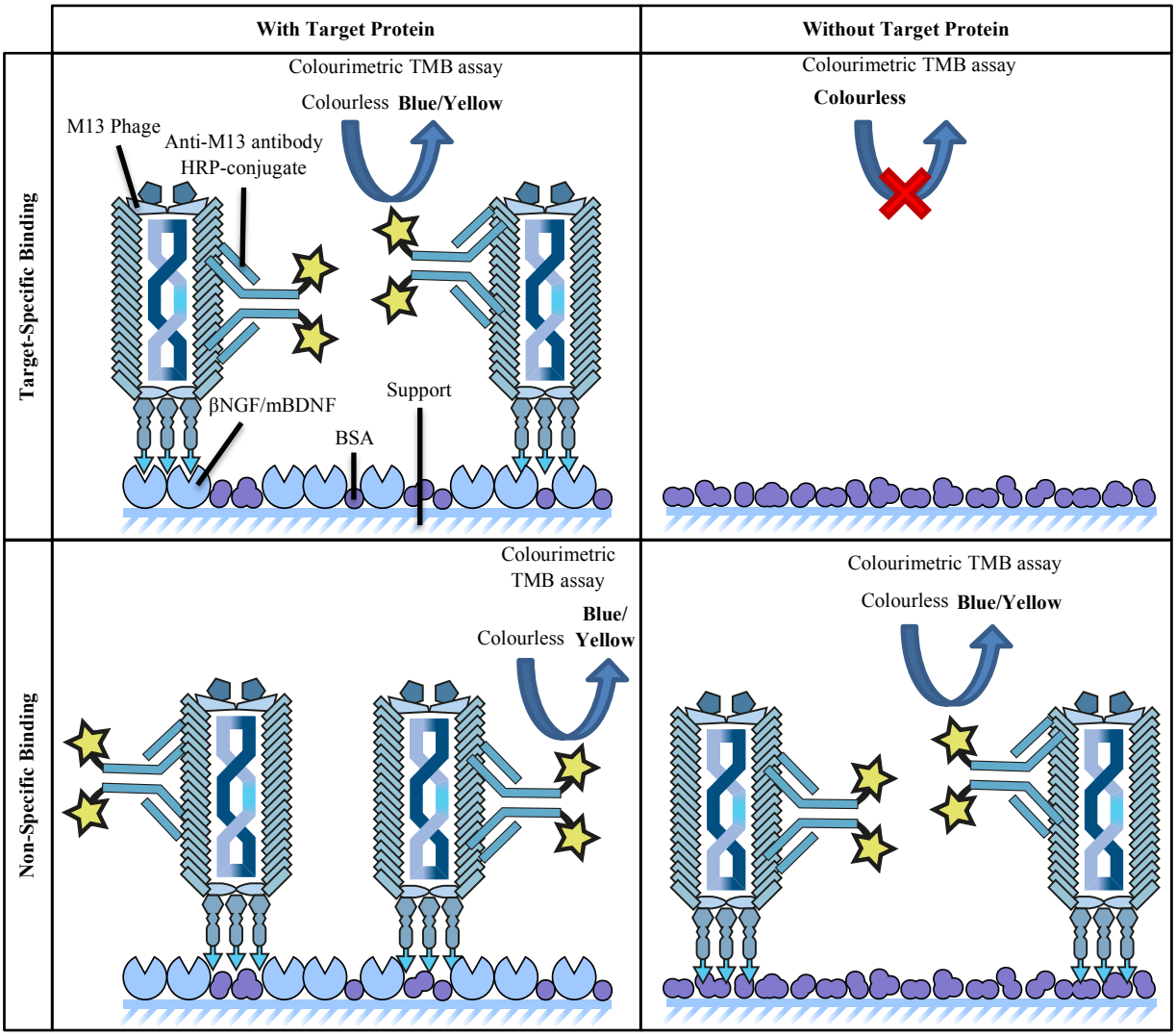



***Figure 43: Phage target specificity assay to check for artefact binding.***

The protocol used to create this assay was based on but deviated from NEB manual E8120. The NEB protocol suggests a phage-titred ELISA with 12 wells per phage, 100-200 µL of 100 µg/mL protein target per well. As stated, the human βNGF and mBDNF used in the panning steps were purchased (Peprotech™, catalogue numbers 450-01 and 450-02): following the NEB protocol would require prohibitive amounts of mBDNF per phage per repeat. As such, , the protein concentration used in these assays was optimised and a range of protein concentrations were explored.

Prior to the commencement of the phage ELISA, the buffer systems used must be explored: if βNGF or mBDNF unfold or misfold in the buffers used then they will be far more adhesive than the native state, and any phages which bind to them are not useful. Protein stability in solution may be measured by thermal shift assay, which involves dissolving the protein of interest in several buffers, some containing stabilising agents,

some with surfactants (0.5% Tween-20). These were then mixed with SYPRO Orange dye (ThermoFisher Scientific, catalogue number S6650),[164] this fluorescent dye undergoes a significant increase in quantum yield upon binding to hydrophobic regions in denatured proteins, and its excitation/emission can be measured using qPCR instrumentation.

Therefore, to assess protein folding stability, the samples of neurotrophin and SYPRO Orange in various buffers are gradually heated. Upon protein unfolding the fluorescence of SYPRO Orange significantly increases. If buffers (HEPES, Tris, PBS) and additives (±274 mM NaCl, ±10% v/v glycerol) affect neurotrophin stability the unfolding transition point shifts. All buffers were prepared to have pH ~7.4, however this was adjusted as needed with 500 mM NaOH or HCl.

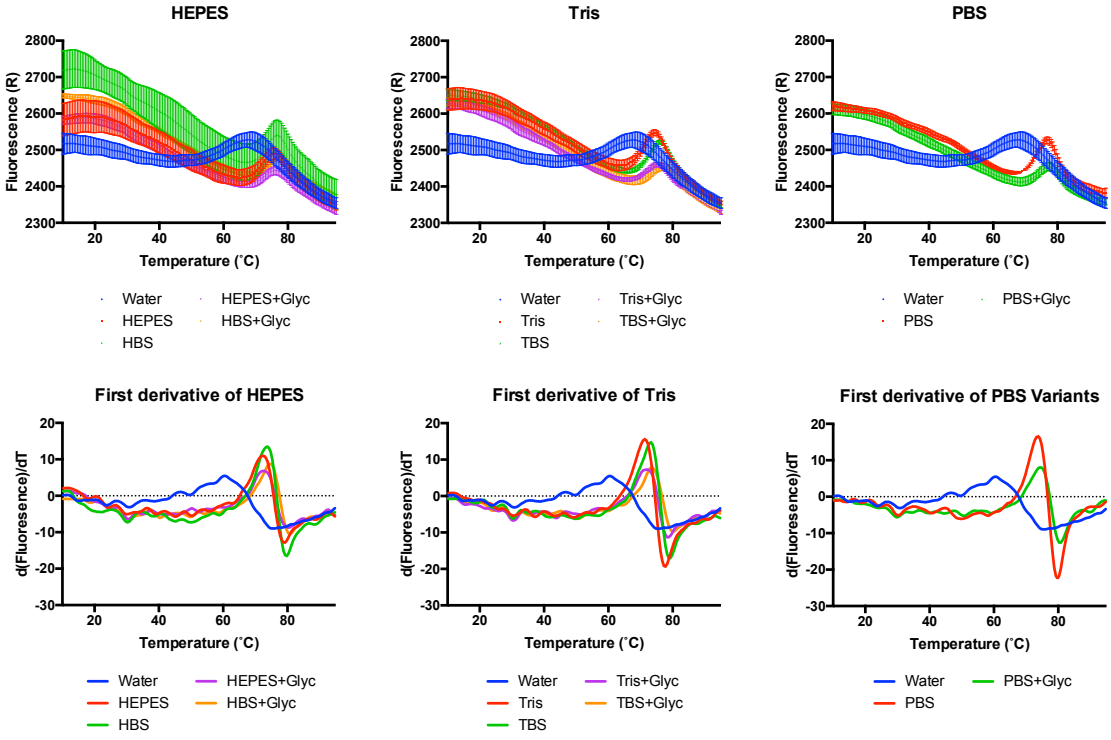



**Figure 44: Thermal shift of βNGF in a variety of buffers.**

***Table 6: Thermal shift assay summary of βNGF melting points in various buffers.***

| Buffer System | βNGF Tm (˚C) | Buffer System | βNGF Tm (˚C) |
|---|---|---|---|
| Water | 60.25 | TBS | 73.25 |
| HEPES | 72.25 | Tris+Glyc | 72.25 |
| HBS | 73.75 | TBS+Glyc | 73.25 |
| HEPES+Glyc | 72.75 | PBS | 73.75 |
| HBS+Glyc | 74.75 | PBS+Glyc | 74.25 |
| Tris | 71.25 | | |

As expected, Table 6 indicates that βNGF is significantly more stable in all of the buffers tested compared to distilled water, and that both NaCl and glycerol improve stability. HBS with glycerol offers the highest βNGF melting point and therefore, stability. PBS with glycerol is a close second, and as creating PBS is far more consistent (using Sigma Aldrich PBS tablets, catalogue number 79382) than HBS (combining out 5 ingredients), PBS with glycerol (PBSG) was used in all future assays. Arguably thermal shift should have been conducted prior to commencing βNGF and mBDNF phage display, however TBS is close to PBS and so the effects of using TBS should be minimal. PBS with Tween-20 (0.5%) and glycerol (10% v/v) was therefore used in a phage binding assay to investigate suitable neurotrophin concentrations for future phage binding assays:

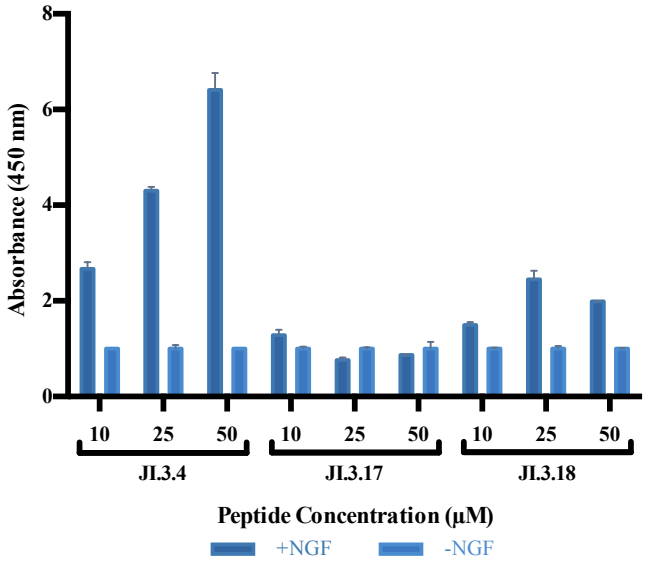
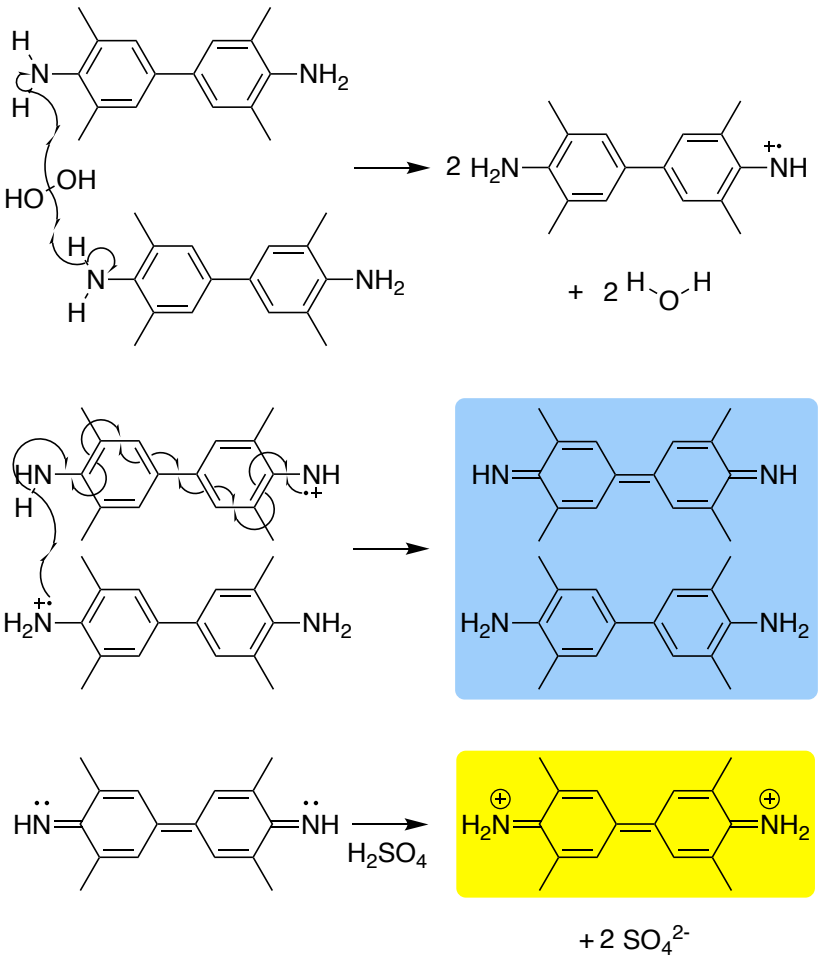



***Figure 45: Phage binding ELISA for varying βNGF concentrations.*** *Mean ± SD n=2, normalised to untreated mean.*

To assess the minimum neurotrophin concentration required to screen phage specificity by ELISA, an optimisation assay was conducted to screen a range of concentrations. Briefly, three phages were randomly selected from the βNGF target screen: JI.3.4, JI.3.17 and JI.3.18 ($X_7$ sequences: PPWYWSF, LKTQLGK, and IGTSVPN, respectively). For each phage to be tested, two wells of a 96-well Greiner Microlon® plate were treated with 25 µL of βNGF at 10, 25 or 50 µg/mL, and two wells were left untreated. The plate was incubated overnight with agitation, then all wells were blocked with a solution of BSA. Plates were incubated, washed, treated with phage at $1x10^{14}$ pfu/well (the concentration recommended by NEB manual E8120) and incubated to permit phage binding. Following

incubation, plates were washed to remove unbound phage, treated with antiM13-HRP conjugate (GE Healthcare #27-9421-0) and incubated. AntiM13-HRP is an anti-pVIII monoclonal antibody conjugated with a horseradish peroxidase (HRP) enzyme and should therefore bind to any remaining M13 phage bound to the plate. The plate was washed again to remove unbound antiM13-HRP. The relative presence of phage was visualised by the addition of Thermo Scientific Pierce 1-Step Ultra TMB ELISA Substrate: if the phages are bound to the plate, the HRP catalyses radical hydrogen peroxide cleavage, which (as shown in Scheme 1) reacts with 3,3',5,5'-tetramethylbenzidine (TMB) to form a blue charge transfer complex. Following incubation, the reaction was stopped by addition of concentrated $H_2SO_4$. This unfolds and deactivates the HRP and stabilises the charge transfer complex into yellow 3,3',5,5'-tetramethylbenzidine diimine, which prevents the reaction from proceeding further. Wells were then tested for absorbance at 450 nm, inferring the relative quantity of phages retained.




***Scheme 1: TMB colourimetric assay reaction.***[165]

As shown in Figure 45, phage binding to plate strongly correlates with increasing βNGF concentrations, and JI.3.4 and JI.3.18 are selective between the βNGF treated wells over the βNGF untreated wells. This suggests that those phages are selective to target over plate/ancillary protein. 25 µL at 25 µM/well neurotrophin was therefore used in all subsequent ELISAs as it gives a good signal to noise window. As stated, phages were selected for this test at random, yet happen to show broad structural differences: $X_7$ sequences: JI.3.4: PPWYWSF, JI.3.17: LKTQLGK, JI.3.18: IGTSVPN), representing high, low and medium lipophilicity. This is also the order of binding strength and selectivity shown in Figure 45, suggesting that the neurotrophins may be quite lipophilic. Phage binding to untreated wells shows no relationship to $X_7$ lipophilicity.

As it was already decided that further phage display pans were required to concentrate on key binding sequences, screening all phages for binding was not necessary. To that end, a quarter of all phages (chosen by random number generation) isolated during Pan 3 were tested by ELISA for binding to their respective target versus binding to the plate:

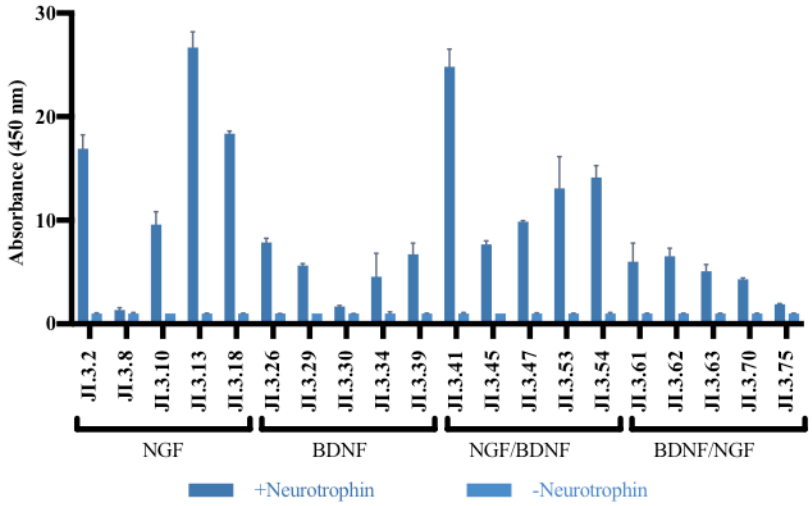



***Figure 46: Selectivity of phage binding to neurotrophin treated or untreated well.*** *Mean ± SD, n=2, normalised to the untreated mean.*

Figure 46 indicates that most phages are highly selective for their neurotrophin over untreated wells, with the exception of JI.3.8, JI.3.30 and JI.3.75 ($X_7$ sequences: QWPQMPQ, SWLHWWQ and TNWATLD respectively) which show either poor binding and poor selectivity. Phages JI.3.2, JI.3.13 and JI.3.41 ($X_7$ sequences: GSSTYYF, VKLWTQQ, and WQARIMN respectively) however show promising selectivity. From this experiment, we can infer that the surface panning procedure used to isolate these

phages has been successful in avoiding non-selective phage, but further panning is required to identify consensus motifs.

#### 3.1.1.3 βNGF and mBDNF Phage Display Pans 4-5

While conducting further rounds of screening is important to identify the strongest binding phage, it has a caveat: over-panning reduces the utility/fidelity of hits for a number of reasons. Firstly, while phage display identifies peptides which bind to the target, it does not screen for inhibitory activity. Over-panning may pull out very strong binders with no inhibitory activity whatsoever and occlude weaker binding peptides with inhibitory properties, e.g. the binding site capable of forming the strongest interaction with any $CX_7C$ peptide may be entirely removed from the neurotrophin surface used to bind its receptor.

Secondly, phage display applies several selection pressures to the phages it isolates, not simply identifying peptides which bind to the target. As stated, false positives include peptide sequences which show affinity for non-target surfaces, such as the solid support (e.g. plastic or affinity beads) or the blocking protein used (e.g. BSA). Plastic binders typically present with high aromaticity (e.g. F, W, H, Y), particularly WXXW, FHXXW, WXW[163] Albumin weakly binds various molecules, for example a study of phage display binding against several species of albumins produced the consensus sequence DICLPRWGCLW.[166] To that end, off-target binders may be identified by ELISA using target-present and target-absent wells.

Finally, over-panning causes overrepresentation of peptide sequences which increase rate of phage replication: the principal role of pIII (the virus coat protein modified to add the variable library) is that of binding to *E. coli* protein TolA on the bacterial F pilus. This allows the virion to access and egress bacteria, thus allowing the phage to replicate. As such, randomising part of pIII changes the rate or ability of a virion to infect or be secreted from a host. This variability of infection/secretion rate results in a bias to the library and therefore two selection pressures are present during phage display – affinity for target and rate of replication during amplification. “Parasitic sequences” allow rapid replication and any peptides resulting from this research will be examined for such sequences. One method of avoiding parasitic sequences is amplification in emulsions, which may be employed if only such sequences result.[167]

A panning balance between identifying strong binders and over-panning was therefore sought, and two further pans were conducted for all four screens (βNGF, mBDNF,

βNGF/mBDNF, mBDNF/βNGF). Stringency was increased by decreasing target concentration from 100 µL of 30 µg/mL to 100 µL of 10 µg/mL, doubling the phage binding time from 45 minutes to 1.5 h, increasing phage count per screen from $1x10^{11}$ to $1x10^{12}$ pfu/well, and finally the duration and agitation of wash steps was increased. Fewer targets and more phage increase competition for binding sites, longer binding and more rigorous washing should result in an improved thermodynamic equilibrium, where stronger binding phage outcompete weaker binding phage.

Pans 4 and 5 were completed for the four screens using the above conditions. Library phage were picked, stored and sequenced, providing the following randomised sequences in the variable loop on phage protein pIII:

***Table 7: Pan 5 N-terminal pIII peptide motifs sequenced from βNGF and mBDNF binding phage.*** *# indicates number of duplicates observed.*

| βNGF Screen | | | mBDNF Screen | | | anti-BDNF βNGF Screen | | | anti-βNGF mBDNF Screen | | |
|---|---|---|---|---|---|---|---|---|---|---|---|
| Code | X7 Region | # | Code | X7 Region | # | Code | X7 Region | # | Code | X7 Region | # |
| JI.5.1 | QHWPWFS | 11 | JI.5.21 | GSAPVRS | | JI.5.41 | PSTVPWS | | JI.5.62 | NPHFYKH | |
| JI.5.5 | GPGTLRV | | JI.5.23 | HMAFKKI | | JI.5.43 | NSFNSGS | 2 | JI.5.64 | NFGSPDQ | |
| JI.5.12 | WTIYLMP | | JI.5.24 | KNIVAPW | | JI.5.44 | NSHRHGA | | JI.5.71 | SGLTRPT | |
| JI.5.13 | SLFSKNY | 7 | JI.5.25 | DPHWPFN | | JI.5.52 | SLNHTVN | | JI.5.72 | YTERTKL | |
| JI.5.14 | GRYMDGG | | JI.5.27 | TMGLTHS | | JI.5.55 | FYKWHSH | | JI.5.73 | NAGHRSQ | |
| JI.5.15 | ENKHTWG | | JI.5.33 | SWLHWWQ | | JI.5.56 | YSNATGS | | | | |
| JI.5.20 | SHIDTQW | | JI.5.36 | GSKINQY | | JI.5.57 | QMNNSDF | | | | |
| | | | JI.5.37 | NAGHLSQ | 9 | JI.5.58 | YELTPGK | | | | |
| | | | JI.5.40 | SLSRLPS | | | | | | | |

As intended, these show several repeats and a number of families/motifs:

***Table 8: $ACX_7CG_3S$ groups identified by ClustalO sequence similarity ranking.[161-162]***

| $X_7$ Group 1 | $X_7$ Group 2 | $X_7$ Group 3 | $X_7$ Group 4 | $X_7$ Group 5 | $X_7$ Group 6 | $X_7$ Misc. |
|---|---|---|---|---|---|---|
| QHWPWFS x11 | SLFSKNY x7 | NAGHLSQ x9 | GSKINQY | YSNATGS | NPHFYKH | WTIYLMP |
| DPHWPFN | SLSRLPS | NFGSPDQ x2 | GSAPVRS | YTERTKL | FYKWHSH | HMAFKKI |
| PSTVPWS | SLNHTVN | NAGHRSQ | GRYMDGG | YELTPGK | ENKHTWG | SHIDTQW |
| KNIVAPW | SGLTRPT | NSHRHGA | GPGTLRV | | | TMGLTHS |
| SWLHWWQ | | NSFNSGS | | | | QMNNSDF |

Interestingly, while JI.5.1 was found only in the βNGF screen, the motif shown in JI.5.13 was found across all four screens, indicating that it is nonspecific. Concerning specificity, the hit peptide sequences were grouped into six groups (and miscellaneous). All of these groups contained sequences from at least two groups, indicating that either none of the motifs identified are βNGF of mBDNF specific in themselves (and if these are specific, that specificity is found in subtle differences), or that the screens themselves were nonspecific between βNGF and mBDNF. If it was the latter, this was to be expected with the target screens, however the anti-target screens were intended to identify some elements of specificity. If this is the case, it may be due to the ratio of targets to the number of phages. For example, in the anti-mBDNF βNGF screen, if there were more mBDNF-binding phage in the library than numbers of mBDNF molecules, not all mBDNF-binding phage would have been sequestered during anti-target screening. For future screens it may be necessary for the anti-target screens to be conducted at higher target concentration. Whether any peptide was specific between βNGF and mBDNF would be seen in later assays.

Concerning whether these phages were identified by design or by random chance, the incidence of each amino acid in the $X_7$ domain of the peptides shown in Table 7 was compared with the observed unbiased library incidence of Table 4, as shown in Table 9:

***Table 9: Observed incidence of amino acids in hit phage variable region, compared with that of the initial unbiased library***

| Amino Acid | Number of Observations | Calculated Observations (%) | Unbiased Library Observations (%) | Observed Frequency (%) | Difference (%) |
|---|---|---|---|---|---|
| Arg | 22 | 9.4 | 5.59 | 4.14 | -1.45 |
| Leu | 18 | 9.4 | 8.53 | 3.38 | -5.15 |
| Ser | 42 | 9.4 | 10.44 | 7.89 | -2.55 |
| Ala | 19 | 6.2 | 5.28 | 3.57 | -1.71 |
| Gly | 23 | 6.2 | 4.22 | 4.32 | 0.10 |
| Pro | 34 | 6.2 | 6.97 | 6.39 | -0.58 |
| Thr | 44 | 6.2 | 9.45 | 8.27 | -1.18 |
| Gln | 13 | 6.2 | 5.31 | 2.44 | -2.87 |
| Val | 16 | 6.2 | 4.18 | 3.01 | -1.17 |
| Asn | 14 | 3.1 | 6.75 | 2.63 | -4.12 |
| Asp | 34 | 3.1 | 3.95 | 6.39 | 2.44 |
| Cys | 0 | 3.1 | 0.59 | 0.00 | -0.59 |
| Glu | 25 | 3.1 | 3.45 | 4.70 | 1.25 |
| His | 32 | 3.1 | 4.98 | 6.02 | 1.04 |
| Ile | 9 | 3.1 | 3.16 | 1.69 | -1.47 |
| Lys | 47 | 3.1 | 5.13 | 8.83 | 3.70 |
| Met | 27 | 3.1 | 4.27 | 5.08 | 0.81 |
| Phe | 20 | 3.1 | 1.94 | 3.76 | 1.82 |
| Trp | 61 | 3.1 | 2.18 | 11.47 | 9.29 |
| Tyr | 32 | 3.1 | 3.64 | 6.02 | 2.38 |

This significant deviance from the unbiased library indicates that the phages were not simply identified by chance.

As stated, further pans may increase hit binding strength, but doing so may occlude weaker binding peptides with inhibitory activity. These phages and peptide sequences were therefore taken forward to phage binding ELISA to assess relative binding strength and target selectivity. ELISA was used to rank phages as this is what is recommended in the NEB manual; the technique is straightforward and similar to phage display panning; however it has a high number of steps to the process, which considerably increases the variability of the results. In hindsight fluorescence polarisation may have been a better assay to use: it is far simpler and due to the size disparity of βNGF or mBDNF to an M13 phage, would provide a strong signal to noise ratio.

### 3.1.1.4 Pan 5 Phage Binding ELISA

Phage were amplified to ELISA concentrations (~$1x10^{14}$ pfu/mL recommended by NEB) and tested by ELISA for their affinity for βNGF and mBDNF at $1x10^{11}$ pfu/mL (100 aM).

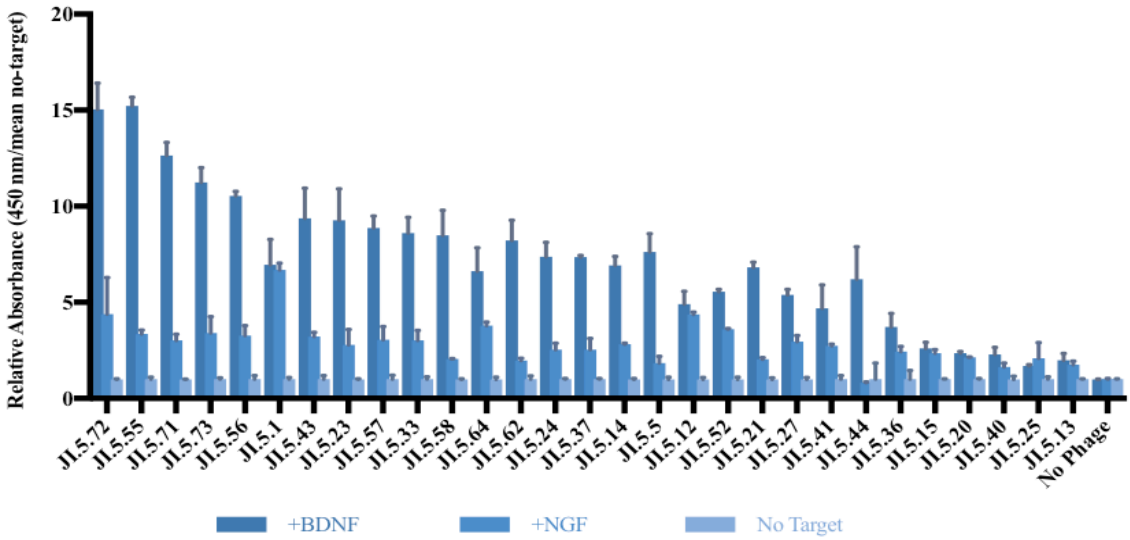



***Figure 47: Graph of pan 5 phage ELISA against mBDNF and βNGF, normalised to untreated mean and ranked by average binding to βNGF and mBDNF.*** *Mean ± SD, n=2.*

ELISA plates were prepared with two wells per phage mBDNF (25 µg/mL, 25 µL per well), two wells βNGF (25 µg/mL, 25 µL per well), two wells untreated. ELISA was conducted at $1x10^{10}$ pfu/mL using GE Healthcare 27942101 HRP/Anti-M13 monoclonal conjugate and TMB (50 µL 1-Step Ultra TMB-ELISA substrate, Thermo Scientific Pierce, quenched with 50 µL 2 M $H_2SO_4$) as a peroxidase assay, and measuring absorbance at 450 nm.

Figure 47 indicates that all phage bind preferentially to βNGF and mBDNF over untreated plate binding, suggesting a successful screen. However, upon amplifying to ELISA concentration, a number of phage isolations (approximately 1/3) showed some white plaques, indicating wild phage contamination as they lack the LacZa gene for the blue/white screen. Despite rigorous cleaning regimens, wild phage contamination is unavoidable when phage display is conducted in an open chemistry/biology lab without appropriate clean-room protocols (e.g. disposable shoe covers). Wild phage contamination may affect the ELISAs and/or the sequencing, therefore purification was undertaken. Wild phages were removed from the affected pools and the phages re-sequenced, and Table 7 was updated for 6 entries (not required for 4). The affected phages were then amplified and the ELISA repeated:

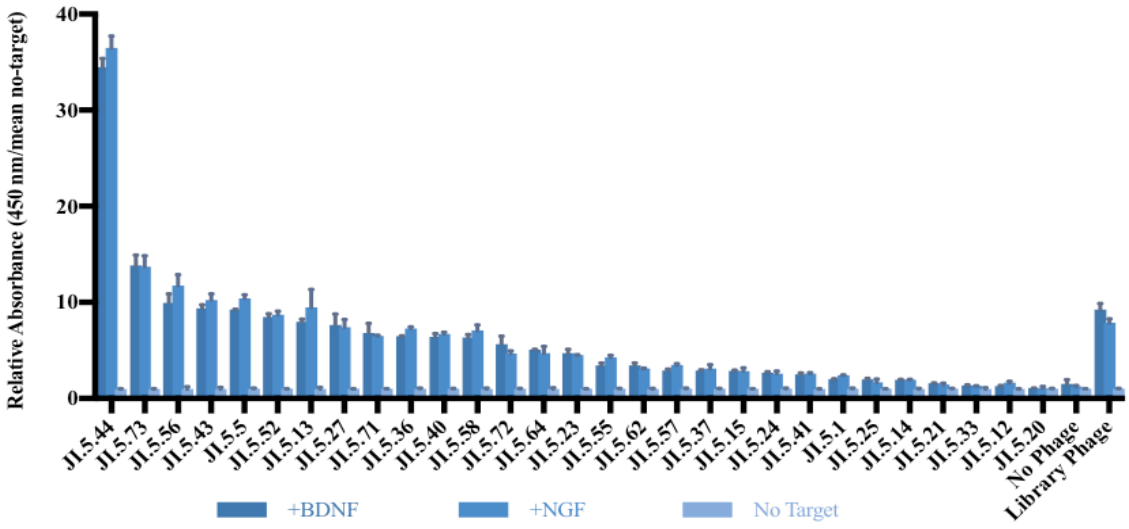



***Figure 48: Graph of pan 5 phage ELISA at 1x10$^{11}$ pfu/mL against mBDNF and βNGF, normalised to non-target binding and ranked by average binding to βNGF and mBDNF.*** *Mean ± SD, n=2.*

Figure 48 indicates that all phages bind preferentially to βNGF and mBDNF over plate. There is some shuffling for position compared with Figure 47, in part due to the removal of wild phage, but also due to the margin for error: the phage are in such high concentration that even with sequential dilution the pipette error will be quite large. A control using wild phage was also attempted, where a white plaque from JI.5.37 was picked, amplified and sequenced. Sequencing returned to show JI.5.37, however titring produced all white phage plaques, indicating a mutation in the LacZa gene. As such, some of the previous contamination may have simply been a mutation, presumably conveying a growth advantage.

The negative control of the unselected ACX$_7$CGGGS library was particularly interesting however: it was assumed that phages which bound to either target to be a rarity, and several rounds of panning was required to identify and amplify strong binders. This ELISA however suggests that while library phage does not bind to untreated wells, binding is nonspecific to either target. To assess whether this issue was systemic, an ELISA using several phages from different screens against several targets was therefore conducted:

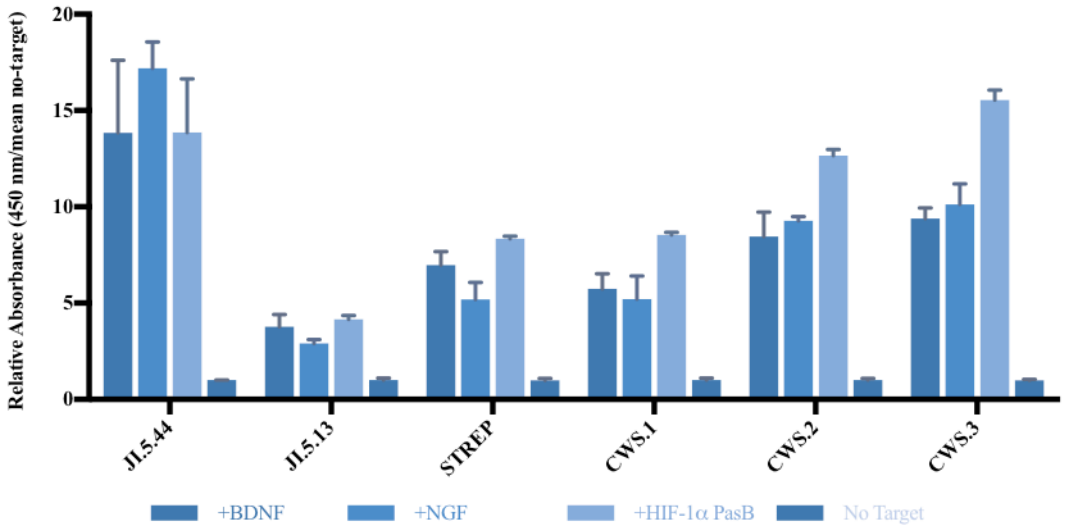



***Figure 49: Graph of phage ELISA at 1x10$^{11}$ pfu/mL against mBDNF, βNGF HIF-2α PasB, normalised to no-target mean.*** *Mean ± SD, n=2.*

The phage from Figure 49 come from various screens: JI.5.44: the highest ranking mBDNF and βNGF binder/no target in the last ELISA, JI.5.13: highest ranking mBDNF/βNGF binder/no target in the last ELISA observed several times during sequencing, STREP: ACGSYVHPQCGGGS, isolated from a control screen against streptavidin, and CWS.1-3 from a phage display screen against HIF-2α PasB conducted in house by C. Shaddick under the supervision of the author. HIF-2α PasB was also expressed and purified by C. Shaddick under the supervision of F. Rowan (unpublished), and has been used as an anti-target control in a number of experiments in this research.

Figure 49 suggests possible ruination for this arm of the project – the phage display may have selected nonsense peptides and/or peptides with high replication rates. To assess whether this is a concentration induced effect and/or if a selectivity window for binding is present, a titred ELISA was conducted using the four highest binders from Figure 48:

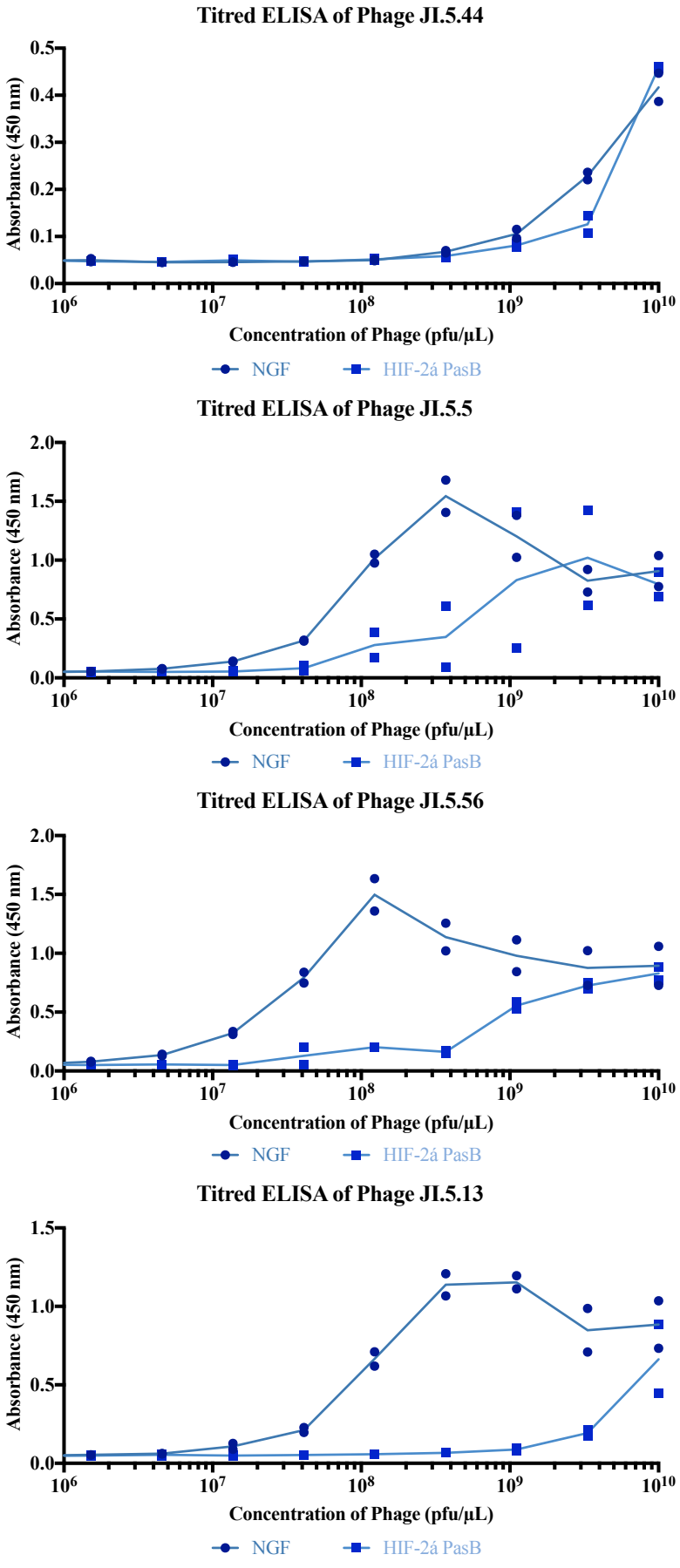



***Figure 50: Titred ELISA of some Pan 5 phage against βNGF and HIF-2α PasB.*** *n=2.*

Figure 50 shows that all phage tested have a significant selectivity binding window between βNGF and HIF-2α PasB. JI.5.5, JI.5.56 and JI.5.13 all peak then decay (an exponentially modified Gaussian distribution, unlike the expected sigmoidal binding curve), this suggests that a concentration-based aggregative effect causes non-specific retention of phage, which caused the binding observed in Figure 48. Interestingly the aggregation effect isn't observed in JI.5.44, which shows weaker binding at lower concentrations than any other phage tested, but higher binding at high concentrations – accounting for the high ranking observed in Figure 48. While there was a concern that these graphs also implied that aggregation occurred during the panning stages, the different binding profiles of these four phages suggest the aggregation is partially sequence-specific, and the panning process has a vast array of sequences. On top of which the ELISAs are conducted in half the volume of pans, at $1x10^{11}$ pfu. To observe binding prior to aggregation effects, the whole pan 5 catalogue was screened by ELISA at $4.6x10^{8}$ pfu/mL (460 zM):

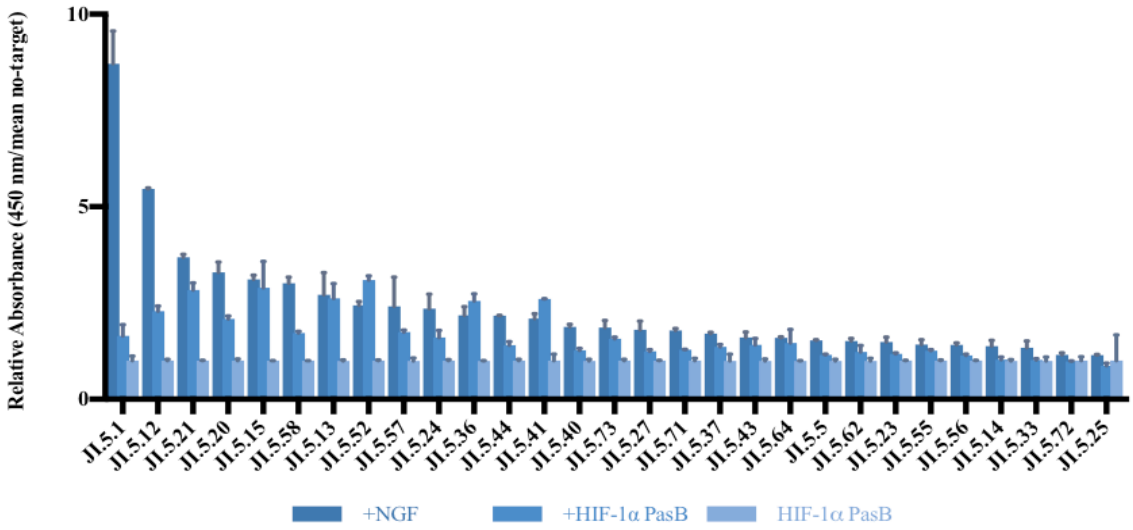



***Figure 51: ELISA of Pan 5 phage against βNGF, HIF-2α PasB or no target, normalised to the mean of the no-target control.*** *n=2.*

Figure 51 highlights a number of particularly interesting peptide sequences with substantial specificity, such as JI.5.1, JI.5.12 and JI.5.58. JI.5.1 was the most frequently observed peptide found during sequencing pan 5, indicating either high binding or a high rate of phage replication (or a combination of the two). Considering the sequence of JI.5.1 (ACQHWPWFSCGGGS) Figure 51 is particularly interesting: the high aromatic content suggests that JI.5.1 is a non-specific plastic binder: plastic binders typically present with high aromaticity: e.g. F, W, H, Y, particularly WXXW, FHXXW, WXW.[163] Figure 51

indicates that JI.5.1 does not bind to the plate (suggesting thorough BSA blocking) and is highly selective between βNGF and the anti-target HIF-2α PasB. It is worth noting however that M13 pIII variable motifs frequently feature an over-representation of proline residues in their peptides.[163, 167-168] This is predominantly because prolines reduce the impact of the variable motif on pIII TolA activity, therefore increasing phage replication rate. Proline is present in 12 of the 30 sequences identified, supporting the idea that no further pans should be conducted. JI.5.12 and JI.5.58, (sequences ACWTIYLMPCGGGS and ACYELTPGKCGGGS) were not selected repeatedly during pan 5, and their binding activity observed in Figure 51 is therefore surprising. This arguably supports further panning so that outlier sequences with strong binding profiles are enriched. As potential parasitic sequences are already emerging, reverting to fresh library stock and conducting ~3 pans entirely using the high stringency protocol may prove more beneficial. However, there is no guarantee that doing so would provide hits any stronger or less parasitic than these.

An experiment which could be added to future phage display screens at this point would be the use of fluorescence polarisation (FP): this is a solution-based binding assay technique that makes use of fact that the degree of polarization of a fluorophore is inversely related to its molecular rotation in solution, when rate of molecular rotation is largely due to size. If, as a fluorophore tumbles in solution it is bound by a significantly larger binding partner then tumbling will decrease significantly. This can be measured as the difference in emission light intensity parallel and perpendicular to the excitation light plane, normalised by the total fluorescence emission intensity.[169] As both βNGF and mBDNF are orders of magnitude smaller than M13 phages, fluorescently labelling the neurotrophins and measuring FP across a range of hit bacteriophage concentrations should provide a strong signal to measure relative phage binding strength in solution.

As stated, the process of phage display screens libraries of phages for their ability to bind to a target. This does not identify peptides capable of target inhibition, and therefore the library of hits cannot be reduced to say JI.5.1 and JI.5.12 for further testing. It is therefore important to screen all hits for their inhibitory activity, as some may show better profiles. Each phage also consists of five copies of pIII, and so each library member's current binding profile (demonstrated by Figure 51) will be modulated to various degrees by the chelate effect. Binding will also be modulated by being fused to pIII, which will affect peptide conformation and orientation. As the intention of this project is to identify small

peptides capable of modulating neurotrophin activity, screening all hits as individual peptides is an important step. As such, 10-20 mg of each peptide was synthesised by WuXi AppTec and confirmed by mass-spec (including disulfide bridge formation). The next step was to develop an inhibition screening platform.

## 3.2 Chapter 3 Conclusions

In this chapter, following a successful positive control screen against streptavidin, phage display was used to screen a library of bacteriophage for the ability of their variable $ACX_7CG_3S$ domain to bind the phage to βNGF or mBDNF. Hit phage were isolated and the ssDNA encoding these variable regions were sequenced and a number of peptide sequences were identified.

To verify that the hit phages were specific to βNGF or mBDNF over the other factors of the screening assay, a specificity assay was developed. This identified a concentration-based specificity issue: at high concentrations, phage binding is non-specific.

Testing across a range of phage concentrations, a concentration was identified at which point a significant selectivity window was identified. All hit phage was then screened for βNGF binding selectivity over either an anti-target or background binding. This identified a number of phage which bound strongly to βNGF over both background and anti-target.

In retrospect, the experiments of this chapter may have been improved by the following: the validity of the resulting hit peptides would have been improved by biasing the library against off-target binders and background artefacts prior to commencing sequencing. This would be achieved by exposing the library to anti-targets and isolating non-binders for use in screening. This technique was omitted as it is not recommended in the NEB manual for the C7C library (Manual E8121). In hindsight however, it may have reduced the number of plastic-binding phages (e.g. those with a high number of tryptophan residues) in the hit phage library, or at least reassured that the presence of tryptophan in hit phages was coincidental.

Secondly, the library of phages was panned five times, at three increasing levels of selection pressures. An increased number of pans biases the resulting library with phages that replicate quickly, the presence of which can be seen in the number of phage with proline residues – a known artefact in pIII M13 bacteriophage screening. An alternative would be to conduct only three pans, replicating the first pan then using the strict

selectivity conditions used in the fourth and fifth pan for the remaining pans. This was not conducted as there was no guarantee that this would produce a different hit phage library.

Finally, there were a number of ELISA assays which would have benefitted from further repetitions/modifications. This is particularly the case for the final full-phage library background selectivity screen, it's a key assay in that it can be used to rank the ability for the phage to be retained in wells, and as such, infers the phage binding strength. The main reason for the lack of repeats and for the lack of a screen against mBDNF was because the relative phage binding strength is of limited value: while it is important to know that the phage binding is selective against background binding, it is relatively inconsequential if a peptide binds *strongly* to βNGF or mBDNF – it is more important that in binding, the peptide is capable of inhibiting neurotrophin-Trk receptor PPIs. As most phages displayed background selectivity and the next stage is to assess inhibitory activity, it was felt that ranking binding to mBDNF was not necessary.

The next step was to create unbound peptides based on the sequenced variable region of the hit phage library. At this point there was no guarantee that peptides which bound to βNGF or mBDNF showed any inhibitory properties of the βNGF-TrkA or mBDNF-TrkB interactions, therefore an assay to investigate the modulatory effect of these peptides had to be developed.

***Table 10: Results from this chapter, ranked by inferred binding affinity in the assay of Figure 51***

| Code | X7 Region | Assays |
|---|---|---|
| JI.5.1 | QHWPWFS | Figure 51: Highly selective between βNGF and HIF2a PasB, very strong binding to βNGF |
| JI.5.12 | WTIYLMP | Figure 51: Highly selective between βNGF and HIF2a PasB, strong binding to βNGF |
| JI.5.21 | GSAPVRS | Figure 51: Selective between βNGF and HIF2a PasB, strong binding to βNGF |
| JI.5.20 | SHIDTQW | Figure 51: Good selectivity between βNGF and HIF2a PasB, strong binding to βNGF |
| JI.5.15 | ENKHTWG | Figure 51: Non-selective between βNGF and HIF2a PasB, strong binding to βNGF |
| JI.5.58 | YELTPGK | Figure 51: Good selectivity between βNGF and HIF2a PasB, strong binding to βNGF |
| JI.5.13 | SLFSKNY | Fig. 48: Selectivity between βNGF and Hif2a PasB at 5x108.<br>Figure 51: Non-selective between βNGF and HIF2a PasB, strong binding to βNGF |
| JI.5.52 | SLNHTVN | Figure 51: Non-selective between βNGF and HIF2a PasB, strong binding to βNGF |
| JI.5.57 | QMNNSDF | Figure 51: Selective between βNGF and HIF2a PasB, strong binding to βNGF |
| JI.5.24 | KNIVAPW | Figure 51: Selective between βNGF and HIF2a PasB, strong binding to βNGF |
| JI.5.36 | GSKINQY | Figure 51: Non-selective between βNGF and HIF2a PasB, strong binding to βNGF |
| JI.5.44 | NSHRHGA | Fig. 48: No selectivity between βNGF and Hif2a PasB.<br>Figure 51: Selective between βNGF and HIF2a PasB, binding to βNGF |
| JI.5.41 | PSTVPWS | Figure 51: Non-selective between βNGF and HIF2a PasB, binding to βNGF |
| JI.5.40 | SLSRLPS | Figure 51: Selective between βNGF and HIF2a PasB, binding to βNGF |
| JI.5.73 | NAGHRSQ | Figure 51: Some selectivity between βNGF and HIF2a PasB, binding to βNGF |
| JI.5.27 | TMGLTHS | Figure 51: Some selectivity between βNGF and HIF2a PasB, binding to βNGF |
| JI.5.71 | SGLTRPT | Figure 51: Some selectivity between βNGF and HIF2a PasB, binding to βNGF |
| JI.5.37 | NAGHLSQ | Figure 51: Some selectivity between βNGF and HIF2a PasB, binding to βNGF |
| JI.5.43 | NSFNSGS | Figure 51: Non-selective between βNGF and HIF2a PasB, binding to βNGF |
| JI.5.64 | NFGSPDQ | Figure 51: Non-selective between βNGF and HIF2a PasB, binding to βNGF |
| JI.5.5 | GPGTLRV | Fig. 48: Selectivity between βNGF and Hif2a PasB at $5x10^8$.<br>Figure 51: Some selectivity between βNGF and HIF2a PasB, binding to βNGF |
| JI.5.62 | NPHFYKH | Figure 51: Some selectivity between βNGF and HIF2a PasB, binding to βNGF |
| JI.5.23 | HMAFKKI | Figure 51: Some selectivity between βNGF and HIF2a PasB, binding to βNGF |
| JI.5.55 | FYKWHSH | Figure 51: Some selectivity between βNGF and HIF2a PasB, binding to βNGF |
| JI.5.56 | YSNATGS | Fig. 48: Selectivity between βNGF and Hif2a PasB at $1x10^8$.<br>Figure 51: Some selectivity between βNGF and HIF2a PasB, binding to βNGF |
| JI.5.14 | GRYMDGG | Figure 51: Some selectivity between βNGF and HIF2a PasB, binding to βNGF |
| JI.5.33 | SWLHWWQ | Figure 51: Some selectivity between βNGF and HIF2a PasB, binding to βNGF |
| JI.5.72 | YTERTKL | Figure 51: Some selectivity between βNGF and HIF2a PasB, binding to βNGF |
| JI.5.25 | DPHWPFN | Figure 51: Near-baseline binding to both βNGF and HIF2a PasB |

# Chapter 4: Screening Identified Peptides for Neurotrophin-Trk PPI Modulatory Activity

## 4.1 Discussion of Suitable Techniques for Investigating PPIs

## 4.2 Two-Component Inhibitory ELISA Development

Screening hit peptides for their ability to inhibit the βNGF to TrkA or mBDNF to TrkB interaction required the development of a suitable assay. It was required to be minimalistic, selective and robust. Searching the literature identified a number of protocols assaying inhibitors of the Trk kinase domains (see Section 1.3.3), however all assays screening for ability to inhibit the neurotrophin-Trk receptor activity used whole cells and either western blot or apoptosis markers, screening for the change in downstream protein activation.[116] This was seen as unfeasible as the cells (e.g. PC12s stably expressing TrkA or TrkB) require a Category 2 containment lab, facilities which weren't available.

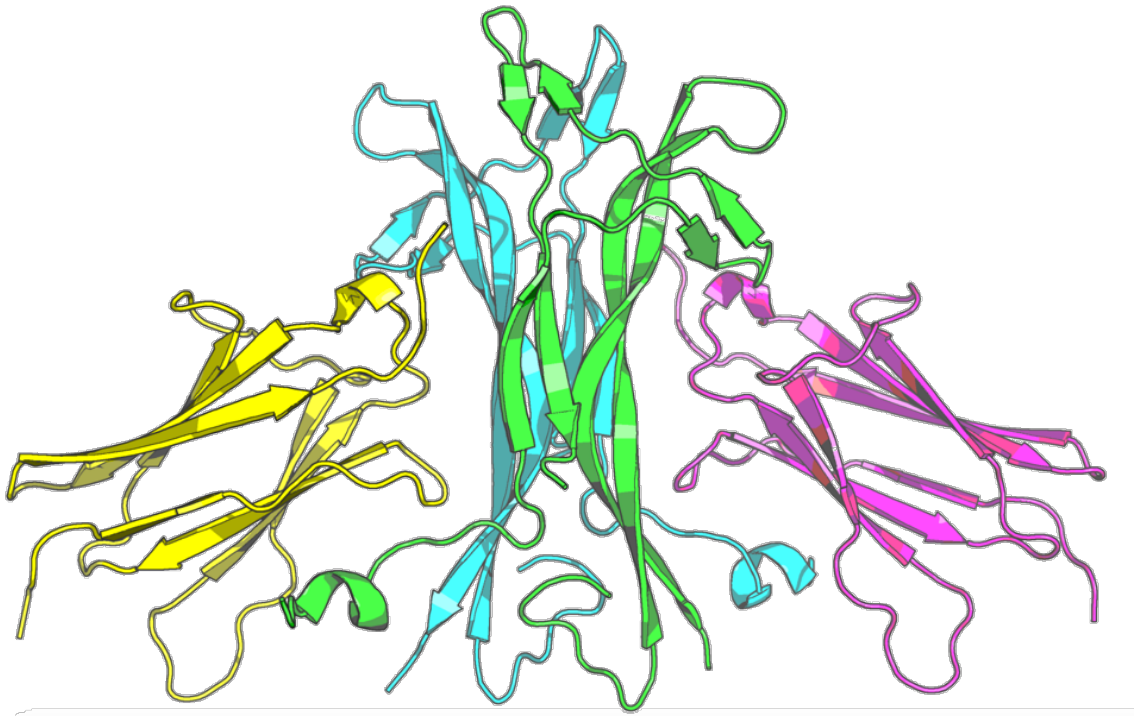


***Figure 52: Crystal structure of βNGF bound by domain 5 of TrkA.*** *RSCB entry 1WWW.*[49]

Developing a novel *in vitro* assay was therefore sought. This was seen as a challenge as both TrkA and TrkB are membrane-bound receptors. While significant advances in isolating membrane-bound proteins have been made, this would add considerable

complexity to this endeavour. Searching the RSCB protein data bank uncovered βNGF bound by the neurotrophin binding domain of TrkA (domain 5), which had been expressed in *E. coli* (Figure 52). By adding tags to the Trk receptors, it was felt that an ELISA assay could be developed:

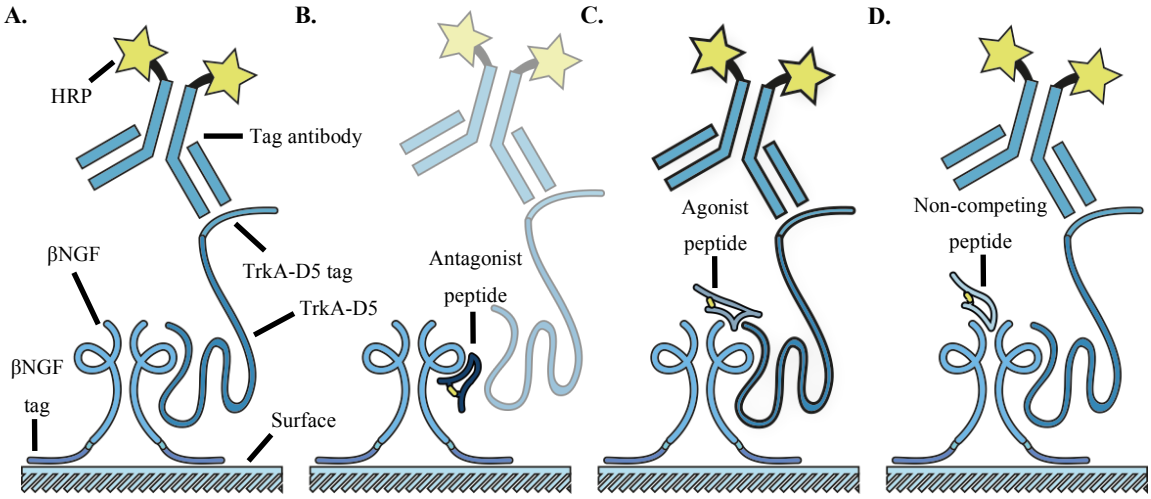



***Figure 53: Overview of the intended two-component ELISA testing for antagonist or agonist peptides.*** *A: positive control, B: antagonist peptide (reduced colour change), C: agonist peptide (increased colour change), D: non-competing peptide (same as positive control).*

To create the inhibitory assay disclosed in Figure 53, the following would need to occur: in cycles of addition, incubation and washing the following are added to a treated plate: 1: tagged βNGF, 2: plate blocking BSA, 3: peptide or blank media (negative control) 4: orthogonally tagged TrkA-D5 and 5: an antibody-colourimetric enzyme conjugate for the tag of TrkA-D5. A colourimetric reaction similar to the phage ELISA is then used to quantify the relative amount of antibody retained.

Other possibilities to the above assay are that the peptide binds to the BSA or plate (tested against a no-neurotrophin control with vs. without peptide) or that that the peptide is a weak binder and is out-competed by TrkA-D5 binding: neither would change the colour output, and if there are other inhibitory peptides with stronger binding profiles then this isn't a concern.

If no inhibitory peptides were identified, decreasing the concentration of TrkA-D5 should reveal the strongest competitive inhibitor. One final possibility is that the peptide either

positively or negatively affects antibody binding to the tagged TrkA-D5. This can be surmounted by changing the tag and antibody, if time permits.

To conclude, development of this assay will require the expression of correctly folded tagged TrkA-D5, TrkB-D5, βNGF and mBDNF. While it is possible to continue using untagged neurotrophin and high-binding polystyrene plates, using tags adds another layer of orthogonality between this assay and the phage ELISA. These and subsequent ELISAs will also use a prodigious amount of protein and as purchased βNGF and mBDNF are very expensive, having an in-house supply should be pursued. The development of methods to create functional expression systems and optimise their isolation and purification for TrkA-D5 and TrkB-D5; and βNGF-$His_6$, OmpA-βNGF-$His_6$, mBDNF-$His_6$ and OmpA-mBDNF-$His_6$ was performed concurrently, but is separated here for ease of comprehension.

### 4.2.1 Expression and Purification of Tagged TrkA-D5 & TrkB-D5

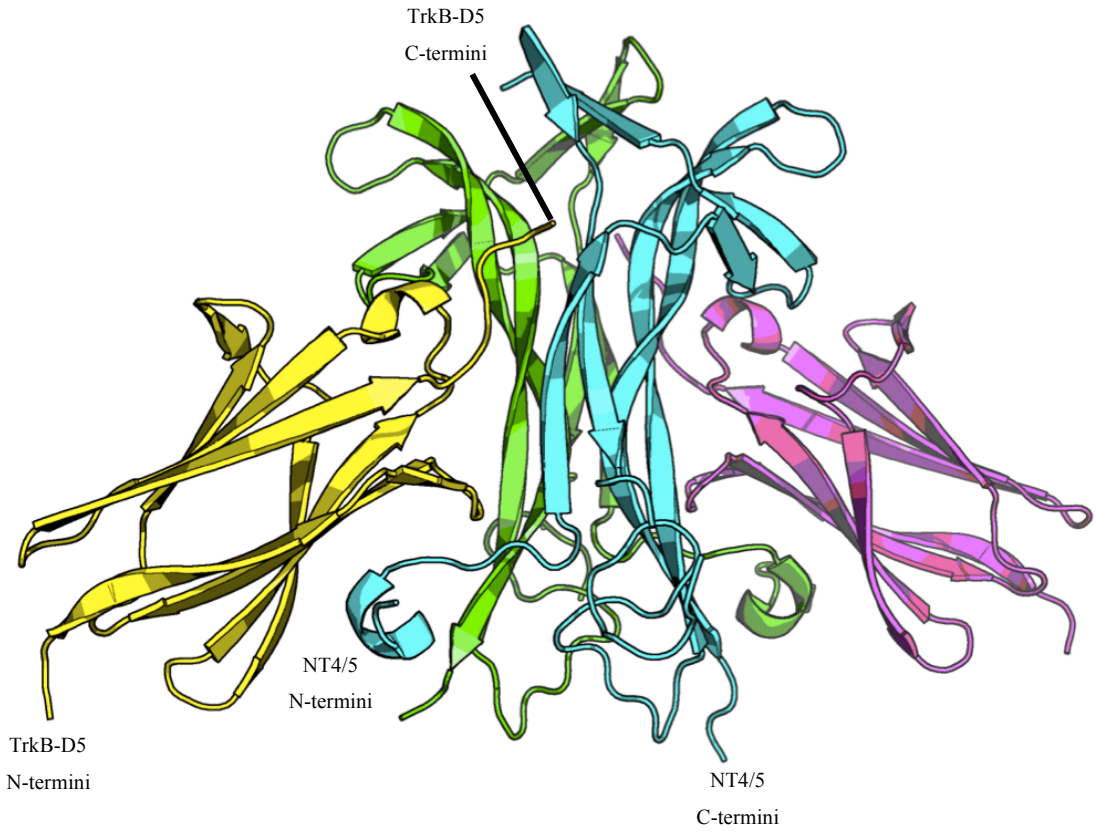



***Figure 54: Crystal structure of TrkB-D5 bound to NT4/5. RSCB PDB entry 1HCF.[170]***

As shown in Figure 54, the N-termini of TrkB-D5 are removed from the neurotrophin binding surface. To clone a tagged version of TrkA-D5 and TrkB-D5, the following was

devised, starting from the N-terminus: a polyhistidine tag, a thrombin cleavage site, a FLAG tag, and either TrkA-D5 or TrkB-D5. Polyhistidine tags ($His_6$, amino acid sequence HHHHHH) are commonly used tags in immobilized metal-affinity chromatography. This takes advantage of the interactions of transition metal ions immobilized on a matrix (commonly $Ni^{2+}$) and certain amino-acid side chains.[171] Histidine is used as the imidazole group has the strongest electron donating group of any amino acid side chain and forms a strong coordinate bond. Peptides and proteins containing consecutive histidine residues are effectively retained on the column matrices and can be later eluted by either adjusting the pH of the column buffer or by the addition of free imidazole to out-compete the protein.[172-173] As polyhistidine tags allow versatile and rapid protein enrichment they were chosen for purifying both Trk and neurotrophin proteins, with the intent of using nickel treated plates for the ELISA. Removal of the TrkA-D5 and TrkB-D5 $His_6$ tags was therefore required to prevent direct binding of Trk proteins to the nickel plate, creating a false-positive response in the ELISA. Therefore a thrombin cleavage site (TCS, amino acid sequence LVPRGS) was added: this motif is selectively cleaved at the R-G bond by the endoprotease thrombin.[174] This allows for the removal of the $His_6$ prior to the ELISA, which may be purified out by size exclusion chromatography. Finally, the FLAG tag (amino acid sequence DYKDDDDK) is an epitope tag.[175] Epitope tags in fusion proteins add the section of an antigen recognised by a readily available antibody to a protein where an antibody isn't available. This allows access to a wide variety of techniques for a fraction of the cost/time of developing a new antibody, or for proteins of low immunogenicity.

The gene block for TrkA-D5 (residues 278-386)[49, 176-177] was optimized for K12 *E. coli* expression and purchased (IDT). This was cloned into the pET28a(+)($His_6$-TCS-FLAG-MCS) under the control of a lac operon using the *NcoI* and *HindIII* restriction sites, and sequence verified. The pET28a(+)($His_6$-TCS-FLAG-MCS) vector was developed in house (A. Ball) from pET28a(+). TrkA-D5 was then replaced with TrkB-D5 (residues 283-385,[49, 178] optimised for K12 *E. coli* expression and purchased from IDT) to create both variants using the *BamHI* and *HindIII* restriction sites, and sequence verified.

Previous efforts to express these proteins in *E. coli* showed a small proportion correctly folded and could be isolated, however the vast majority misfolded and is packaged into inclusion bodies in the insoluble fraction.[49, 177] The misfolded protein cannot be used in assays in this state, and must be denatured by strong chaotropes then refolded through gradual chaotrope reduction: a challenging and time-consuming process. In an effort to

increase the amount of correctly folded TrkA-D5 and TrkB-D5, SHuffle T7 Express *E. coli* cells (NEB catalogue: C3029) were used for expression. These cells allow greater disulfide bond formation in *E. coli*, and it was hoped this and the highly polar $His_6$ and FLAG tags would permit improved solubility and folding. For more information on SHuffle T7 Express cells, see Section 4.2.2.1.

To assess various expression conditions and identify the success of using SHuffle T7 Express cells, a test-expression was performed: the pET28a(+)(TrkA-D5) and pET28a(+)(TrkB-D5) plasmids were chemically transformed into SHuffle T7 Express *E. coli* and expression of TrkA-D5 or TrkB-D5 was induced with IPTG, screening at two concentrations across two temperatures in 10 mL of culture per condition. Cells were then lysed by freeze-thaw and sonication, the proteins separated into soluble and insoluble fractions and thermally denatured in Laemmli buffer before separated by SDS PAGE. Figure 55 indicates that both TrkA-D5 and TrkB-D5 expression can be induced, especially at 1 mM IPTG and 37 ˚C, however the vast majority of expressed protein is still present in the insoluble fraction.

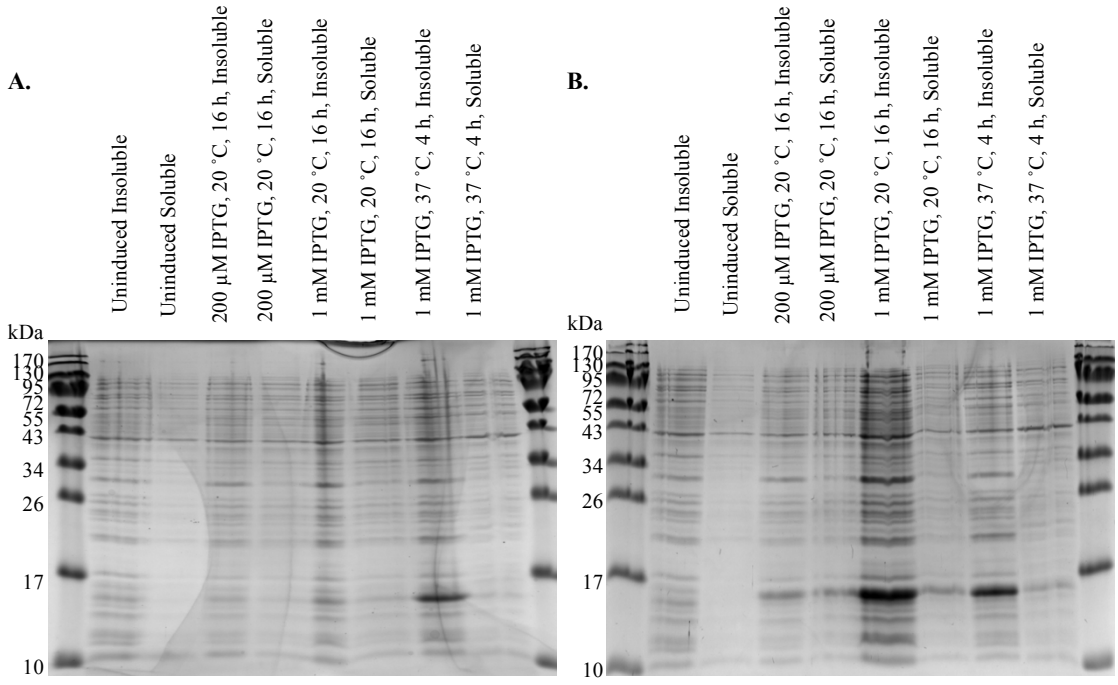



***Figure 55: SDS PAGE of a small-scale test expression of A: TrkA-D5 and B: TrkB-D5 in SHuffle T7 Express E. coli.***

The TrkA-D5 and TrkB-D5 expressed here have the advantage of affinity tags: despite the low proportion of TrkA-D5 and TrkB-D5 expressed in a soluble form, to assess whether

significant enrichment was possible, a mid-scale test was performed, enriching the TrkA-D5 or TrkB-D5 expressed in the soluble fraction by Nickel affinity column chromatography:

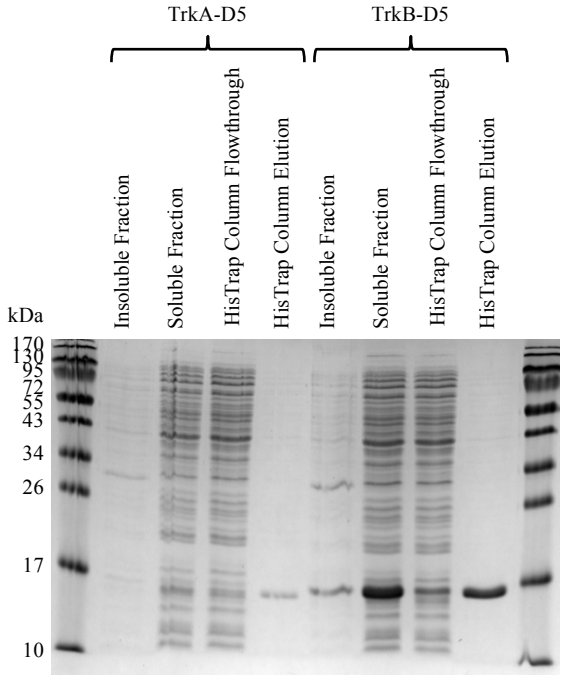



***Figure 56: SDS PAGE of a mid-scale test of TrkA-D5 and TrkB-D5 expression in SHuffle T7 Express, using a HisTrap nickel affinity column to purify.***

Using an 800 mL scale expression of TrkA-D5 and TrkB-D5 in SHuffle T7 Express was conducted. Fusion protein expression was induced after reaching the log growth phase using 1 mM IPTG. The cultures were incubated at 37 ˚C for 4 h before lysis and harvesting as before. A test purification was performed on the soluble protein fraction using a 1 mL GE Healthcare HisTrap FF column.

As shown in Figure 56, the test was a success: soluble TrkA-D5 and TrkB-D5 were isolated and enriched. Significant upscaling was required however as a thrombin cleavage, second HisTrap and a further “polishing” purification step was required to ensure sufficient product, purity and monomeric state: polymeric proteins would be non-functional, size exclusion chromatography allows isolation of monomeric TrkA-D5 and TrkB-D5, as well as removing any other proteins which bound to the HisTrap. Note: the samples in Figure 56 have been thermally and chemically denatured, a non-denatured process would be required to observe polymeric state by SDS PAGE. This mid-scale test expression and HisTrap purification only produced 0.3 and 0.2 mgs of TrkA-D5 and TrkB-D5, which is

insufficient for the further purification required. A 3 L expression at 37 ˚C for 4 h was therefore performed:

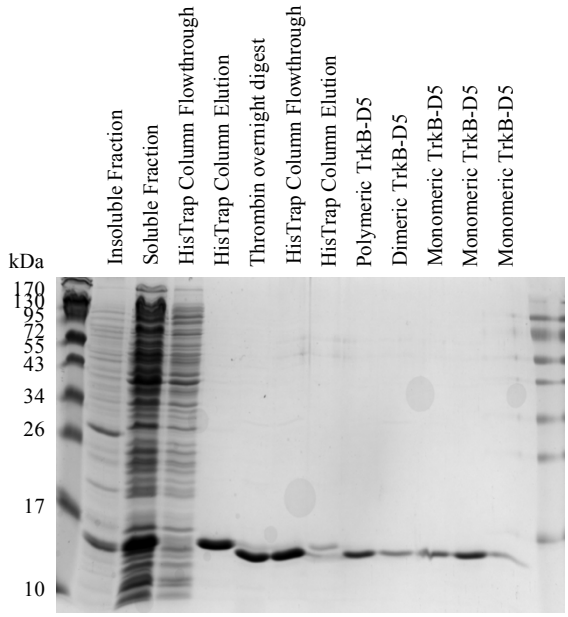



***Figure 57: SDS PAGE of a 3 L TrkB-D5 expression and purification from SHuffle T7 Express cells.***

As shown in Figure 57, the soluble fraction from a lysed 3 L expression of TrkB-D5 in SHuffle T7 Express was passed through a HisTrap nickel column. The bound fraction was eluted from the column by increasing the concentration of imidazole in the eluent, and collected. This was then dialysed into fresh column binding buffer (lowering imidazole from 250 mM to 20 mM) for 2 h at 4 ˚C before the addition of thrombin (whose catalytic activity is inhibited by high concentrations of imidazole) and further incubated overnight at 4 ˚C. Following cleavage, the thrombin, uncleaved protein and any unintended proteins which previously bound to the column were removed by a second pass through a HisTrap column: the cleaved protein now lacks the $His_6$ tag, and therefore passes through without impedance. The mixture is then purified further by size exclusion chromatography, successfully isolating 0.4 mg of cleaved, monomeric TrkB-D5. This is very low considering the extensive testing required for a large range of peptides. Alternative cell lines were therefore investigated, which may be more suited to high expression rates. The pET28a(+) TrkA-D5 and TrkB-D5 plasmids were therefore transformed into BL21 DE3 cells and a small scale test expression conducted, with protein identity further indicated by western blot. To indicate polymeric state, a non-denaturing Laemmli buffer was used

(lacking DTT) the proteins were still thermally denatured however to permit the SDS PAGE to separate by mass.

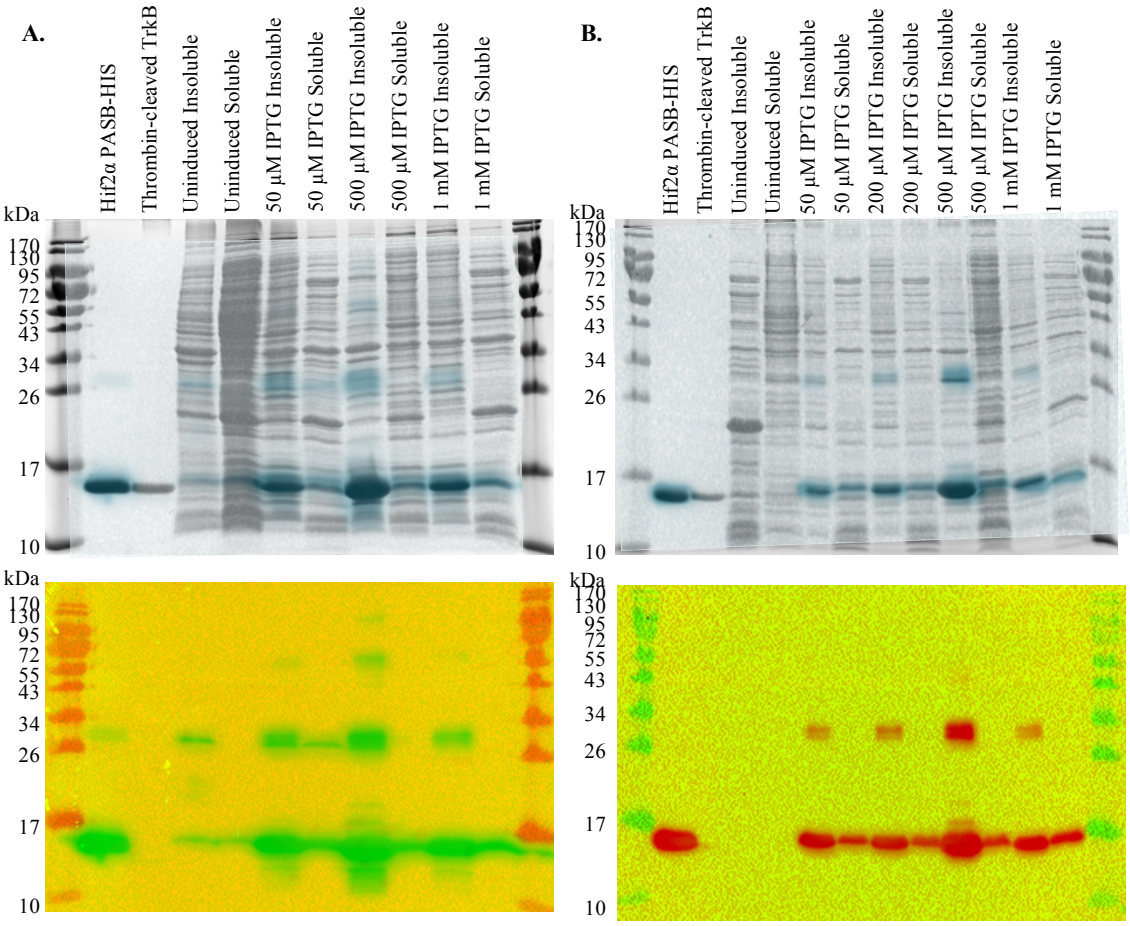



***Figure 58: SDS PAGE of a small-scale test expression of A. TrkA-D5 and B. Anti-His$_6$ western blot.*** *TrkB-D5 in BL21 DE3 E. coli, superimposed with an anti-His$_6$ western blot of a duplicate gel. TrkA-D5: 16.3 kDa, TrkB-D5: 16.0 kDa.*

Despite Figure 55 Indicating that at 37 ˚C SHuffle cells produced more TrkA-D5 and TrkB-D5 than at 20 ˚C, the above BL21 DE3 test expression was conducted at 20 ˚C for 16 h. Current understanding is that expression at lower temperatures permits greater soluble protein production in proteins prone to aggregation. This is thought to be due to slower bacterial replication and translation, therefore a lower metabolic strain of protein overexpression, lowering toxicity and producing more protein overall.

Both Figure 58A and Figure 58B indicated that 500 µM IPTG induction is the optimum for protein expression: 1 mM may prove too toxic and reduce overall yield. These expression conditions were therefore used in all future TrkA-D5 and TrkB-D5 expression. Some leaky

expression was observed in TrkA-D5 expression, which may have caused the reduced expression (compared to TrkB-D5) observed throughout: leaky expression would increase metabolic load unnecessarily during the bacterial logarithmic growth phase.

Also, of interest is the observation of monomeric, dimeric, trimeric and even tetrameric TrkA-D5 and TrkB-D5, even observed in the soluble fraction. As these proteins are chemically but not thermally denatured, this is presumably due to the formation of linking disulfide bridges from the two cysteines present in both Trk proteins. This reiterates the requirement for size-exclusion chromatography, as it is important to isolate monomeric protein.

A soluble fraction isolation of purified, cleaved and monomeric TrkA-D5 and TrkB-D5 from a 1 L expression in BL21 DE3 yielded 0.4 mg and 0.3 mg. Despite doubling the amount of isolated protein per litre of expression, this is still insufficient, therefore a method for purification from the insoluble fraction was sought. Although this has been successfully conducted previously,[49, 177] the addition of the $His_6$ tag and advances in protein purification methodology meant that a novel approach may allow the isolation of TrkA-D5 and TrkB-D5 in higher quantities, rates and purity than previously possible. A protocol was therefore developed, combining two methods from the literature regarding the isolation of inclusion bodies[179] with the complete unfolding and slow refolding of proteins into their soluble state,[180] followed by the previous purification, thrombin cleavage and size exclusion chromatography steps. Some customization was required due to the equipment available and the later use of these proteins: e.g. use of β-mercaptoethanol (β-ME) in place of dithiothreitol as dithiothreitol reduces the efficiency of HisTrap columns. For the full protocol, see Section 7.3.3.

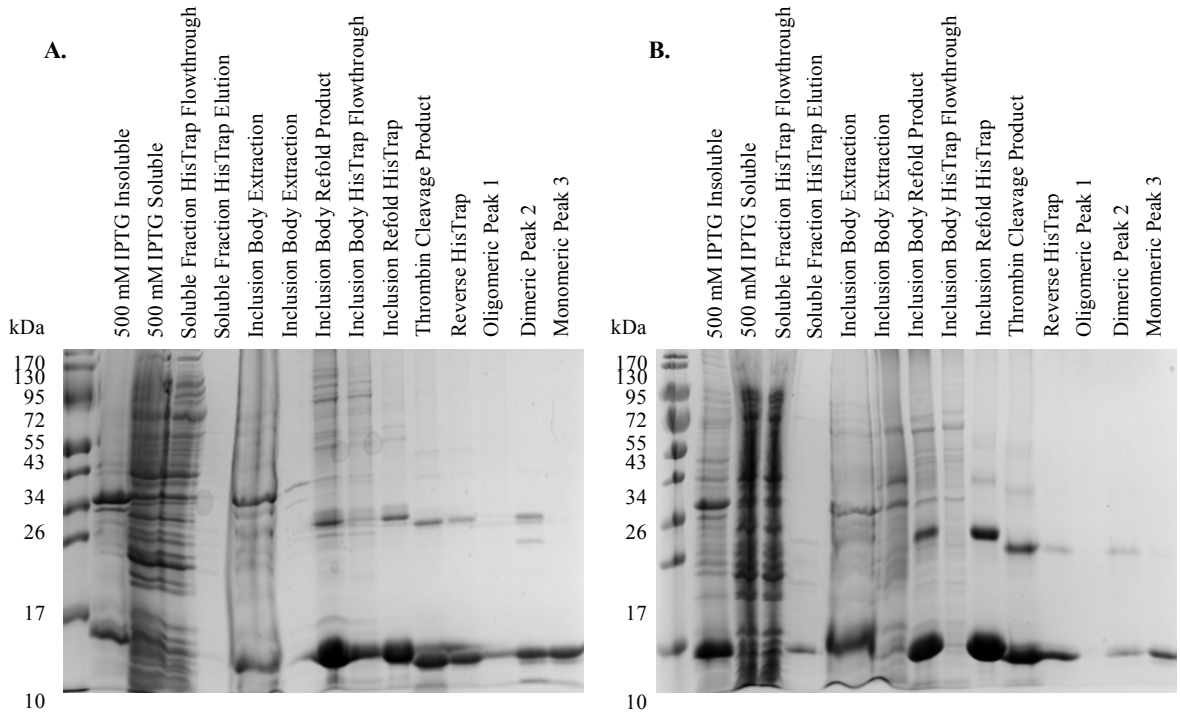



***Figure 59: SDS PAGE of the expression, unfolding, refolding and purification of A: TrkA-D5 and B: TrkB-D5.***

Two 3 L expression of BL21 DE3 *E. coli* was induced to express TrkA-D5 or TrkB-D5 from their pET28a(+) plasmids using 500 μM IPTG at 20 ˚C overnight. The cells were isolated by centrifugation, resuspended in inclusion body lysis buffer and lysed by freeze/thaw and sonication. Inclusion body proteins, unbroken cells and large cellular debris were then isolated by centrifugation. The inclusion body proteins were cleaned by repeated resuspension in inclusion body wash buffer and centrifugation before being resuspended in inclusion body extraction buffer. A very high chaotrope concentration and β-ME is used to unfold the inclusion body proteins and reduce disulfide bridges. Sequential dialysis was used to slowly lower the concentration of chaotrope and disulfide bridge reductants to gradually promote protein refolding. Finally, the protein was dialysed into HisTrap binding buffer, and soluble proteins were isolated by centrifugation. The supernatant was then purified as before: use of a HisTrap column, dialysis back into HisTrap binding buffer and $His_6$ cleavage with thrombin; HisTrap collecting column flowthrough, and size exclusion chromatography. Using this protocol, 6.3 and 8.4 mgs of purified, $His_6$ cleaved and soluble TrkA-D5 and TrkB-D5 were isolated.

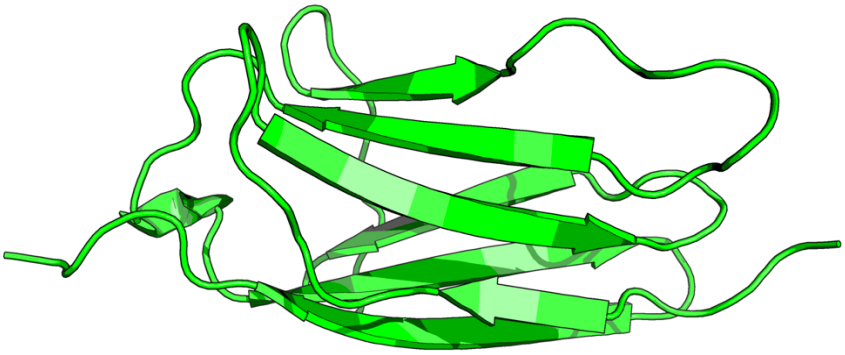


***Figure 60: Crystal structure of TrkA-D5, highlighting the predominantly antiparallel β-sheet secondary structure.*** *RCSB PDB entry 1WWW.*[49]

As Figure 60 and Figure 54 indicate, TrkA-D5 and TrkB-D5 are almost entirely antiparallel β-sheet and random loops, with one small α-helix. An attempt was therefore made to assess the success of refolding through the use of circular dichroism (CD) spectroscopy. This technique measures the change in absorbance between right-hand circularly polarised light and left-hand circularly polarised light across a range of wavelengths. As Figure 61A indicates, protein secondary structure displays distinct absorbance motifs and the secondary structure of a sample may therefore be inferred.

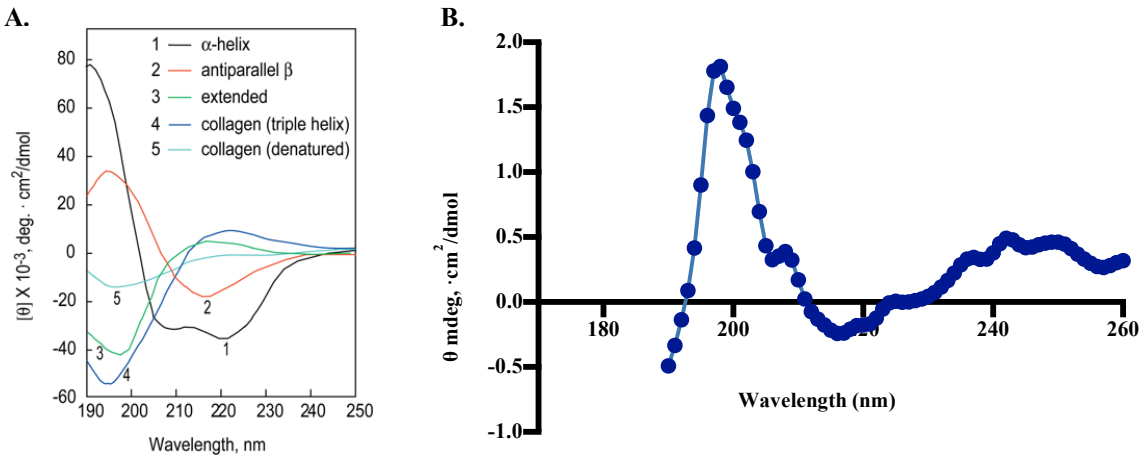



***Figure 61A: CD spectra of polypeptides and proteins with some representative secondary structure.*** [181] ***Figure 61B: CD spectra of TrkA-D5, indicating mainly anti-parallel β-sheet secondary structure.***

Figure 61A: 1: poly-L-lysine in an α-helix conformation at pH 11.1. 2: poly-L-lysine the in antiparallel *β*-sheet conformation at pH 11.1 after heating. 3: poly-L-lysine in the random coil/extended left-hand helix conformation at pH 5.7. 4-5: placental collagen in the native triple-helix and denatured conformations.

As Figure 61B indicates that the refolded TrkA-D5 contains mostly antiparallel $\beta$-sheet and random coil motifs. The signal strength is far lower than optimum however: total light absorbance was observed at typical working concentrations (0.5 mg/mL protein) even when using short path lengths (0.5 and 0.1 mm). This may be due to the protein itself, or absorbent artefacts in the buffer, despite a buffer exchange (GE Healthcare PD-10 desalting columns) into 10 mM phosphate buffer at pH 7.4. Lower protein concentrations managed to produce the above spectra, however TrkB-D5 spectra were deemed to have too high signal-noise for any useful conclusions to be drawn.

Proof of successful refolding was later inferred in Section 4.2.3 by the selective binding of TrkA-D5 and TrkB-D5 to their respective neurotrophins, and lack of TrkA-D5 or TrkB-D5 binding to HIF-2α PasB. Finally, after the protein created during the initial production of TrkA-D5 and TrkB-D5 was expended, expression and purification was repeated. The proteins were tested by two-component ELISA for their ability to bind their respective neurotrophin: while TrkA-D5 recognised βNGF, TrkB-D5 did not recognise mBDNF. This suggests that the TrkB-D5 produced during this second isolation had failed to refold correctly. This was ostensibly due to attempting to refold at an increased inclusion body concentration from the previous attempt: expression media was slightly scaled up resulting in a larger cell pellet. The apparatus used in the previous attempt was insufficient for the amount of dialysis tubing needed and a higher concentration was used, resulting in the observed lack of TrkB-D5 binding (Figure 62) indicating that misfolding can occur and highlighting the need for sufficient activity testing prior to usage (see Figure 75). One final test would be to take a sample of TrkA-D5 or TrkB-D5 which bound to its respective neurotrophin, thermally denature the samples and assess the change in binding activity.

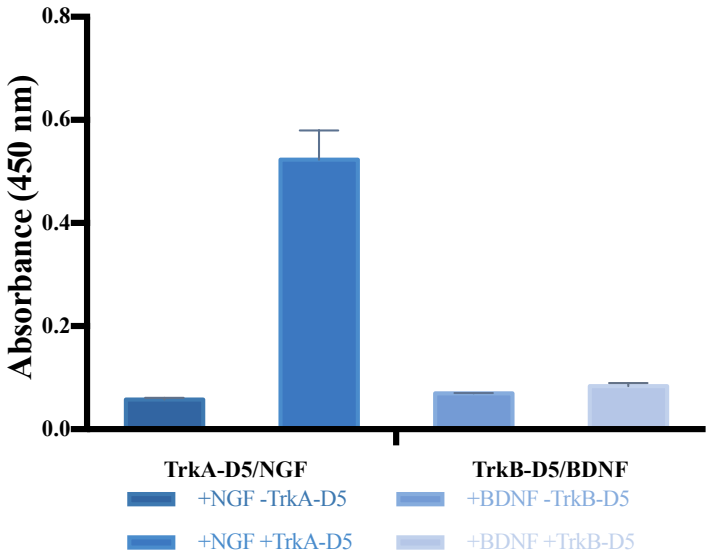



***Figure 62: Neurotrophin binding ELISAs of the second synthesis of TrkA-D5 and TrkB-D5.*** *Mean ± SD, n=2.*

## 4.2.2 Expression and Purification of βNGF & mBDNF

As stated previously, the proposed ELISAs and further testing would use significant quantities of both βNGF and mBDNF. As these are considerably expensive, an attempt was made to synthesise tagged versions of both βNGF and mBDNF.

### 4.2.2.1 *E. coli* Disulfide Bridge Formation

While bacterial expression is generally a quick and cost-effective method for producing recombinant proteins, synthesising proteins in certain structural classes (such as those with extensive PTMs) has proved problematic. One such class is that of proteins which are reliant on specific disulfide bond formation for their stability. This is especially true of small secretory proteins, where a small size results in a smaller hydrophobic effect (the main protein folding force) and stability is therefore supplemented by disulfide bridges. Both eukaryotic and prokaryotic cells have reducing cytoplasmic environments (preventing the formation of disulfide bridges) requiring oxidative cellular compartments. To use these compartments—the endoplasmic reticulum and the periplasm, respectively—requires an elaborate system of aggregation-preventing chaperones and folding catalysts. These not only ensure that disulfide bridges are formed (oxidoreductase activity), but (should a protein have more than two cysteines) that the correct cysteines are connected (isomerase activity). As the oxidoreductase activity preferentially links consecutive cysteine bridges in

*E. coli* this isomerase activity is vital to prevent the formation of improper interactions. These proteins are highly specialised and some require specific protein sequences for recognition and activity. Should eukaryotic proteins (such as βNGF and mBDNF) be expressed in prokaryotic cells this mismatch can lead to the eukaryotic protein being poorly or improperly expressed, leading to aggregation of misfolded protein.

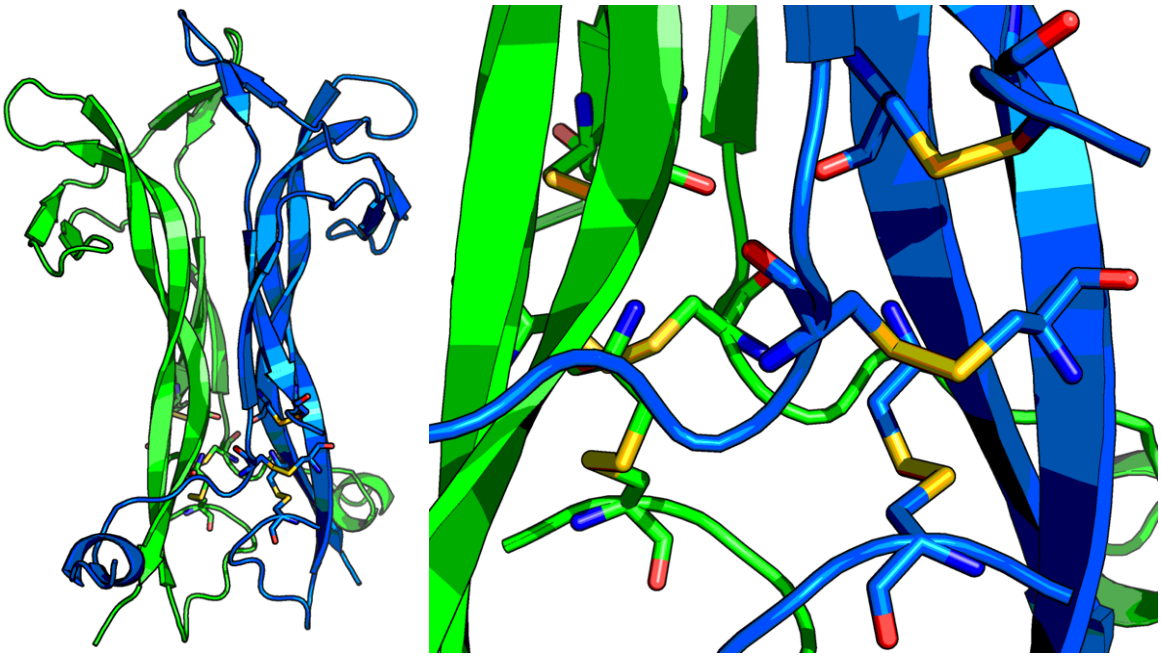


***Figure 63: Dimeric βNGF (PDB 1WWW[49]), highlighting the six intramolecular disulfide bridges per dimer of neurotrophin (C136-C201 C179-C229 and C189-C231).***

During the development of numerous mBDNF based RTHS, literature searches of neurotrophin expression in *E. coli* were limited to mBDNF. Upon expanding this project to also identifying βNGF inhibitors, new concepts came to light: soluble, functional βNGF expression in *E. coli* is critically affected by the overexpression of a number of *E. coli* proteins critical to the formation and particularly the isomerisation of disulfide bridges in *E. coli*. [144] Identifying this link subsequently identified that the expression of functional, soluble mBDNF in *E. coli* is also reliant on the overexpression of the same disulfide bridge isomerisation proteins,[145] which may explain the observed inability to form functional RTHS. When considering expressing both βNGF and mBDNF in *E. coli*, this overexpression must therefore be accounted for. What follows is an explanation of disulfide bond formation and isomerisation in eukaryotic and prokaryotic cells, in an endeavour to explain their importance of such overexpression.

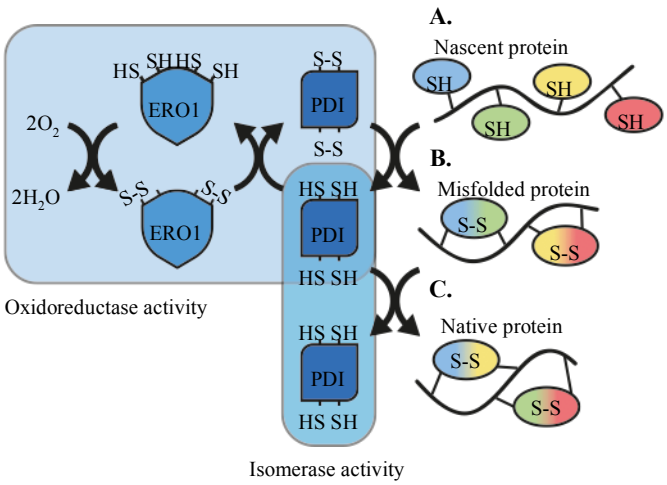



***Figure 64: Eukaryotic non-consecutive disulfide bridge formation in the endoplasmic reticulum.***

In eukaryotic cells an amino acid endoplasmic reticulum retention signal (KDEL) promotes migration to the endoplasmic reticulum.[182] Following translation, a nascent protein bearing that sequence is inserted into the endoplasmic reticulum with reduced cysteines. Protein disulfide isomerase (PDI) is present in millimolar concentrations inside the endoplasmic reticulum[183] and acts as a chaperone, preventing aggregation and providing both oxidoreductase and isomerase activity. As shown in Figure 64, PDI oxidises pairs of cysteines into disulfide bridges. This early stage of protein folding is highly error prone, and the resulting incorrect oxidation may result in mispairing or correct pairing which temporarily impedes further folding. Fortunately, PDI is also able to act as a reductase and break disulfide bridges, or as an isomerase and shuffle disulfide bridges between pairs of cysteines, should the result be energetically more favourable. The equilibria of reduced and oxidised PDI is maintained by endoplasmic oxidoreductin 1 (Ero1).[184] Proteins are excreted from the endoplasmic reticulum when the retention signal is cleaved, plus some lose affinity for PDI when fully folded.[182, 185]

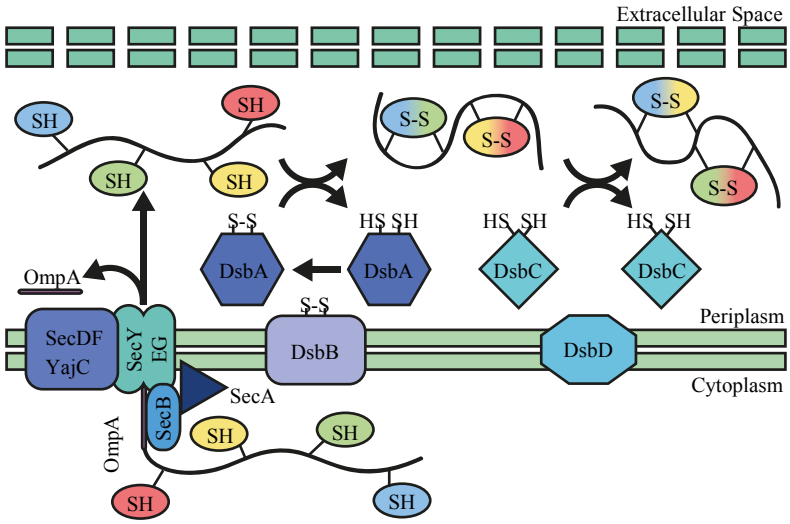



***Figure 65: Prokaryotic non-consecutive disulfide bridge formation in the periplasm.***

Prokaryotic cells follow a slightly different course when oxidising and isomerising disulfide bonds: A number of amino acid sequences have been identified for their ability to direct nascent proteins to the periplasm.[186] The most commonly used leader sequences in chemical biology to produce recombinant proteins in *E. coli* are OmpA and PelB, which both use the Sec pathway.[187-188] Following translation they are recognised and bound by the highly acidic chaperone protein SecB, which prevents aggregation and targets bound proteins to the Sec translocase. This consists of a peripheral associated ATPase (SecA) and a membrane-embedded heterotrimeric protein conducting channel consisting of SecY, SecE and SecG. SecA accepts secretory proteins from SecB and drives their translocation across the membrane.[189-190] The Sec translocase also has a second heterotrimeric component consisting of SecD, SecF and YajC. Its function is less clear: overexpression of SecD and SecF improve the export of proteins with mutant leader peptides, and knockout studies are non-viable at low temperatures.[191] Once inside the periplasm, the nascent protein is exposed to the oxidative machinery of the bacterium. This primarily consists of the disulfide-forming pair of proteins DsbA and DsbB, and the disulfide-isomerising pair of proteins DsbC and DsbD. DsbA is the primary periplasmic disulfide bridge donor, catalysing their introduction to nascent proteins *consecutively along the amino acid sequence*. DsbA is supported by DsbB, a cytoplasmic membrane-bound protein and the primary disulfide bridge forming enzyme: DsbB forms *de novo* disulfide bonds and transfers them to DsbA.[192] DsbC acts to isomerase misfolded disulfide bridges in a similar manner to PDI. It's partner DsbD maintains DsbC in the reduced state by transferring electrons from cytosolic thioredoxin. It is this consecutive disulfide bridge formation of

DsbA followed by the transfer to DsbC which can lead to the misfolding of eukaryotic proteins when expressed in *E. coli*: the recognition sites and sequences are different between eukaryotic and prokaryotic proteins, therefore leaky recognition by DsbA or DsbC, or a failed transfer between DsbA and DsbC may rapidly lead to the aggregation of misfolded protein. The consecutive formation of disulfide bridges by DsbA is especially problematic for the expression of βNGF and mBDNF, who each have three linking non-consecutive disulfide bridges: Cys136-Cys201, Cys179-Cys229 and Cys189-Cys231; and Cys141-Cys208, Cys186-Cys237 and Cys196-Cys239 respectively. Expression systems for βNGF and mBDNF were therefore sought, identifying NEB SHuffle T7 Express. This BL21-based E. coli has an oxidising cytosol and constitutive overexpression of cytoplasmic DsbC,[193] which was found to be the most critical for βNGF and mBDNF expression.[144-145]

#### 4.2.2.2 βNGF and mBDNF expression

The gene for mature human βNGF (residues 122-241)[194] tagged with both an N-terminal OmpA periplasmic leader sequence (MKKTAIALAVALAGFATVAQA)[187-188] and a C-terminal His6 affinity tag (with appropriate linkers, digestion sites and digestion overhangs) was optimised for K12 based *E. coli* expression[133] and purchased. A copy of the gene block was amplified by PCR with modifying primers to create a variant lacking the OmpA tag. As SHuffle T7 Express cells have an oxidising cytoplasm and constitutively expresses cytoplasmic DsbC,[193] directing proteins to the periplasm shouldn't be necessary but both with and without OmpA were attempted. Both gene blocks were then cloned into an empty pET28a(+) vector using the *HindIII* and *NcoI* restriction endonuclease sites and sequence verified. It should be noted that while there is a $His_6$ tag present in blank pET28a(+), the linking amino acid sequence between it and the MCS isn't optimal. Therefore, the above constructs were inserted as a complete reading frame. A silent mutation was given to mBDNF from p16THCP(mBDNF-FL-434D) during its creation, introducing an internal *NcoI* site. This was removed by KOD polymerase-based SDM and sequence verified. It was then amplified by PCR using modifying primers to add the appropriate restriction endonuclease sites at both 5'- and 3'-ends. Copies of both pET28a(+)(OmpA-βNGF-$His_6$) and pET28a(+)(βNGF-$His_6$) had their βNGF gene replaced with the above mBDNF construct using the *HindIII* and *NcoI* restriction endonuclease sites and were sequence verified. Whilst the mBDNF cloning was being conducted, the βNGF

expression plasmids were chemically transformed into SHuffle T7 Express cells and a small-scale test expression was conducted:

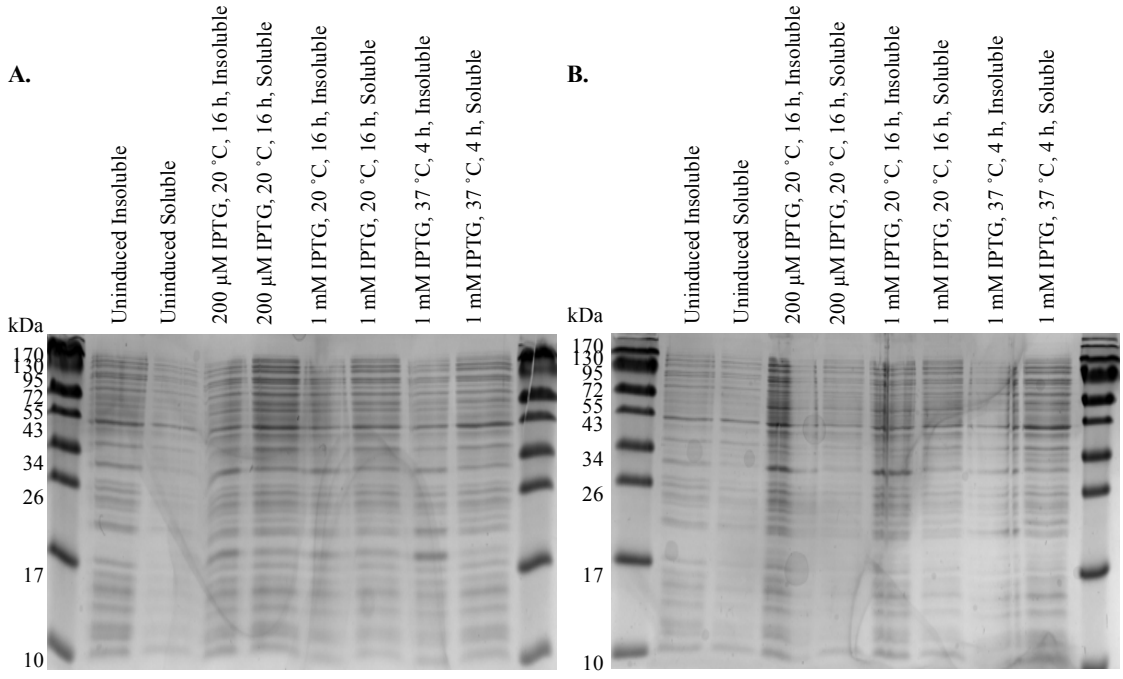



***Figure 66: SDS PAGE of a small-scale test expression of A: βNGF-His$_6$ and B: OmpA-βNGF-His$_6$in SHuffle T7 Express E. coli.***

While **Figure 66** indicates that expression of βNGF-His$_6$ and OmpA-βNGF-His$_6$ is unsuccessful (no additional bands are observed at 15.178 kDa and 17.876 kDa, respectively), this may be an artefact of small-scale expression: conducted as 10 mL of culture in a 50 mL falcon tube, insufficient aeration may be occurring and affecting protein expression. Aeration is critical to protein expression in *E. coli*[195] as anaerobic growth causes the expression of over 200 genes, greatly increasing metabolic load and hampering the amount of heterologous protein produced.[196] The 1 mM IPTG, 37 ˚C 4 h condition for both βNGF-His$_6$ and OmpA-βNGF-His$_6$ expression was therefore scaled up to a 50 mL culture in a 250 mL Erlenmeyer flask, and the soluble fraction was used in HisTrap affinity chromatography (as used during TrkA-D5 and TrkB-D5 purification) in an attempt to ascertain whether any neurotrophin was being produced. A fresh transformation of pET28a(+) plasmids into chemically competent SHuffle T7 cells was used each time expression was conducted hereafter, incubated (37 ˚C, overnight) and used to create a 1% culture in fresh media. This was done to prevent mutations in cDNA, which could produce inactive protein. In-house, using freshly transformed cultures have also been shown to

produce far more recombinant protein (3-4x) than a culture made from a -80 ˚C bacterial stock used identically (F. Rowan).

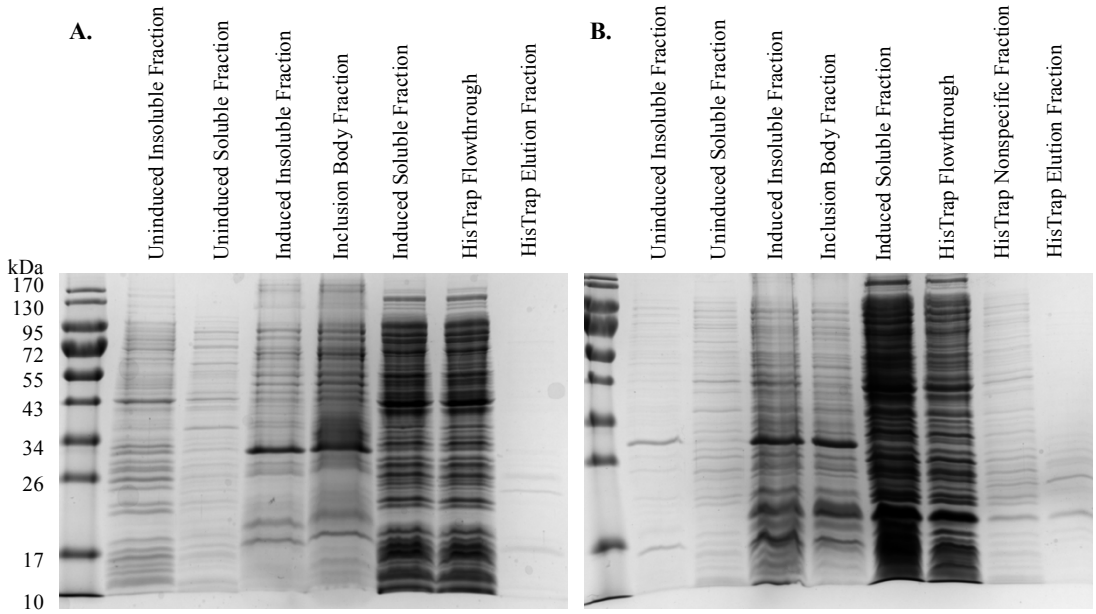



***Figure 67: SDS PAGE of a mid-scale test expression of A: mBDNF-His$_6$ and B: OmpA-mBDNF-His$_6$ in SHuffle T7 Express E. coli.*** *Non-denaturing Laemmli buffer was used to preserve polymeric state.*

Figure 67 indicates that very little mBDNF-His$_6$ and some OmpA-mBDNF-His$_6$ could be recovered from the soluble fraction. The inclusion body fraction (prepared as TrkA-D5 and TrkB-D5 were) was also added and both mBDNF-His$_6$ and OmpA-mBDNF-His$_6$ appear to have significant quantities of inclusion bodies present. This indicates significant aggregation, possibly due to misfolding. Again, using a lower expression temperature here may yield more correctly folded soluble protein. This is a commonly used technique, especially when attempting to express proteins suspected of aggregation: it slows the rate of protein synthesis and folding kinetics, decreasing the hydrophobic interactions involved in aggregation.[197] One caveat is that oxygen dissolution also decreased with lowering temperatures, therefore efforts should be made to ensure sufficient aeration.

Figure 67B also shows the HisTrap non-specific elution: after flowing the filtered soluble fraction through the HisTrap column, non-specific binders were eluted by raising the imidazole concentration from 20 mM to 43 mM. Specific binders are then eluted by raising the imidazole concentration to 250 mM. This fraction was included in the gel to ensure that the His$_6$ tag wasn't eluting early. While some of both mBDNF-His$_6$ and OmpA-mBDNF-

$His_6$ is produced, it's not nearly enough to meet the requirements of this project. Further optimisation is therefore required, and a deeper understanding of how the bacteria are processing the homologous proteins.

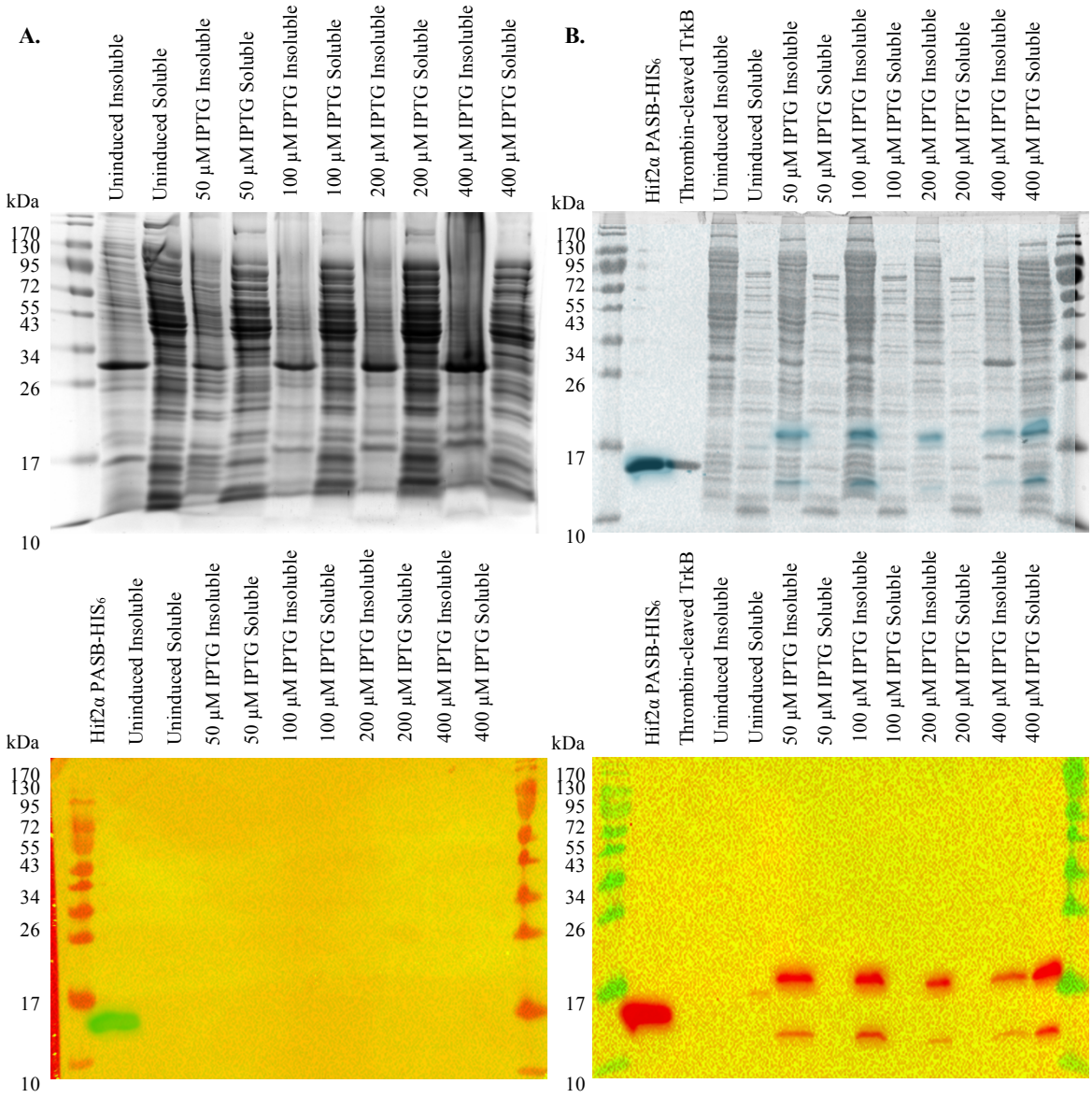



***Figure 68: SDS PAGE of a mid-scale test expression of A. βNGF-$His_6$ and B. OmpA-βNGF-$His_6$ in SHuffle T7 Express E. coli, superimposed with an anti-$His_6$ western blot of a duplicate gel.***

To that end, the mid-scale 50 mL culture in 250 mL flask test expression was repeated (Figure 68 and Figure 69), changing the LB media for Terrific Broth (TB) media: this increases the available nucleic acid precursors and changes the bacterial carbon source from catabolised amino acids to glycerol at non-rate limiting concentrations. It also contains a phosphate buffer to maintain physiological pH, preventing growth impedance

due to acidic metabolite release during exponential growth. LB media generally serves well in most chemical biology, but has a diauxie at $OD_{600}$ 0.3 (presumably at the exhaustion of a media metabolite) slowing overall growth and typically reaches a maximum cell-density of $OD_{600}$ 7.0.[198] With the differences outlined above, TB media typically reaches a maximum cell density of $OD_{600}$ 18-20, yielding 4-7 times the DNA product.[199] In addition to changing the media, the inducer concentration was significantly lowered: should the expression products be inhibiting growth then reducing their rate of expression should increase overall yield. SDS PAGE was also combined with an anti-$His_6$ western blot to undeniably identify the band containing the fusion proteins.

The gels and blots shown in Figure 68 indicate that no βNGF-$His_6$ and some OmpA-βNGF-$His_6$ was produced during this expression. However, as the $His_6$ tag was applied to the C-termini and proteins are biosynthesised from N-termini to C-termini, this may be due to incomplete translation and a stalling of the ribosome. As the codons encrypting the βNGF gene were optimised for expression in K12 *E. coli* and OmpA-βNGF-$His_6$ successfully expresses, this is unlikely to be due to rare codons and a depletion of the necessary tRNA, and therefore it's presumable that the OmpA tag and linker aids the solubility of the emerging nascent protein, supporting further translation. This is surprising due to the sequence of the OmpA tag (MKKTAIALAVALAGFATVAQA)[187-188] which is at first glance more hydrophobic than hydrophilic. A future iteration could therefore be the addition of a solubility tag at the N-termini, such as maltose binding protein, with a thrombin cleavage site to allow isolation of the neurotrophin.[200] As the 400 mM IPTG OmpA-βNGF-$His_6$ induction produced a surprisingly large amount of soluble heterologous protein, that was investigated first. NB: these gels were created using the Laemmli buffer lacking DTT: two bands indicates that the upper band is a dimer.

In Figure 68B, at 400 μM IPTG, it appears as though significant amounts of OmpA-βNGF-$His_6$ were present in the soluble fraction, however this was likely due to the high amount of inclusion bodies present in the sample: an insufficient separation or filtration of the soluble fraction may have pulled some inclusion bodies into the soluble fraction. As such, this experiment should have been repeated.

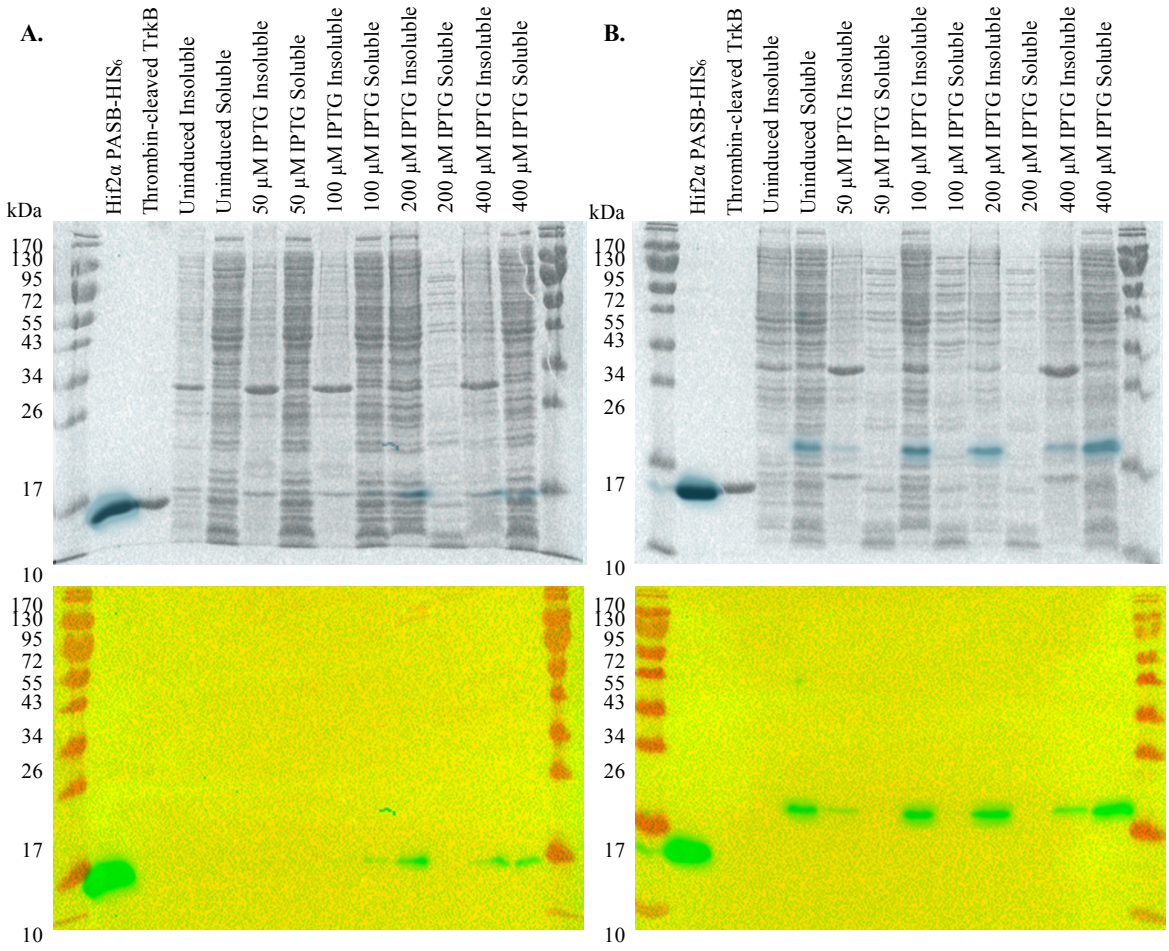



***Figure 69: SDS PAGE of a small-scale test expression of A. mBDNF-His$_6$ and B. OmpA-mBDNF-His$_6$ in SHuffle T7 Express E. coli, superimposed with an anti-His$_6$ western blot of a duplicate gel.***

Figure 69 indicates a similar expression profile for mBDNF-His$_6$ and OmpA-mBDNF-His$_6$ as their βNGF counterparts: low expression for the fusion proteins lacking the OmpA tag, although some and interestingly soluble protein is produced during the 200 µM and 400 µM mBDNF-His$_6$ expression. Similar to OmpA-βNGF-His$_6$, the most favourable expression conditions appear to be the 400 µM IPTG. This was therefore used in a large-scale expression: 1 L cultures of SHuffle T7 Express bearing the pET28a(+) plasmids of either OmpA-βNGF-His$_6$ and OmpA-mBDNF-His$_6$ were induced to express overnight at 20 ˚C. 2L Baffled Erlenmeyer flasks containing 500 mL culture each were used to increase the oxygen content by increasing agitation. Antifoam 204 was added to prevent foaming: foams decrease oxygen dissolution, hampering *E. coli* growth and ultimately homologous protein expression.[201] This expression was lysed and the soluble fraction was purified in a HisTrap FF nickel affinity chromatography column, isolating 0.1 mg of OmpA-βNGF-His$_6$ and 0.2 mg OmpA-mBDNF-His$_6$. This is insufficient for the needs of this project and

therefore further scale-up was investigated: a Brunswick Scientific Co. Bioflo 110 fermenter equipped with a 7.5L vessel was used to express a 6 L culture of SHuffle T7 Express cells expressing OmpA-mBDNF-$His_6$ using 400 μM IPTG:

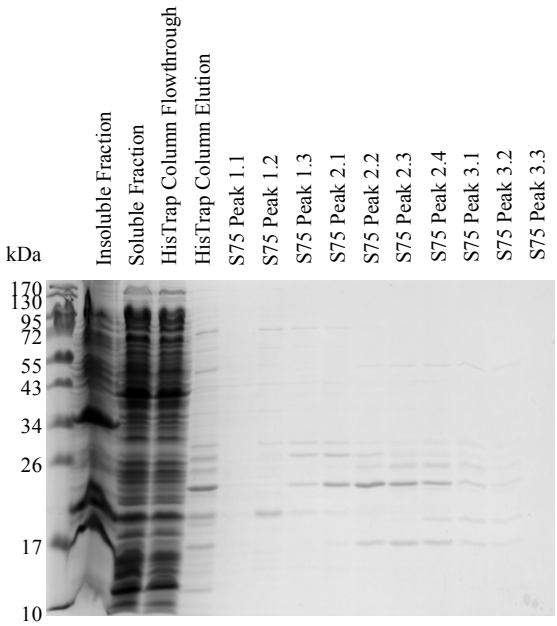



***Figure 70: SDS PAGE of a 5 L large-scale bioreactor expression of OmpA-mBDNF-$His_6$ in SHuffle T7 Express, induced with 400 μM IPTG.*** *Samples were purified by HisTrap FF nickel affinity columns and s75 size-exclusion chromatography.*

While the soluble fraction of the lysed *E. coli* used to create Figure 70 were passed through two consecutive 1 g HisTrap FF columns in buffer containing 20 mM imidazole (binding proteins with high nickel affinity), and the column was then flushed with buffer containing 43 mM imidazole to remove any non-specific binding, the flush was cut a little short and the column eluted with buffer containing 250 mM imidazole. This caused the multiple bands present in the HisTrap Column Elution column of Figure 70 and resulted in the presence of several peaks in the S75 column (peaks were subdivided into leading edge, middle and trailing edge, creating e.g. peak 1.1, 1.2 and 1.3). By mass the band/column containing OmpA-mBDNF-$His_6$ is peak 1.2. This process would have been repeated to isolate OmpA-mBDNF-$His_6$ in far higher purity if it weren't for the fact that even at a 5 L scale this only produced ~0.4 mg of (impure) OmpA-mBDNF-$His_6$.

It's possible that the low expression rates are also caused by *E. coli* toxicity of the expressed proteins: killing or retarding growth in cells obviously hampers protein

production. In an attempt to decrease toxicity an alternative induction technique was investigated. Auto-induction media (AIM) uses fermentable sugars as carbon sources (which can decrease pH and inhibit protein production), yet contains a phosphate buffer to maintain physiological pH. The main advantage to AIM is the gentle induction conditions, which are thought to prevent the induced toxic effects of homologous protein expression in *E. coli*.[202]

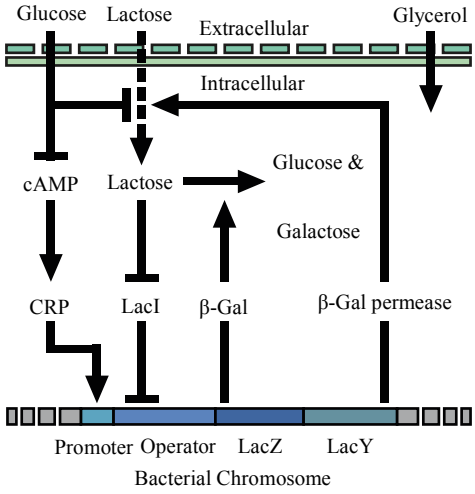



***Figure 71: Overview of Lac operon used in auto-induction media.***

AIM contains a short-term carbon source (glucose), a long-term carbon source (glycerol) and a delayed carbon source (lactose). As shown in Figure 71, before glucose is expended, it inhibits both the active import of lactose and the promotion of the expression of LacZ and LacY. Early growth in AIM media therefore uses glucose and inhibits the intake of lactose. With low intracellular lactose concentrations, the LacI repressor isn't inhibited, allowing it to further suppress the expression of LacZ and LacY. The expression of any fusion proteins under a similar LacI control (such as OmpA-mBDNF-$His_6$) are similarly repressed, preventing leaky expression. When glucose is expended as a fuel source, lactose passively diffuses into the cell, inhibits LacI and permits the expression of LacZ and LacY. These encode β-galactosidase (which cleaves lactose into glucose and galactose, the first step in its metabolism), and β-galactoside permease, which actively transports β-galactosides (such as lactose) into the bacterium. As such, AIM media is a delayed induction media with a slow on-rate: the bacteria initially use glucose as a fuel source and heavily repress the expression of LacZ, LacY and the fusion proteins described in this section (which are under a T7Lac promoter). A 1 L 37 ˚C overnight expression was therefore attempted:

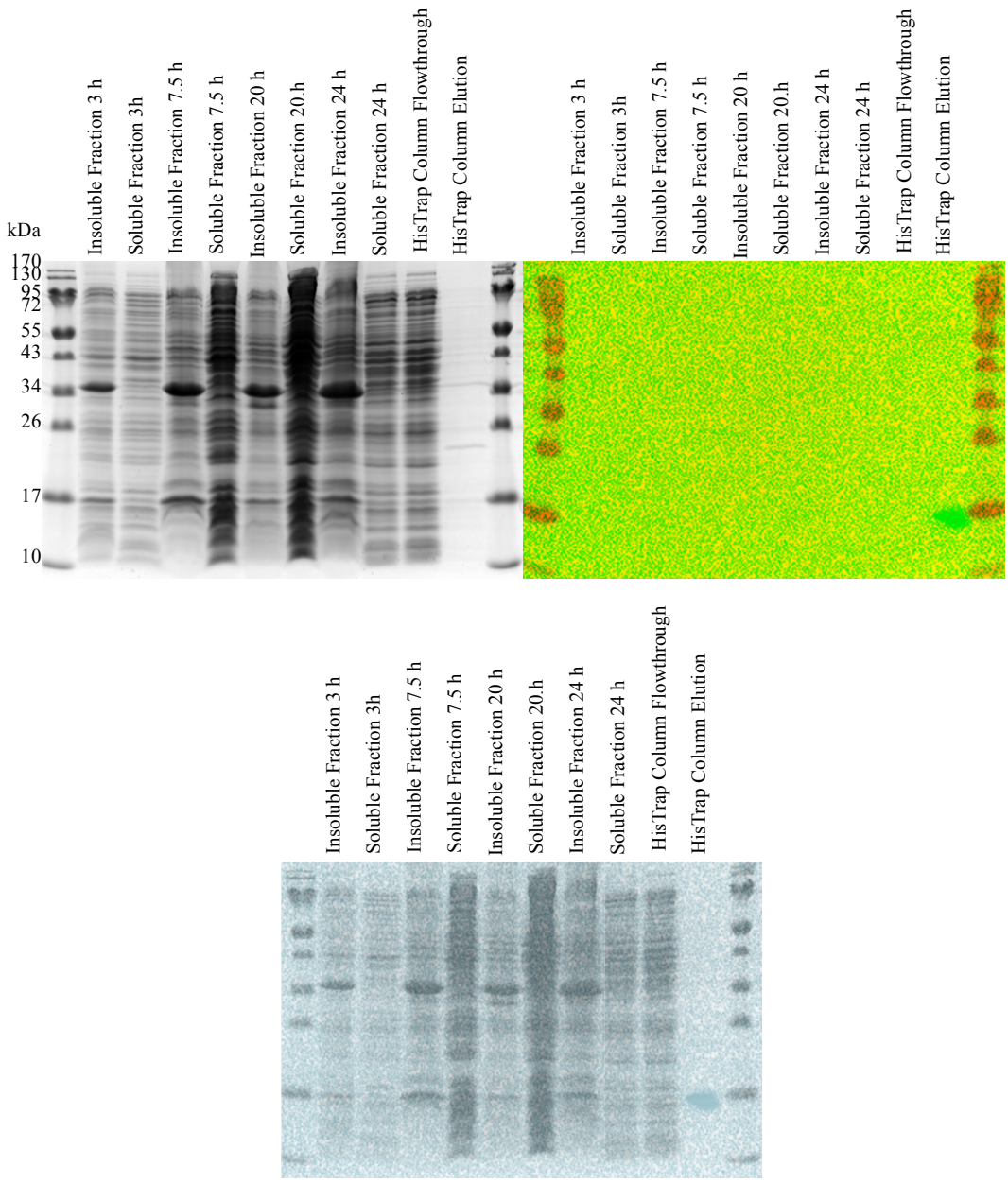



***Figure 72: Time course SDS PAGE, anti-$His_6$ western blot and overlay from a 1 L expression of OmpA-mBDNF-$His_6$ in auto-induction media.***

Unlike in previous gel images, in Figure 72 the SDS PAGE has been included without the western blot overlaid. This has been included to indicate that while a $His_6$ tag has been identified during this anti-$His_6$ western blot, the actual band in the SDS PAGE is very faint. It's also worth noting that this was only identified following an enrichment on a HisTrap column (isolating 200 µg of protein), and looking at the SDS PAGE, the correct band isn't even the major species present in that fraction. OmpA-mBDNF-$His_6$ is below detection levels at all points across the time course, indicating that either it induced very poorly, or the glucose wasn't expended until very late in the incubation. As this was the

standard protocol for AIM it is unlikely to be significantly improved upon and therefore other methods of expressing βNGF-$His_6$ and mBDNF-$His_6$ were investigated.

As stated earlier, Figure 67 and Figure 68 indicate that βNGF-$His_6$ and mBDNF-$His_6$ express poorly compared to OmpA-βNGF-$His_6$ and OmpA-mBDNF-$His_6$, presumably causing truncations during translation due to a difference in solubility. Attempts were made to clone variants with added solubility tags, however this was unsuccessful. At this point the bacterial synthesis of sufficient quantities of tagged βNGF and mBDNF was seen as too complex, and commercial sources were sought. Regrettably, the recommended sources only sold untagged versions of these proteins, therefore the intention of using nickel-affinity surfaces for ELISA protocols had to be set aside in place of the further use of high-binding polystyrene plates. This does however raise the issue of off-target binding: one of the advantages of tagging βNGF and mBDNF was to change the physical support used in the initial phage display to nickel treated plates. This intention was to add a layer of orthogonality between off-target binding.

### 4.2.3 ELISA Development & Testing

During this section, an assay was developed to assess the ability of the peptides discovered in Section 3.1.1.4, to inhibit or activate the binding of βNGF to TrkA-D5 and mBDNF to TrkB-D5. The library of 30 peptides were then screened for antagonist or agonist activity, allowing a more in-depth ELISA binding assay to be performed.

#### 4.2.3.1 Two-Component ELISA Design

As in the phage binding ELISA assays, a cycle of addition, incubation and washings was used to consecutively add to a polystyrene high-binding plate: target protein, BSA, either TrkA-D5 or TrkB-D5 (at a range of concentrations), mouse anti-FLAG antibody, anti-mouse IgG HRP conjugate and 1-Step Ultra TMB-ELISA substrate. Following a final incubation, the colourimetric reaction was ceased with $H_2SO_4$ before measuring absorbance at 450 nm.

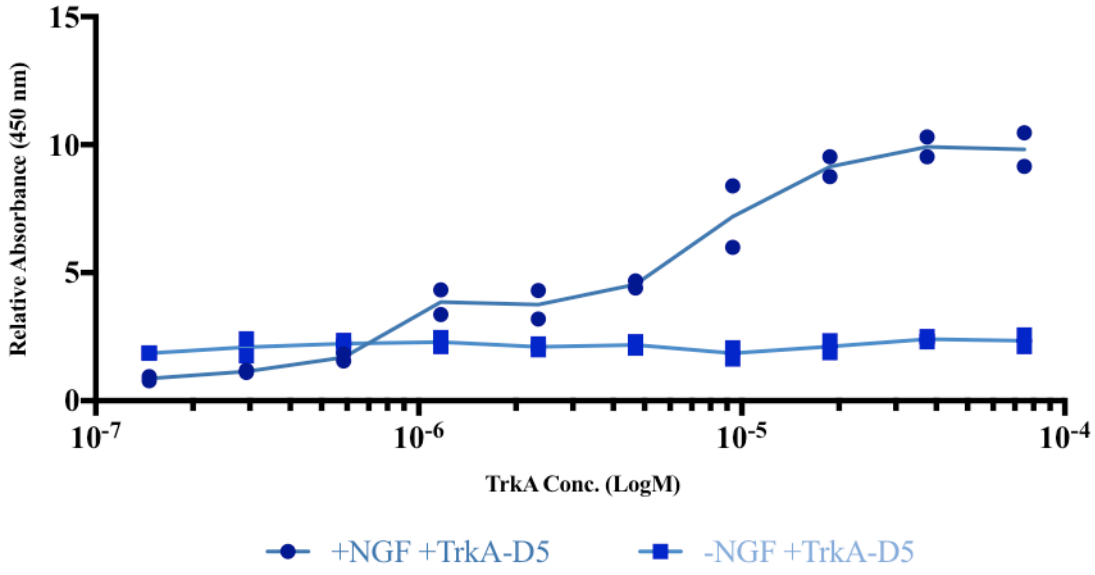



***Figure 73: Two component ELISA of TrkA-D5 binding βNGF, normalised to a +βNGF -TrkA-D5 negative control.*** *n=2.*

With an average relative absorbance of 2.28, the −βNGF +TrkA-D5 does show some affinity for the untreated wells, but this is not dose-dependent, suggesting a limited number of binding sites available on either the BSA or polystyrene plate, constant across the range of TrkA-D5 concentrations. +βNGF +TrkA-D5 shows a classic dose-dependent sigmoidal response, indicative of successful binding. An interpolation of the curve provides an EC50 of 5.60 µM ±4.05 µM. fortunately there is a significant window between the −βNGF +TrkA-D5 and the +βNGF +TrkA-D5 condition. 10 µM of TrkA-D5 was therefore used in all future experiments to provide a point near the midway of the curve, but with a reasonable window between baseline and total inhibition.

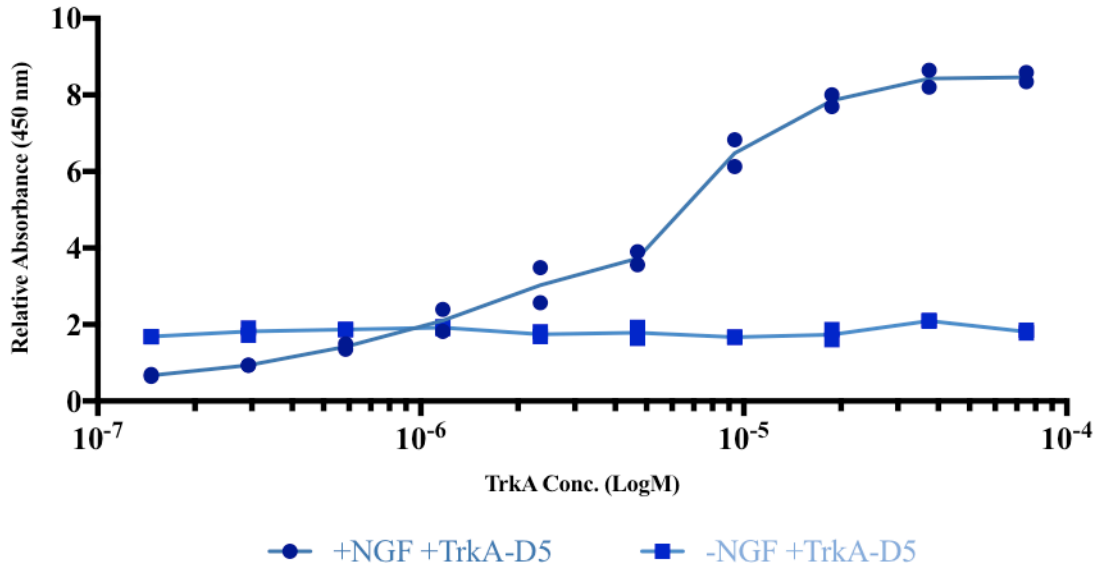



***Figure 74: Two component ELISA of TrkB-D5 binding mBDNF, normalised to a +mBDNF –TrkB-D5 negative control.*** *n=2.*

Figure 74 shows a similar trend to Figure 73: −mBDNF +TrkB-D5 shows some affinity for the untreated plate, but there is a significant binding window above 10 µM TrkB-D5. Interpolation of the curve indicates an EC50 of 6.28 µM ±2.10 µM. 10 µM TrkB-D5 was therefore used in all subsequent ELISAs.

The above graphs show the absorbance of ±βNGF +TrkA-D5 or ±mBDNF +TrkB-D5 relative to +βNGF –TrkA-D5 or +mBDNF –TrkB-D5 negative controls. It's worth noting that the +mBDNF –TrkB-D5 control showed significantly more absorption than the +βNGF –TrkA-D5 control, accounting for the difference in vertical axis scale between the two graphs. These tests were performed in staggered parallel but the TMB reaction for the mBDNF tests was permitted to react slightly longer, accounting for this variability.

Whether TrkA-D5 and TrkB-D5 are selectively binding βNGF and mBDNF was then assessed. Due to the use of size-exclusion chromatography it is unlikely that TrkA-D5 and TrkB-D5 are folded in such a way to be entirely nonspecific: any molecules that were such would self-adhere and be retained on the column. Testing whether they are selective to their neurotrophin over the other neurotrophin, or whether they bind to an anti-target was therefore used to assess selectivity activity. Using the concentrations outlined above, an ELISA was designed testing the affinity of a range of combinations of neurotrophin, receptor and an anti-target, Hif2α PASB:

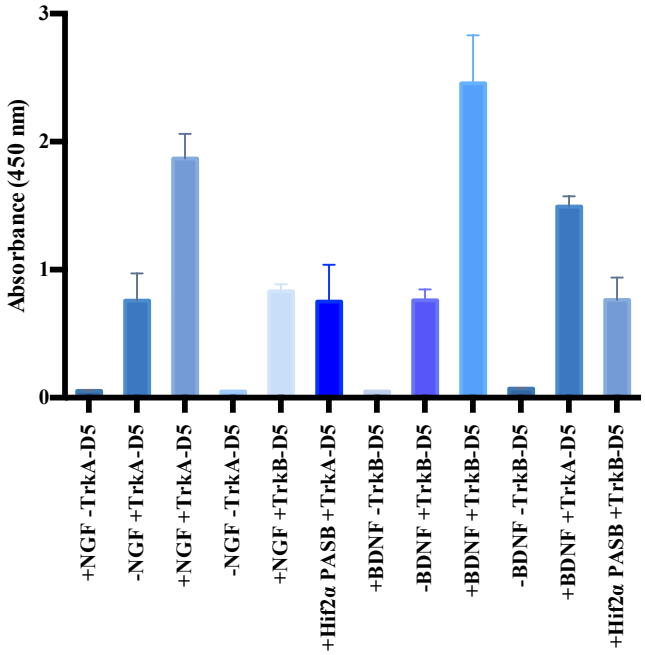



***Figure 75: ELISA to assess the selectivity of expressed, refolded and purified TrkA-D5 and TrkB-D5.*** *Mean ± SD, n=2*

Figure 75 indicates that both TrkA-D5 and TrkB-D5 demonstrate excellent selectivity windows of 200-300% over baseline. The negative controls (+βNGF −TrkA-D5, −βNGF −TrkA-D5, +mBDNF −TrkB-D5 and −mBDNF −TrkB-D5) indicate the background 1-Step Ultra TMB-ELISA degradation observed in this experiment is minimal, and neither βNGF or mBDNF, nor the BSA ancillary blocking proteins are capable of catalysing substrate degradation. Both the −βNGF +TrkA-D5 and −mBDNF +TrkB-D5 negative controls indicate baseline TrkA-D5 and TrkB-D5 retention, indicating that both TrkA-D5 and TrkB-D5 show some affinity for the BSA capping the high-binding plates. This is acceptable however as the +βNGF +TrkA-D5 and +mBDNF +TrkB-D5 positive controls show absorbance at 2-3× baseline TrkA-D5/TrkB-D5 retention. As both βNGF and mBDNF are at low concentration (1 µM) this indicates a significant retention and binding affinity compared with the negative control. The +βNGF +TrkB-D5 and +mBDNF +TrkA-D5 negative controls were to assess whether the expressed TrkA-D5 and TrkB-D5 were selective for their respective neurotrophins. As the membrane-bound receptors these domains are derived from are selective then this is a strong test of whether correct refolding has been achieved. +βNGF +TrkB-D5 indicates complete selectivity, as TrkB-D5 retention demonstrates parity with the –mBDNF +TrkB-D5 control. Conversely the +mBDNF +TrkA-D5 control indicates that TrkA-D5 has some affinity for mBDNF, which may be for a number of reasons: a concentration-based effect (the concentrations used in

this experiment are far higher than *in vivo* conditions), possible incomplete folding, using an isolated domain of a multi-domain protein reducing selectivity, lack of an essential PTM (TrkA-D5 (i.e. residues 278-386 of TrkA) contains one disulfide bridge and *five* suspected glycosylation sites, which will not be correctly addressed in *E. coli*[203]), the addition of an epitope FLAG tag modulating selectivity or off-target thrombin cleavage removing a section of the protein. These do not need tested due to the selectivity shown elsewhere. Testing hit peptide specificity will be important downstream, and future work may involve screening hits against a range of human proteins .

As this colourimetric enzymatic reaction is light and heat sensitive, these experiments proved difficult to replicate exactly. Light shielding was straightforward but temperature regulation proved problematic: trends were always retained, but scale always varied. 1-Step Ultra TMB-ELISA substrate is stored at 4 ˚C and had to be raised to room temperature prior to usage. If incubated at RTP for too long and the reaction will slowly proceed due to peroxide degradation, too short and the cool reagent will slow the temperature-sensitive enzymatic reaction. Early attempts simply placed the 250 mL bottle at RTP to rest for 30 min but this proved too variable. Later experiments used a 2 mL aliquot of 1-Step Ultra TMB-ELISA substrate placed in a darkened falcon tube, suspended for 30 min in a water bath that had been allowed to reach room temperature over 3 h. This proved to make these ELISAs considerably closer to parity when replicated, but not significantly so. This could have been improved by probing the temperature of a sample of the warmed 1-Step Ultra TMB-ELISA prior to usage, which would have avoided contamination and significantly improved experimental consistency. The following ELISAs are therefore to be treated as a guide only, providing insight into binding and inhibition but further, more accurate assays are required to probe binding constants etc.

#### 4.2.3.2 Two-Component Inhibitory ELISA of the Peptide Library

Free peptides allow precise control of concentration, avoids the avidity effect of pentavalent phage display and by removing the phage the peptides may be used at far higher concentrations. Assaying the peptides for their inhibitory affect was therefore conducted to minimise artefacts introduced through phage display.

As stated previously, to expedite this research WuXi AppTec were contracted to synthesise all 30 $ACX_7CG_3S$ peptides identified by this research, as free, soluble peptides. On arrival they were characterised by liquid chromatography mass spectrometry (LCMS), which also

provided a semi-qualitative measure of purity: LCMS indicated that the peptides were the only species present in the sample. In retrospect, in addition to LCMS, analytical HPLC should have been used to quantitatively assess purity. Later these peptides were re-synthesised (with purity assessed by analytical HPLC) and parity was found in the LCMS results (as shown in Section 7.3.5.4).

The $G_3S$ linker section is included as to do otherwise would introduce a negatively charged carboxylate, proximal to the variable region. When displayed on a phage this charge was not present and may substantially affect binding.

All peptides were screened at two concentrations for their ability to inhibit or activate both βNGF-TrkA-D5 binding, and mBDNF-TrkB-D5 binding, providing an indication of selectivity. This differs from the protocol used to create Figure 73 and Figure 74 in that the peptides (or PBST buffer for the controls) are added after the plates following the wash step after the BSA blocking. The plate is then incubated to allow the peptide to bind before addition of TrkA-D5 or TrkB-D5. The protocol then proceeds as before.

Figure 76 indicates that the majority of peptides do not inhibit TrkA-D5 binding to βNGF, and most actually increase binding. This is likely due to the hydrophobic nature of the majority of the peptides discovered through this phage display screen: phage display selects phages capable of target cohesion, hydrophobicity is a non-directional attraction prone to a lack of specificity. Of particular note are JI.5.12 (ACWTIYLMPCGGGS) and JI.5.58 (ACYELTPGKCGGGS) which inhibit TrkA-D5 binding to βNGF. JI.5.12 is particularly interesting due to the ranking of JI.5.12 in Figure 51, where it was ranked the second highest binder, showing a significant selectivity window between βNGF and mBDNF. JI.5.58 was ranked sixth in Figure 51 and showed a reasonable selectivity between βNGF and mBDNF. Of the peptides which increased TrkA-D5 binding, JI.1.14 (ACGRYMDGGCGGGS) and JI.5.55 (ACFYKWHSHCGGGS) show the largest effect. JI.1.14 is surprising as it is neither particularly hydrophobic, nor does it contain proline, which is known to be overrepresented in C7C library panning, occurring in >50% of hits.[204] With five out of seven variable amino acids bearing an aromatic residue, the activity shown by JI.5.55 is expected. Of particular note is the activity displayed by JI.5.1 (ACQHWPWFSCGGGS): with the highest reoccurrence during phage display (11 of the 20 phages sequenced for the βNGF screen) exceptionally high aromatic/hydrophobic content and the highest ranking in the Figure 51 phage ELISA, it is particularly surprising

that it had little to no effect on βNGF binding TrkA-D5. This suggests that where JI.5.1 binds with βNGF is discontinuous with the βNGF-TrkA-D5 binding site.

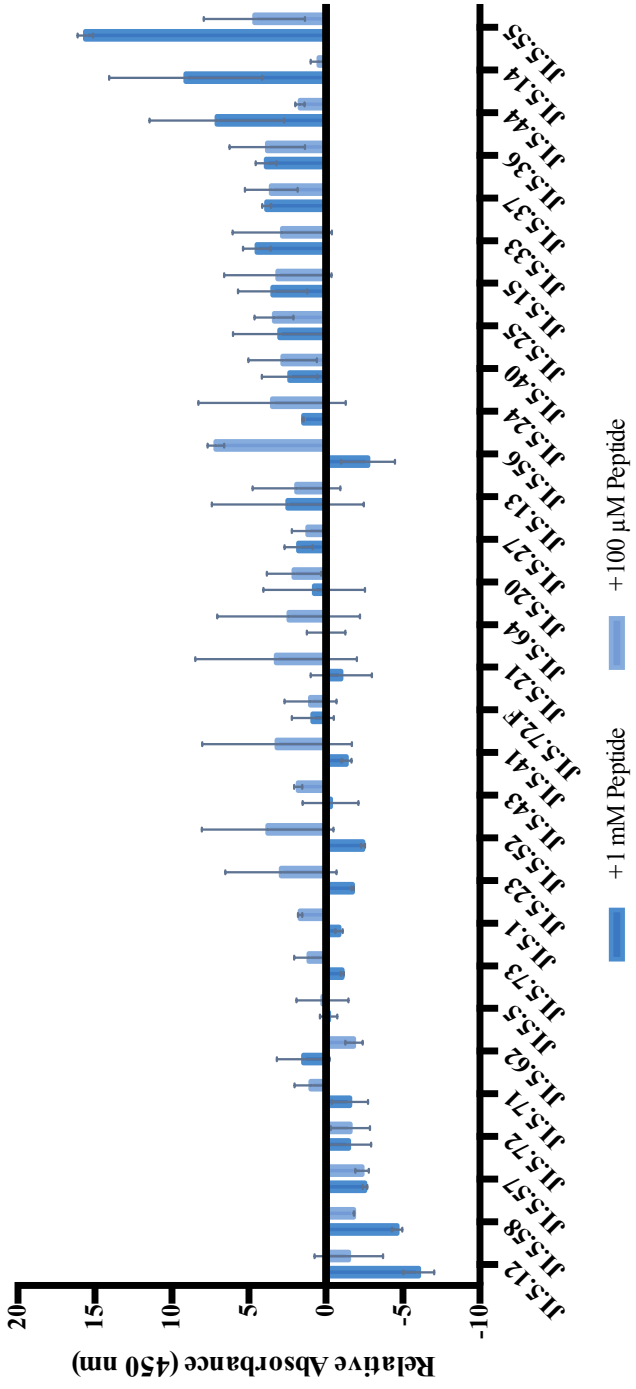



***Figure 76: Two-component inhibition ELISA of βNGF and TrkA-D5 binding.*** *Normalised to a –βNGF +TrkA-D5 negative control and a +βNGF +TrkA-D5 positive control: positive values therefore indicate PPI agonism and negative values PPI antagonism. Ranked by average relative absorbance. Mean ± SD, n=2.*

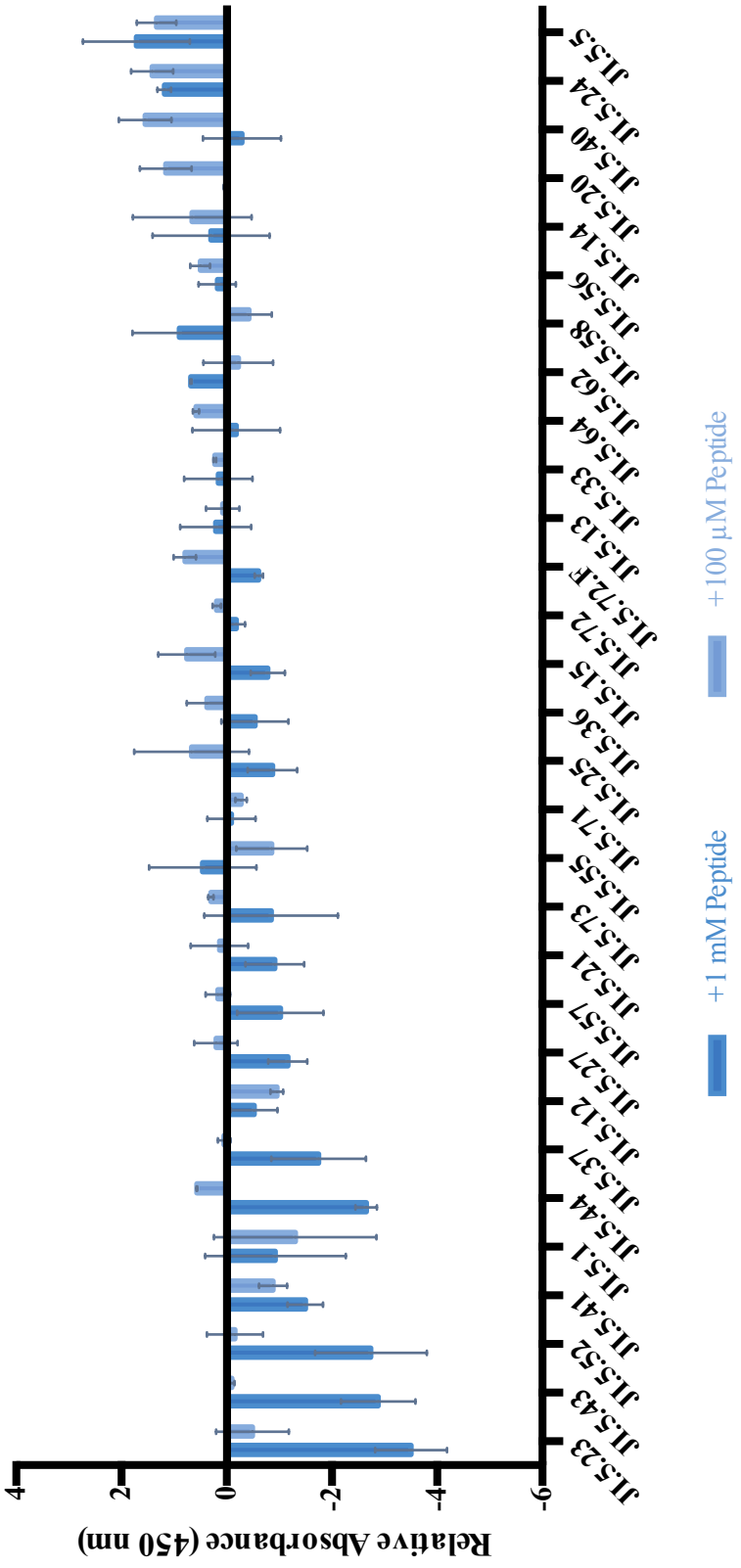



***Figure 77: Two-component inhibition ELISA of mBDNF and TrkB-D5 binding.*** *Normalised to a –mBDNF +TrkB-D5 negative control and a +mBDNF +TrkB-D5 positive control: positive values therefore indicate PPI agonism and negative values PPI antagonism. Ranked by average relative absorbance. Mean ± SD, n=2.*

Considering the hit peptides are being screened against highly similar neurotrophins and their receptors (TrkA-D5 and TrkB-D5 also have high sequence similarity), the difference between Figure 76 and Figure 77 is surprising: in Figure 76 the trend is mostly agonistic, whereas Figure 77 is mostly antagonistic. As expected however, most peptides show little to no activity, indicative of binding outside of the βNGF-TrkA-D5 or mBDNF-TrkB-D5 binding site, or that the peptides are out-competed by TrkA-D5 or TrkB-D5. While JI.5.12 is shown to inhibit mBDNF-TrkB-D5 binding, it shows a far greater degree of disruption with βNGF-TrkA-D5 in Figure 76, corroborating the selectivity indicated by Figure 51. JI.5.58, JI.5.14 and JI.5.55 also show very little mBDNF-TrkB-D5 activity: particularly interesting in the case of the βNGF agonist JI.5.55, which was assumed to be non-selective. Concerning mBDNF-TrkB-D5 activity, of particular interest in Figure 77 are JI.5.23 (ACHMAFKKICGGGS), JI.5.43 (ACNSFNSGSCGGGS), JI.5.52 (ACSLNHTVNCGGGS), and arguably JI.5.44 (ACNSHRHGACGGGS) and JI.5.37 (ACNAGHLSQCGGGS). JI.5.23 is surprising as it was one of the weaker binders in the phage ELISA assay (Figure 51), suggesting that it's affinity window was different to say JI.5.1, possibly having high activity but low affinity—which would also account for the very small change from baseline for the 0.1 μM measurement. The same is true of JI.5.43 and JI.5.37, which were ranked towards the back in the Figure 51 binding affinity assay. JI.5.44 showed medium affinity, and JI.5.52 was one of only three peptides which demonstrated a preferred binding to mBDNF than βNGF.

Regarding the affinity of the peptides screened in these two experiments: considering the nature of the interaction they are affecting (Figure 73 and Figure 74), it was expected that their activity drops sharply between 100 μM and 1 μM. Protein-protein interactions are large interacting surfaces and their inhibition by initial-hit small molecules is usually of micromolar magnitude. While in this case a better indication of dose-dependent inhibition and comparative inhibitor strength would have been observed by measuring at say 100 μM and 20 μM—or better still at three concentration points—this experiment was truly a venture into the unknown: it may have identified several peptides with strong activity, testing at 1 μM may have allowed the rapid identification of the peptide with the strongest affinity. The experiment is also considerably expensive: merely in peptide and mBDNF each iteration of the experiment approaches four figures. As such, minimising screening the whole library was an important factor in the experimental design: peptides identified by it can now be focussed on and a more in-depth binding profile can be sought. Overall the experiment was a success: it has identified a number of antagonists and agonists from the

peptide hit library with distinct (selective) activity between βNGF-TrkA-D5 or mBDNF-TrkB-D5.

Moving forward, it was necessary for an in-depth assessment of the binding of the putative βNGF antagonists JI.5.12 and JI.5.58, βNGF agonists JI.5.14, and JI.5.55; and putative mBDNF antagonists JI.5.23, JI.5.43, JI.5.52, JI.5.44 JI.5.37. The next steps therefore were to perform focused ELISAs of these peptides at a range of peptide concentrations.

### 4.2.4 Lead Peptide Titred ELISA

To address binding and confirm the dose-dependent activity observed in Figure 76 and Figure 77, assays were performed linking the inhibition or activation of βNGF TrkA-D5, or mBDNF TrkB-D5 binding with peptide concentration. These ELISAs were performed following a similar protocol as used with Figure 76 and Figure 77 but with eight sequentially diluted concentrations of lead peptide ranging from 1 mM to 10 µM:

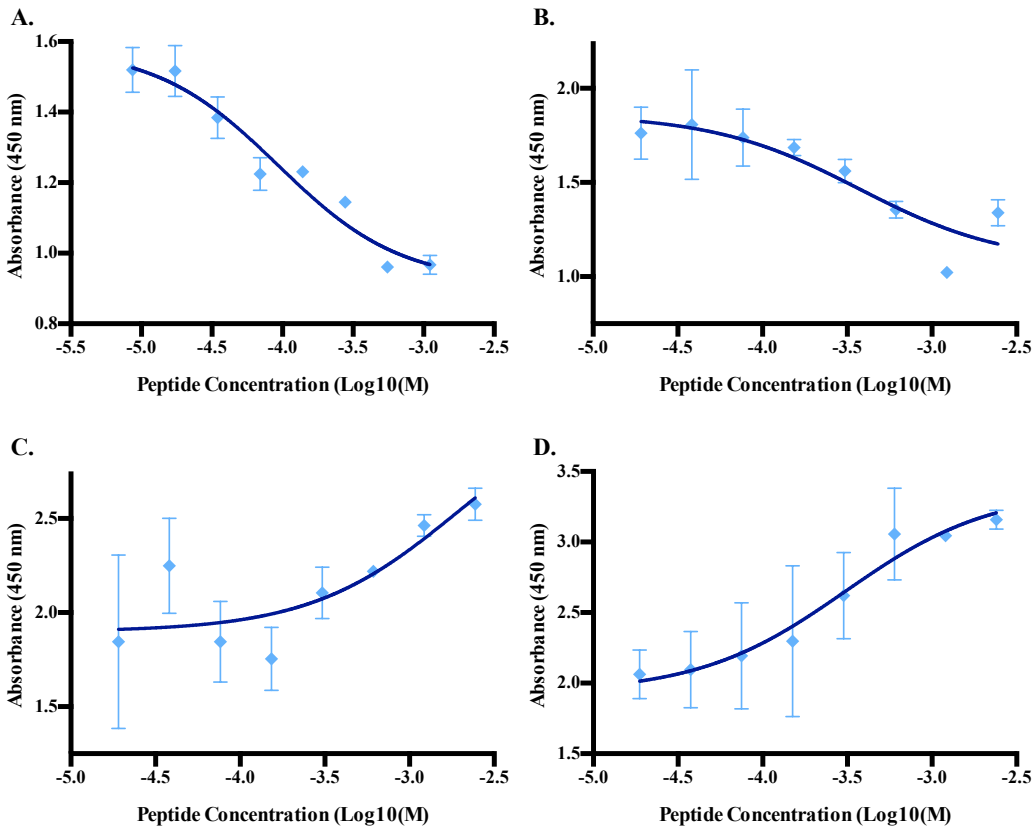



***Figure 78: Titred peptide ELISAs of lead βNGF peptides A. JI.5.12, B. JI.5.58, C. JI.5.14 and D. JI.5.55.*** *Normalised to a +βNGF –TrkA-D5 negative control. Mean ± SD, n=2.*

Despite the trends observed in Figure 78 following the expected directions (i.e. downwards for antagonists JI.5.12 and JI.5.58, upwards for agonists JI.5.14 and JI.5.55) the titred peptide ELISAs produced less than ideal data: there is high variability observed in all but Figure 78A. Including error, divergence from a flat line is small in some experiments (such as Figure 78C). Multiple repeats were attempted but displayed a similar variability. This may be due to the addition of DMSO (working concentration: 5%) and Tween-20 (working concentration: 0.5%) used during the assays. Solvent systems for these peptide ELISAs were explored during the optimisation of Figure 76 and Figure 77 and this was found to be the lowest level of DMSO possible to fully solvate certain hydrophobic peptides such as JI.5.1. Both DMSO and Tween-20 act as chaotropes and disrupt protein-protein interactions, obfuscating observable results. JI.5.12 is the best of these four and displays a tight grouping of results, but may simply be the middle of a sigmoidal curve: extending the range of concentrations in both directions could significantly improve the information gleaned in this experiment. This was attempted but the experiment failed in the final 1-Step Ultra TMB reaction. Interpolation of the curves should be taken *cum grano salis*, but recorded IC50s were as follows: JI.5.12: 93.03 μM ±49.9, JI.5.58: 371.5 μM ±307, JI.5.14: 1.90 mM ±1.85 and JI.5.55: 307.9 μM ±240. βNGF

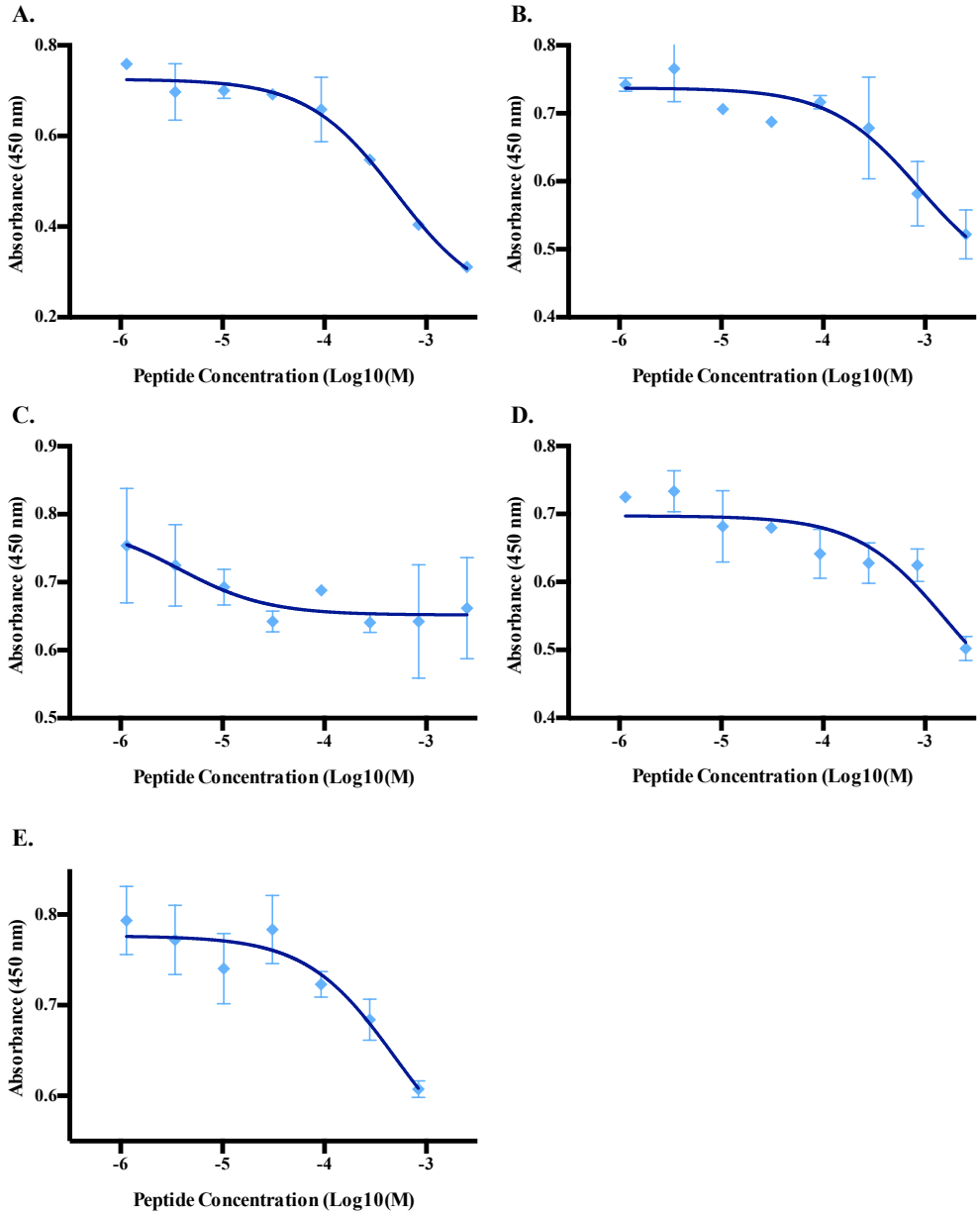



***Figure 79: Titred peptide ELISAs of lead mBDNF peptides A. JI.5.23, B. JI.5.37, C. JI.5.43, D. JI.5.44 and E. JI.5.52.*** *Normalised to a + mBDNF –TrkB-D5 negative control. Mean ± SD, n=2.*

Similar to Figure 78, the titred peptide ELISA experiments used to create Figure 79 would benefit from further experimentation and optimisation of experimental range. Repeats were attempted, but showed similar variability, presumably due to the relatively high concentration of DMSO used in the buffer media. While Figure 79A, B, D and E do appear to show coherent binding events (unlike the flat line observed with JI.5.43 in Figure 79C), they would benefit from experimenting at higher concentrations. As the binding sigmoidal curves do not bottom out, the observed interpolations cannot be used to measure IC50.

Between checking peptide identity and purity by mass-spec, solvent optimisation, whole-hit library screening ELISAs, repeats, titred peptide ELISAs and repeats, some peptides had now been completely expended. In-house synthesis of the 9 lead peptides was therefore conducted. This allowed a far greater reliance on the identity and purity of the peptides used, and permitted binding, inhibition and cellular testing.

## 4.3 Chapter 4 Conclusions

The aim of this chapter was to screen the peptide sequences identified by phage display for their ability to modulate the βNGF-TrkA or mBDNF-TrkB PPIs. To that end, an assay was developed where these interactions caused a quantifiable colour change, as such the inhibition of these interactions decreased the colour change. The peptides were screened for their modulatory activity and a number of agonists and antagonists were identified.

In the process of developing this assay, significant research was conducted into the bacterial expression of tagged versions of βNGF, mBDNF, TrkA and TrkB. Through considerable optimisation, methods to isolate clean, soluble, correctly folded, monomeric, tagged TrkA and TrkB were developed. Despite protracted attempts at optimisation of the expression of tagged versions of βNGF and mBDNF, no method could be developed which was capable of isolating soluble, correctly folded protein using the available techniques. To that end, untagged βNGF and mBDNF were used for the above assays.

The use of untagged βNGF and mBDNF in the modulatory assay required the continued use of high binding polystyrene as a support (as used in the phage display screen). The idea of using tagged versions was intended to add a layer of orthogonality between the phage display screen and the modulatory binding assay: the initial modulatory binding assay would use nickel chelation binding plates in place of high binding polystyrene as a support. It is unlikely that any small peptides which bound to the highly aromatic high-binding polystyrene would bind to the highly polar ionic nickel supports, which should significantly decrease background binding.

Conversely, adding a tag to βNGF or mBDNF for the modulatory assay orients the proteins on the surface of the substrate, which could bias the screen towards or away from orientations which permit binding or inhibition of binding to their respective Trk. An advantage to using high-binding polystyrene plates is that the neurotrophins are highly likely to bind to the plate across a number of orientations. Ideally, the use of tagged

neurotrophins with a long, flexible linker to permit a range of orientations would have been preferred.

In hindsight, as it is a key assay it would have been pertinent to perform further repeats of the modulatory binding assay. It was found that because of the number of variables present, the results of repeats of these assays are challenging to combine and are more suited to identifying trends of activity rather than absolute activity. In retrospect, further repeats could have represented individually such that comparisons in modulatory activity could have been drawn.

To conclude, a number of peptides were identified with agonist and antagonist activity for the βNGF-TrkA or mBDNF-TrkB PPIs. The next step was to verify and quantify these affects using a range of techniques.

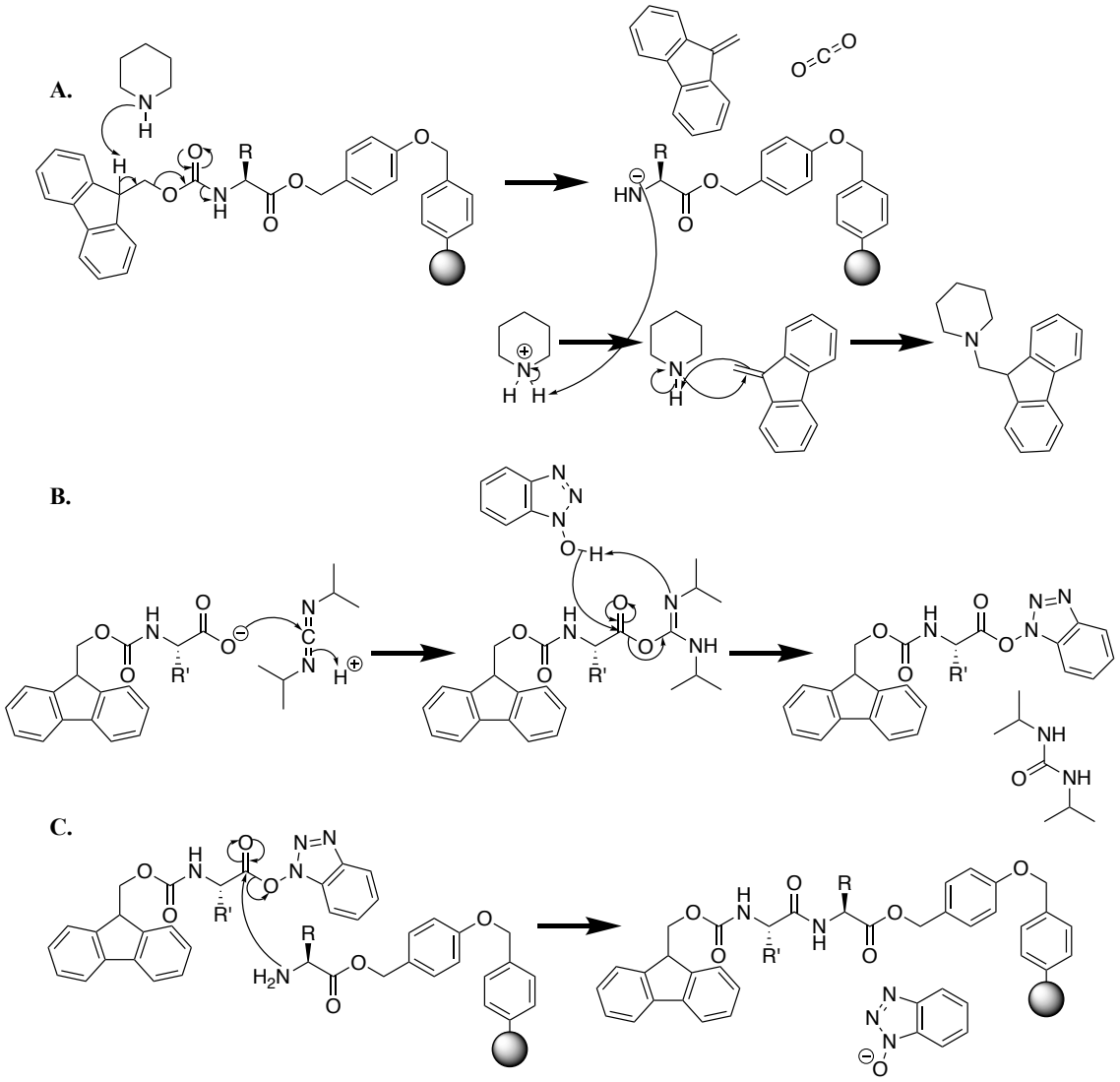
# Chapter 5: Development of Approaches to Determine the Modulatory Effect of Identified Binders

## 5.1 Lead Peptide Solid Phase Peptide Synthesis

Standard solid-phase peptide synthesis (SPPS) was used to synthesise JI.5.12, JI.5.14, JI.5.23, JI.5.37, JI.5.43, JI.5.44, JI.5.52, JI.5.55 and JI.5.58; as well as JI.5.1 and JI.5.13. These last were also included due to their phage display proclivity compared to other entries. SPPS allows for the controlled stepwise addition of protected amino acids to a growing peptide chain. It overcomes many of the solubility issues present in solution-phase peptide synthesis and provides convenient purification procedures.[205] Standard SPPS requires protection of the backbone amine by either a fluorenylmethyloxycarbonyl (Fmoc) or a tert-butyloxycarbonyl (Boc) group. With both Fmoc and Boc SPPS strategies, side-chain cross-reactions are prevented by orthogonal protecting methodology. Like most standard SPPS, the Fmoc methodology was chosen over Boc due to the greater degree of orthogonality: TFA is used iteratively to deprotect Boc-amides, but also cleaves some side-chain protecting groups in each cycle and progressively removes some peptide from the polymer support. Fmoc methodology is more robust and generally yields a cleaner crude product: mild base is used to remove the Fmoc group, however an acid-labile Wang linker resin was used in combination with acid-labile side-chain protecting groups.

Unlike biological peptide synthesis, SPPS adds amino acids from C-termini to N-termini. As all lead peptides have an $ACX_7CG_3S$ structure, this allows a scale-up to produce $CG_3S$-Wang, which were then split and a Schlenk line used to quadruplex peptide synthesis. This was used to add the individual $ACX_7$ sequences prior to cleavage and deprotection. As such, at a 250 mmol/final peptide scale the Fmoc protecting group was removed from pre-loaded S-Wang resin using 20 % piperidine in DMF (Scheme 2A). The next Fmoc-protected amino acid could then be added, however it is necessary to activate the carboxylic acid beforehand due to the non-spontaneous nature of amide bond formation requiring the elimination of $H_2O$.[206] A plethora of coupling reagents exist, here the initial activation was conducted using a carbodiimide to produce an *O*-acylurea. *N,N′*-diisopropylcarbodiimide (DIC) was used in this synthesis as unlike say *N,N′*-dicyclohexylcarbodiimide, the diisopropylurea by-product is DMF soluble, allowing simple purification by filtration. DIC is however a very strong leaving group and may lead to the racemisation of the amino acid α-carbon via an 5(4H)-oxazolone intermediate. To

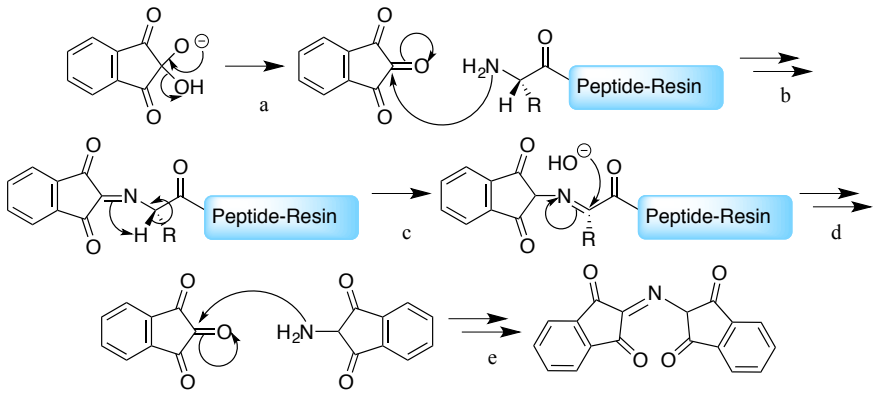
prevent this, the additive hydroxybenzotriazole (HOBt) was used. This mechanism of SPPS consists of DIC protonation by the amino acid carboxylic acid and the subsequent nucleophilic attack on the carbodiimide to form the acylurea. This can undergo a slow rearrangement to form an N-acylurea side reaction, or a fast reaction with HOBt to produce an active HOBt ester (HOBt is pre-mixed with the amino acid prior to DIC addition to promote this).




***Scheme 2A: Fmoc deprotection, Scheme 2B: DIC and HOBt preparatory reaction Scheme 2C: amide coupling reaction***

To ensure that every Fmoc deprotection or amino acid coupling had proceeded to completion—which may be hindered due to amino acid sequence or side-chain protecting group steric hindrance—after every coupling or deprotection a sample of the product was tested for the presence of free amines using the Kaiser test. This qualitative test uses

2,2-dihydroxyindane-1,3-dione (ninhydrin) to react with free primary amines to form Ruhemann's Purple.[207-208]




***Scheme 3: Kaiser test reaction mechanism.*** *A: thermal decay (~120 ˚C), b: imine formation and condensation, c: imine rearrangement, d: imine hydrolysis, e: Ruhemann's Purple formation by nucleophilic attack with the newly formed amine with a second molecule of indantrione.*

Note that if the Kaiser test is performed on a secondary amine the Scheme 3c cannot proceed and the formation of the yellow-orange imine (rather than the dark violet Ruhemann's purple) must be relied upon. If following coupling or Fmoc deprotection the Kaiser test was unsuccessful the coupling or deprotection reaction was repeated until a successful Kaiser test was observed. Peptides were then formed by the iterative process of Fmoc deprotection and amino acid coupling until the desired sequence was produced. The peptide was then simultaneously cleaved from the resin and acid-labile side-chain protecting groups removed using a cleavage cocktail of trifluoroacetic acid (TFA) and scavengers (i.e. triisopropylsilane (TIS) and water to prevent side reactions.[209].

Following filtration to remove the expended Wang resin, volatile reagents (such as TFA) were then removed *in vacuo* and the crude peptides purified using flash reverse phase chromatography using a Biotage® SNAP Ultra C18 column and a shallow $H_2O$:acetonitrile (ACN) gradient. Both solvents used in this chromatography were doped with TFA (0.1%) to aid resolution. The lead peptides were then lyophilised, isolating 23.3-67.8 mgs of peptide. Peptides then underwent hairpin cyclisation by disulfide bridge formation using iodine.[210] Briefly, the peptides were dissolved in acetic acid (75 % v/v), and to the mixture was added dropwise an iodine solution (10% w/v in MeOH) until a stable orange colour was created. The reaction was then stirred (1 h, RTP) and excess iodine quenched by the

dropwise addition of sodium ascorbate solution (20 mM). The product was then purified by reverse-phase HPLC ($H_2O$/ACN gradient) and lyophilised, isolating 9.6-31.7 mgs of final peptide. Disulfide bond formation was confirmed by the observed change in mass following the iodine reaction. All lead peptides were analysed by mass-spec and analytical HPLC. MSMS was considered, however it was advised that for the molecular weight the variability was too high. In hindsight, NMR should have been used: COSY, TOCSY, NOESY, HMQC and HSQC combined should provide sufficient data for full characterisation of all peptides. Their structures are shown in Figure 80, Figure 81 and Figure 82.

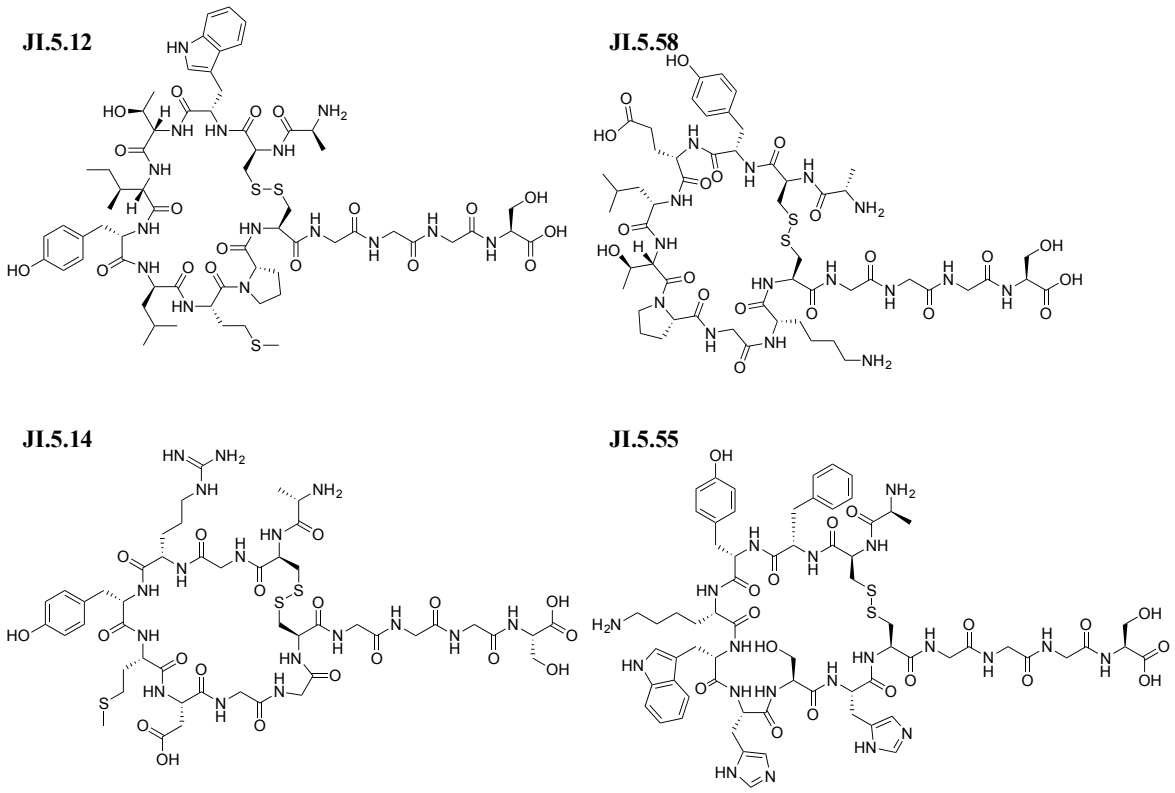



***Figure 80: Structures of peptides selected by phage display as βNGF agonists or antagonists.***

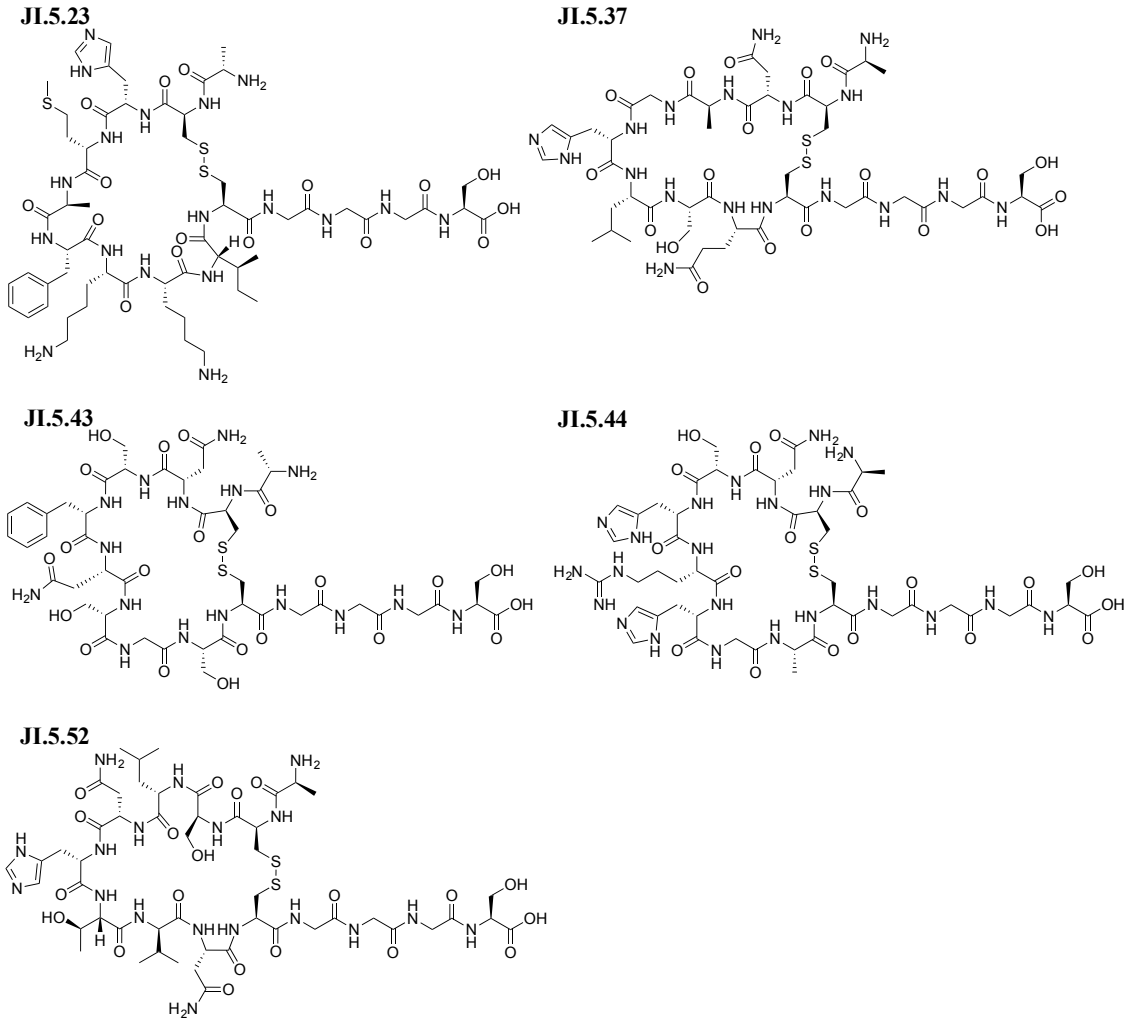



***Figure 81: Structures of peptides selected by phage display as mBDNF antagonists.***

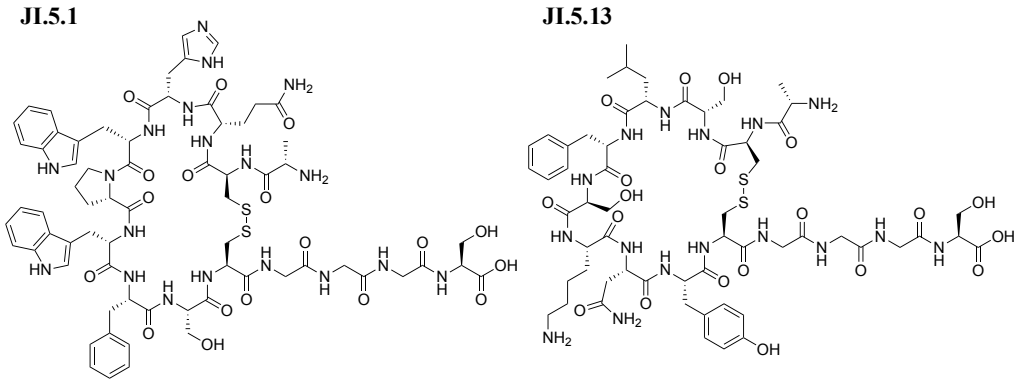



***Figure 82: Structures of peptides selected by βNGF and mBDNF phage display which display interesting properties.***

To investigate whether these peptides had been characterised previously (which would provide a basis of comparison with these peptides), the above structures were individually

converted into the SMILES format and PubChem was searched for identical entries. Unsurprisingly, none of the peptides had been previously identified.

***Table 11: Collated characterisation data from SPPS of lead peptides***

| | | | Mass Spectroscopy (m/z) | | | | Analytical HPLC | |
|---|---|---|---|---|---|---|---|---|
| | **mg** | **µmol** | **Species** | **Synthesised** | **Purchased** | **Expected** | **Retention (min)** | **%** |
| JI.5.1 | 11.2 | 7.36 | $(M+2H)^{2+}$ | 761.60 | 761.60 | 761.80 | 19.80 | 95.70 |
| | | | | | | | 20.66 | 4.30 |
| JI.5.12 | 6.5 | 4.45 | $(M+H)^{+}$ | 1457.90 | 1457.00 | 1457.61 | 22.91 | 77.30 |
| | | | $(M+2H)^{2+}$ | 729.40 | 729.30 | 729.31 | 23.49 | 22.70 |
| JI.5.13 | 9.6 | 6.89 | $(M+H)^{+}$ | 1392.80 | 1392.20 | 1393.58 | 23.16 | 75.62 |
| | | | $(M+2H)^{2+}$ | 696.90 | 696.00 | 697.29 | 23.64 | 24.38 |
| JI.5.14.5 | 5.8 | 4.49 | $(M+H)^{+}$ | 1288.60 | 1288.90 | 1291.47 | 12.45 | 100.00 |
| | | | $(M+2H)^{2+}$ | 645.20 | 645.40 | 646.24 | | |
| JI.5.14.7 | 2.8 | 2.17 | $(M+H)^{+}$ | 1288.70 | 1288.90 | 1291.47 | 12.45 | 100.00 |
| | | | $(M+2H)^{2+}$ | 645.20 | 645.40 | 646.24 | | |
| JI.5.23.5 | 9.8 | 6.95 | $(M+2H)^{2+}$ | 704.90 | 705.30 | 706.34 | 14.84 | 56.70 |
| | | | $(M+3H)^{3+}$ | 470.40 | 470.40 | 471.23 | 15.02 | 43.30 |
| | | | $(M+4H)^{4+}$ | 353.10 | 353.20 | 353.67 | | |
| JI.5.23.6 | 21.9 | 15.52 | $(M+2H)^{2+}$ | 704.90 | 705.30 | 706.34 | 14.84 | 18.40 |
| | | | $(M+3H)^{3+}$ | 470.40 | 470.40 | 471.23 | 15.02 | 81.60 |
| | | | $(M+4H)^{4+}$ | 353.10 | 353.20 | 353.67 | | |
| JI.5.37 | 18.9 | 14.99 | $(M+H)^{+}$ | 1259.70 | | 1261.50 | 13.11 | 96.75 |
| | | | $(M+2H)^{2+}$ | 630.60 | 630.80 | 631.25 | 13.21 | 3.25 |
| JI.5.43 | 10.6 | 8.51 | $(M+H)^{+}$ | 1245.40 | 1245.80 | 1246.43 | 12.07 | 100.00 |
| | | | $(M+2H)^{2+}$ | 623.60 | 623.80 | 623.60 | | |
| JI.5.44 | 13.9 | 10.57 | $(M+H)^{+}$ | 1312.70 | 1312.60 | 1315.54 | 20.03 | 100.00 |
| | | | $(M+2H)^{2+}$ | 656.80 | 656.80 | 658.27 | | |
| | | | $(M+3H)^{3+}$ | 438.30 | 438.30 | 439.18 | | |
| | | | $(M+4H)^{4+}$ | 328.90 | | 329.64 | | |
| JI.5.52 | 12.5 | 9.48 | $(M+H)^{+}$ | 1317.40 | | 1319.54 | 12.63 | 100.00 |
| | | | $(M+2H)^{2+}$ | 659.70 | | 660.28 | | |
| JI.5.55 | 26.8 | 17.40 | $(M+2H)^{2+}$ | 769.80 | 770.10 | 771.32 | 14.90 | 94.65 |
| | | | $(M+3H)^{3+}$ | 513.70 | 513.90 | 514.55 | 14.66 | 5.35 |
| | | | $(M+4H)^{4+}$ | 385.60 | 385.70 | 386.17 | | |
| JI.5.58 | 16.4 | 12.22 | $(M+H)^{+}$ | 1341.30 | 1341.20 | 1342.57 | 12.04 | 70.29 |
| | | | $(M+2H)^{2+}$ | 671.40 | 671.30 | 671.79 | 14.91 | 29.71 |

Upon characterisation, several peptides showed more than one retention time by analytical HPLC but the same bass by Mass Spec. From this we deduce the presence of diastereomers (which peptides and to what degree is shown in Table 11), presumably this was due to the presence of cysteines (which are known to be susceptible to racemisation despite HOBt usage).[211] Ideally peptides would either be separated by chiral HPLC or resynthesised using reagents with improved anti-racemisation properties (e.g. HOAt, HATU, PyBOP).[212] However, it was felt that binding constants should be investigated, and that preliminary *in*

*vitro* testing should be attempted. If peptides showed activity then resynthesis or purification could be investigated.

## 5.2 Peptide Binding Characterisation by Microscale Thermophoresis

### 5.2.1 Introduction to Microscale Thermophoresis

Due to the high variability observed in titred peptide ELISAs, a new method was sought for the quantification of peptide binding constants. This variability was primarily due to the high DMSO and surfactant concentrations required to dissolve particularly hydrophobic proteins during the hit screening effort of 30 peptides. With only 9 lead peptides (most of which are reasonably hydrophilic) a more tailored solvent system may be developed to minimise protein disruption.

Considering suitable assay systems, SPR, ITC and microscale thermophoresis (MST) were considered. MST was chosen for its solution-based approach, minimal protein consumption and the ability to perform both direct and competition binding assays.

MST makes use of the thermophoretic effect: the directed motion of molecules along temperature gradients. This is performed by using an infrared (IR) laser to heat a small volume of solution, and measuring the rate of molecular movement along the thermal gradient. This motion is affected by molecule size, charge, solvation shell or conformation; if a binding partner is added to the media then this rate of motion will change. If the molecule has been fluorescently tagged then an excitation light may be used to visualise its position in the solution. By measuring the change in fluorescence at the site of heating, the motion of the molecules (thermophoresis) is inferred. Therefore, by keeping a constant fluorescent partner concentration and measuring across a range of non-fluorescent binding partner concentrations, EC50 concentrations may be ascertained. Microscale thermophoresis minimises protein consumption by using low-volume, thin-walled capillaries for each sample. An overview of how MST may be used to measure binding events is shown in in Figure 83.

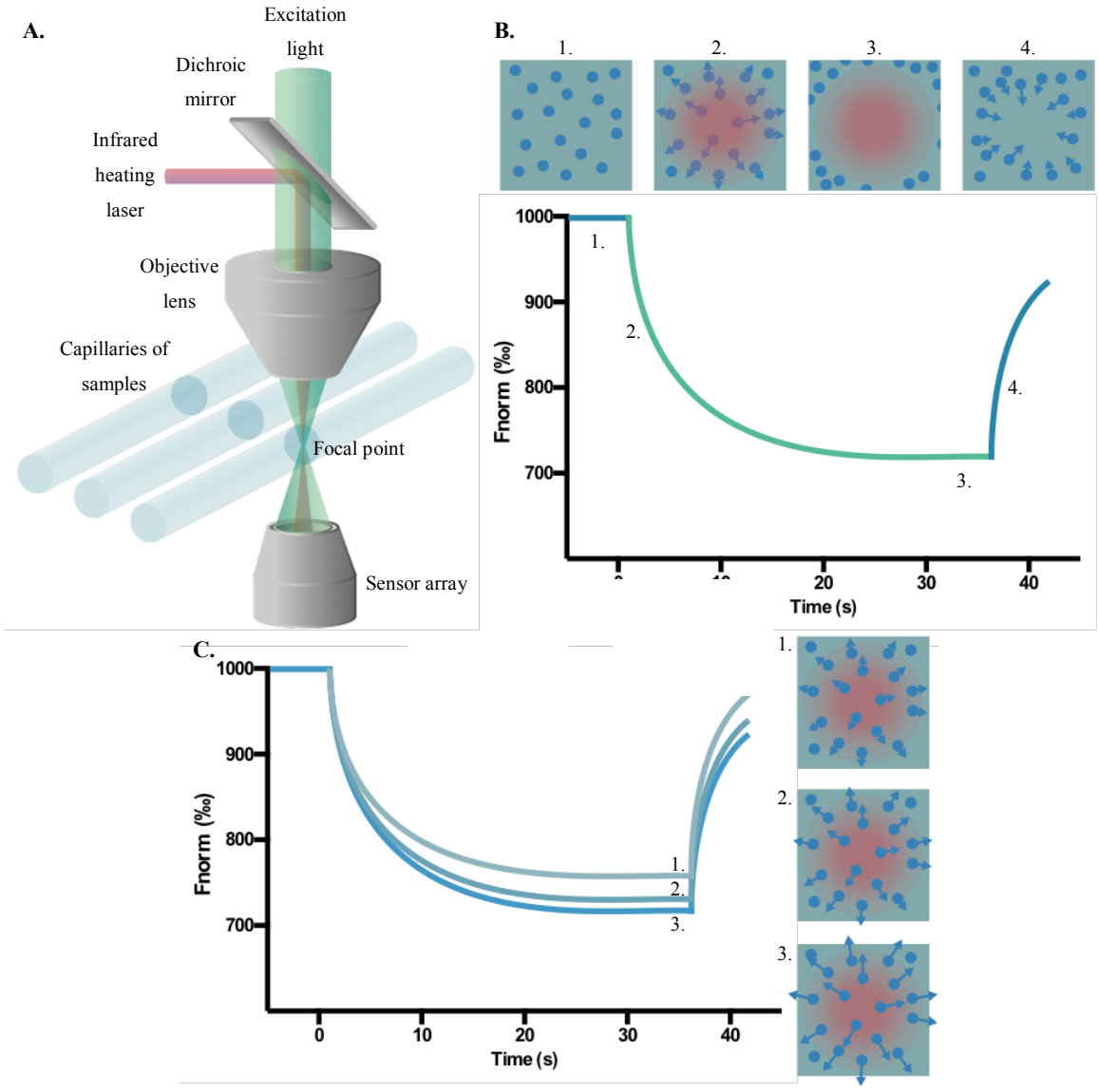



***Figure 83A: Schematic of MST device. Figure 83B: Fluorescence readout stages during an MST experiment. Figure 83C: Fluorescence readout across a range of binding partner concentrations.***

*Figure 83B: 1: Initial conditions: a homogenous mixture. 2. Thermophoresis: heat is applied, creating a thermal gradient the net movement of molecules is away from the focal point of the laser. 3: Steady state: is no net movement of molecules as diffusion matches the thermophoretic effect. 4: Back-diffusion: the net movement of molecules is back into the area as the gradient is removed. Figure 83C: MST measurement for samples with different concentrations of binding partner: 1: Fully bound (low motility), 2: Partially bound (medium motility), 3: Completely unbound (high motility).*

### 5.2.2 Microscale Thermophoresis Overview and Results

Both direct- and competitive-binding MST assays were performed across the library of lead peptides, none of which were able to produce coherent results. This was felt to be due to the labelling technique used to attach fluorescent probes to βNGF and mBDNF: following the Nanotemper Monolith NT™ Protein Labelling Kit RED-NHS manual (Catalogue number L001), NT-647-NHS dye was covalently attached to free amines on the surface of these proteins. This is one of two common, commercially available methods to attach such probes, the alternative is to attach at surface cysteine residues: neither βNGF or mBDNF have such residues. Concerning the labelling method used, due to the locations of amines on the surface of βNGF and mBDNF (Figure 84) it was felt that dye labelling had ameliorated binding of both peptide to βNGF or mBDNF and βNGF or mBDNF to TrkA or TrkB. With such binding nullified, no discernible results could be made.

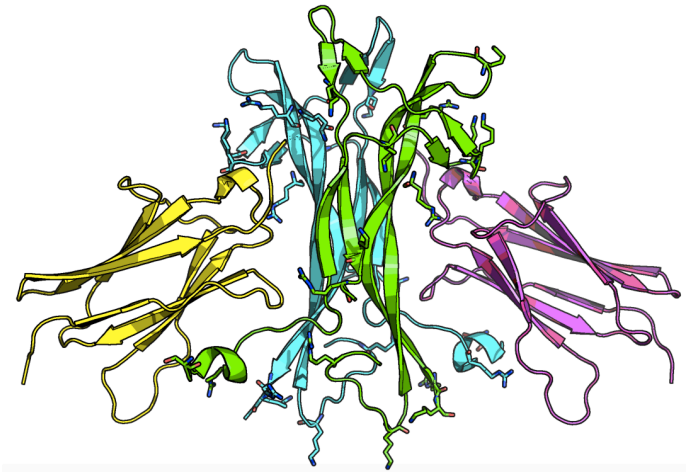


***Figure 84: Crystal structure of βNGF bound by TrkA-D5, highlighting the N-termini, lysine and arginine residues of βNGF. RSCB entry 1WWW.[49]***

If this technique was to be used in the future, it may be worth either attempting to label the TrkA-D5 or the TrkB-D5, or to synthesise βNGF or mBDNF with a surface-available cysteine at the C-termini. Alternatively, a fluorescently labelled peptide may also be used, however given the size of the peptides, this may affect binding.

Finally, an opportunity for collaboration within the University of Southampton became apparent: Dr K. Deinhardt and P. Patil of the Institute for Life Sciences were investigating neuronal morphology and signalling changes induced by βNGF and mBDNF using a well-known cell model, TrkB/PC12.[215] They agreed to perform some preliminary *in vitro* testing of the original unlabelled lead peptides. If the peptides showed activity (particularly if they

agreed with the agonist/antagonist ELISA data) this would provide a strong indication that these peptides were biologically active. Further research could then be used to ascertain the true binding strength these lead peptides display. As cellular testing involves considerably more complex processes than have been used thus far, there is a concern for specificity. This is slightly mitigated as neurotrophin inhibition is extracellular and considering the highly polar nature of their structure it is highly unlikely that any lead peptide is cell-permeable. It is generally considered that most peptides are too polar to be cell permeable, this greatly reduces the number of available targets the peptides can interact with. The cell permeability of a compound may be assessed using a parallel artificial membrane permeability assay (PAMPA), which assesses passive permeability of a compound from one chamber to a second when the chambers are interposed by an artificial membrane. Following incubation, compound concentration in both chambers is measured and compared with starting conditions. This identifies not only how much is capable of passively permeating the membrane, but also how much of the compound is retained on/in the artificial membrane.

## 5.3 *In Vitro* Peptide Testing

As stated, TrkB/PC12 cells are widely used as a model to investigate neuronal differentiation due to βNGF and mBDNF morphological induction. Growth of these rat pheochromocytoma cells in media containing βNGF or mBDNF causes the cells to differentiate into sympathetic neuron-like cells, characterised by the extension of neurites (neuritogenesis) and the flattening of cell bodies due to somatic enlargement. This morphological change is due to the stable expression of TrkA, TrkB and $p75^{NTR}$ in the cell membrane, and the activation of downstream signalling cascades by the autophosphorylation of TrkA and TrkB upon binding βNGF and mBDNF.[215] These assays were performed to investigate whether the lead peptides were capable of agonising or antagonising these downstream cascades, or affecting the morphological changes.

Two experiments were therefore devised: two western blot experiments to investigate lead peptide short-term effects, and two morphology experiments to explore the long-term effects.

### 5.3.1 Lead Peptide Activation/Inhibition Western Blot Assays

To investigate the ability of lead peptides to modulate βNGF-TrkA or mBDNF-TrkB activity, assays were conducted investigating whether a peptide could raise or lower the downstream phosphorylation of proteins activated by this activity. While direct measurement of TrkA and TrkB phosphorylation is possible, the amplification effect of downstream activation greatly improves signal to noise.

Commonly, 50-100 ng/mL of βNGF or mBDNF is used to induce TrkB/PC12 differentiation. In this case, it was felt that this would greatly oversaturate the Trk receptors, masking any agonistic/antagonistic activity by the lead peptides. This was corroborated by an identical differentiation of TrkB/PC12 cells grown in media containing 5-100 ng/mL of βNGF or mBDNF. 10 ng/mL βNGF or mBDNF was therefore used in inhibitory experiments. Considering agonist activity, a minimal activation was sought, to which peptide activity could improve upon. Overnight differentiation experiments showed minimal induction at 1 ng/mL βNGF, or 0.1 ng/mL mBDNF (a difference potentially due to different receptor expression levels, binding constants or downstream effector proteins), therefore for experiments investigating the ability of lead peptides to increase βNGF-TrkA or mBDNF-TrkB activity above baseline, 1 ng/mL βNGF and 0.1 ng/mL mBDNF were used.

For both the antagonist and agonist western blot experiments, TrkB/PC12 cells were prepared and serum starved in DMEM media for one hour. For antagonist assays, 10 ng/mL βNGF or mBDNF was mixed with a lead peptide and incubated for 30-60 minutes. For activation assays, 1 ng/mL βNGF and 0.1 ng/mL mBDNF were similarly mixed with peptide and incubated. These cocktails were then added to the prepared TrkB/PC12 cells and incubated for 10 minutes. Cells were then lysed following the Iwasaka protocol[215] (the addition of 50 mM Tris-HCl (pH 7.4), 150 mM NaCl, 1% nonidet P-40, 1 mM sodium vanadate, 1 mM phenylmethylsulfonyl fluoride, 10 µg/mL leupeptin, 10 µg/mL pepstatin), and the cell lysate centrifuged. The proteins were separated by SDS PAGE prior to being transferred to a nitrocellulose membrane. The membrane was then blotted with BSA before being treated with anti-pAkt-Ser473 (60 kDa), anti-p44/p42 (42/44 kDa) and anti-GAPDH (37 kDa) antibodies. Antibodies were then imaged using HRP-anti-mouse IgG monoclonal antibody conjugate. Blots were photographed and quantified by densitometry. Bands were then normalised using the anti-GAPDH loading control.

These experiments were performed in triplicate using a single fresh lead peptide dissolved stock (dissolved to 1.5 mM in PBS with 5% glycerol, 0.05% Tween-20 and 2% DMSO) with start points at 1, 3 and 7 days. The effects seen in the following western blots reduce between repeats to eventually no effect. This may be due to the hydrolysis-sensitive nature of the disulfide bridge stapling the peptides into conformation. Regrettably, the stocks were not investigated by mass-spec to assess whether the disulfide bond had been reduced.

This suggests that future iterations of these peptides should be fabricated to be hydrolysis-resistant to retain conformation. This may be achieved by replacing the disulfide bridge with an alkene or alkane linker, or through backbone cyclisation. These techniques would also prevent proteolysis and should extend the compounds half-life *in vivo*.

Because of this change in activity, only the day 1 gels are included here. Only sufficient lyophilised peptide remained to investigate morphological changes in duplicate and no further testing.

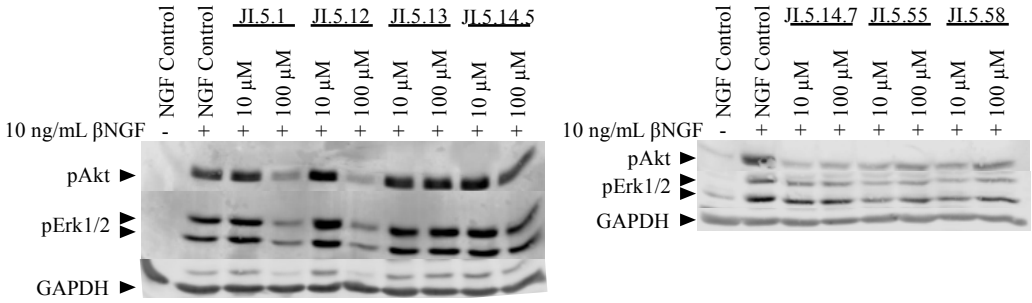



***Figure 85: SDS PAGE western blot of the βNGF antagonist in vitro assay.***

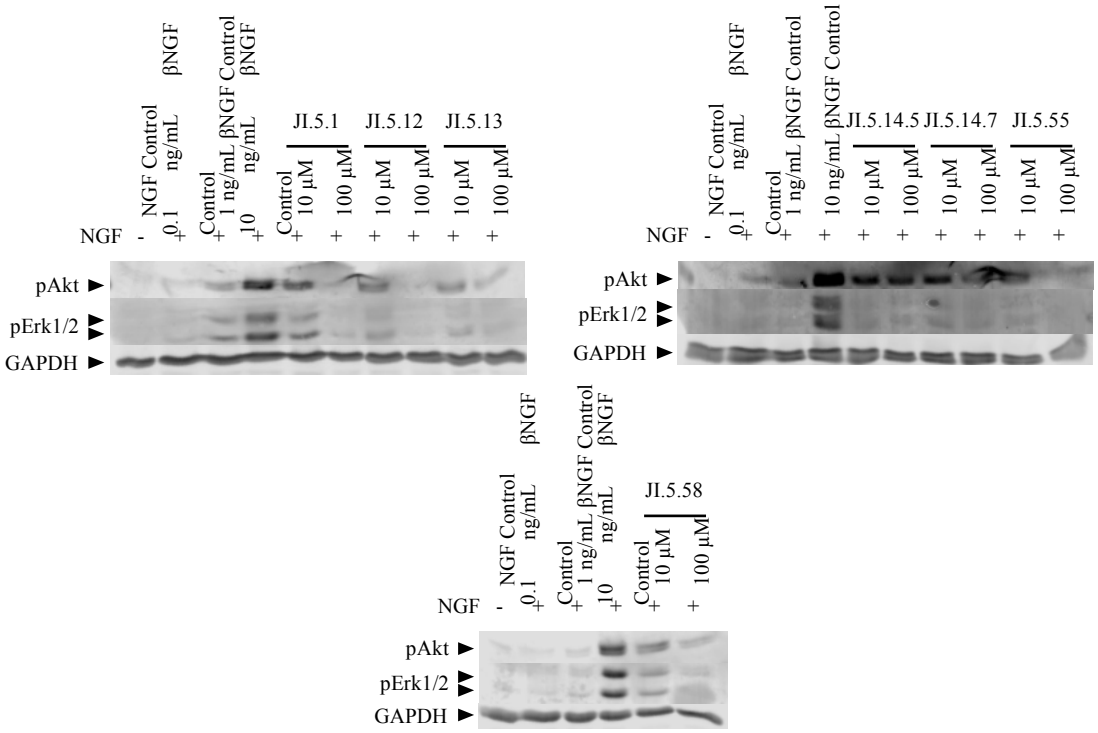



***Figure 86: SDS PAGE western blot of the βNGF agonist in vitro assay.***

Figure 85 and Figure 86 indicate that a number of peptides display clear biological activity. Figure 85 indicates that JI.5.1 and JI.5.12 display clear antagonistic activity at 100 µM, similarly upheld in Figure 86. Perhaps subtler is the antagonistic activity of JI.58 displayed mildly in Figure 85 yet clearly in Figure 86. Regarding agonist activity, Figure 86 indicates that JI.5.14 shows some activity in this regard, reinforced by Figure 85.

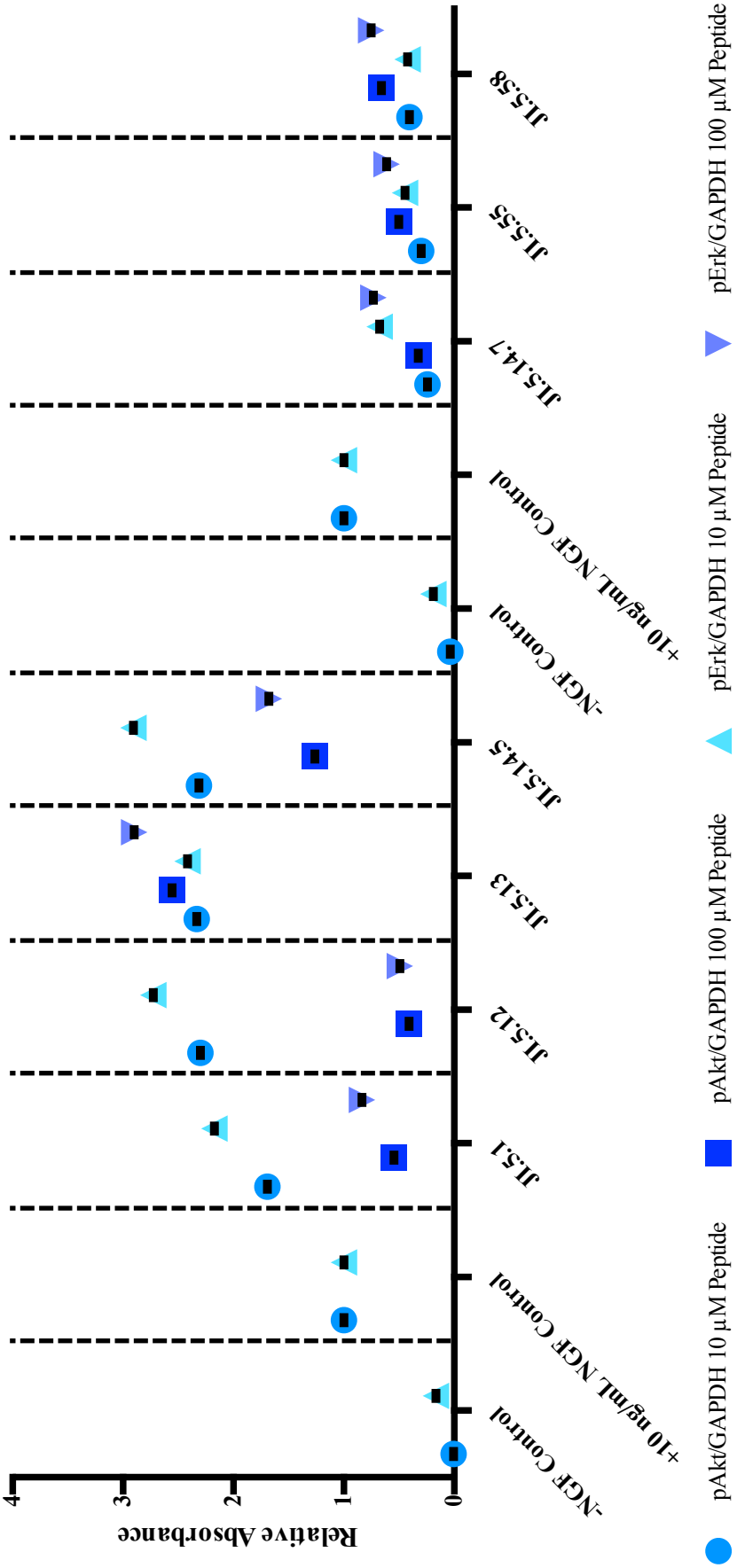



***Figure 87: Western blot densitometry measurements of βNGF antagonist in vitro assays.***

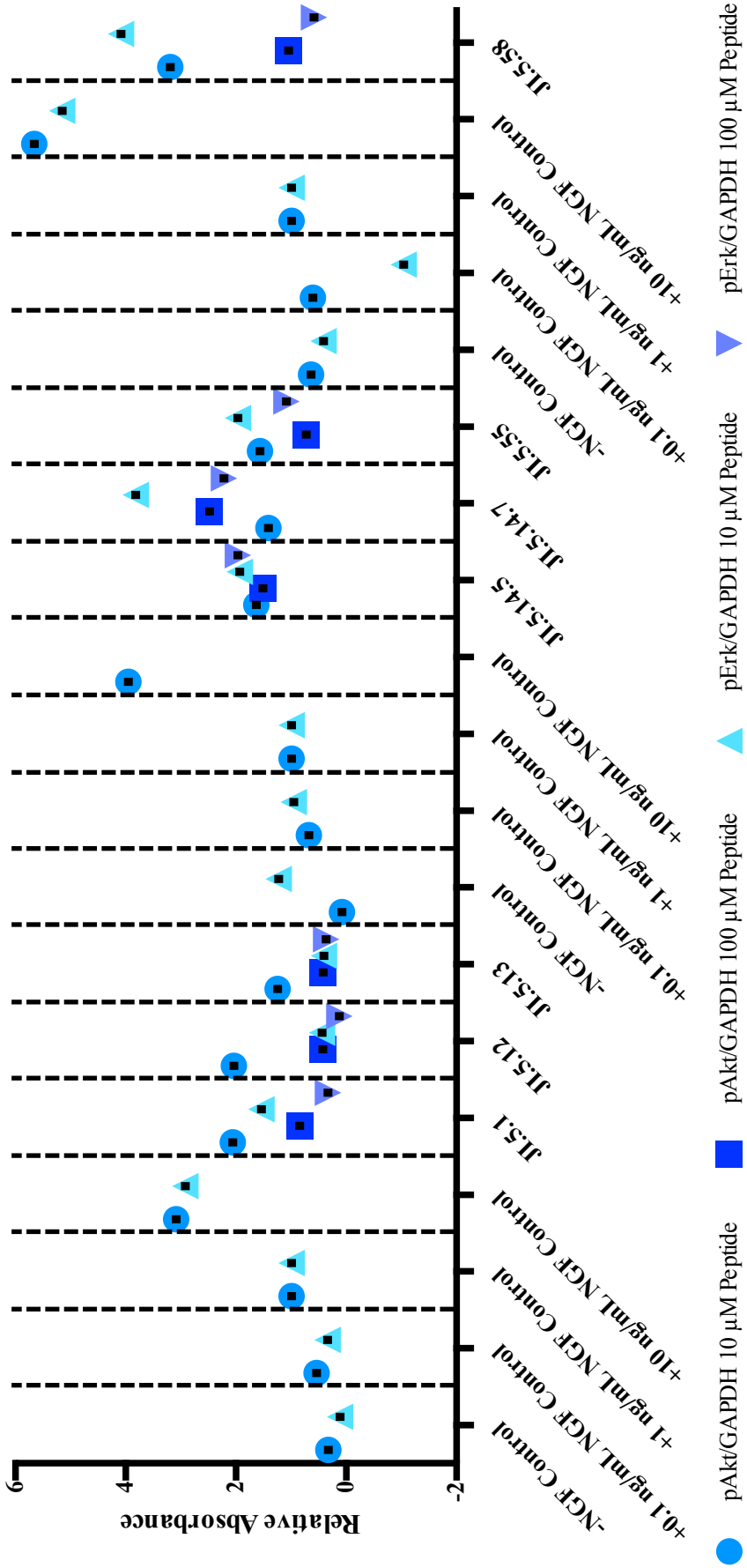



***Figure 88: Western blot densitometry measurements of βNGF agonist in vitro assays.***

As stated, pixel densitometry was used to quantify the above western blots, however due to "smiling", gel bubbles and variable background these should not be used quantitatively, merely qualitatively. Nevertheless, Figure 87 and Figure 88 supports the indications of Figure 85 by showing the antagonistic activity of JI.5.1, JI.5.12, and JI.5.58, and the agonistic activity of JI.5.14. Excluding JI.5.1 which showed no activity, this strongly corroborates the βNGF antagonist or agonist activity shown in the two-component peptide activity ELISA shown in Figure 76.

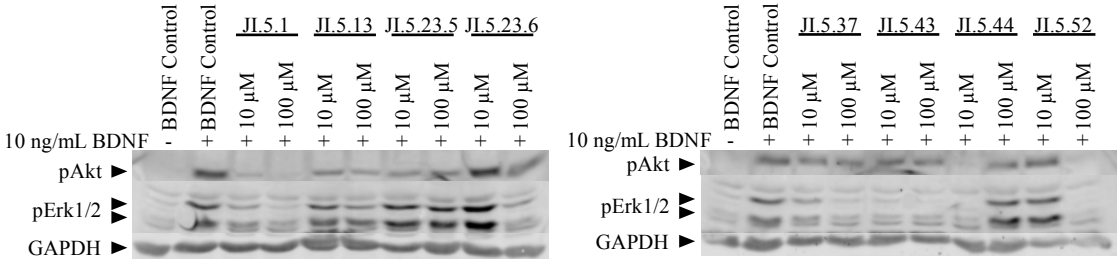



***Figure 89: SDS PAGE western blot of the mBDNF antagonist in vitro assay.***

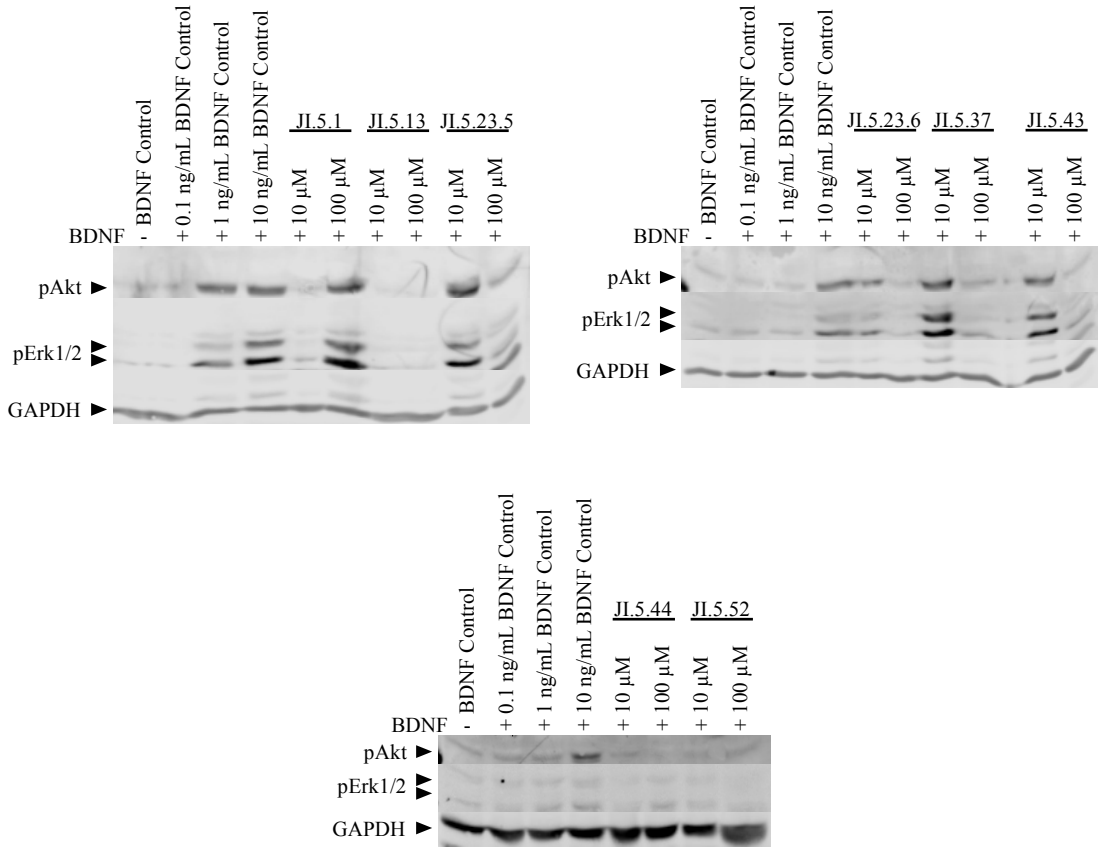



***Figure 90: SDS PAGE western blot of the mBDNF agonist in vitro assay.***

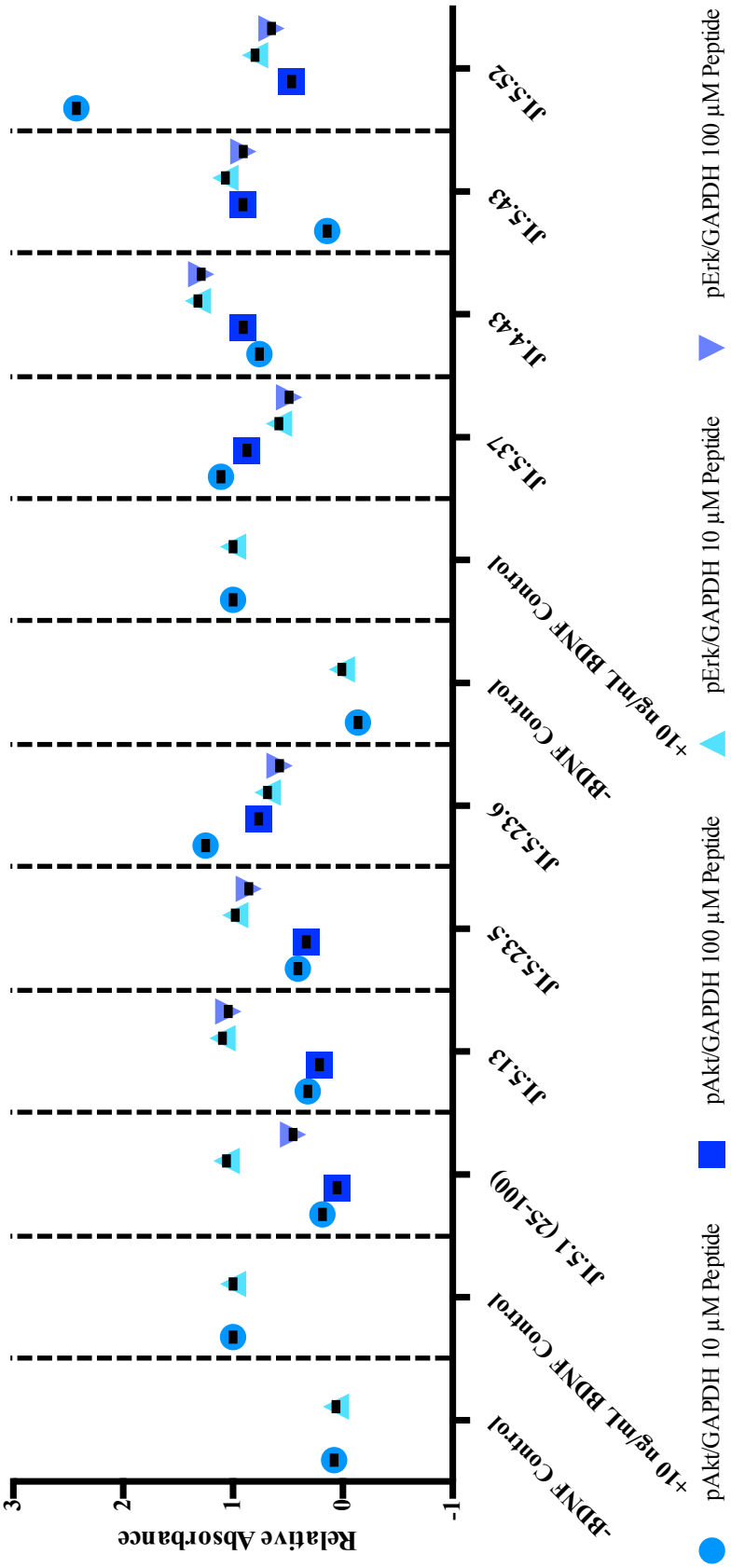



***Figure 91: Western blot densitometry measurements of mBDNF antagonist in vitro assays.***

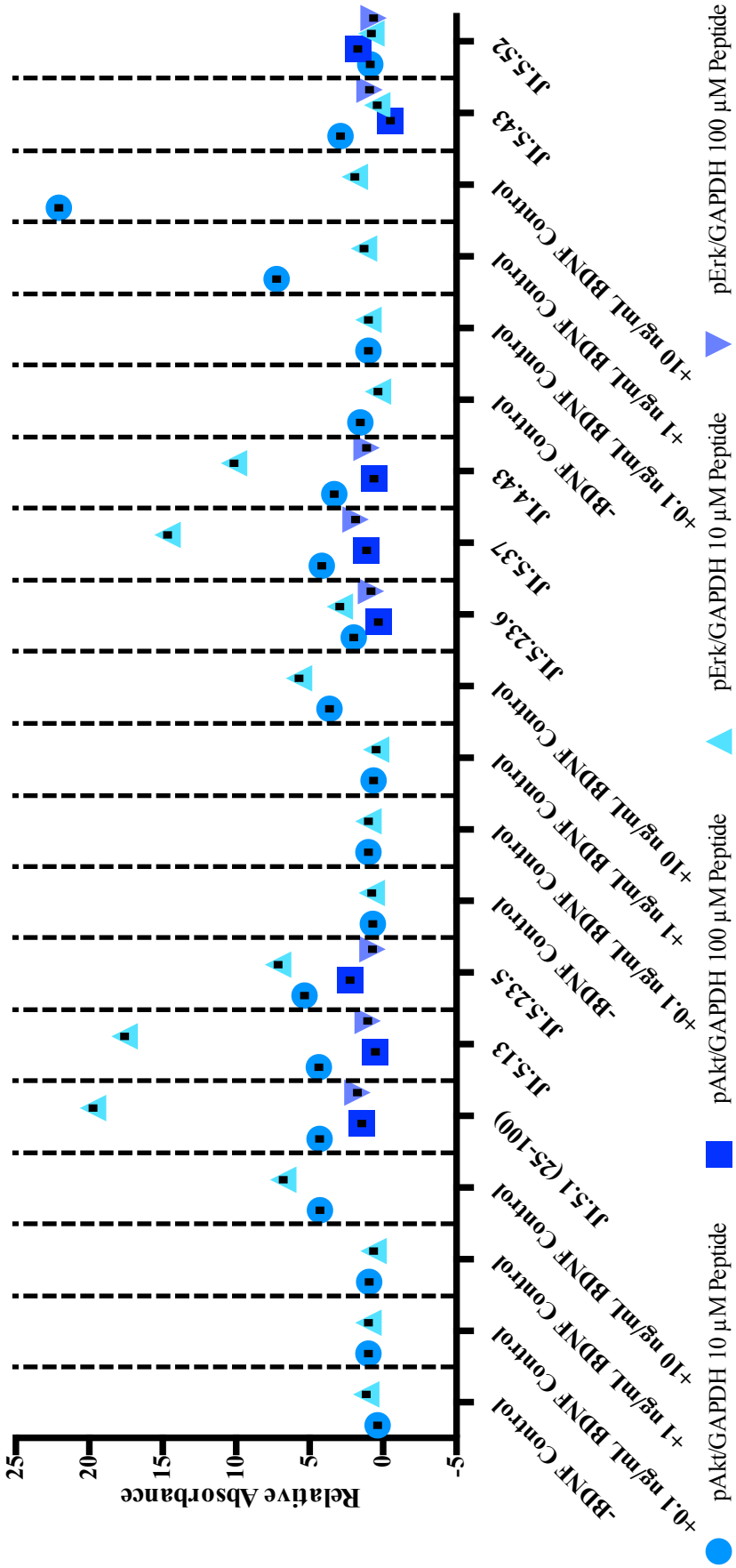



***Figure 92: Western blot densitometry measurements of mBDNF agonist in vitro assays.***

Figure 89 and Figure 90 similarly corroborate the antagonistic activity shown in the mBDNF-TrkB-D5 peptide screening ELISA of Figure 77. Figure 89 indicates that JI.5.23 and JI.5.52 strongly antagonise mBDNF-TrkB, supported by Figure 90. A subtler inhibition is also seen for JI.5.37, JI.5.43 and JI.5.44 in Figure 90. JI.5.1 and JI.5.13 are where these western blots possibly deviate from the ELISA data: these indicate that JI.5.1 has both agonistic and antagonistic activity (it was baseline-antagonistic in Figure 77), and JI.5.13 shows a mild antagonistic activity in Figure 90 (baseline in Figure 77). This may be due to non-specific interactions within the TrkB/PC12 cells.

Figure 91 and Figure 94 qualitatively agrees with Figure 89, Figure 90 and Figure 77, indicating that JI.5.23, JI.5.52, JI.5.37, JI.5.43 and JI.5.44 inhibit mBDNF-TrkB activity.

To conclude, the western blot *in vitro* peptide activity data has identified several peptides which agonise or antagonise βNGF-TrkA or mBDNF-TrkB activity. What's more, this data correlates with the two-component ELISA screening assay data, verifying the information gleaned.

### 5.3.2 Morphology Assays

To investigate whether peptides could modulate the long-term effects βNGF and mBDNF have on TrkB/PC12 cells, 10 ng/mL, 1 ng/mL and 0.1 ng/mL βNGF and mBDNF samples were mixed with lead peptide and incubated for 30-60 mins. Similar to the western blot protocol, TrkB/PC12 cells were prepared and serum starved for 1 h. Cells were then treated with mixtures of neurotrophin and peptide—the same concentrations as previously: 10 ng/μL for inhibition experiments, 0.1 ng/mL βNGF and 1 ng/mL mBDNF for agonist experiments—and incubated. Cells were imaged at 24, 48 and 72 h post-neurotrophin addition, and 100 cells from each duplicate set of each condition were measured. At time of publication only the 48 h have been processed and therefore included in this report.

Neurite length was determined by relative length to cell body diameter, with lengths grouped into <3x, 3-5x and >5x cell body diameter. Neurite lengths of <3x cell body diameter represent un-differentiated cells, 3-5x represent partial differentiation and >5x represent full differentiation. As such, antagonism is identified as a decrease in cells with >5x relative neurite length, and agonism is identified as a decrease in cells with <3x relative neurite length. With the peptide degradation observed during the western blots, it

was unknown whether activity would be observed during this extended exposure to cell media and the metabolites that cells produce.

JI.5.1 and JI.5.12 were initially included in the morphology assays, yet proved cytotoxic presumably due to precipitation: these two were the most hydrophobic of the lead peptides and considerable effort was expended attempting to optimise the solvent system to them. These were retested by creating 250 µM stocks (diluted to the working 100 µM), unlike the remaining peptides which were in 1.5 mM stocks. This resulted in an increased DMSO, glycerol and surfactant concentration in the media and therefore required a unique DMEM-only peptide-negative control. As such, these have been included in separate charts found below. At time of publication this had only been performed once however.

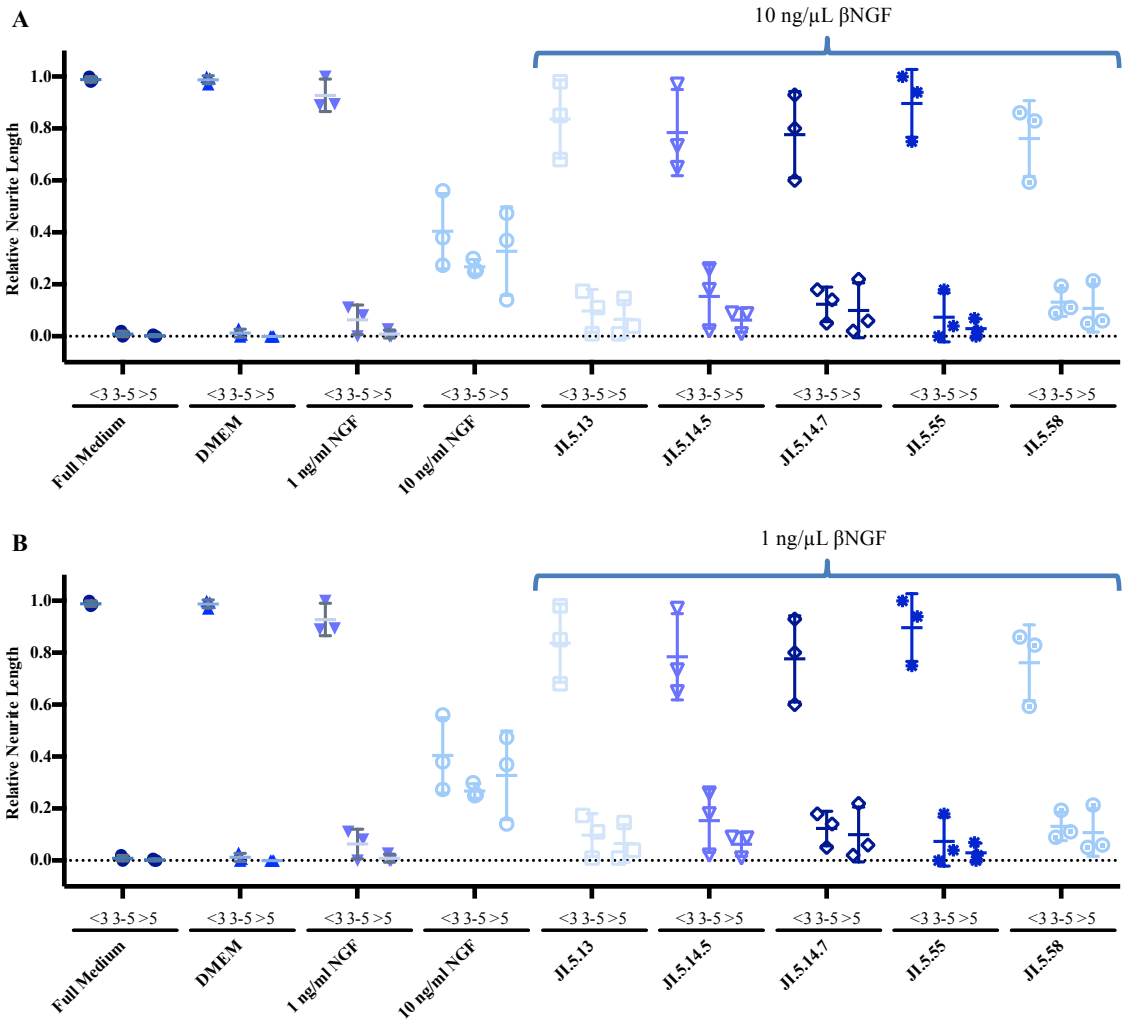



***Figure 93: βNGF morphology assays of A: antagonist and B: agonist activity.*** *Mean ± SD, n=3 with 100 measurements per condition per repeat.*

Despite the successful controls which show no differentiation without βNGF and strong differentiation with βNGF, Figure 93A displays considerable variability in the conditions with added peptide. Inspecting the raw data reveals a strong pattern: in the first experiment, no antagonistic behaviour is observed, yet in the repeat all peptides (except JI.5.14.5) display antagonistic activity. Arguably the most antagonistic is JI.5.58 and JI.5.13 however variability is too large to draw any strong conclusions. Figure 93B does not share this pattern of first vs. second repeat and the results therefore hold slightly more validity, however all peptides merely show mild agonist activity, the strongest being arguably JI.5.14.7.

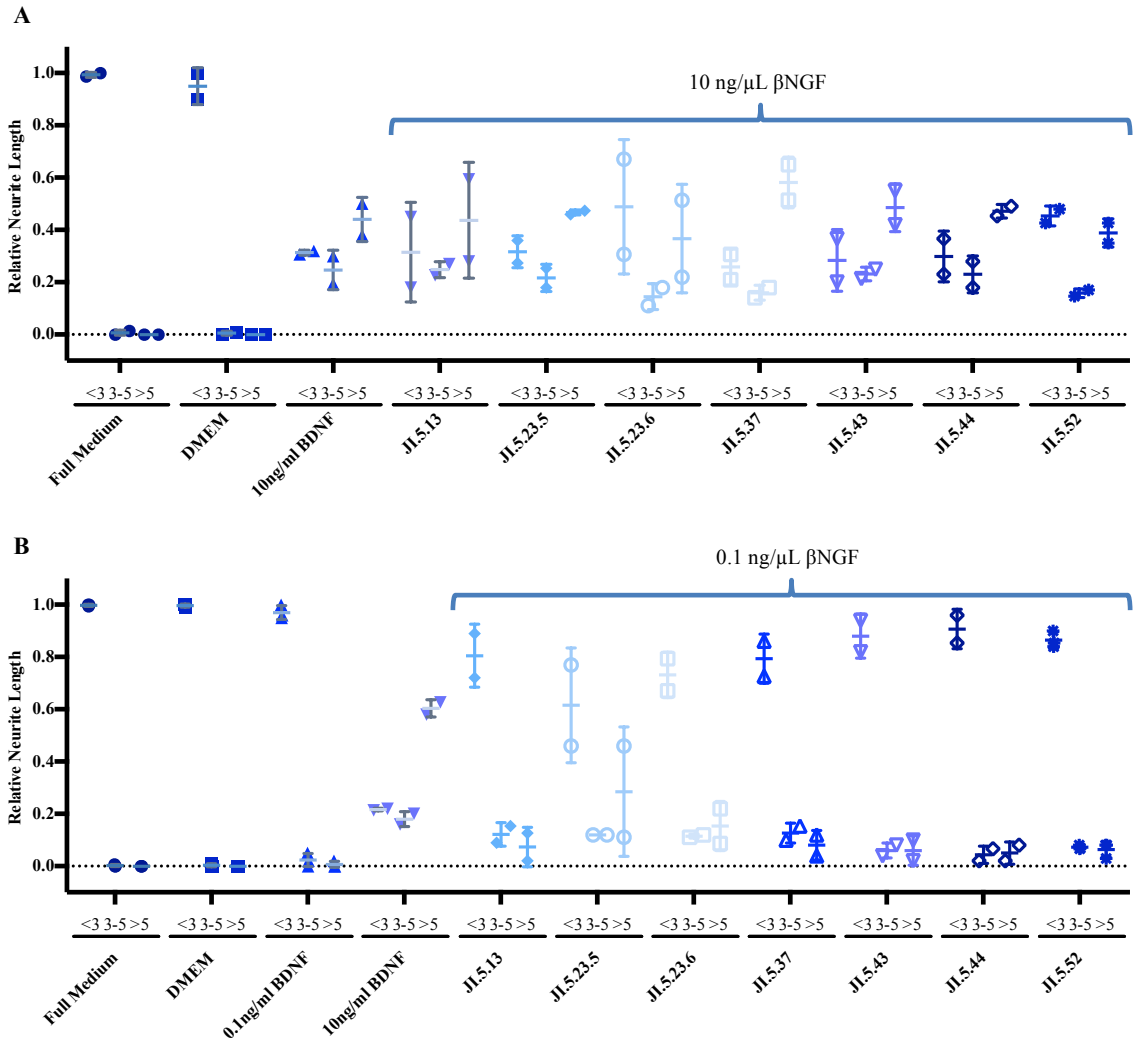



***Figure 94: mBDNF morphology assays of A: antagonist and B: agonist activity.*** *Mean ± SD, n=2 with 100 measurements per condition per repeat.*

Fortunately, Figure 94A does not mimic the distinct variability pattern found in Figure 93A. Regrettably most peptides show no activity whatsoever, with the possible exception

of JI.5.13 and JI.5.23.6, however the variability is too high to be certain. Figure 94A shows a similar lack of efficacy with the exception of JI.5.23 (either), which display some agonist activity (running contra to the antagonist activity displayed thus far).

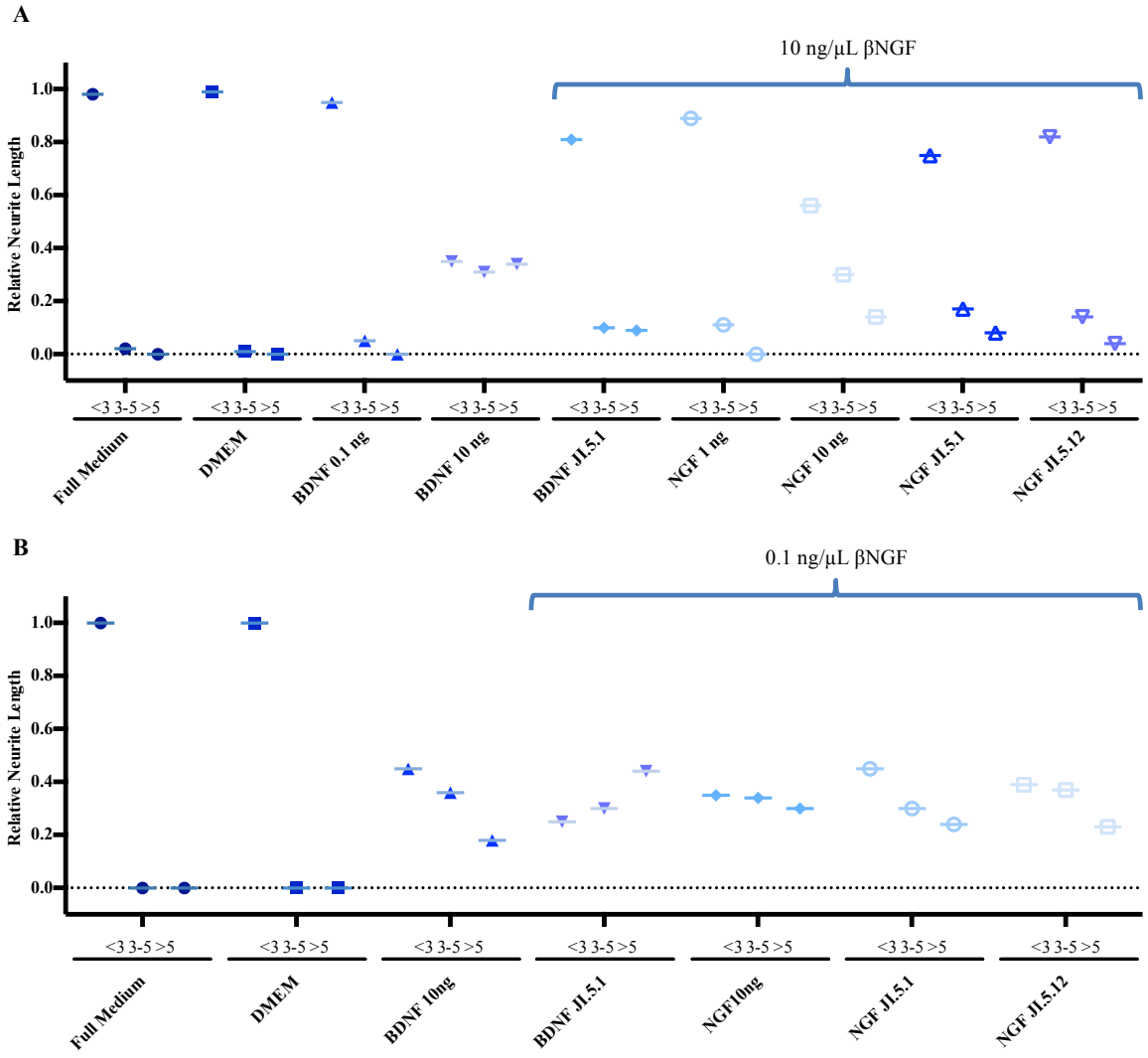



***Figure 95: mBDNF morphology assays of A: antagonist and B: agonist activity.*** *n=1 with 100 measurements per condition.*

Given that the 10 ng of neurotrophin positive controls do not fully differentiate, Figure 95 indicates that the cells cannot function correctly in the media containing increased DMSO and surfactant. No conclusions should therefore be brought from this data and a solubility tag may be required to further study these peptides.

To conclude, this morphology data suggests that all peptides display little to no long-term effects when incubated (37 ˚C) for several days with cancer cells. This is to be expected

given the disulfide bonded hairpin structure of the peptides, and strongly suggests the use of analogues which are hydrolysis or reduction resistant.

## 5.4 Chapter 5 Conclusions

The aim of this chapter was to verify and quantify the agonist or antagonist activity of peptides identified in Chapter 4. A number of MST based assays were attempted, focussing on amine tagging βNGF or mBDNF and either measuring direct peptide binding or competitive binding with TrkA or TrkB. These proved unsuccessful, which is thought to be due to the location of the amines on βNGF or mBDNF – the putative binding site for TrkA or TrkB. As such, it was felt that amine tagging βNGF and mBDNF removed the ability to bind to TrkA or TrkB. In hindsight, amine tagging of TrkA or TrkB for a competitive binding assay with untagged βNGF or BDNF should have been attempted.

Alternatively, ITC and SPR could have been used to quantitatively assess binding and inhibitory activity. ITC is attractive as it is a tag-free method of assessing binding. SPR would be useful as tagged TrkA or TrkB could be bound to the chip and βNGF or mBDNF could be flowed past at a constant concentration in the presence or absence of peptides. These assays would therefore be part of potential future work in this area.

Finally, *in vitro* testing was used to assay modulatory activity of these peptides against rat pheochromocytoma cells which stably express TrkA and TrkB cell membrane receptors. Adding βNGF or mBDNF to the cell media causes signalling cascades in these cells, therefore peptides were pre-incubated with βNGF or mBDNF prior to addition to the media. Modulatory activity was therefore measured by western blot to assess the divergence of signalling cascade phosphorylation from baseline. The signalling cascades also initiate measureable morphological changes of the cells, so a second assay was conducted to assess long-term peptide modulatory effect.

The above western blot assay verified the modulatory effect of a number of peptides, however this effect was ameliorated in the morphological assay. This change in activity may be due to the known susceptibility of a disulphide bridge to reduction in aqueous media: the protracted aqueous conditions of the morphological assay may have removed the conformational restriction of the peptides, which may have been critical to activity. As such, synthesising hairpin-stapled peptides analogues would form part of future research in this area.

***Table 12: Collated qualitative results of modulatory ELISA and* in vitro *assays***

| | | **Modulatory Binding ELISA (Figure 76 & Figure 77)** | | **Titred ELISAs (Figure 78 & Figure 79)** | | ***In vitro* Western Blot (Figure 85-Figure 92)** | |
|---|---|---|---|---|---|---|---|
| **Code** | **X7 Region** | **NGF** | **mBDNF** | **NGF** | **mBDNF** | **NGF** | **mBDNF** |
| JI.5.1 | QHWPWFS | | | | | Antagonist | |
| JI.5.5 | GPGTLRV | Agonist | Agonist | | | | |
| JI.5.12 | WTIYLMP | Antagonist | | Antagonist | | Antagonist | |
| JI.5.14 | GRYMDGG | Agonist | | Agonist | | Agonist | |
| JI.5.15 | ENKHTWG | Agonist | | | | | |
| JI.5.20 | SHIDTQW | | | | | | |
| JI.5.21 | GSAPVRS | | | | | | |
| JI.5.23 | HMAFKKI | | Antagonist | | Antagonist | | Antagonist |
| JI.5.24 | KNIVAPW | | Agonist | | | | |
| JI.5.25 | DPHWPFN | Agonist | | | | | |
| JI.5.27 | TMGLTHS | | | | | | |
| JI.5.33 | SWLHWWQ | Agonist | | | | | |
| JI.5.36 | GSKINQY | Agonist | | | | | |
| JI.5.37 | NAGHLSQ | Agonist | Antagonist | | Antagonist | | Antagonist |
| JI.5.40 | SLSRLPS | Agonist | | | | | |
| JI.5.41 | PSTVPWS | | Antagonist | | | | |
| JI.5.43 | NSFNSGS | | Antagonist | | Antagonist | | Antagonist |
| JI.5.44 | NSHRHGA | Agonist | Antagonist | | Antagonist | | Antagonist |
| JI.5.52 | SLNHTVN | | Antagonist | | Antagonist | | Antagonist |
| JI.5.55 | FYKWHSH | Agonist | | Agonist | | | |
| JI.5.56 | YSNATGS | | | | | | |
| JI.5.57 | QMNNSDF | Antagonist | | | | | |
| JI.5.58 | YELTPGK | Antagonist | | Antagonist | | Antagonist | |
| JI.5.62 | NPHFYKH | | | | | | |
| JI.5.64 | NFGSPDQ | | | | | | |
| JI.5.71 | SGLTRPT | | | | | | |
| JI.5.72 | YTERTKL | Antagonist | | | | | |
| JI.5.73 | NAGHRSQ | | | | | | |

Table 12 indicates that the majority of qualitative data is consistent throughout the three key assays of this research, and that the effects are specific between βNGF and mBDNF.

It is however surprising that for the most part these results have shown that these peptides are specific between βNGF and mBDNF; considering the high sequence

It would of course require qualitative assays such as ITC or SPR to be able to rank these fully, which will form a large part of the future work of this project.

# Chapter 6: Thesis Overview, Conclusions and Future Work

## 6.1 Thesis Introduction

βNGF and mBDNF are autocrine and paracrine proteins used for extracellular communication in nerve cells. Their dysregulation has been linked with a number of disease states such as chronic pain,[11, 13-15, 17] various cancers[26-29] and alzheimer's.[34-36] It is felt that their selective modulation (both inhibition and activation) could be used to treat these diseases from a novel direction. However, despite nearly thirty years of research in this area, there is only one pan-Trk inhibitor currently in the clinic for treating a form of cancer, and one βNGF inhibitor in Phase III trials. A new route towards modulating βNGF and mBDNF was therefore proposed: using oligopeptides as scaffolds to enter a chemical space beyond Lipinski's rules:[20] as protein-protein interactions occur via large surfaces, small molecule inhibition may not be the most appropriate solution. As such, phage display was selected as a technique to screen large peptide libraries (1 trillion members) for their ability to bind to either βNGF or mBDNF. While pVIII based M13 phage display has been used against βNGF in the development of AMG819, no other phage display has been used against either βNGF or mBDNF. As stated previously, AMG819 failed at phase 1 trials due to an unacceptably promiscuous immunogenic epitope. That study used a variable 20-mer peptide fused to M13 pVIII[101] There is no guarantee that changing to the $ACX_7CG_3S$ motif used in this pIII based M13 phage display does not show this immunological propensity, but it is to be hoped.

## 6.2 Overview and Conclusions

As stated, the NEB C7C library was selected to screen against βNGF and mBDNF. This was used successfully in a streptavidin control screen to ensure correct use of technique by selecting the HPQ motif. An unbiased $ACX_7CG_3S$ pIII M13 phage library was then screened for affinity for βNGF and mBDNF using a surface panning protocol. Three pans were conducted and several phages were isolated, sequenced, and tested for specificity between neurotrophin and ancillary protein/plastic support. Most phages considerably passed this selectivity test, however it was felt that the motifs identified showed too high variability and that further pans were required. Two more pans were conducted, using conditions of greater stringency. Sequencing the phages isolated from these pans revealed a number of repeated sequences and motifs, and the phages were therefore taken forward to the next stage. Phage specificity between target and support was repeated and—

following some concentration-based aggregation issues—the phages were found to have a good selectivity window between their neurotrophins, the ancillary BSA, plastic support and some even showed strong selectivity against an anti-target (HIF-2α PasB, Figure 51).

Next, the hit peptides had to be assessed for their ability to modulate βNGF-TrkA-D5 and mBDNF-TrkB-D5 activity. Based on a crystal structure of βNGF bound by the neurotrophin-binding domain of its receptor, TrkA,[49] a two-component ELISA assay was designed. This required significant optimisation in the *E. coli* expression, refolding and purification of FLAG tagged TrkA-D5 and TrkB-D5. An attempt was made to similarly express tagged βNGF and mBDNF as this would allow far greater flexibility for further experiments, however baculovirus transformed insect cells remain the only feasible route to expressing human βNGF and mBDNF: expression techniques outside the scope available to this project.

The above protein assay was developed and optimised, and thanks to kind Pfizer backing all 30 hit peptides were purchased and screened for their ability to modulate βNGF-TrkA-D5 and mBDNF-TrkB-D5 interactions. As predicted, most failed to show significant modulatory effect, presumably due to binding to a surface other than the TrkA-D5 or TrkB-D5 binding site or from being out-competed by TrkA-D5 or TrkB-D5. Several peptides did however modulate βNGF-TrkA-D5 or mBDNF-TrkB-D5 binding, both positively (agonists) and negatively (antagonists). These lead peptides were further investigated by ELISA by measuring their modulatory effects over a range of concentrations. While trends were retained and IC50s were in the expected μM range, error was particularly high: presumably due to the relatively high concentration of DMSO in the sample. This DMSO had been included as it was necessary to dissolve some hit peptides, but screening the lead peptides in this fashion would have benefitted from bespoke DMSO concentrations to minimise their effects.

At this point some purchased peptide stocks had been expended, therefore solid-phase peptide synthesis was used to produce more. These were cyclised by disulfide bond and used in direct- and competition binding assays using microscale thermophoresis. Potentially this is a fast, accurate assay and can be used for a wider range of experiments. Unfortunately no coherent binding signals could be generated by this project—potentially due to fluorescently labelling the TrkA-D5 binding site of βNGF, or the TrkB-D5 binding site of mBDNF. Synthesising fluorescently labelled peptides was attempted but sufficient quantities of peptides in reasonable purity could not be isolated. Future work in this area

would be to fully ascertain lead peptide binding data, which could be performed in a number of ways: as stated, the TrkA-D5 or TrkB-D5 could be fluorescently labelled for MST, βNGF and mBDNF could be synthesised to have an additional cysteine on their surface for fluorescent tagging, or better yet use a label free method such as surface plasmon resonance (SPR) or isothermal titration calorimetry (ITC). These label-free techniques can be used to accurately measure binding events with far lower assay artefacts—particularly with ITC, which also tests in solution. As they test using far larger volumes than MST they consume significantly more protein per experiment (hence the attempt with MST).

The final stage in this project was to test the biological efficacy of the lead peptides. This final proof of concept was performed by assessing the change in downstream phosphorylation of TrkA or TrkB signalling cascades. The βNGF assays suggested that JI.5.58, JI.5.1 and JI.5.12 warrant further investigation as antagonists of βNGF, and JI.5.14 does as an agonist. The mBDNF assays confirmed that JI.5.23, JI.5.52 and JI.5.44 warrant further investigations as mBDNF antagonists. This data correlates with the two-component ELISA screening data, adding weight to the argument.

Morphology studies were also conducted to test whether lead peptides could antagonise or agonise the long-term physical effects of βNGF or mBDNF on TrkB/PC12 cells. These and the repeats of the western blot highlighted the fragile nature of the peptides however: they gradually degrade in aqueous media, presumably due to reduction of the disulfide bonds stapling their conformation as hairpins.

## 6.3 Future Work

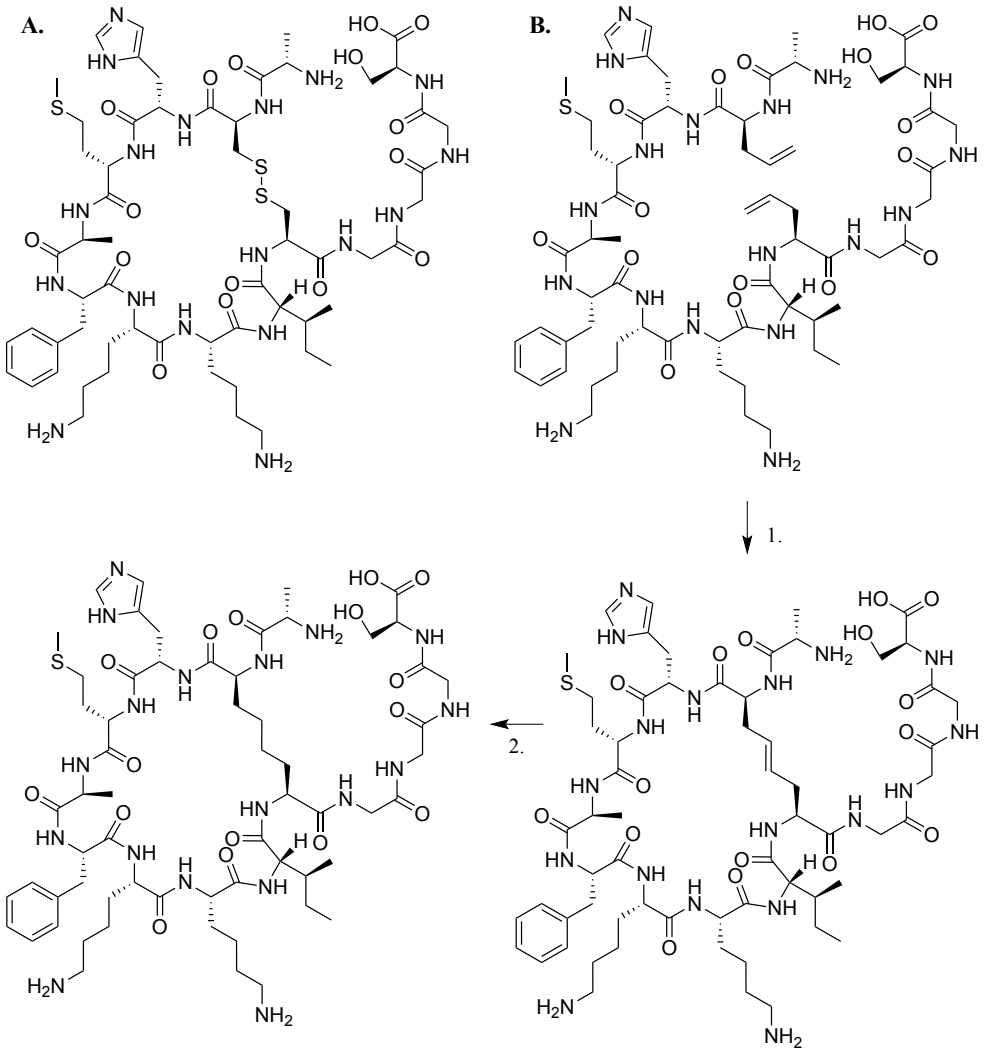
Moving forward, as stated it is very important to uncover the binding strength of the lead peptides as it allows their quantitative ranking and therefore the focus of future research. It would also be invaluable to identify the active motif of various lead peptides. This is typically performed on peptide-based lead compounds using alanine scanning: synthesising variants of a lead peptide where one residue is replaced by alanine. The binding strength of the series is then tested, allowing the binding contribution of each amino acid side chain to be assessed. Binding contribution is not only related to the type and location of motifs which permit intermolecular bonds to be formed, but also intramolecular interactions, including stoichiometry: larger constituents such as a Trp residue may affect the peptide conformation differently than Ala or Gly. Uncovering the binding contribution of each

amino acid also allows simplification or modulation of the lead peptide to have added functionality or better properties such as improved solubility.

This research focussed on the inhibition of βNGF/TrkA and mBDNF/TrkB PPI activity, it has not investigated whether the peptides could inhibit βNGF/$p75^{NTR}$ or mBDNF/$p75^{NTR}$ PPI activity, nor whether the hits are selective between mature neurotrophins and pro-neurotrophins. The former would be a perfectly valid extension of this work, the latter would be a key characterisation for any lead compound. Indeed, lead compounds would have to be screened for specificity across a range of human proteins as part of lead development.

A covalent warhead may be added to an area of a peptide not involved in binding, allowing the peptide binding site to be uncovered. Alanine scanning also allows a second-generation of that peptide to be explored: swapping key amino acids with analogues in an attempt to improve binding strength and prevent dissociation. If a binding site can be uncovered then modelling may be used to investigate the binding conformer. As such, rational design may be employed to make analogues.

As stated it is likely that the disulfide bridge is critically important to maintaining the correct conformation for biological activity. Unfortunately, this bond is readily reduced, therefore a key second generation lead peptide would be to replace the cysteines with reduction-resistant analogues such as an alkene/alkane bond. This should dramatically improve the serum half-life of the active conformation, and prevent proteolysis. To do so, cysteine is easily replaced by allyl glycine during SPPS, and metathesis can be used to form an alkene hairpin lead peptide analogue. The alkene may then be selectively hydrogenated to form an alkane, whose bond angles are closer to the disulfide bridge. The alkene may produce a better conformer however, so both should be tested.




***Scheme 4: Second generation alkene/alkane disulfide bridge analogues.*** *Scheme 4A: JI.5.23. Scheme 4B: synthesis of a JI.5.23 alkene or alkane analogue using allyl glycine. 1: Grubb's second generation catalyst in DCM. 2: $H_2$, Pd/C in MeOH.*

Finally, while further research is warranted by all lead peptides, in hindsight JI.5.5 should have undergone further investigation. On inspection of Figure 76 and Figure 77, JI.5.5 appears to be non-specific between βNGF and mBDNF, however this is the only peptide which showed dose-responsive agonist activity of mBDNF.

To conclude, this project has identified a number of novel peptides capable of either positively or negatively modulating βNGF or mBDNF activity. Some have proven to be biologically active, and through development may offer a unique and novel approach to treating a number of critical diseases.

***Table 13: Lead peptide activity***

| Code | X7 Region | Activity | Code | X7 Region | Activity |
|---|---|---|---|---|---|
| JI.5.5 | GPGTLRV | NGF and mBDNF Agonist | JI.5.43 | NSFNSGS | mBDNF Antagonist |
| JI.5.12 | WTIYLMP | NGF Antagonist | JI.5.44 | NSHRHGA | mBDNF Antagonist |
| JI.5.14 | GRYMDGG | NGF Agonist | JI.5.52 | SLNHTVN | mBDNF Antagonist |
| JI.5.23 | HMAFKKI | mBDNF Antagonist | JI.5.55 | FYKWHSH | NGF Agonist |
| JI.5.37 | NAGHLSQ | mBDNF Antagonist | JI.5.58 | YELTPGK | NGF Antagonist |

Summary of potential future work:

1. Synthesise reduction-resistant analogues of lead peptides using allyl glycine/metathesis/hydrogenation strategy
2. Characterise binding to target and modulatory activity using SPR and/or ITC, so that leads can be ranked and prioritised
3. Use alanine scanning to identify the lead peptide active motifs
4. Use that data to develop next-generation analogues.
5. Test all of the above for their activity in cells, particularly assessing whether the reduction-resistant strategy was effective.

# Chapter 7: Experimental

## 7.1 Materials and Equipment

All chemicals were purchased from Fisher Scientific, Sigma Aldrich (UK), Novabiochem (Merck Millipore) or Matrix Scientific and were used unmodified. HPLC grade solvents were purchased from Scientific and used unmodified. Primers and gene blocks were purchased from Eurofins MWG or Integrated DNA Technologies. All restriction enzymes and buffers were purchased from New England Biolabs, all polymerase enzymes were purchased from Promega. Primers, genes and gene blocks were synthesised by Eurofins MWG Operon or Integrated DNA Technologies.

All sterilisation by autoclave was conducted with a LTE Touchclave-R following the manufacturer's instructions. All centrifugation of 1.5 mL Eppendorf tubes were centrifuged with a Fisher Scientific Accuspin Micro, larger samples were centrifuged with a Thermo Electron Corporation Heraeus Biofuge Primo R Centrifuge, following the manufacturer's instructions. All DNA concentrations were identified with a NanoDrop ND1000 Spectrophotometer following the manufacturer's instructions for DNA. All agarose and SDS-PAGE gels were separated using a BioRad Power Pack Basic and visualised with a BioRad Universal Hood II imager using BioRad Quantity One software, following the manufacturer's instructions. All electroporation was conducted with a Bio-Rad Micro Pulser electroporator following the manufacturer's instructions. All heat-killing of enzymes was performed using a Grant QBA1 for samples in 1.5 mL Eppendorf tubes, and with an Eppendorf Mastercycler Personal for samples in 250 µL PCR tubes. FPLC was conducted using a GE Healthcare Life ÄKTAprime Plus following the manufacturer's instructions. Size exclusion chromatography was conducted using a GE Healthcare HiLoad Superdex 16/600 75PG prep grade column. Affinity purification was conducted using 1 mL GE Healthcare HisTrap FF columns. HPLC was conducted using an HPLC Waters system. Mass spectrometry was performed on a Waters 2MD Single Quadrupole mass spectrometer by the University of Southampton MS service using a C18 reverse phase program. All Agar plates were incubated in a Heraeus Function Line incubator, liquid cultures were incubated in a Thermo Scientific Max Q 6000. Opacity of bacterial cultures was measured using a Varian Cary 100 Bio UV-Visible Spectrophotometer tuned to 600 nm, following the manufacturer's instructions. All restriction sites were identified using EnzymeX software. All DNA sequencing was performed by Eurofins MWG. All

sonication was conducted using a MSE Soniprep 150Plus following the manufacturer's instructions. ELISA results were measured using a Tecan Infinite M200 Pro micro-plate reader. Large scale protein bacterial culture was performed using an Eppendorf UK Bioflo 110 fermenter following the manufacturer's instructions. MST was performed using a Nanotemper Monolith NT.115 instrument following the manufacturer's instructions. Water baths used were either A Grant SubAqua 5 and a Clifton water bath, containing an aqueous solution of Wak Chemie AquaClean (0.5 % v/v). All water was purified using a Millipore Elix Advantage 3 following the manufacturer's instruction.

## 7.2 Preparation of Materials

### 7.2.1 Agarose Gel

Agarose (1% w/v) was dissolved in Tris-acetate-EDTA (TAE) buffer and heated by microwave (800 W, 2 min). After dissolution, ethidium bromide (~0.625 mg/mL, 1 drop per 50 mL) was added and mixed by swirling. This was then allowed to set in a cast (~20 min) before usage.

### 7.2.2 Antibiotic Stock Solutions

Antibiotic stock solutions were created under sterile conditions through the dissolution of the antibiotic into autoclaved deionised water or biological grade ethanol (as indicated), mixed by inversion and filtered through a 0.22 µm Millipore filter before storage at 4˚C.

***Table 14: Antibiotic concentrations.***

| Antibiotic | Solvent | Stock Concentration | Working Concentration (Plasmid) | Working Concentration (Chromosome) | Storage |
|---|---|---|---|---|---|
| Carbenicillin | H2O | 100 mg/mL | 100 µg/mL | 50 µg/mL | 4 ˚C |
| Chloramphenicol | EtOH | 35 mg/mL | 35 µg/mL | 17.5 µg/mL | 4 ˚C |
| Kanamycin | H2O | 50 mg/mL | 50 µg/mL | 25 µg/mL | 4 ˚C |
| Spectinomycin | H2O | 50 mg/mL | 50 µg/mL | 25 µg/mL | 4 ˚C |
| Tetracycline | 1:1 EtOH:H2O | 20 mg/mL | 20 µg/mL | 10 µg/mL | -20 ˚C |

### 7.2.3 Antibody Blocking Buffer

PBS with non-fat dry milk (2% w/v), prepared fresh daily.

### 7.2.4 Auto-induction Media

$Na_2HPO_4$ (6 g/L), $KH_2PO_4$ (3 g/L), pH 7.2. Bacto-Tryptone (20 g/L), yeast extract (5 g/L), NaCl (5 g/L) dissolved in deionised water and autoclaved. To this was added filter-sterilised glycerol (60% v/v, 10 mL/L), glucose (10% w/v, 5 mL/L) and lactose (8% w/v, 25 mL).

### 7.2.5 Biotin Streptavidin Elution Buffer

Biotin (100 mM) in TBS.

### 7.2.6 Blocking Buffer

$NaHCO_3$ (0.1 M pH 8.6), BSA (5 mg/ml). Filter sterilized and stored at 4°C.

### 7.2.7 Coomassie Destain Solution

$H_2O$ (700 mL), MeOH (Bio-reagent grade, 5 M), glacial acetic acid (2.3 M).

### 7.2.8 Coomassie Stain

Coomassie G-250 (3 mM), glacial acetic acid (2.3 M), methanol (Bio-reagent grade, 11 M), $H_2O$ (450 mL)

### 7.2.9 Glutathione (Oxidised)

Oxidised glutathione (0.1 M) in $H_2O$, pH 7.0 using NaOH. Stored at -20 ˚C and used within 1 month.

### 7.2.10 Glutathione (Reduced)

Reduced glutathione (0.1 M) in $H_2O$, pH 7.0 using NaOH. Stored at -20 ˚C and used within 1 month.

### 7.2.11 HEPES Buffered Saline

Dextrose (2.0 g/L), HEPES (10 g/L), KCl (0.74 g/L), NaCl (16 g/L), $Na_2HPO_4.2H_2O$ (0.27 g/L).

### 7.2.12 HisTrap Column Binding Buffer

PBS with imidazole (20 mM) in autoclaved deionised water, the pH adjusted to 7.8.

### 7.2.13 HisTrap Column Elution Buffer

PBS and imidazole (250 mM) in autoclaved deionised water pH adjusted to 7.8.

### 7.2.14 HisTrap Lysis Buffer

PBS with glycerol (10% v/v) and imidazole (20 mM) with Pierce Protease Inhibitor Mini Tablets (catalogue number 88666) at manufacturer's recommended concentration.

### 7.2.15 Inclusion Body Lysis Buffer

Tris HCl (100 mM, pH 7.0), EDTA (5 mM), β-mercaptoethanol (2 mM), benzamidine HCl (5 mM). Prepared fresh every time.

### 7.2.16 Inclusion Body Wash Buffer

Tris HCl (100 mM, pH 7.0), EDTA (5 mM), β-mercaptoethanol (2 mM), urea (2 M), Triton X-100 (2% v/v). β-ME, urea and Triton X-100 were added immediately prior to use, and versions were prepared with and without the urea and Triton X-100.

### 7.2.17 Inclusion Body Extraction Buffer

Glycine (14.4 mM), NaOH (156 mM), reduced glutathione (5 mM), guanidine hydrochloride (8 M), β-mercaptoethanol (2 mM), adjusted to pH 9.6 with NaOH (2 M) or HCl (2 M).

### 7.2.18 Inclusion Body Folding Buffer A

Glycine (3.45 mM), NaOH (1.56 mM), glycerol (10% v/v), reduced glutathione (1 mM), oxidised glutathione (100 µM), urea (4 M), adjusted to pH 9.6 with NaOH (2 M) or HCl (2 M).

### 7.2.19 Inclusion Body Folding Buffer B

Ethanolamine hydrochloride (60 mM), glycerol (10% v/v), reduced glutathione (100 µM), oxidised glutathione (10 µM), adjusted to pH 9.6 with NaOH (2 M) or HCl (2 M).

### 7.2.20 Intein Extraction Buffer

Tris.HCl (20 mM), TCEP (1 mM), NaCl (0.5 mM), in autoclaved deionised water, the pH adjusted to 7.8.

### 7.2.21 Iodide Buffer

Tris-HCl (10 mM, pH 8.0), EDTA (1 mM), sodium iodide (4 M). Stored at room temperature in the dark. Discarded if colour is evident.

### 7.2.22 IPTG/Xgal Stock

IPTG (5.25 mmol), Xgal (2.5 mmol) 1.25:1:25 mass/mass/volume in molecular biology grade dimethylformamide (DMF), stored (-20 ˚C).

### 7.2.23 Laemmli Buffer

Tris.HCl (100 mM), SDS (4 %), glycerol (20 %), DTT (50 mM) and trace bromophenol blue, pH 6.8, in freshly autoclaved deionised water.

### 7.2.24 Laemmli Buffer (Non-Denaturing)

SDS (4% v/v), glycerol (20 %), Tris.HCl (120 mM), adjusted to pH 6.8, bromophenol blue (0.02%).

### 7.2.25 LB Agar/IPTG/Xgal/Tet Plates

LB Agar was mixed, autoclaved and cooled (~62 ˚C). IPTG/Xgal Stock (0.1%) and Tet stock (0.1%) was added and the mixture pour into plates. Once set, plates were stored at 4°C in the dark due to light sensitivity of both Xgal and Tet.

### 7.2.26 LB Agar Tet Plates

LB Agar was mixed, autoclaved and cooled (~62 ˚C). Tetracycline Stock (0.1%) was added and the mixture poured into plates. These were stored at 4°C in the dark. Plates were not used if brown or black.

### 7.2.27 Lysogeny Broth

Lysogeny broth (LB) broth powder (25 g/L, Fisher BioReagents) dissolved in deionised water and autoclaved.

### 7.2.28 Lysogeny Broth (for ER2738)

Bacto-Tryptone (10 g/L), yeast extract (5 g/L), NaCl (5 g/L) dissolved in deionised water and autoclaved (Note: this has a lower salt concentration than standard LB).

### 7.2.29 Lysogeny Broth Agar Plates

LB agar powder (10 g, Fluka Analytical) dissolved in deionised water (4 g per 100 mL), autoclaved (120 ˚C, 20 minutes) and cooled (RTP). A microwave (800 W, 7-10 min) was used to liquefy agar as desired. Agar was allowed to cool (~65 ˚C) before the relevant antibiotic was added. Agar (~25 mL) was poured into petri dishes to set (~20 min). Plates were then dried in the incubator (~20 min, 37 °C) before usage.

### 7.2.30 Minimal Media Salt Stock

$(NH_4)_2SO_4$ (75.6 mM), $K_2HPO_4$ (602.8 mM), $KH_2PO_4$ (771.6 mM) and sodium citrate monobasic (23.4 mM), dissolved in freshly autoclaved deionised water.

### 7.2.31 PEG/NaCl Phage Storage Solution

20% (w/v) polyethylene glycol–8000, 2.5 M NaCl. Autoclaved and thoroughly mixed to combine the separated layers whilst still warm. Stored at room temperature.

### 7.2.32 Phosphate Buffered Saline (PBS)

NaCl (137 mM), KCl (2.7 mM) and phosphate (10 mM) pH 7.4 at 25 °C.

### 7.2.33 PBST

PBS with added Tween 20, percentage given as indicated. Prepared fresh daily.

### 7.2.34 pH Phage Elution Buffer

Glycine (0.2 M) dissolved into deionised water and the pH adjusted to 2.2 with HCl. BSA was then added (1 mg/ml).

### 7.2.35 pH Phage Elution Neutralisation Buffer

Tris.HCl (1 M) dissolved in deionised water and the pH adjusted to 9.1 with NaOH.

### 7.2.36 Plating Buffer

$NaHCO_3$ (0.1 M) (pH 8.6) dissolved in deionised water and filter sterilized. Distributed into aliquots (10 mL), stored at 4°C.

### 7.2.37 Protein Storage Buffer

PBS with glycerol (10% v/v).

### 7.2.38 SDS Running Buffer

Tris base (25 mM), glycine (250 mM), SDS (2 %).

### 7.2.39 Sodium Iodide Buffer

Tris-HCl (10 mM) dissolved in deionised water and the pH adjusted to 8.0 with HCl, EDTA (1 mM), NaI (4 M). Stored at room temperature in the dark, discarded if colour changes.

### 7.2.40 Streptavidin Stock Solution

Lyophilized Streptavidin (1.5 mg) in 1 ml sodium phosphate (10 mM, pH 7.2), NaCl (10 mM). Aliquoted (100 µL) and stored (–20°C).

### 7.2.41 Super Optimal Broth with Catabolite Repression (SOC) Media

A solution of $MgCl_2$ (1 M, 500 µL), $MgSO_4$ (2 M, 500 µL), and glucose solution (20%, 500 µL) (all solutions made using freshly autoclaved deionised water) was added to freshly autoclaved LB agar broth (50 mL). The solution was then filtered (0.22 µM, Millipore, UK), and stored in aliquots (10 mL, 4 ˚C).

### 7.2.42 TAE Buffer

Tris base (2 M), acetic acid anhydride (1 M), EDTA (50 mM), in deionised water. This was then autoclaved.

### 7.2.43 TBFI Buffer

Potassium acetate (30 mM), RbCl (100 mM), CaCl2 (10 mM), MnCl2 (50 mM) and glycerol (15% v/v) dissolved in autoclaved deionised water, pH (5.8) adjusted with acetic acid (1%).

### 7.2.44 TBFII Buffer

A mixture of 3-(N-morpholino)propanesulfonic acid (10 mM), CaCl2 (10 mM), RbCl (75 mM), and glycerol (15% v/v) was created, dissolved in autoclaved deionised water. The pH (6.5) adjusted with NaOH.

#### 7.2.45 Terrific Broth (TB)

Bacto-Tryptone (12 g/L), yeast extract (24 g/L), glycerol (4 mL/L) dissolved in 90% of final volume deionised water and autoclaved. Once cooled <60 ˚C, add the final 10% as a filter-sterilised solution of $KH_2PO_4$ (170 mM) and $K_2HPO_4$ (720 mM).

#### 7.2.46 Top Agar

Per litre $H_2O$: 10 g Bacto-Tryptone, 5 g yeast extract, 5 g NaCl, 7 g Bacto-Agar. This was autoclaved and dispensed into 50 ml aliquots. Stored solid at room temperature, melted in a microwave as needed.

#### 7.2.47 Tris Buffered Saline (TBS)

Tris-HCl (50 mM pH 7.5), NaCl (150 mM). Autoclaved and stored at room temperature.

## 7.3 General Procedures

### 7.3.1 Bacterial Manipulation

#### 7.3.1.1 Storing Bacterial Stock

A sample of bacterial culture (900 µL) was diluted with dimethylsulfoxide (100 µL) and stored (-80 ˚C).

#### 7.3.1.2 Growing Bacterial Culture

A solution of LB broth (10 mL) was treated with relevant antibiotic and a sterile pipette tip was used to add the desired bacterium from either a colony, liquid culture or 10% DMSO frozen stock. This was then incubated (37 ˚C, overnight, agitation at 200 rpm) to provide the bacterial culture.

#### 7.3.1.3 Plasmid Mini-Prep

Plasmids were extracted from bacterial culture and purified using a Thermo Scientific GeneJET Plasmid Miniprep Kit following the manufacturer's instructions.

#### 7.3.1.4 Competent Cell Preparation and Usage

##### 7.3.1.4.1 Preparation and Transformation into Chemically Competent Cells

A bacterial culture was prepared and incubated overnight with shaking (37 ˚C, 200 RPM) in LB broth (10 mL) with relevant antibiotics to grow the strain. A sample (250 µL) of this bacterial culture was then added to fresh LB broth (25 mL) with relevant antibiotic and incubated (37 ˚C) until an $OD_{600}$ of 0.5-0.7 was obtained. This was then centrifuged (1000 *g*, 15 min, 4 ˚C), the supernatant discarded and the pellet resuspended in TBFI buffer (5 mL, 0 ˚C). The solution was then centrifuged (1000 *g*, 15 min, 4 ˚C), the supernatant discarded and the pellet resuspended in TBFII buffer (1 mL, 0 ˚C). The solution was then divided into aliquots (100 µL) and stored (-80 ˚C).

An aliquot of chemically competent cells was defrosted (10 min, 0 ˚C). The desired plasmid (~250 ng) was introduced, mixed by flicking and the solution rested (30 min, 0 ˚C) before being heat-shocked in a water bath (42 ˚C, 30 s). This was then rested on ice (2-3 min) before being transferred into SOC media (895 µL), which was then incubated (37 ˚C, 1 h), centrifuged (1000 *g*, 15 min, 4 ˚C), the pellet resuspended in some of the supernatant (100 µL), spread on LB agar plates containing the relevant antibiotic and incubated (37 ˚C, overnight).

##### 7.3.1.4.2 Preparation and Transformation of Electrocompetent Cells

A bacterial culture was prepared and incubated overnight with shaking (37 ˚C, 200 RPM) in LB broth (10 mL) with relevant antibiotics to grow the strain. LB broth (250 mL) was inoculated with bacterial culture (1% v/v), which was then incubated (37 ˚C with agitation) until an $OD_{600}$ of 0.6 was obtained. This was then chilled in ice slurry (15 mins). The culture was then divided (4 x 50 mL aliquots) and centrifuged (1000 *g*, 15 min). The supernatant was discarded and the pellet resuspended in ice-cold glycerol solution (10 % aq., 1 mL initial resuspension before a final dilution to 50 mL per aliquot) before being centrifuged again (1100 *g*, 4 ˚C, 15 min). The supernatant was discarded and the pellet resuspended in ice-cold glycerol solution (10 % aq. 1 mL initial resuspension before a final dilution to 20 mL per aliquot) before being centrifuged again (1100 *g*, 4 ˚C, 15 min). The supernatant was discarded and the pellet resuspended in ice-cold glycerol solution (10 % aq. 1 mL) and the six solutions combined into two solutions before being diluted with more glycerol (10 % aq, final volume 10 mL) before being centrifuged again (1100 *g*, 4 ˚C, 15 min). The supernatant was discarded and the pellet resuspended in ice-cold glycerol

solution (10 % aq. 1 mL) and the two solutions combined into one solution before being diluted with more glycerol (10 % aq., final volume 5 mL) before being centrifuged again (1100 *g*, 4 ˚C, 15 min). The supernatant was discarded and the pellet resuspended in ice-cold glycerol solution (10 % aq. 1 mL), this was then divided into pre-cooled (on dry ice) aliquots (100 µL solution each) and stored (-80 ˚C).

Per condition, an aliquot of electrocompetent cells (100 µL), was thawed on ice. Per condition SOC (898 µL), an empty culture tube and an electroporation cuvette were chilled on ice. Per condition a falcon tube was filled with water (~10 mL) and warmed (37 ˚C). Dialysed (3-5 h on a Millipore 13 mm 0.025 µM nitrocellulose filter floating on 1 L deionised water) plasmid (2 µL) was added to the cells, the aliquots were flicked to mix. The mixture was then added to a chilled electroporation cuvette (Biorad, UK 0.1 cm) and placed in a Bio-Rad Micropulser Electroporator set to *E. coli* (EC1). After one pulse (1.8 KV), SOC (898 µL, 0 ˚C) was immediately added, before transfer to the culture tubes on ice. The cultures were then incubated (37 ˚C, 1 h, in water baths). Cultures were then chilled (15 mins, 0 ˚C) and plated on selective LB agar (per plate: 25 mL LB agar, 62.5 µL Spectinomycin stock solution, 62.5 µL Carbenicillin stock solution). This was then incubated (37 ˚C, overnight). Colonies were then picked and inspected using mixed primer PCR.

#### 7.3.1.4.3 Preparation, Transformation and Integration into Electrocompetent Cells with Helper Plasmid

Bacterial culture of *SNS118*_pAH69 was created and incubated overnight with shaking (37 ˚C) in LB broth (10 mL) with Spec (25 µL stock solution) and Camp (25 µL stock solution) to grow the strain. LB broth (250 mL) was inoculated at 1% (2.5 mL overnight culture), which was then incubated (37 ˚C with agitation) until an $OD_{600}$ of 0.4 was obtained. The culture was then incubated (42 ˚C water bath with shaking) until an $OD_{600}$ of 0.6 was obtained before being chilled in ice slurry (15 mins). The culture was then divided (4 x 50 mL aliquots) and centrifuged (1000 *g*, 15 min). The supernatant was discarded and the pellet resuspended in ice-cold glycerol solution (10 % aq. 1 mL initial resuspension before a final dilution to 50 mL per aliquot) before being centrifuged again (1100 *g*, 4 ˚C, 15 min). The supernatant was discarded and the pellet resuspended in ice-cold glycerol solution (10 % aq. 1 mL initial resuspension before a final dilution to 20 mL per aliquot) before being centrifuged again (1100 *g*, 4 ˚C, 15 min). The supernatant was discarded and the pellet resuspended in ice-cold glycerol solution (10 % aq. 1 mL) and the six solutions

combined into two solutions before being diluted with more glycerol (10 % aq. 8 mL) before being centrifuged again (1100 *g*, 4 ˚C, 15 min). The supernatant was discarded and the pellet resuspended in ice-cold glycerol solution (10 % aq. 1 mL) and the two solutions combined into one solution before being diluted with more glycerol (10 % aq. 3 mL) before being centrifuged again (1100 *g*, 4 ˚C, 15 min). The supernatant was discarded and the pellet resuspended in ice-cold glycerol solution (10 % aq. 1 mL), this was then divided into pre-cooled (on dry ice) aliquots (100 µL solution each) and stored (-80 ˚C).

Per condition SOC (898 µL) an empty culture tube and an electroporation cuvette were chilled on ice. Two times per condition falcon tubes were filled with water (~10 mL) and warmed (32 ˚C, 42 ˚C). Per condition, an aliquot of electrocompetent cells with helper plasmid (100 µL), was thawed on ice (10 min). Dialysed (3-5 h on a Millipore 13 mm 0.025 µM nitrocellulose filter floating on 1 L water) plasmid (2 µL) was added to the cells, the aliquots were flicked to mix. The mixture was then added to a chilled electroporation cuvette (Biorad, UK 0.1 cm) and placed in a Bio-Rad Micropulser Electroporator set to *E. coli* (EC1). After one pulse (1.8 KV), SOC (898 µL, 0 ˚C) was immediately added, before transfer to the culture tubes on ice. The cultures were then incubated (32 ˚C, 1 h, in water baths), followed by integration/curing incubation (42 ˚C, 1h, water baths). Cultures were then chilled (15 mins, 0 ˚C) and plated on selective LB agar (per plate: 25 mL LB agar, 62.5 µL Spectinomycin stock solution, 62.5 µL Carbenicillin stock solution). This was then incubated (37 ˚C, overnight). Colonies were then picked and inspected using mixed primer and split primer PCR.

#### 7.3.1.5 Repressor Efficacy and Toxicity Drop Spotting

##### 7.3.1.5.1 Minimal Media Plate and LB Plate Preparation

Per condition (i.e. harsh, mild), Agar powder (2.8 g) was mixed with deionized water (150 ml) and autoclaved. Upon prompt removal from the autoclave, to each mixture was added 10x Minimal media salt stock (18.75 mL), Glycerol (7.5 mL, 50% v/v) and freshly autoclaved deionised water (13.5 mL). The agar was then allowed to warm in an oven (~65 °C) before being treated with Spectinomycin (25 µg/mL) and $MgSO_4$ (1 M, 187.5 µL). An agar plate (20 mL) was made at this point (“000”), before addition of kanamycin (harsh: 50 µg/mL, mild: 25 µg/mL) and 3-AT (harsh: 5 mM, mild: 2.5 mM) to the remaining agar. Agar jelly plates (20 mL each) were then created with 0, 10, 25, 75 and 150 µM IPTG, allowed to set (15 min) and dried (37 ˚C, 20 min) before usage.

LB agar (8 g) was mixed with 200 mL deionized water) and autoclaved. The liquid agar was then allowed to cool in an oven (~65 °C) before being treated with Spectinomycin (25 µg/mL). An agar plate (20 mL) was made at this point ("000"), and agar jelly plates (20 mL each) were created with 10, 25, 75 and 150 µM IPTG allowed to set (15 min) and dried (37 ˚C, 20 min) before usage.

#### 7.3.1.5.2 Drop Spotting

A bacterial culture was prepared and incubated overnight with shaking (37 ˚C, 200 RPM) in LB broth (10 mL) with relevant antibiotics to grow the strain. Solutions of cell cultures ($10^{-2}$, $10^{-3}$, $10^{-4}$, $10^{-5}$, $10^{-6}$, $10^{-7}$%) were prepared by inoculating glycerol (50% v/v, 180 µL) with overnight bacterial culture (20 µL), then serial diluting that sample (20 µL each) into fresh glycerol (50% v/v, 180 µL). Samples (2.5 µL) of each dilution were dropped onto the relevant agar plate and incubated (37 °C, repressor efficacy testing: 72 h, toxicity testing: overnight).

### 7.3.2 DNA Manipulation

#### 7.3.2.1 PCR

##### 7.3.2.1.1 PCR Primer Design

PCR primers were designed using the first 15-20 nucleotides of the 5′ region (forward) and the reverse compliment of the final 15-20 nucleotides of the 3′ region (reverse). The length of the primers were adjusted so that GC% = >45%, <55%, and $\Delta T_m$ = 5˚C. When required, relevant restriction endonuclease sites were added, preceded/succeeded (5′ vs. 3′ respectively) by a digestion overhang (usually GTTGTT) to allow optimum digestion efficiency. For specific primer sequences, see the Primer Table in the Appendix

##### 7.3.2.1.2 GoTaq Polymerase

A mix of autoclaved deionised water (32.5 µL), 5x GoTaq buffer (10 µL), dNTP bases (1 µL, 20 mM), forward primer (2 µL, 10 pmol/µL), reverse primer (2 µL, 10 pmol/µL), DNA template (1 µL), G2 Taq polymerase (0.25 µL) was placed in a BioRad Mycycler. Typical cycle: initial denaturation (95 ˚C, 1 min), melting (95 ˚C, 2 min), anneal (temperature specified in the text, 30 s), extension (72 ˚C, 1 min/Kb), cycled 34 times

before final extension (72 ˚C, 5 min) and holding (4 ˚C). The PCR products were then spin column purified before use.

#### 7.3.2.1.3 Q5 Polymerase

Brought to 0 ˚C then mixed, autoclaved deionised water (32.5 µL), 5x Q5 buffer (10 µL), dNTP bases (1 µL, 20 mM), forward primer (2.5 µL, 10 pmol/µL), reverse primer (2.5 µL, 10 pmol/µL), DNA template (1 µL), was mixed with Q5 polymerase (-20 ˚C, 0.5 µL). This was placed in a BioRad Mycycler. Typical cycle: initial (98 ˚C, 30 s), melting (98 ˚C, 10 s), anneal (temperature specified in the text, 20 s), extension (72 ˚C, 30 s/Kb), cycled 30 times before final extension (72 ˚C, 2 min) and holding (4 ˚C). The PCR products were then spin column purified before use.

#### 7.3.2.1.4 Pfu Polymerase

Brought to 0 ˚C then mixed, autoclaved deionised water (32.5 µL), 10X PFU DNA polymerase buffer with $MgSO_4$ (5 µL), dNTP bases (1 µL, 20 mM), forward primer (2.5 µL, 10 pmol/µL), reverse primer (2.5 µL, 10 pmol/µL), DNA template (~50 ng), was mixed with Pfu polymerase (-20 ˚C, 0.5 µL). This was placed in a BioRad Mycycler. Typical cycle: initial (95 ˚C, 2 min), melting (95 ˚C, 10 s), anneal (temperature specified in the text, 20 s), extension (72 ˚C, 30 s/Kb), cycled 30 times before final extension (72 ˚C, 2 min) and holding (4 ˚C). The PCR products were then spin column purified before use.

#### 7.3.2.1.5 KOD Polymerase SDM

SDM primers were made using a 15-20 nucleotide overhang in both directions from the intended mutagenesis site, adjusting length so that GC% = >45%, <55% (forward primer) the reverse compliment sequence was also purchased (reverse primer). Brought to 0 ˚C then mixed, autoclaved deionised water (32.6 µL), 10X KOD buffer #1 (5 µL), dNTP bases (5 µL, 20 mM), $MgCl_2$ (25 mM), forward primer (2 µL, 10 pmol/µL), reverse primer (2 µL, 10 pmol/µL), DNA template (1 µL), was mixed with KOD DNA polymerase (-20 ˚C, 0.4 µL). This mixture was repeated, replacing buffer #1 with buffer #2. These were placed in a BioRad Mycycler. Cycle: initial (98 ˚C, 15 s), melting (98 ˚C, 15 s), anneal (58 ˚C, 5 s), extension (72 ˚C, 10 s/Kb), cycled 30 times before final extension (72 ˚C, 1 min) and holding (4 ˚C). *Dpn*I (1 µL) was added to each tube to digest methylated template and incubated (37 ˚C, 1 h). The PCR products were then spin column purified, a sample (~5

µL) used to assess PCR success, and the effective PCR product chemically transformed into the relevant chemically competent cell line.

#### 7.3.2.1.6 Colony PCR

Colonies picked from agar plates were separately mixed with autoclaved deionised water (6.25 µL), GoTaq 5x green buffer (2 µL), dNTP bases (1 µL, 20 mM), forward primer (0.25 µL, 10 pmol/µL), reverse primer (0.25 µL, 10 pmol/µL) and GoTaq polymerase (0.05 µL) was placed in a BioRad Mycycler. Typical cycle: initial (95 ˚C, 5 min), melting (95 ˚C, 5 min), anneal (temperature specified in the text, 30 s), extension (72 ˚C, 1 min), cycled 30 times before final extension (72 ˚C, 5 min) and holding (4 ˚C).

#### 7.3.2.1.7 Mixed-Primer PCR

A mix of autoclaved deionised water (2.9 µL), 5x GoTaq buffer (2 µL), dNTP bases (1 µL, 20 mM), P1 primer (1 µL, 10 pmol/µL), P2 primer (1 µL, 10 pmol/µL), P3 primer (1 µL, 10 pmol/µL), P4 primer (1 µL, 10 pmol/µL), Taq polymerase (0.1 µL) and a colony picking was placed in a BioRad Mycycler The following PCR programme was used: initial melting (2 min, 95 ˚C), cycle: melting (30 s, 95 ˚C), annealing (30 s, 55 ˚C), extension (30s, 72 ˚C), cycled 30 times before a final extension (2 min, 72 ˚C) and holding (4 ˚C).

#### 7.3.2.1.8 Split-Primer PCR

A master mix was created, quantities multiplied per category (i.e. the following quantities x no template control, positive control, negative control, item(s) to be tested): autoclaved deionised water (28.1 µL), GoTaq 5x green buffer (9 µL), dNTP bases (4.5 µL, 20 mM) and GoTaq polymerase (0.25 µL). This was divided into four aliquots (10.45 µL per condition), A, B, C and D. To A was added (per condition) primers P1 (1 µL, 10 pmol/µL) and P4 (1 µL, 10 pmol/µL) (no integration). To B was added (per condition) primers P1 (1 µL, 10 pmol/µL) and P2 (1 µL, 10 pmol/µL) (integration). To C was added (per condition) primers P3 (1 µL, 10 pmol/µL) and P4 (1 µL, 10 pmol/µL) (integration). To aliquot D was added (per condition) primers P3 (1 µL, 10 pmol/µL) and P2 (1 µL, 10 pmol/µL) (multiple integration). A, B, C and D were then divided per condition into aliquots (10 µL) and samples (0.2 µL) of the culture to be tested were added to all four. These were then mixed by flicking, centrifuged briefly to bring to the bottom of the tube and placed in a BioRad Mycycler. The following PCR programme was used: initial melting (2 min, 95 ˚C), cycle:

melting (30 s, 95 ˚C), annealing (30 s, 55 ˚C), extension (30s, 72 ˚C), cycled 30 times before a final extension (2 min, 72 ˚C) and holding (4 ˚C).

#### 7.3.2.2 Spin Column Purification

Spin column purification was performed using a Thermo Scientific GeneJET PCR Purification Kit following the manufacturer's instructions.

#### 7.3.2.3 Gel Purification

Dependent on the size of the desired DNA fragment, the following Agarose gel concentrations were used; >5000 Kb: 0.8%, >1000 <5000: 1%, <1000: 1.2%. These were created using Agarose powder (0.8 g, 1 g, 1.2 g, Fisher Analytical) and 1x TAE buffer (100 mL). This was boiled by microwave (2-3 min, 800W) and ethidium bromide (2 drops) added before the mixture was swirled. The ethidium bromide agarose gel mixture was then poured into a gel channel and the appropriate comb inserted. The gel was allowed to set (~5 minutes) before being placed in an electrophoresis box and immersed in 1x TAE buffer. The DNA was mixed thoroughly with green GoTaq reaction buffer (10% v/v) then loaded into wells with NEB 2-Log DNA Ladder for reference. This was then separated by charge using electrophoresis (100 V, 30 min, 400 mA, BioRad PowerPac Basic). The desired DNA fraction was excised gel and purified using a Thermo Scientific GeneJET PCR Purification Kit following the manufacturer's instructions.

#### 7.3.2.4 Restriction Endonuclease Digestion

For the enzyme(s) used, the NEB recommended buffer (5 µL) was mixed with template (~2000 ng) and diluted to 48 µL with freshly autoclaved water. To this was added restriction enzyme 1 (1 µL,) and restriction enzyme 2 (1 µL). TSAP or rSAP were used to remove phosphate groups and prevent religation in vectors (not used with inserts). Reaction timescale was >2x the NEB recommended time, but using the recommended temperature. Following denaturing (NEB recommended temperature and duration), the mixture was then spin column purified. A test-digestion uses $1/5^{th}$ of the above quantities and is not purified; it is used in electrophoresis and imaging.

#### 7.3.2.5 Ligation

Amounts of prepared digested vector and insert were calculated as

follows:

*Equation 1:*
$$ng\ of\ insert = \left(\frac{length\ of\ insert\ (kb)}{length\ of\ vector(kb)}\right) \times amount\ of\ vector\ (ng)$$

Each ligation mix contains digested vector DNA (~100 ng), digested insert DNA (*n* ng, depending on m/m insert to vector ratio), T4 DNA ligase buffer (1 µL), autoclaved deionised water (to a final volume of 10 µL). To this was added T4 DNA ligase (0.5 µL) before gentle mixing by pipette and storage (4 ˚C, overnight of 16 ˚C, 1h). Typically, 1:3, 1:6 and 1:9 insert to vector ratios were used, as well as a control using autoclaved deionised water in place of insert, to assess vector religation.

### 7.3.3 Protein Manipulation

#### 7.3.3.1 Circular Dichroism

CD analysis was performed on Jasco-720 instrument using a 450W xenon short-arc lamp, calibrated with ammonium d-camphorsulphonate (0.6 mg $ml^{-1}$ in deionised water). Samples were analysed using 1, 0.5 and 0.1 mm cuvettes. CD analysis was conducted at room temperature with a 1 nm step size, scanning speed of 20 nm $min^{-1}$ and ten scans per sample. The samples had concentrations of 0.3 µM in 1 mL of phosphate buffer (10 mM sodium phosphate, pH 7.3).

#### 7.3.3.2 MST

Microscale thermophoresis was conducted using a NanoTemper Monolith NT.115 system following the manufacturer's instructions. A 45% Excitation LED power and either 20 or 40% IR-laser power was used during experiments. MST was recorded using a 5 s, 30 s, 5 s laser off-on-off cycle.

#### 7.3.3.3 Peptide ELISAs

Following the same protocol as described in Section 7.3.4.3.1, Greiner Microlon® high binding polystyrene plates were prepared with the desired protein targets and anti-targets; and incubated (4 ˚C, overnight).

The following day the proteins were removed by aspiration and all relevant wells filled with Blocking Buffer (350 µL) and incubated (RTP, mild agitation, 1 h). A separate plate

was prepared for protein dilutions and all necessary wells similarly filled with Blocking Buffer and incubated. A falcon tube was similarly prepared with Blocking Buffer for use as a vessel to dilute TrkA-D5 or TrkB-D5. Blocking buffer was then removed from the second plate and the wells washed 6 times with TBST (0.5% V/V TWEEN-20), before being used to serially dilute the peptides to the required concentrations in TBST (0.5% V/V TWEEN-20) with DMSO (5% v/v)). The primary plate was then similarly washed before adding 50 µL of a diluted peptide per well, and incubated (RTP, 2 h, mild agitation). Meanwhile TrkA-D5 or TrkB-D5 was diluted to desired concentrations in TBST (0.5% V/V TWEEN-20) with DMSO (5% v/v). The primary plate was then washed again, 6 times with TBST (0.5% V/V TWEEN-20) with DMSO (5% v/v), before the addition of TrkA-D5 or TrkB-D5 and further incubation (1 h, RTP with agitation). The plate was then washed again, 6 times with TBST (0.5% V/V TWEEN-20) with DMSO (5% v/v) before the addition of Antibody Blocking buffer (100 µL) and the plates incubated (RTP, 1 h, mild agitation). Plates were then washed again 6 times with PBST (0.05% Tween-20, 200 µL/well) before the addition of anti-FLAG mouse IgG monoclonal antibody (Sigma Aldrich, Catalogue number: F3165) in antibody blocking buffer (1:5000 dilution, 100 µL). The plates were then incubated (RTP, 1 h, mild agitation) before a final wash step 6 times with PBST (0.05% Tween-20). To each well was then added 1-Step Ultra TMB (50 µL) before further incubation (RTP, 15-min with agitation). The reaction was then halted by the addition of $H_2SO_4$ (50 µL, 2 M) and incubate (RTP, 5 min with agitation) before reading the absorbance of each well (420 nm).

#### 7.3.3.4 Protein Unfolding and Refolding

The protocol to unfold, refold and purify TrkA-D5 and TrkB-D5 from expressed inclusion bodies into soluble protein was the amalgamation of two protocols[179-180] adapted for the available equipment and purification methods (such as using β-ME in place of DTT to permit nickel affinity chromatography). As such the protocol used is outlined here:

The plasmid of interest was transformed into a fresh aliquot of chemically competent cells and grown overnight in fresh LB media. This was used to create a 2% (v/v) LB mixture (800 mL-3 L) in an Erlenmeyer or baffled flask 3-4x the volume of the solution and incubated (37 ˚C) with agitation until an OD600 of 0.6-0.8 was achieved. A 10 mL sample was taken as an uninduced control, which was centrifuged and the pellet frozen (-80 ˚C). The remaining bacterial culture was induced to express using IPTG (final concentrations provided in the text) Cultures were then incubated at either 30 ˚C for 4h, or at 18 ˚C

overnight. Bacteria were isolated by centrifugation and the supernatant removed. Pellets were then frozen (-80 ˚C) before being resuspended in Inclusion Body Lysis Buffer (4 mL/g original cell pellet, 0˚C) and lysed on ice by sonication using an MSE Soniprep 150Plus using a 50:50 on/off 30s cycle for 10 minutes. The mixture was then centrifuged (1 h, 0 ˚C, 20,000 ×*g*) to pellet unbroken cells, large cellular debris and inclusion bodies. The pellet was then thoroughly resuspended in Inclusion Body Wash Buffer (the variant containing urea and Triton-X, 10 mL/g original cell pellet, 0˚C). This was then repeatedly (3×) centrifuged (30 min, 0 ˚C, 20,000 ×*g*) and resuspended in urea/Triton-X Inclusion Body Wash Buffer (5 mL/g original cell pellet, 0˚C) or until the supernatant was clear. At this point it was resuspended in Inclusion Body Wash Buffer lacking urea or Triton-X (5 mL/g original cell pellet, 0˚C) before a final centrifugation (30 min, 0 ˚C, 20,000 ×*g*) and storage (-80 ˚C).

The inclusion body pellet was then thoroughly resuspended in Inclusion Body Extraction Buffer (2.5 mL/g original cell pellet, 0˚C) and clarified by sonication on ice using a 50:50 on/off 10s cycle for 1 minute. This was then mixed with an equal volume of Inclusion Body Folding Buffer A (0 ˚C) and dialysed into 25× the mixtures volume of Inclusion Body Folding Buffer A (0 ˚C, 16 h with agitation) using Thermo Scientific SnakeSkin dialysis tubing (10 K MWCO, 16 mm I.D, catalogue number 88243). The mixture was then dialysed into Inclusion Body Folding Buffer B (0 ˚C, 8 h with agitation) before being dialysed into HisTrap Column Binding Buffer (0 ˚C, 16 h with agitation). During this process, significant aggregation and misfolded protein occurs. This was removed by centrifugation (1 h, 0 ˚C, 20,000 ×*g*) and the supernatant used in nickel affinity chromatography and thrombin cleavage (Section 7.3.3.8) and size-exclusion chromatography (Section 7.3.3.9).

### 7.3.3.5 Protein Expression - Small Scale Test

The plasmid of interest was transformed into a fresh aliquot of chemically competent cells and grown overnight in fresh LB media. This was used to create a 2% (v/v) LB mixture (50 mL) in a 250 mL Erlenmeyer flask and incubated (37 ˚C) with agitation until an OD600 of 0.6-0.8 was achieved. The mixture was then subdivided (10 mL, in falcon tubes) and expression in all but one aliquot was induced to express at various IPTG concentrations (the remainder acting as the uninduced control). Cultures were then incubated at either 30 ˚C for 4h, or at 18 ˚C overnight. Bacteria were isolated by centrifugation and the supernatant removed. Pellets were then frozen (-80 ˚C) and resuspended in HisTrap lysis

buffer (4 mL/g wet weight cells). 400 µL samples were then sonicated in a water bath in 30/30s cycles of in the bath or on ice for 10 minutes. Samples were then centrifuged and the supernatant (soluble fraction) separated from the pellet (insoluble fraction). 10 µl of the soluble fraction was then mixed with Laemmli stain (50/50 v/v). A pinhead of the insoluble fraction was resuspended in 100 µL of lysis buffer, and 10 µL was mixed with Laemmli stain (50/50 v/v). Both samples were then denatured (70 ˚C, 10 min) and loaded onto an SDS gel (15%) was created, and protein/Laemmli buffer mixture loaded into wells, with 170 KDa PageRuler Prestained Protein Ladder (Thermo Scientific, UK) as a reference. The gel was then submerged in SDS running buffer and subjected to electrophoresis (150 V, 50 min). The proteins were visualised by submerging the gel in Coomassie stain (8 min), then being submerged in Coomassie destain solution (overnight).

#### 7.3.3.6 Protein Expression - Mid-Large Scale

The plasmid of interest was transformed into a fresh aliquot of chemically competent cells and grown overnight in fresh LB media. This was used to create a 2% (v/v) LB mixture (250 mL-3 L) in an Erlenmeyer or baffled flask 3-4x the volume of the solution and incubated (37 ˚C) with agitation until an OD600 of 0.6-0.8 was achieved. A 10 mL sample was taken as an uninduced control, which was centrifuged and the pellet frozen (-80 ˚C). The remaining bacterial culture was induced to express using IPTG (final concentrations provided in the text) Cultures were then incubated at either 30 ˚C for 4h, or at 18 ˚C overnight. Bacteria were isolated by centrifugation and the supernatant removed. Pellets were then frozen (-80 ˚C) and resuspended in HisTrap lysis buffer (4 mL/g wet weight of cells) and combined. Resuspended *E. coli* were then sonicated on ice using a MSE Soniprep 150Plus using a 50:50 on/off 30s cycle for 10 minutes. The uninduced sample pellet was similarly resuspended and lysed. The cellular debris was then centrifuged and the supernatant (soluble fraction) separated from the pellet (insoluble fraction). Samples of all were kept for SDS PAGE & Western Blot. The soluble induced fraction was then used for HisTrap and Size Exclusion Chromatography; or for unfolding, refolding and then HisTrap and Size Exclusion Chromatography.

#### 7.3.3.7 Protein Imaging

##### 7.3.3.7.1 SDS PAGE

Bisacrylamide gels were prepared using the following recipe:

***Table 15: Formula for bisacrylamide gels for SDS PAGE***

| | Acrylamide Concentration | | |
|---|---|---|---|
| | 10% | 12% | 15% |
| Autoclaved deionised water | 9.9 mL | 10.2 mL | 7.0 mL |
| Tris-base (1.5 M pH 8.8) | 6.3 mL | 7.5 mL | 7.5 mL |
| SDS (10 % w/v) | 0.25 mL | 0.30 mL | 0.30 mL |
| Acrylamide/Bisacrylamide (30%/0.8% w/v) | 8.3 mL | 12.0 mL | 15.0 mL |
| Ammonium persulphate (10% w/v) | 0.25 mL | 0.25 mL | 0.15 mL |
| Tetramethylethylenediamine | 0.02 mL | 0.02 mL | 0.02 mL |

Once set, the above gels were capped with stacking gel and a comb inserted to create wells once set:

***Table 16: Formula for stacking gel bisacrylamide gels for SDS PAGE***

| | |
|---|---|
| Autoclaved deionised water | 3.38 mL |
| Tris-base (1.5 M pH 6.8) | 1.5 mL |
| SDS (10 % w/v) | 0.06 mL |
| Acrylamide/Bisacrylamide (30%/0.8% w/v) | 1 mL |
| Ammonium persulphate (10% w/v) | 0.06 mL |
| Tetramethylethylenediamine | 0.003 mL |

Once set, gels were stored in a sealed humid container (4 ˚C) until needed. At this point, protein samples were mixed with 2x Laemmli buffer and incubated (95 ˚C, 10 min). Samples were then loaded in the gel in Running Buffer, and separated by electrophoresis using a BioRad Power Pack Basic (150 V, ~65 min, RTP). Gels were then stained with Coomassie Stain (30 min, RTP with agitation) before being clarified with Coomassie Destain (16h, RTP). Gels were then imaged using a BioRad Universal Hood II imager with BioRad Quantity One software.

#### 7.3.3.7.2 Western Blot

To produce western blot images duplicate SDS PAGE gels were created using the protocol in Section 7.3.3.7 deviating in that one was stained/destained as usual, however the proteins of the other gel were left unstained and instead transferred onto nitrocellulose membranes (Protran, Whatman) using a BioRad Power Pack Basic (400 mA, 1h, -20 ˚C). Blots were then blocked with milk PBST solution (5% w/v, 0.05% Tween-20, 1 h, RTP), followed by incubation with the primary antibody (1/5000 dilution in milk PBST, 5% w/v, 0.05% Tween-20, 1 h, RTP). The gel was then rinsed with PBST (0.05% Tween-20, 5 min, RTP) before treatment with the secondary antibody (1/15000 dilution in milk PBST 5% w/v, 0.05% Tween-20, 1 h, RTP). The membrane was washed a second time with PBST (0.05% Tween-20, 5 min, RTP) before detection using ECL reagent (Pierce). This was allowed to react in the dark for 1 minute prior to imaging the gel using the BioRad Universal Hood II imager with BioRad Quantity One software.

### 7.3.3.8 Protein Purification – HisTrap Affinity Chromatography

Following Section 7.3.3.4: Protein Unfolding and Refolding or Section 7.3.3.6: Protein Expression - Mid-Large Scale, refolded protein or soluble fractions were purified by filtration (0.22 μm nitrocellulose Millipore filter) to remove cell debris and insoluble protein, and the filtrate loaded onto a HisTrap FF 1 g column for nickel affinity chromatography. Bound proteins were eluted using HisTrap Column Elution Buffer (containing 250 mM imidazole). Where thrombin cleavage was required, the eluent was dialysed (1 h, 4 ˚C) using Thermo Scientific SnakeSkin dialysis tubing (10 K molecular weight cut off (MWCO), 16 mm I.D, catalogue number 88243) into HisTrap Column Binding Buffer (25× initial volume). After an hour of dialysis, thrombin (10 units per mg of protein) was added and incubation continued (16 h, 4 ˚C). The following morning this mixture was re-filtered (0.22 μm nitrocellulose Millipore filter) in case of aggregation and passed through a HisTrap FF 1 g column. If size exclusion chromatography was required, see Section 7.3.3.9.

### 7.3.3.9 Protein Purification – Size Exclusion Chromatography

Continuing from Section 7.3.3.8, proteins in HisTrap Column Elution Buffer were purified using a GE Healthcare HiLoad Superdex 16/600 75PG prep grade column pre-loaded with Protein Storage Buffer, at a flow rate of 1.5 mg/min at room temperature. Protein was

detected at 280 nm wavelength. Peaks were analysed by SDS PAGE (usually with non-denaturing Laemmli buffer) and western blot. Useful fractions were combined and concentrated using GE Healthcare Vivaspin 500 columns with a MWCO of 5000 until the desired concentration was obtained. Proteins were then aliquoted and stored (-80 ˚C).

#### 7.3.3.10 Thermal Shift

A thermal shift assay was conducted using a Bio-Rad CFX Connect Real-Time qPCR system. Samples of βNGF were serially diluted into a range of buffers (HEPES, HBS, Tris, TBS and PBS; all with and without glycerol (10% v/v)) containing SYPRO Orange (working concentration recommended by manufacturer) to a final βNGF concentration of 2.5 μM. These were then placed in a Greiner Cellstar® plate (catalogue number: 655083) and the plates sealed with an optically clear adhesive sheet. The plate was centrifuged then the thermal shift tested using a Bio-Rad CFX Connect Real-Time qPCR system testing across 10-100 ˚C, measuring at 570 nm.

### 7.3.4 Phage Protocols

As the NEB manual for the C7C library (Manual E8121) was heavily clarified/modified (due to high ambiguity, available equipment and to make it far more approachable) the protocols followed in this research are included below:

#### 7.3.4.1 Measuring Phage Concentration

Measuring the number of phage present in a sample: phages were heavily diluted and used to infect a fresh culture of ER2738, this is then plated on a blue/white screen. This allows phage quantification and qualifies whether the sample contains library phage or wild phage. Using a very low dilution ensures a low multiplicity of infection (MOI) resulting in one phage plaque equalling one original phage.

A 1% culture of ER2738 from a fresh overnight culture was incubated at 37 ˚C with agitation until it reached an $OD_{600}$ 0.5-0.6. During bacterial incubation time aliquots of top agar were melted and aliquoted (3 mL) into sealed sterile culture tubes, one per expected phage dilution. Tubes were maintained at 45°C in a water bath. One LB/IPTG/Xgal plate per expected dilution was dried and warmed at 37°C until ready for use. Phage samples (10 μL) were diluted to 1 mL with LB by the following factors: unamplified phage: $10^1$, $10^2$, $10^3$, $10^4$, amplified phage: $10^6$, $10^8$, $10^{10}$, $10^{12}$. Fresh anti-aerosolising filtered pipette tips

were used throughout. Upon reaching an $OD_{600}$ of 0.5-0.6, 10 µL of each phage sample was added to separate 200 µL aliquots of the ER2738 culture. These were then vortexed and incubated (RTP, 5 min) before being added to an aliquot of the prepared Top Agar. This was *immediately* vortexed and poured over a pre-warmed LB/IPTG/Xgal plate. Plates were then tilted and rotated gently to spread the Top Agar evenly. After cooling (5 min), plates were capped with a loose lid, inverted and incubated (37 ˚C, overnight). Plates bearing approximately 100 plaques were counted their plaque forming units (pfu) calculated.

#### 7.3.4.2 Storage of Phage Solutions

Working phage solutions were stored for no longer than a month in suspensions of LB with $1/6^{th}$ volume of NaCl/PEG buffer at 4 ˚C. Long-term stocks were created by following the Plaque Amplification protocol, incubating samples (65 ˚C, 15 mins) to kill residual *E. coli*, and diluting 1:1 with glycerol before storage (-20 ˚C). Samples are purportedly stable for up to 5 years.

#### 7.3.4.3 Phage Display Surface Panning Procedure

##### 7.3.4.3.1 Initial Target Plate Preparation

The target protein was diluted from stock (1 mg/mL) into plate binding buffer and an aliquot (100 µL) was added to one well of a Greiner Microlon® high binding polystyrene plates (catalogue number: 655061). Plates were then swirled to distribute the solution around the base of the well and incubated (37 ˚C, overnight) with gentle agitation in a humidified container (i.e. a sealable plastic box lined with damp paper towels). A 250 mL Erlenmeyer flask was sterilised using Virkon and autoclaved. A 10 mL LB (treated with Tet) overnight culture was created from a fortnightly stock streak LB Agar Tet plate of ER2738 from the -80 ˚C stored stock.

##### 7.3.4.3.2 Initial Pan and Binding Phage Amplification

The previously prepared well was emptied—throughout this protocol all media movements occurred by aspiration with anti-aerosol filtered pipette tips—and filled with blocking buffer (350 µL) before being incubated (4 ˚C, 1 h). The overnight culture of ER2738 was used to create a 1% solution in fresh LB treated with Tet and incubated (37 ˚C, ~2 h) until an $OD_{600}$ of 0.5-0.6 was reached, at which point it was put on ice. The blocking buffer was

then removed and the plate washed 6 times with TBST (0.1%, 200 µL) before the addition of a 100-fold representation of the library diluted with TBST (0.1% 100 µL final volume). Plates were gently agitated (1 h). Meanwhile LB Agar IPTG/Xgal/Tet plates were dried and warmed (37 ˚C, until needed), Top Agar aliquots were melted, re-aliquoted and maintained in a 45 ˚C water bath. Non-binding phage were then removed by aspiration and the plate washed 10 times with TBST (0.1%) before the addition of pH phage elution buffer (100 µL) and a gently agitated incubation (no more than 20 minutes). The eluate was then aspirated into a microcentrifuge tube and neutralised with pH phage elution neutralisation buffer (15 µL). Phage concentration was then ascertained using a 10 µL sample following the protocol mentioned in Section 7.3.4.1. The remaining phage solution was amplified by adding it to a fresh 20 mL LB Tet 1% ER2738 culture made from the overnight stock. This was then incubated in the sterile 250 mL Erlenmeyer flask prepared previously (37 ˚C, 5 h). Amplified phage were then isolated by centrifugation (10 min, 12,000 g, 4 ˚C). The supernatant was then re-spun and the upper 80% supernatant removed. To this was added PEG/NaCl Phage Buffer (1/6 volume). Phage were then allowed to precipitate (4 ˚C, overnight) and another ER2738 10 mL LB Tet culture was created from the fortnightly stock streak plate and incubated (37 ˚C, overnight).

#### 7.3.4.3.3 Initial Phage Purification and Plate Preparation

The overnight phage titre plates were used to assess that no wild phage were present, and that a reasonable number of phage had been selected (reducing pfu by ~8 orders of magnitude). The overnight ER2738 culture was used to create a 1% culture in LB Tet, this was incubated (37 ˚C, ~2 h) until an $OD_{600}$ of 0.5-0.6 was reached, at which point it was kept on ice. Meanwhile LB Agar IPTG/Xgal/Tet plates were dried and warmed (37 ˚C, until needed), Top Agar aliquots were melted, re-aliquoted and maintained in a 45 ˚C water bath. The overnight phage PEG precipitation was twice centrifuged (12,000 g, 15 min, 4 ˚C) and the supernatant aspirated and discarded. The pellet was then resuspended in TBS (1 mL) and transferred to a microcentrifuge tube before being re-spun (17,000 g, 5 min). The supernatant was then transferred to a fresh microcentrifuge tube and re-precipitated by adding PEG/NaCl Phage Buffer (1/6 volume) and incubating on ice (60 min). The precipitate was then isolated by repeated centrifugation (17,000 g, 10 min) and discarding the supernatant (twice). The pellet was resuspended in TBS (200 µL) before being centrifuged (17,000 g, 1 min). The upper 80% of the supernatant was then transferred to a fresh microcentrifuge tube. This is the amplified eluate, and the concentration ascertained

by phage titring. Half was converted into a long-term stock following the protocol outlined in Section 7.3.4.1 and stored (-20 ˚C). As in Section 7.3.4.3.1 a fresh high-binding plate was prepared with target, a 250 mL Erlenmeyer flask was sterilised and an overnight culture of ER2738 was prepared from the fortnightly stock and incubated (37 ˚C, overnight).

#### 7.3.4.3.4 Intermediate Pans and Purifications

The concentration of amplified phages were ascertained (~$1x10^{13-14}$ pfu/ml) using the overnight phage titre plates. Sections 7.3.4.3.2 and 7.3.4.3.3 were then repeated as needed using this new input phage concentration and using increased PBST Tween-20 concentrations (0.5 % v/v).

#### 7.3.4.3.5 Final Pan

For the final pan, panning was conducted as in Section 7.3.4.3.2 (again using increased PBST Tween-20 concentrations) but phage were not amplified. Phage concentration was ascertained as before using the LB Agar IPTG/Xgal/Tet plates in a blue/white screen overnight for no longer than 18 h (deletions may occur if incubated for too long) and the plates sealed (parafilm), inverted and stored (4 ˚C, no more than 3 days). An overnight culture of ER2738 in 10 mL LB Tet was prepared from the fortnightly stock and incubated (37 ˚C, overnight).Plaque Amplification for Sequencing and ELISA

A 1% ER2738 LB Tet culture was prepared from the overnight stock and 1 mL aliquots added to 50 mL falcon tubes, one for each phage/plaque to be characterised. Using a sterile filtered pipette tip, individual blue plaques were stabbed and used to inoculate the above 1 mL aliquots with library phage. Phage/Bacteria cultures were then incubated (37 ˚C, 4 h with agitation) before being transferred to microcentrifuge tubes and the phage isolated by centrifugation (17,000 g, 1 min). Supernatants were transferred to fresh tubes and re-spun. Per phage, the following occurred: the upper 800 µL was transferred by aspiration to a fresh tube and 300 µL used to create a phage storage stock. Concentrations were ascertained by phage titre measurement. The remaining 500 µL of the supernatant was transferred by aspiration to a fresh tube, precipitated by the addition of PEG/NaCl Phage Buffer (1/6 volume), mixed by inversion and incubated (20 min, RTP). The precipitate was then isolated by centrifugation (17,000 g, 10 min) and the supernatant discarded. Centrifugation and supernatant aspiration was then repeated before pellet resuspension in Sodium Iodide Buffer (100 µL), mixing by tapping the tube vigorously. To this was added

ethanol (molecular biology grade, >99.8%) and the mixture incubated (20 min, RTP) before ssDNA isolation by centrifugation (17,000 g, 10 min). The supernatant was discarded and the pellet resuspended in ethanol (500 µL, -20 ˚C, molecular biology grade diluted to 70% with deionised water sterilised by filtration through a 0.22 µm nitrocellulose Millipore filter) before being re-spun (17,000 g, 10 min). The supernatant was discarded and the pellet briefly dried under vacuum before being resuspended in sterilised deionised water (30 µL). By this point, each aliquot holds the isolated and purified ssDNA of a single M13 phage species. They were then used to sequence the phage they were picked from using the -96 gIII primer. The remainder was stored (-20 ˚C).

### 7.3.4.4 Phage ELISA Binding Assay with Direct Target Coating

#### 7.3.4.4.1 Phage Amplification and Purification

Prior to the ELISA, phage were amplified to high concentrations. The phage storage stock generated in Section 0 (5 µL per phage) was used to inoculate separate cultures of ER2738 (20 mL, 1% v/v solution from a fresh overnight culture made with the fortnightly stock, in a Virkon and autoclave sterilised 250 mL flask) and the cultures incubated (37 ˚C, 4.5-5 h). The culture was transferred to a centrifuge tube and spun (12,000 g, 10 min, 4 ˚C). The supernatant was then transferred to a fresh centrifuge tube and re-spun. The upper 80% of the supernatant was transferred by aspiration and the phage precipitated by the addition of PEG/NaCl Phage Buffer (1/6 original volume) and incubated (4 ˚C, overnight). A fresh overnight culture of ER2738 was prepared from the fortnightly stock streak plate. The following day this was used to create a fresh 1% culture, and grown to $OD_{600}$ 0.5-0.6 before being chilled on ice. The phage precipitations were isolated by centrifugation (12,000 g, 15 min, 4 ˚C) and the supernatant discarded. The pellet was then resuspended in TBS (1 mL) and transferred to a microcentrifuge tube before being centrifuged further (17,000 g, 5 min) to pellet residual cells. The supernatant was then transferred to a fresh tube and phage re-precipitated by the addition of PEG/NaCl Phage Buffer (1/6 original volume) and incubated (1 h, on ice). Phage were then isolated by centrifugation (17,000 g, 10 min) and the supernatant discarded. Phage were then resuspended in TBS (50 µL), making the final isolated, amplified stock ready for an ELISA, and may be stored (4 ˚C) for several weeks without loss of titre. Phage concentration was then ascertained by following the protocol described in Section 7.3.4.1, it should be ~$1x10^{14}$ pfu/mL.

#### 7.3.4.4.2 Phage ELISA

Following the same protocol as described in Section 7.3.4.3.1, Greiner Microlon® high binding polystyrene plates were prepared with the desired protein targets and anti-targets; and incubated (4 ˚C, overnight).

The following day the proteins were removed by aspiration and all relevant wells filled with Blocking Buffer (350 µL) and incubated (RTP, mild agitation, 1 h). A separate plate was prepared for phage dilutions and all necessary wells similarly filled with Blocking Buffer and incubated. Blocking buffer was then removed from the second plate and the wells washed 6 times with TBST (0.5% V/V TWEEN-20), before being used to serially dilute the phage to the required concentrations in more TBST (0.5% V/V TWEEN-20). The primary plate was then similarly washed before adding 50 µL of a diluted phage per well, and incubated (RTP, 2 h, mild agitation). The primary plate was then washed again, 6 times with TBST (0.5% V/V TWEEN-20). To each well was then added Antibody Blocking buffer (100 µL) and the plates incubated (RTP, 1 h, mild agitation). Plates were then washed again 6 times with PBST (0.05% Tween-20, 200 µL/well) before the addition of HRP-conjugated anti-M13 monoclonal antibody (GE Healthcare. #27-9421-01) in antibody blocking buffer (1:5000 dilution, 100 µL). The plates were then incubated (RTP, 1 h, mild agitation) before a final wash step 6 times with PBST (0.05% Tween-20). To each well was then added 1-Step Ultra TMB (50 µL) before further incubation (RTP, 15-min with agitation). The reaction was then halted by the addition of $H_2SO_4$ (50 µL, 2 M) and incubate (RTP, 5 min with agitation) before reading the absorbance of each well (420 nm).

### 7.3.5 Solid-Phase Peptide Synthesis

#### 7.3.5.1 General SPPS Protocol, Disulfide Cyclisation and Purification

All peptides were prepared following this general scheme. Serine Wang resin (0.25 mmol) was swelled in DMF (20 min) before the DMF was removed by vacuum filtration. The Fmoc protecting the serine's C-terminal was deprotected using piperidine solution (20% v/v in DMF, 20 min), the solution suspended and agitated on a sinter funnel using bubbled argon. The resin was then washed three times with DMF, then three times with dichloromethane (DCM) before three times with diethyl ether, the solvent removed each time by vacuum filtration. A Kaiser test was used to confirm Fmoc deprotection (Section

7.3.5.2), turning indigo in the presence of a free amine. Separately, a solution of Fmoc-protected amino acid (0.75 mmol) and HOBt (0.75 mmol) was prepared in DMF. Following incubation (5 min, RTP) to this was added DIC (1.5 mmol) and the solution was thoroughly mixed before being added to the deprotected Wang resin. This was suspended and agitated by argon and allowed to react (45 min, RTP). The resin was then washed again as before with DMF, DCM and diethyl ether. A Kaiser test was performed, and coupling verified by no colour change. Deprotection and coupling was repeated as needed until the desired linear peptide was synthesised.

Linear peptides were then cleaved from the resin and the side chain protecting groups were simultaneously cleaved using a cocktail of TFA (95% v/v), $H_2O$ (2.5% v/v) and TIS (2.5% v/v), stirred in a sealed argon atmosphere. The TFA was removed *in vacuo* and the sample washed with DCM and methanol. The residue was purified by trituration using diethyl ether, filtered and dried before being purified by flash reverse phase chromatography using a Biotage® SNAP Ultra C18 column. This typically used the following program, however the gradient was adapted as needed with increasing/decreasing hydrophilicity to ensure the desired peak was eluted from the column 50-60% of the way through the solvent gradient:

***Table 17: RP-HPLC Biotage program used in general SPPS of linear peptides.***

| Column Volumes | Water (+0.1% TFA) % | Acetonitrile (+0.1% TFA) % |
|---|---|---|
| Pre-loaded | 100 | 0 |
| 1 | 100 | 0 |
| 1 | 85 | 15 |
| 10 (gradient) | 85-40 | 15-60 |
| 3 | 40 | 60 |
| 3 | 0 | 100 |
| 3 | 100 | 0 |

Fractions containing the desired linear peptide were confirmed by mass spectroscopy, combined, lyophilised and stored (-20 ˚C). To form the disulfide bond to turn the linear peptides into hairpin conformers, the peptides were dissolved in acetic acid (75% aq.). To this a solution of iodine (10% w/v in methanol) was added dropwise until a stable orange colour was produced. The mixture was then stirred (1 h, RTP) and quenched by dropwise addition of sodium ascorbate (20 mM, aq). Water, acetic acid and methanol was removed *in vacuo* and the mixture purified by reverse-phase HPLC generally using the following program but again adapting the gradient so that the desired peak fell 50-60% of the way up the gradient.

***Table 18: RP-HPLC program used in general SPPS of hairpin peptides.***

| Column Volumes | Water (+0.1% TFA) % | Acetonitrile (+0.1% TFA) % |
|---|---|---|
| Pre-loaded | 100 | 0 |
| 1 | 100 | 0 |
| 1 | 80 | 20 |
| 10 (gradient) | 80-35 | 20-65 |
| 3 | 35 | 65 |
| 3 | 0 | 100 |
| 3 | 100 | 0 |

Fractions containing the desired peaks were identified by mass spectrometry, combined, lyophilised and stored (-20 ˚C). Cyclisation was confirmed by a shift in mass equivalent to removing two hydrogens. Final lead peptides were analysed by mass spectrometry and analytical reverse phase HPLC.

### 7.3.5.2 Kaiser Test

For each Kaiser test a sample of Wang resin beads was removed and to it added potassium cyanide (0.4 mL, 2 mM in pyridine) and ninhydrin (0.6 mL, 280 mM, in ethanol). The mixture was then heated (135 ˚C, 30 s). If the beads or solution turned violet a deprotected amine was present. If the beads turned orange either a secondary amine was present, or certain Fmoc protected amino acids (particularly cysteine) were present. If the beads and solution stayed yellow then no primary amine was present.

### 7.3.5.3 Analytical HPLC

All analytical HPLC was conducted using a Waters XSelect CSH C18 5 μM column, with dimensions 4.6 by 250 mm, using the following program:

***Table 19: Analytical RP-HPLC program used the analysis of linear peptides.***

| Column Volumes | Water (+0.1% TFA) % | Acetonitrile (+0.1% TFA) % |
|---|---|---|
| Pre-loaded | 95 | 5 |
| 1 | 95 | 5 |
| 25 (gradient) | 95-50 | 5-50 |
| 5 | 50 | 50 |
| 5 (gradient) | 50-5 | 50-95 |
| 5 | 5 | 95 |
| 5 (gradient) | 5-95 | 95-5 |
| 5 | 95 | 5 |

### 7.3.5.4 Lead Peptide Synthesis

#### 7.3.5.4.1 JI.5.1

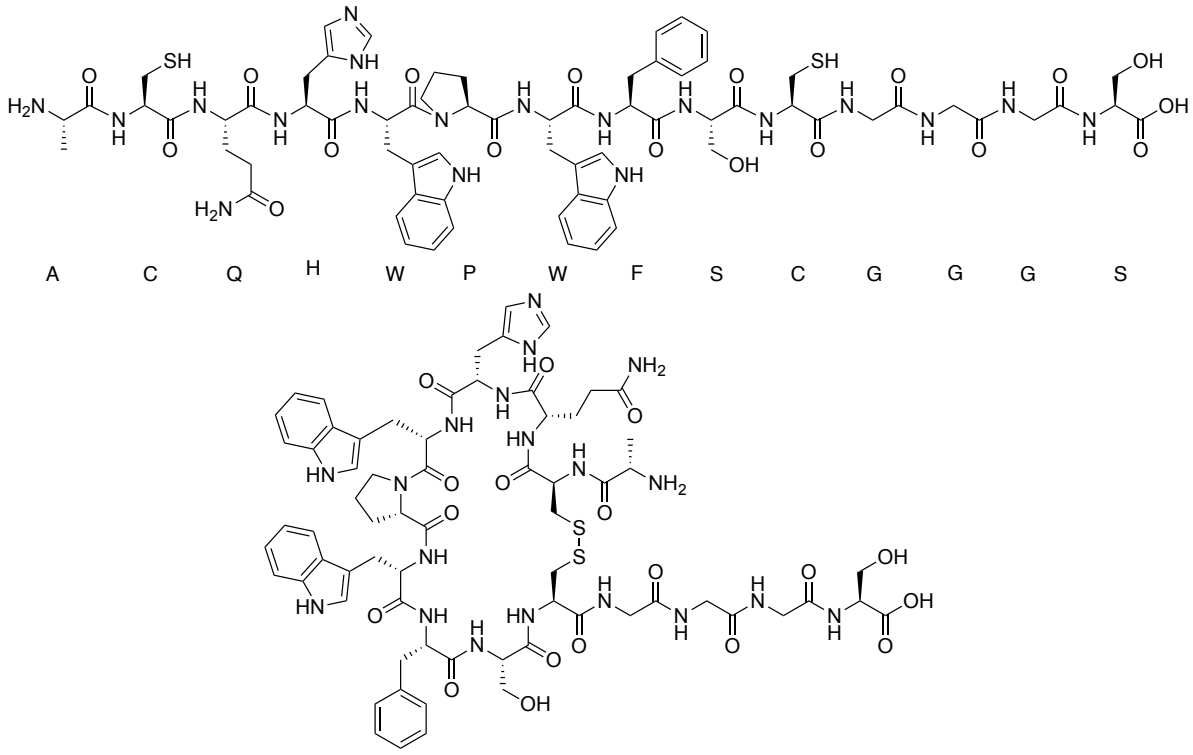



***Figure 96: Linear and hairpin disulfide cyclised JI.5.1***

JI.5.1 was synthesised using the procedure outlined in Section 7.3.5.1. After the first purification (by Biotage) the linear peptide product, 40.1 mg, 26.5 µmol (10.6% yield) was isolated. This was analysed by MS (ES+) *m/z*: 762.5 ($(M+2H)^{2+}$ expected exact mass: 762.80), 508.7 ($(M+3H)^{3+}$ expected exact mass: 508.87).

After disulfide bridge formation and HPLC purification, the peptide was lyophilised and analysed: 11.2 mg, 7.36 µmol (27.7% step yield, 2.9% overall yield) was isolated, MS (ES+) m/z: 761.6 ($(M+2H)^{2+}$ expected exact mass: 761.80). Analytical HPLC (280 nm): 19.8 min 95.7%, 20.656 min 4.3%. The WuXi version of this peptide was analysed by MS (ES+) *m/z*: 761.6 ($(M+2H)^{2+}$ expected exact mass: 761.80), confirming parity of newly synthesised peptide with the purchased variant.

### 7.3.5.4.2 JI.5.12

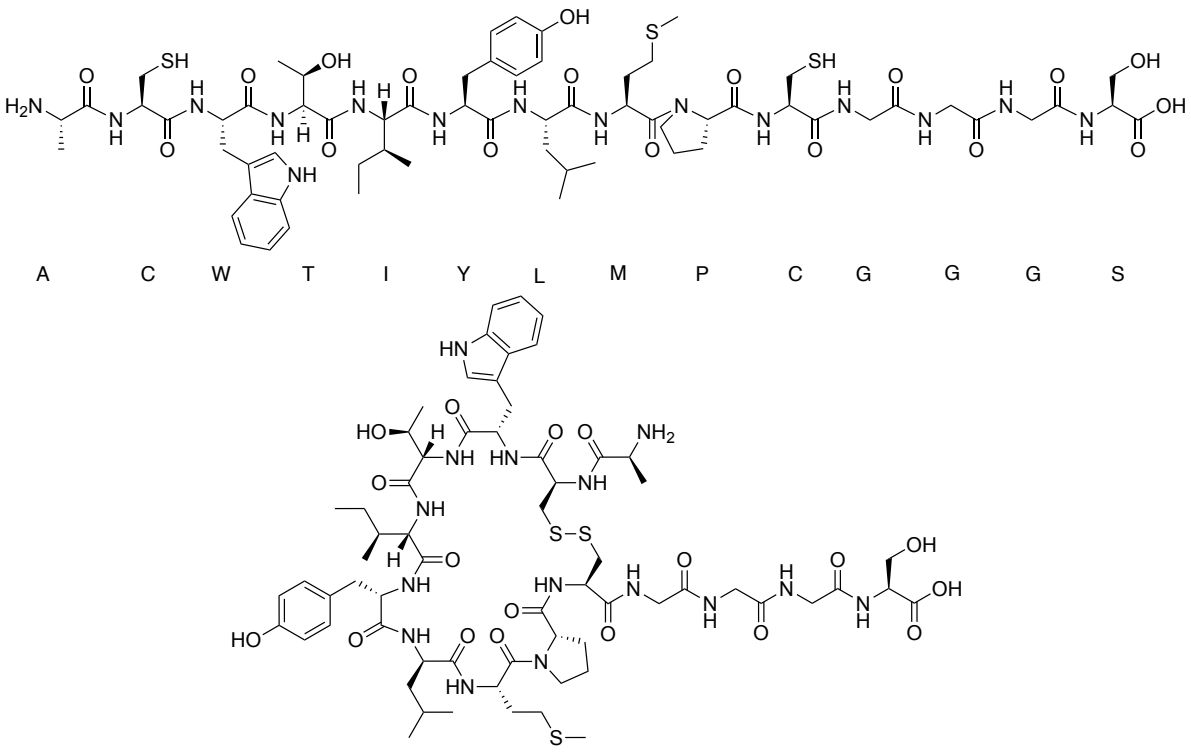



**Figure 97: Linear and hairpin disulfide cyclised JI.5.12**

JI.5.12 was synthesised using the procedure outlined in Section 7.3.5.1. After the first purification (by Biotage) the linear peptide product, 23.5 mg, 16.1 µmol (6.4% yield) was isolated. This was analysed by MS (ES+) *m/z*: 1458.8 ($(M+H)^{+}$ expected exact mass: 1459.63), 730.4 ($(M+2H)^{2+}$ expected exact mass: 730.32), 1480.9 ($(M+Na)^{+}$ expected exact mass: 1481.61).

After disulfide bridge formation and HPLC purification, the peptide was lyophilised and analysed: 6.5 mg, 4.45 µmol (27.7% step yield, 1.78% overall yield) was isolated, MS (ES+) m/z: 1457.9 ($(M+H)^+$ expected exact mass: 1457.61), 729.4 ($(M+2H)^{2+}$ expected exact mass: 729.31). Analytical HPLC (280 nm): 22.908 min 77.3%, 23.488 min 22.7%. The WuXi version of this peptide was analysed by MS (ES+) *m/z*: 1457.0 ($(M+H)^+$ expected exact mass: 1457.61), 729.3 ($(M+2H)^{2+}$ expected exact mass: 729.31), confirming parity of newly synthesised peptide with the purchased variant.

7.3.5.4.3 JI.5.13

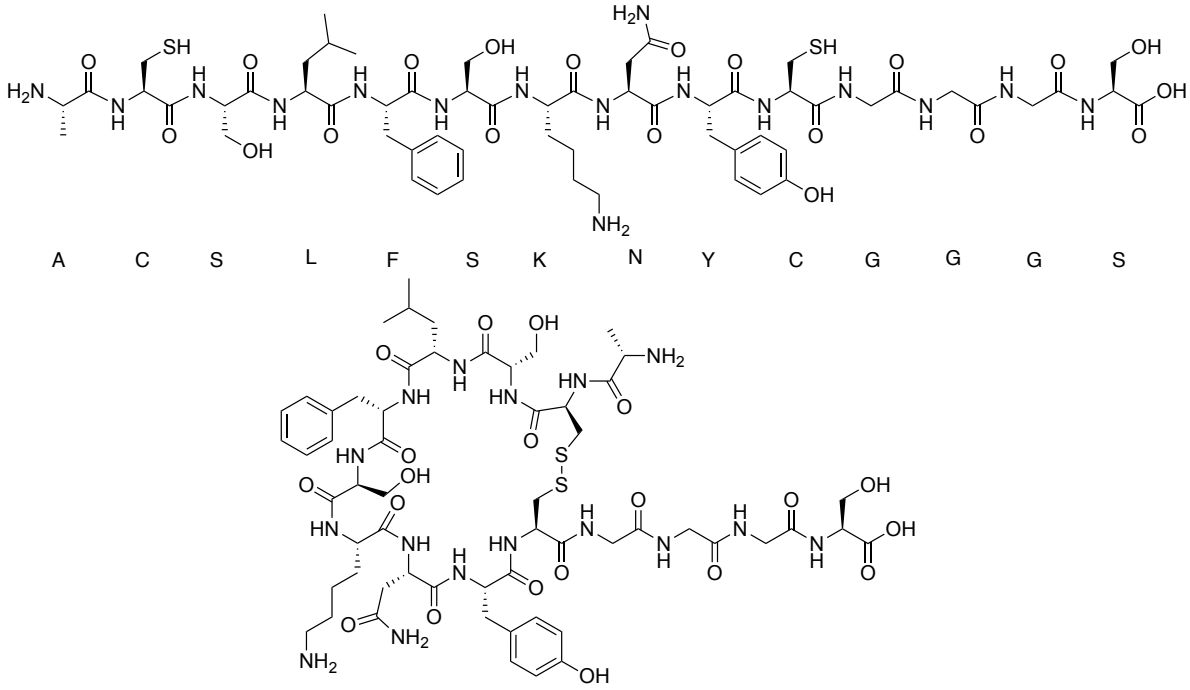



**Figure 98: Linear and hairpin disulfide cyclised JI.5.13**

JI.5.13 was synthesised using the procedure outlined in Section 7.3.5.1. After the first purification (by Biotage) the linear peptide product, 55.4 mg, 39.72 µmol (15.89% yield) was isolated. This was analysed by MS (ES+) *m/z*: 1394.1 ($(M+H)^+$ expected exact mass: 1395.6), 697.9 ($(M+2H)^{2+}$ expected exact mass: 698.3).

After disulfide bridge formation and HPLC purification, the peptide was lyophilised and analysed: 9.6 mg, 6.89 µmol (17.35% step yield, 2.76% overall yield) was isolated, MS (ES+) m/z: 1392.8 ($(M+H)^+$ expected exact mass: 1393.58), 696.9 ($(M+2H)^{2+}$ expected exact mass: 697.29). Analytical HPLC (280 nm): 23.163 min 75.62 %, 23.6357 min 24.38%. The WuXi version of this peptide was analysed by MS (ES+) *m/z*: 1392.2

($(M+H)^+$ expected exact mass: 1393.58), 696.00 ($(M+2H)^{2+}$ expected exact mass: 697.29), confirming parity of newly synthesised peptide with the purchased variant.

7.3.5.4.4 JI.5.14

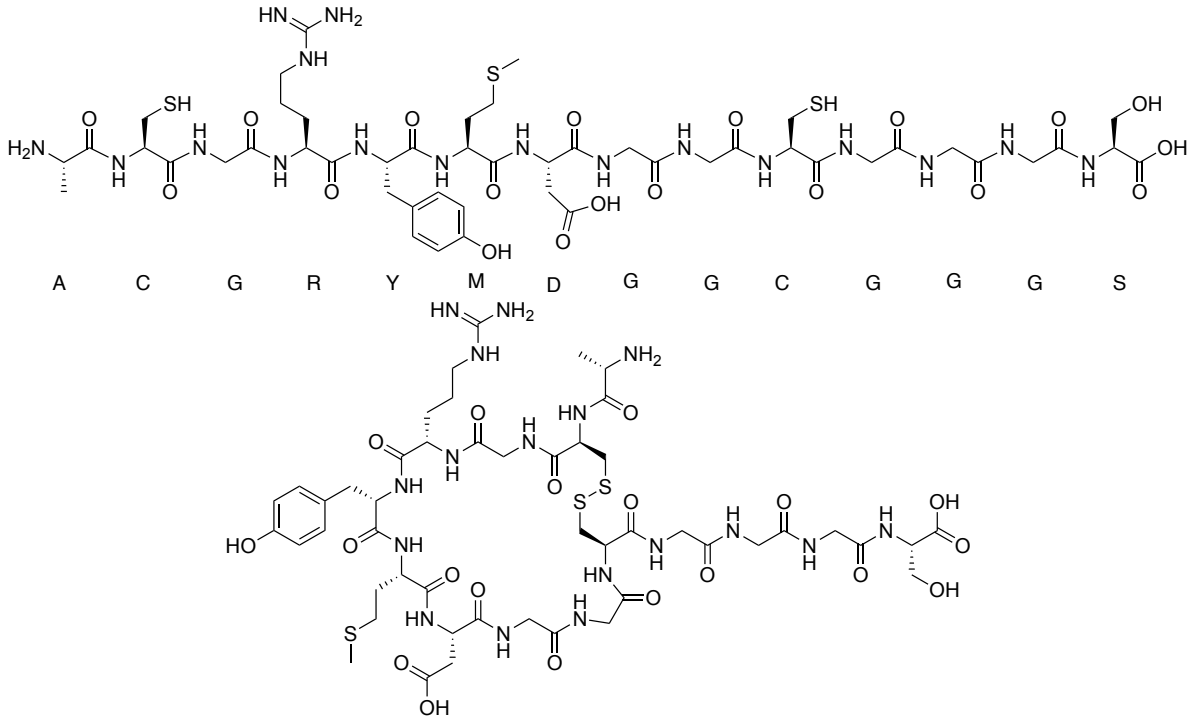



**Figure 99: Linear and hairpin disulfide cyclised JI.5.14**

JI.5.14 was synthesised using the procedure outlined in Section 7.3.5.1. After the first purification (by Biotage) the linear peptide product, 44.5 mg, 34.43 µmol (13.77% yield) was isolated. This was analysed by MS (ES+) *m/z*: 1290.9 ($(M+H)^+$ expected exact mass: 1293.48), 646.1 ($(M+2H)^{2+}$ expected exact mass: 647.25).

After disulfide bridge formation and HPLC purification, two enantiomers were separated: JI.5.14.5 and JI.5.14.7. These were was lyophilised and analysed: JI.5.14.5: 5.8 mg, 4.49 µmol (13.05% step yield, 1.80% overall yield) was isolated, MS (ES+) m/z: 1288.6 ($(M+H)^+$ expected exact mass: 1291.47), 645.2 ($(M+H)^{2+}$ expected exact mass: 646.24). Analytical HPLC (280 nm): 12.46 min 100%.

JI.5.14.7: 2.8 mg, 2.17 µmol (6.30% step yield, 0.87% overall yield), MS (ES+) m/z: 1288.7 ($(M+H)^+$ expected exact mass: 1291.47), 645.2 ($(M+H)^{2+}$ expected exact mass: 646.24). Analytical HPLC (280 nm): 12.45 min 100%. NB: the analytical HPLC shows almost the same retention time for both 14.5 and 14.7, but these eluted at different times

from the preparative HPLC. By mass spec these are identical. It was assumed these are enantiomers, but this should dramatically affect the analytical HPLC. The WuXi version of this peptide was analysed by MS (ES+) *m/z* 1288.9 $((M+H)^{+}$ expected exact mass: 1291.47), 645.4 $((M+H)^{2+}$ expected exact mass: 646.24), confirming parity of newly synthesised peptide with the purchased variant.

7.3.5.4.5 JI.5.23

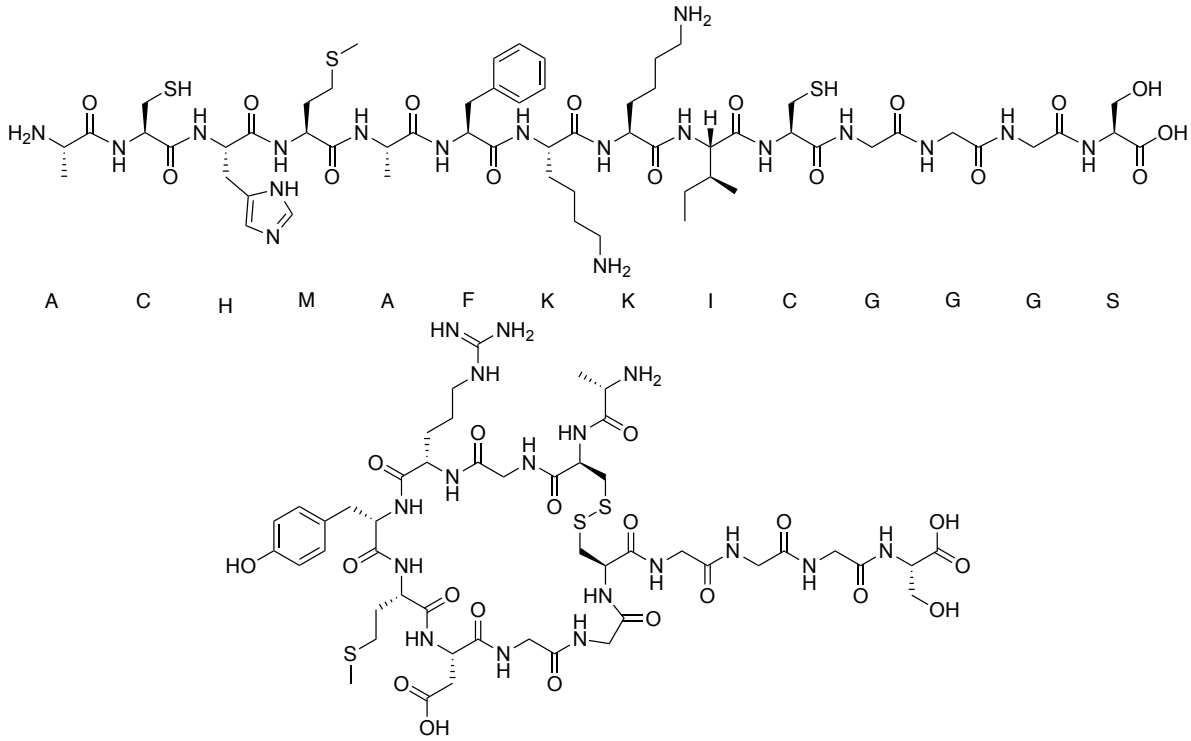



**Figure 100: Linear and hairpin disulfide cyclised JI.5.23**

JI.5.23 was synthesised using the procedure outlined in Section 7.3.5.1. After the first purification (by Biotage) the linear peptide product, 67.8 mg, 47.99 µmol (19.19% yield) was isolated. This was analysed by MS (ES+) *m/z*: 705.8 $((M+2H)^{2+}$ expected exact mass: 707.34), 471.1 $((M+3H)^{3+}$ expected exact mass: 471.9) 353.7 $((M+4H)^{4+}$ expected exact mass: 354.18).

After disulfide bridge formation and HPLC purification, two enantiomers were partially separated: 23.5 and 23.6. These were lyophilised and analysed: 23.5: 9.8 mg, 6.95 µmol (14.47% step yield, 2.78% overall yield) was isolated, MS (ES+) m/z: 704.9 $((M+2H)^{2+}$ expected exact mass: 706.34), 470.4 $((M+3H)^{3+}$ expected exact mass: 471.23), 353.1 $((M+4H)^{4+}$ expected exact mass: 353.67). Analytical HPLC (280 nm): 14.843 min 56.7%,

15.018 min 43.3%. 23.6: 21.9 mg, 15.52 µmol (32.35% step yield, 6.21% overall yield), MS (ES+) m/z: 704.9 ((M+2H)$^{2+}$ expected exact mass: 706.34), 470.4 ((M+3H)$^{3+}$ expected exact mass: 471.23), 353.1 ((M+4H)$^{4+}$ expected exact mass: 353.67). Analytical HPLC (280 nm): 14.841 min 18.4%, 15.019 min 81.6%. As these have the same masses but different analytical HPLC times, JI.5.23.5 and JI.5.23.6 represent enantiomers. JI.5.23.5 therefore represents a 50:50 mixture of enantiomers, JI.5.23.6 represents a 1:4 mixture. If these show different inhibitory properties then JI.5.23 can be resynthesised and purified with a more cautious HPLC gradient to try to isolate one enantiomer. The WuXi version of this peptide was analysed by MS (ES+) *m/z*: 705.3 ((M+2H)$^{2+}$ expected exact mass: 706.34), 470.4 ((M+3H)$^{3+}$ expected exact mass: 471.23), 353.2 ((M+4H)$^{4+}$ expected exact mass: 353.67), confirming parity of newly synthesised peptide with the purchased variant.

### 7.3.5.4.6 JI.5.37

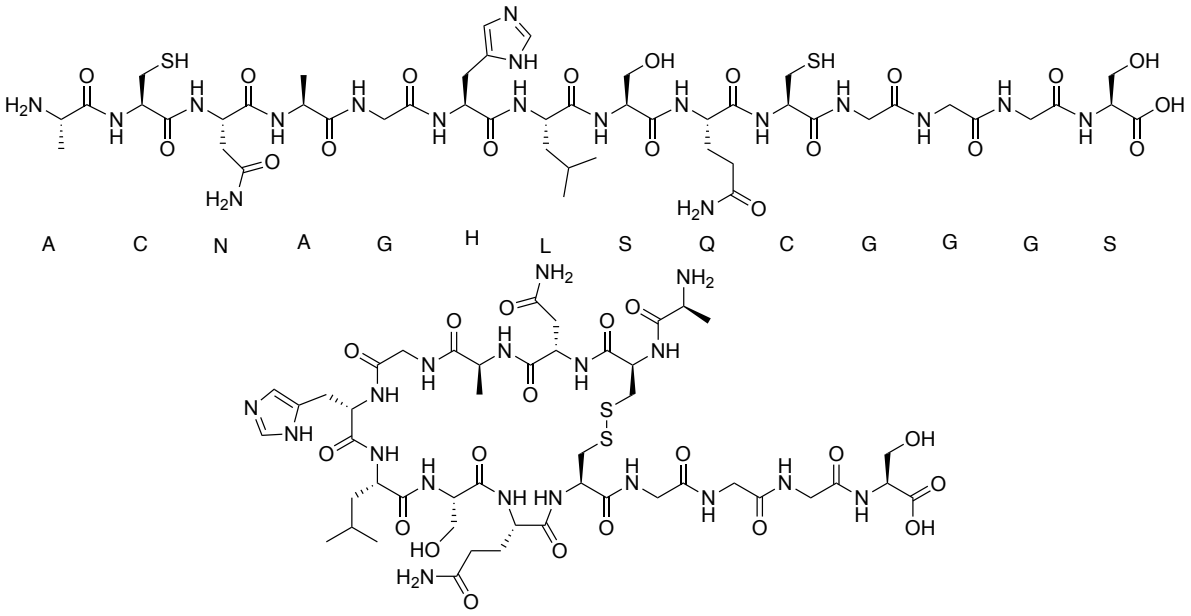



**Figure 101: Linear and hairpin disulfide cyclised JI.5.37**

JI.5.37 was synthesised using the procedure outlined in Section 7.3.5.1. After the first purification (by Biotage) the linear peptide product, 62.0 mg, 49.11 µmol (19.64% yield) was isolated. This was analysed by MS (ES+) *m/z*: 1262.9 ((M+H)$^{+}$ expected exact mass: 1263.52), 631.7 ((M+2H)$^{2+}$ expected exact mass: 632.26), 421.5 ((M+3H)$^{3+}$ expected exact mass: 421.84).

After disulfide bridge formation and HPLC purification, the peptide was lyophilised and analysed: 18.9 mg, 14.99 µmol (30.53% step yield, 6.00% overall yield) was isolated, MS

(ES+) m/z: 1259.7 ((M+H)$^+$ expected exact mass: 1261.5), 630.6 ((M+2H)$^{2+}$ expected exact mass: 631.25). Analytical HPLC (280 nm): 13.105 min 96.75%, 13.213 min 3.25%. The WuXi version of this peptide was analysed by MS (ES+) *m/z*: 630.8 ((M+2H)$^{2+}$ expected exact mass: 631.25), confirming parity of newly synthesised peptide with the purchased variant.

### 7.3.5.4.7 JI.5.43

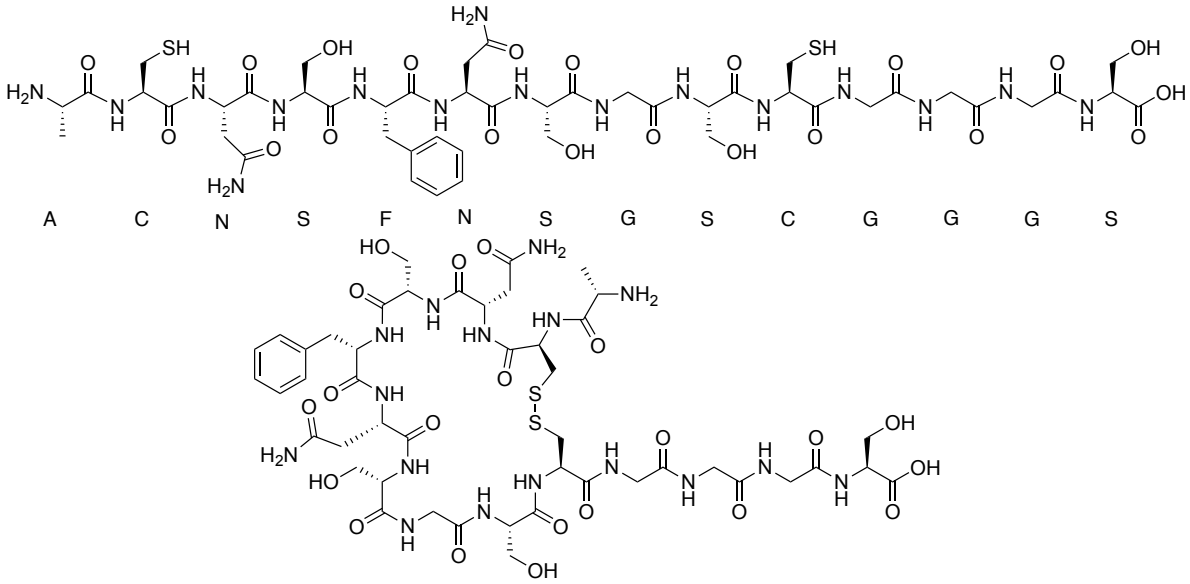



**Figure 102: Linear and hairpin disulfide cyclised JI.5.43**

JI.5.43 was synthesised using the procedure outlined in Section 7.3.5.1. After the first purification (by Biotage) the linear peptide product, 35.0 mg, 28.06 µmol (11.22% yield) was isolated. This was analysed by MS (ES+) *m/z*: 1247.8 ((M+H)$^+$ expected exact mass: 1248.45), 624.6 ((M+2H)$^{2+}$ expected exact mass: 624.73).

After disulfide bridge formation and HPLC purification, the peptide was lyophilised and analysed: 10.6 mg, 8.51 µmol (30.34% step yield, 3.41% overall yield) was isolated, MS (ES+) m/z: 1245.4 ((M+H)$^+$ expected exact mass: 1246.43), 623.6 ((M+2H)$^{2+}$ expected exact mass: 623.6). Analytical HPLC (280 nm): 12.07 min. The WuXi version of this peptide was analysed by MS (ES+) *m/z*: 1245.8 ((M+H)$^+$ expected exact mass: 1246.43), 623.8 ((M+2H)$^{2+}$ expected exact mass: 623.6), confirming parity of newly synthesised peptide with the purchased variant.

7.3.5.4.8 JI.5.44

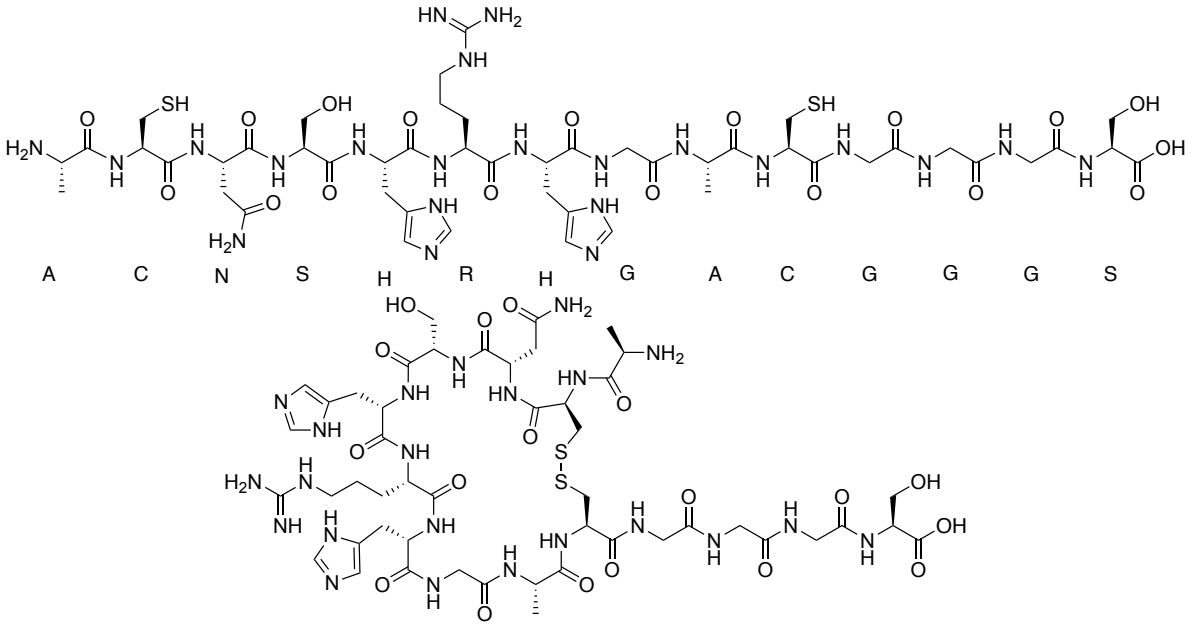



**Figure 103: Linear and hairpin disulfide cyclised JI.5.44**

JI.5.44 was synthesised using the procedure outlined in Section 7.3.5.1. After the first purification (by Biotage) the linear peptide product, 64.0 mg, 48.61 µmol (19.44% yield) was isolated. This was analysed by MS (ES+) *m/z*: 1314.5 ($(M+H)^+$ expected exact mass: 1317.55), 657.8 ($(M+2H)^{2+}$ expected exact mass: 659.28), 329.5 ($(M+3H)^{3+}$ expected exact mass: 330.14).

After disulfide bridge formation and HPLC purification, the peptide was lyophilised and analysed: 13.9 mg, 10.57 µmol (21.75% step yield, 4.23% overall yield) was isolated, MS (ES+) m/z: 1312.7 ($(M+H)^+$ expected exact mass: 1315.54), 656.8 ($(M+2H)^{2+}$ expected exact mass: 658.27), 438.3 ($(M+3H)^{3+}$ expected exact mass: 439.18), 328.9 ($(M+4H)^{4+}$ expected exact mass: 329.64). Analytical HPLC (280 nm): 20.03 min. The WuXi version of this peptide was analysed by MS (ES+) *m/z*: 1312.6 ($(M+H)^+$ expected exact mass: 1315.54), 656.8 ($(M+2H)^{2+}$ expected exact mass: 658.27), 438.3 ($(M+3H)^{3+}$ expected exact mass: 439.18), confirming parity of newly synthesised peptide with the purchased variant.

7.3.5.4.9 JI.5.52

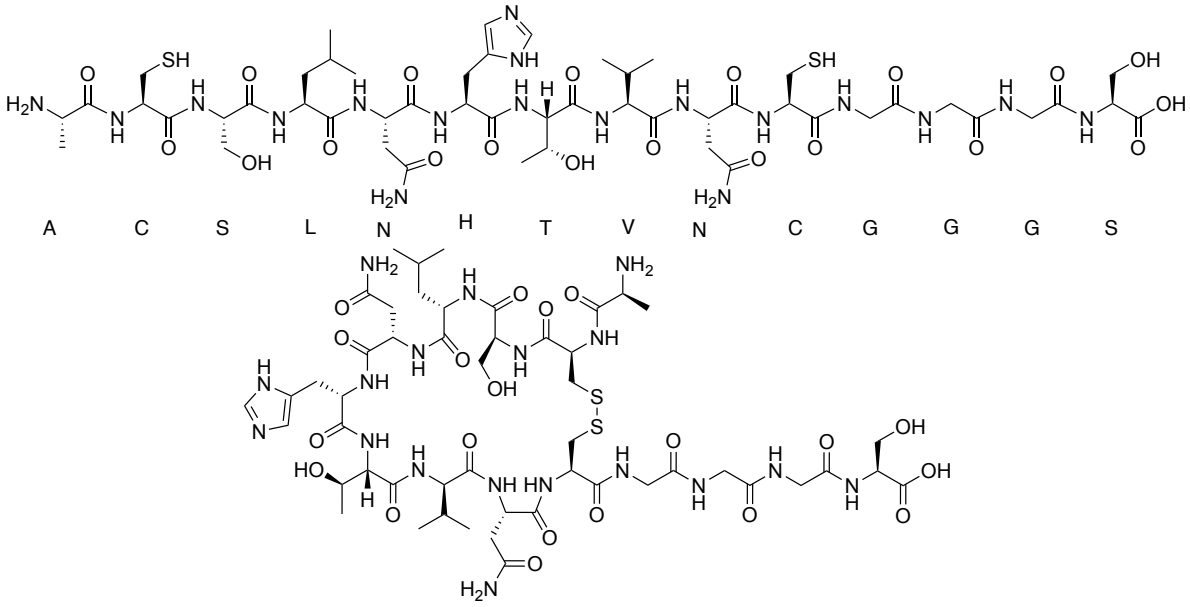



**Figure 104: Linear and hairpin disulfide cyclised JI.5.52**

JI.5.52 was synthesised using the procedure outlined in Section 7.3.5.1. After the first purification (by Biotage) the linear peptide product, 36.4 mg, 27.56 µmol (11.03% yield) was isolated. This was analysed by MS (ES+) *m/z*: 1320.6 ($(M+H)^+$ expected exact mass: 1321.56), 660.7 ($(M+2H)^{2+}$ expected exact mass: 661.28).

After disulfide bridge formation and HPLC purification, the peptide was lyophilised and analysed: 12.5 mg, 9.48 µmol (34.39% step yield, 3.79% overall yield) was isolated, MS (ES+) m/z: 1317.4 ($(M+H)^+$ expected exact mass: 1319.54), 659.7 ($(M+2H)^{2+}$ expected exact mass: 660.28). Analytical HPLC (280 nm): 12.63 min. The WuXi version of this peptide was analysed by MS (ES+) *m/z*: 1318.1 ($(M+H)^+$ expected exact mass: 1319.54), 659.9 ($(M+2H)^{2+}$ expected exact mass: 660.28), confirming parity of newly synthesised peptide with the purchased variant.

7.3.5.4.10 JI.5.55

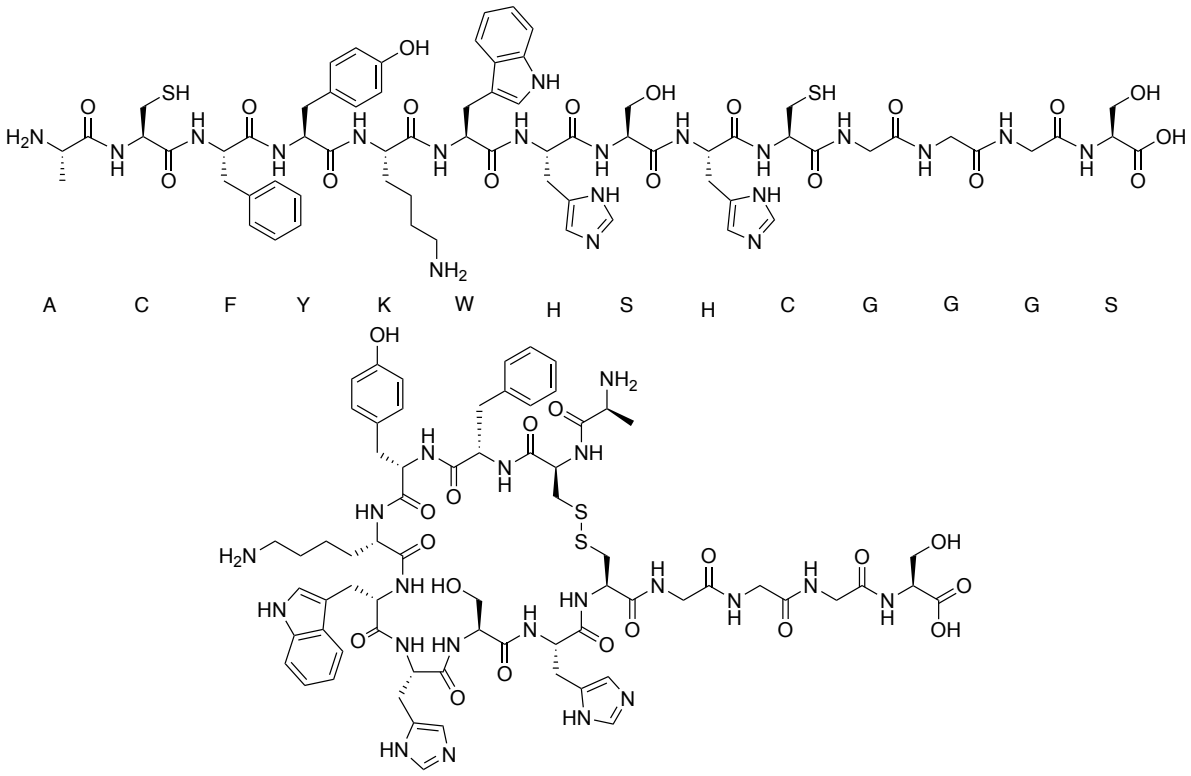



**Figure 105: Linear and hairpin disulfide cyclised JI.5.55**

JI.5.55 was synthesised using the procedure outlined in Section 7.3.5.1. After the first purification (by Biotage) the linear peptide product, 66.2 mg, 42.91 µmol (17.17% yield) was isolated. This was analysed by MS (ES+) *m/z*: 770.9 ($(M+2H)^{2+}$ expected exact mass: 772.33), 514.6 ($(M+3H)^{3+}$ expected exact mass: 515.22), 386.1 ($(M+4H)^{4+}$ expected exact mass: 386.67).

After disulfide bridge formation and HPLC purification, the peptide was lyophilised and analysed: 26.8 mg, 17.40 µmol (40.54% step yield, 6.96% overall yield) was isolated, MS (ES+) m/z: 769.8 ($(M+2H)^{2+}$ expected exact mass: 771.32), 513.7 ($(M+3H)^{3+}$ expected exact mass: 514.55), 385.6 ($(M+4H)^{4+}$ expected exact mass: 386.17). Analytical HPLC (280 nm): 14.901 min 94.65%, 14.657 min 5.35%. The WuXi version of this peptide was analysed by MS (ES+) *m/z*: 770.1 ($(M+2H)^{2+}$ expected exact mass: 771,32), 513.9 ($(M+3H)^{3+}$ expected exact mass: 514.55), 385.7 ($(M+4H)^{4+}$ expected exact mass: 386.17), confirming parity of newly synthesised peptide with the purchased variant.

7.3.5.4.11 JI.5.58

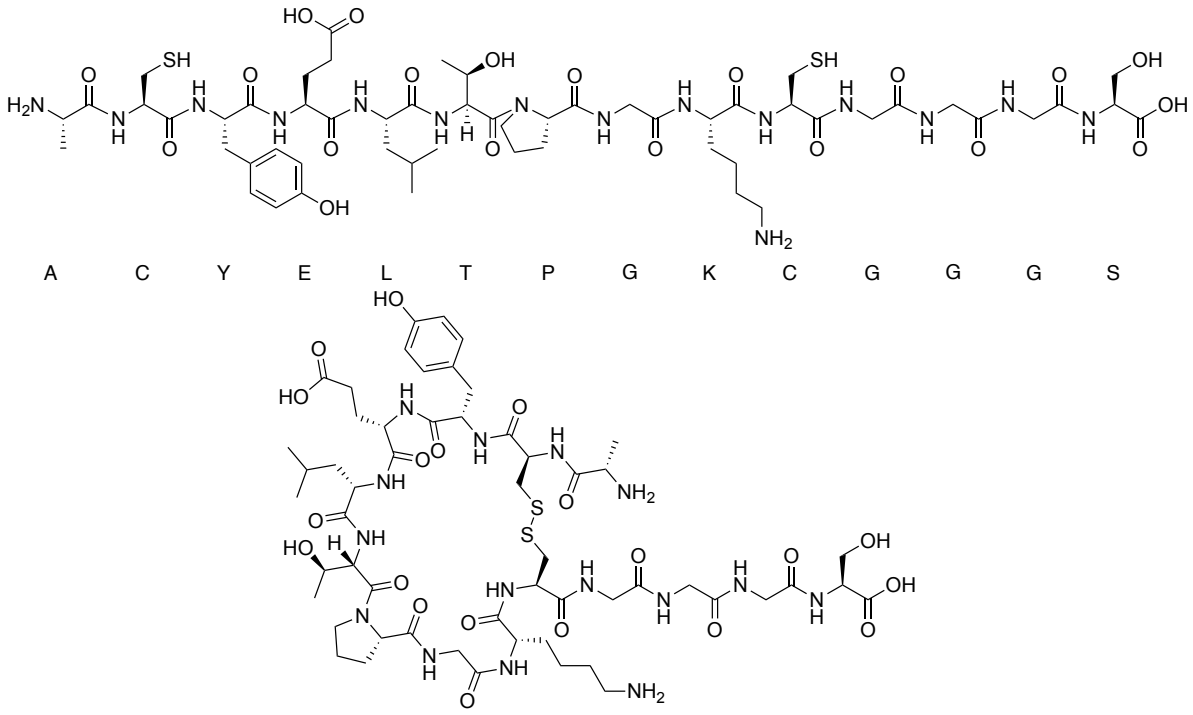



**Figure 106: Linear and hairpin disulfide cyclised JI.5.58.**

JI.5.58 was synthesised using the procedure outlined in Section 7.3.5.1. After the first purification (by Biotage) the linear peptide product, 41.1 mg, 30.59 µmol (12.24% yield) was isolated. This was analysed by MS (ES+) *m/z*: 1343.7 ($(M+H)^+$ expected exact mass: 1344.59), 672.4 ($(M+2H)^{2+}$ expected exact mass: 672.80), 448.9 ($(M+3H)^{3+}$ expected exact mass: 448.87).

After disulfide bridge formation and HPLC purification, the peptide was lyophilised and analysed: 16.4 mg, 12.22 µmol (39.96% step yield, 4.89% overall yield) was isolated, MS (ES+) m/z: 1341.3 ($(M+H)^+$ expected exact mass: 1342.57), 671.4 ($(M+2H)^{2+}$ expected exact mass: 671.79). Analytical HPLC (280 nm): 12.035 min 70.29%, 14.907 min 29.71%. The WuXi version of this peptide was analysed by MS (ES+) *m/z*: 1341.2 ($(M+H)^+$ expected exact mass: 1342.57), 671.3 ($(M+2H)^{2+}$ expected exact mass: 671.79). confirming parity of newly synthesised peptide with the purchased variant.

## 7.3.6 Cloning

### 7.3.6.1 Reverse Two-Hybrid Systems

#### 7.3.6.1.1 pTHCP16(434-mBDNF)

pEX-A2(mBDNF) (Eurofins MWG) was transformed into chemically competent *DH5α*. Cultures of *DH5α*_pEX-A2(mBDNF) and *DH5α*_pTHCP16(434-Blank) (provided by A. Male) were prepared and the plasmids isolated and subjected to digestion with *Sac*I-HF and *Bam*HI-HF in Cutsmart buffer. Digested pTHCP16 was then treated with TSAP (1 µL, 1 h, 37 ˚C). Purified digested vector and insert were then ligated together and transformed into chemically competent *DH5α E. coli* cells and incubated on LB agar containing Camp overnight. The resulting colonies were inspected using colony PCR (primers: M13-49, SEQ1R, $T_m$ anneal: 52 ˚C) and two positive colonies were cultured, the insert sequence verified (primer SEQ1R, FR02268827 and FR02268828) and pTHCP16(434-mBDNF)-4_12/11/13 was used in all future work.

pTHCP16(434-mBDNF)-4_12/11/13 was used to create pAH68(434-mBDNF).

#### 7.3.6.1.2 pAH68(434-mBDNF)

434-mBDNF was amplified out of pTHCP16(434-mBDNF)-4_12/11/13 by PCR (primers: M13-49, Seq-1R, anneal: 52 ˚C). *DH5α*PIR+Low_pAH68(434-BTB) was cultured and the plasmids isolated. These were subjected to digestion by *Nde*I and *Sac*I-HF in Cutsmart buffer. Digested pAH68 was treated with TSAP (1 µL, 1 h, 37 ˚C). Purified digested vector and insert were then ligated together and transformed into *DH5α*Pir+Low *E. coli* cells and incubated on LB agar containing CAMP overnight. The resulting colonies were inspected using colony PCR (primers: M13-49/P2, $T_m$ anneal: 51 ˚C) and a selection of positive colonies were cultured, the insert sequence verified (primer: M13-49, FR02268961) and used in all future work.

pAH68(434-mBDNF) was transformed and integrated into electrocompetent *SNS118*_pAH69 cells, then used in repressor efficacy and toxicity drop spotting.

#### 7.3.6.1.3 pTHCP16(434-TrmBDNF-30)

Using pTHCP16(434-mBDNF) as a template, PCR-TrmBDNF-30 was created by PCR (GoTaq polymerase, primers: BD-Rev/BD-Tr30-F, $T_m$: 51˚C). Cultures of

*DH5α*_pTHCP16(434-Blank) were prepared and the plasmids isolated and subjected to digestion with *Bam*HI-HF and *Sac*I-HF in Cutsmart buffer. Digested pTHCP16 was then treated with TSAP (1 µL, 1 h, 37 ˚C). Purified digested vector and insert were then ligated together and transformed into *DH5α E. coli* cells and incubated on LB agar containing Camp overnight. The resulting colonies were inspected using colony PCR (primers: BD-Rev and M13-49, $T_m$ anneal: 51 ˚C) and a selection of positive colonies were cultured, the insert sequence verified (primer: M13-49, FR02301023).

This was transformed into chemically competent *SNS118 E. coli* cells for repressor efficacy and toxicity shutdown testing, and used to create pAH68(434-TrmBDNF-30).

#### 7.3.6.1.4 pAH68(434-TrmBDNF-30)

Using pAH68(434-TrmBDNF-30) as a template, PCR-434-TrmBDNF-30 was created by PCR (GoTaq polymerase, primers: M13-49/BDRev, $T_m$: 51˚C). Cultures of *DH5α*Pir+ _pAH68(434-mBDNF) were prepared and the plasmids isolated and subjected to digestion with *Nde*I and *Sac*I-HF in Cutsmart buffer. Digested pAH68 was then treated with TSAP (1 µL, 1 h, 37 ˚C). Purified digested vector and insert were then ligated together and transformed into *DH5αPir+ E. coli* cells and incubated on LB agar containing Camp overnight. The resulting colonies were inspected using colony PCR (primers: BD-TrBD-30/BD-Rev, $T_m$ anneal: 51 ˚C) and a selection of positive colonies were cultured, the insert sequence verified (primer: M13-49, FR02270516).

pAH68(434-TrmBDNF-30) was integrated into *SNS118 E. coli* and used in repressor efficacy and toxicity shutdown testing.

#### 7.3.6.1.5 pTHCP16(434-TrmBDNF-38)

Using pTHCP16(434-mBDNF) as a template, PCR-TrmBDNF-38 was created by PCR (GoTaq polymerase, primers: BD-Rev/BD-Tr38-F, $T_m$: 51˚C). Cultures of *DH5α*_pTHCP16(434-Blank) were prepared and the plasmids isolated and subjected to digestion with *Bam*HI-HF and *Sac*I-HF in Cutsmart buffer. Digested pTHCP16 was then treated with TSAP (1 µL, 1 h, 37 ˚C). Purified digested vector and insert were then ligated together and transformed into *DH5α E. coli* cells and incubated on LB agar containing Camp overnight. The resulting colonies were inspected using colony PCR (primers: BD-Rev and M13-49, $T_m$ anneal: 51 ˚C) and a selection of positive colonies were cultured, the insert sequence verified (primer: M13-49, FR02270509).

This was used to create pAH68(434-TrmBDNF-38).

#### 7.3.6.1.6 pAH68(434-TrmBDNF-38)

Using pAH68(434-TrmBDNF-38) as a template, PCR-434-TrmBDNF-38 was created by PCR (GoTaq polymerase, primers: M13-49/BDRev, $T_m$: 51˚C). Cultures of *DH5α*Pir+ _pAH68(434-mBDNF) were prepared and the plasmids isolated and subjected to digestion with *Nde*I and *Sac*I-HF in Cutsmart buffer. Digested pAH68 was then treated with TSAP (1 µL, 1 h, 37 ˚C). Purified digested vector and insert were then ligated together and transformed into *DH5αPir+ E. coli* cells and incubated on LB agar containing Camp overnight. The resulting colonies were inspected using colony PCR (primers: BD-TrBD-38/BD-Rev, $T_m$ anneal: 51 ˚C) and a selection of positive colonies were cultured, the insert sequence verified (primer: M13-49, FR02270554).

pAH68(434-TrmBDNF-38) was integrated into *SNS118 E. coli* and used in repressor efficacy and toxicity shutdown testing.

#### 7.3.6.1.7 pTHCP16(434-TrmBDNF-44)

Using pTHCP16(434-mBDNF) as a template, PCR-TrmBDNF-44 was created by PCR (GoTaq polymerase, primers: BD-Rev/BD-Tr44-F, $T_m$: 51˚C). Cultures of *DH5α*_pTHCP16(434-Blank) were prepared and the plasmids isolated and subjected to digestion with *Bam*HI-HF and *Sac*I-HF in Cutsmart buffer. Digested pTHCP16 was then treated with TSAP (1 µL, 1 h, 37 ˚C). Purified digested vector and insert were then ligated together and transformed into *DH5α E. coli* cells and incubated on LB agar containing Camp overnight. The resulting colonies were inspected using colony PCR (primers: BD-Rev and M13-49, $T_m$ anneal: 51 ˚C) and a selection of positive colonies were cultured, the insert sequence verified (primer: M13-49, FR02301070).

This was transformed into chemically competent *SNS118 E. coli* cells for repressor efficacy and toxicity shutdown testing, and used to create pAH68(434-TrmBDNF-44).

#### 7.3.6.1.8 pAH68(434-TrmBDNF-44)

Using pAH68(434-TrmBDNF-44) as a template, PCR-434-TrmBDNF-44 was created by PCR (GoTaq polymerase, primers: M13-49/BDRev, $T_m$: 51˚C). Cultures of *DH5α*Pir+ _pAH68(434-mBDNF) were prepared and the plasmids isolated and subjected to digestion with *Nde*I and *Sac*I-HF in Cutsmart buffer. Digested pAH68 was then treated with TSAP

(1 µL, 1 h, 37 ˚C). Purified digested vector and insert were then ligated together and transformed into *DH5αPir+ E. coli* cells and incubated on LB agar containing Camp overnight. The resulting colonies were inspected using colony PCR (primers: BD-TrBD-38/BD-Rev, $T_m$ anneal: 51 ˚C) and a selection of positive colonies were cultured, the insert sequence verified (primer: M13-49, FR02270519).

pAH68(434-TrmBDNF-44) was integrated into *SNS118 E. coli* and used in repressor efficacy and toxicity shutdown testing.

#### 7.3.6.1.9 pAH68(mBDNF-FL-434)

A gene block ("mBDNF-FL-434") containing digestion overhangs (GTTGTT), an *Nde*I site, mBDNF, a *Bam*HI site, FL3[141], 434, a *Sac*I site and digestion overhangs (AACAAC) was amplified by PCR (Q5 polymerase, primers: BD-CT-F, BD-CT-434-R, $T_m$: 70˚C). Cultures of *DH5αPir+*_pAH68(BTB) were prepared and the plasmids isolated and subjected to digestion with *Nde*I and *Sac*I in Cutsmart buffer. Digested pAH68 was then treated with rSAP (1 µL, 1 h, 37 ˚C). Purified digested vector and insert were then ligated together and transformed into *DH5αPir+E. coli* cells and incubated on LB agar containing Camp overnight. The resulting colonies were inspected using colony PCR (primers: M13-49/ BD-CT-434-R, $T_m$ anneal: 68 ˚C) and a selection of positive colonies were cultured, the insert sequence verified (primer: M13-49, FR02269947).

pAH68(mBDNF-FL-434) was integrated into the chromosome of *SNS118 E. coli* and used in repressor efficacy and toxicity drop spotting.

#### 7.3.6.1.10 p16THCP(mBDNF-FL-434D)

pAH68(mBDNF-FL-434) was used as a template for GoTaq PCR using primers BD-CT-F and 434D-SacI-R. This was spin column purified and digested at the *BamHI* and *SacI* sites before further purification. Cultures of pAH68(434-TrmBDNF-38) were grown and their plasmids harvested before digestion at the *BamHI-HF* and *SacI* sites, and treatment with rSAP to prevent vector religation. The digested and purified by agarose gel electrophoresis and gel excision. Digested and purified vector and insert were ligated together and chemically transformed into *DH5α E. coli* cells. These were then incubated on LB agar containing Camp overnight. The resulting colonies were inspected using colony PCR (primers: M13-49 and 434D-SacI-R) and a selection of positive colonies were cultured, the insert sequence verified (primer: M13-49), identifying a K → R mutation in

p16THCP(mBDNF-FL-434D) due to the use of GoTaq. This was rectified with KOD polymerase SDM using the 434D-SDM-F and 434D-SDM-R primers. This was chemically transformed into *DH5α* cells and plated on LB agar containing Camp and incubated overnight. Colonies were picked and sequenced verified from LacI to NCR and mBDNF-FL-434D (p16-MscI-F, p16-LacI-F, M13-49).

#### 7.3.6.1.11 pAH68(mBDNF-FL-434D)

p16THCP(mBDNF-FL-434D) was transformed into GM2929 cells to prevent DNA methylation. These were cultured and the plasmids harvested for digestion at the *MscI* and *SacI* sites. LacI-NCR-mBDNF-FL-434D was isolated by agarose gel electrophoresis and purified. Fresh pAH68 was purchased from the CGSC, Yale (catalogue number: 70955), transformed into *DH5α* and cultured. The plasmids were harvested and digested at the *SmaI* and SacI sites before rSAP treatment to prevent vector religation. The digested vector was isolated by agarose gel electrophoresis and purified. Purified digested vector and insert were then ligated together, chemically transformed into *DH5α E. coli* cells and incubated on LB agar containing Camp overnight. The resulting colonies were inspected using colony PCR (primers: M13-49 and 434D-SacI-R). A selection of positive colonies were cultured, the insert sequence verified (primers: p16-MscI-F, p16-LacI-F, M13-49).

pAH68(mBDNF-FL-434D) was integrated into the chromosome of *SNS118 E. coli* and used in repressor efficacy and toxicity drop spotting.

### 7.3.6.2 Expression Plasmids

#### 7.3.6.2.1 pET28a(+)(TrkA-D5)

The gene block for TrkA-D5 (residues 278-386)[49, 176-177] was optimized for *E. coli* expression and the codons for a flexible linker was added at the 5′ end, plus appropriate restriction sites. This was then purchased (Integrated DNA Technologies) and amplified by Pfu polymerase PCR using primers TrkA-D5/TrkB-D5-Fwd and TrkA-D5-R. This was then digested at the *BamHI* and *HindIII* sites and purified. A bacterial culture of DH5α pET28a(+)($His_6$-TCS-FLAG) (provided by A. Ball) was used to create cultures. The plasmids were harvested, digested (*BamHI* and *HindIII*) and treated with rSAP to prevent vector religation. The digested vector was removed by agarose gel electrophoresis and gel excision. Purified digested vector and insert were ligated and transformed into DH5α cells and plated on LB agar containing Kanamycin as a selective pressure. Colonies were picked

and confirmed using colony PCR and using primers TrkA-D5/TrkB-D5-Fwd and TrkA-D5-R. Successful colonies were picked, cultured, harvested and sequenced verified using TrkA-D5/TrkB-D5-Fwd.

pET28a(+)($His_6$-TCS-FLAG-FL-TrkA-D5) was chemically transformed into expression cell lines as needed.

#### 7.3.6.2.2 pET28a(+)(TrkB-D5)

The gene block for TrkB-D5 (residues 283-385) [49, 176-177][49, 178] was optimized for *E. coli* expression and the codons for a flexible linker was added at the 5′ end, plus appropriate restriction sites. This was then purchased (Integrated DNA Technologies) and amplified by Pfu polymerase PCR using primers TrkA-D5/TrkB-D5-Fwd and TrkB-D5-R. This was then digested at the *BamHI* and *HindIII* sites and purified. Cultures of DH5α pET28a(+)($His_6$-TCS-FLAG-FL-TrkA) were prepared and the vector harvested and digested (*BamHI* and *HindIII*) and treated with rSAP to prevent vector religation. The digested vector was removed by agarose gel electrophoresis and gel excision. Purified digested vector and insert were ligated and transformed into DH5α cells and plated on LB agar containing Kanamycin as a selective pressure. Colonies were picked and confirmed using colony PCR and using primers TrkA-D5/TrkB-D5-Fwd and TrkA-D5-R. Successful colonies were picked, cultured, harvested and sequenced verified using TrkA-D5/TrkB-D5-Fwd.

pET28a(+)($His_6$-TCS-FLAG-FL-TrkA-D5) was chemically transformed into expression cell lines as needed.

#### 7.3.6.2.3 pET28a(+)(βNGF-$His_6$)

The gene for mature human βNGF (residues 122-241) tagged with both an N-terminal OmpA periplasmic leader sequence and a C-terminal $His_6$ affinity tag (with appropriate linkers, digestion sites and digestion overhangs) was optimised for K12 based *E. coli* expression and purchased (IDT). This was amplified by Pfu PCR using primers βNGF-Ex-FL and $His_6$-Rev, purified, digested at the *NcoI* and *HindIII* sites and purified by spin column. Cultures of DH5α pET28a(+) were prepared and harvested. The plasmids were digested at their *NcoI* and *HindIII* sites, treated with rSAP to prevent vector religation and purified by gel electrophoresis. The digested and purified to produce and purified insert and vector were ligated and chemically transformed into DH5α cells. These were grown

overnight on LB agar plates containing kanamycin to select for successful transformation. Colonies were picked and colony PCR (GoTaq, βNGF-Ex-F and $His_6$-Rev) was used to select *E. coli* bearing the correct vector. These were cultured and the plasmids harvested and sequence verified using the $His_6$-Rev primer.

pET28a(+)(βNGF-$His_6$) was chemically transformed into expression cell lines as needed.

#### 7.3.6.2.4 pET28a(+)(OmpA-βNGF-$His_6$)

The gene for mature human βNGF (residues 122-241) tagged with both an N-terminal OmpA periplasmic leader sequence and a C-terminal $His_6$ affinity tag (with appropriate linkers, digestion sites and digestion overhangs) was optimised for K12 based *E. coli* expression and purchased (IDT). This was amplified by Pfu PCR using primers OmpA-GB-Fwd and $His_6$-Rev, purified, digested at the *NcoI* and *HindIII* sites and purified by spin column. Cultures of DH5α pET28a(+) were prepared and harvested. The plasmids were digested at their *NcoI* and *HindIII* sites, treated with rSAP to prevent vector religation and purified by gel electrophoresis. The digested and purified to produce and purified insert and vector were ligated and chemically transformed into DH5α cells. These were grown overnight on LB agar plates containing kanamycin to select for successful transformation. Colonies were picked and colony PCR (GoTaq, OmpA-GB-Fwd and $His_6$-Rev) was used to select *E. coli* bearing the correct vector. These were cultured and the plasmids harvested and sequence verified using the $His_6$-Rev primer.

pET28a(+)(OmpA-βNGF-$His_6$) was chemically transformed into expression cell lines as needed.

#### 7.3.6.2.5 pET28a(+)(mBDNF-$His_6$)

The mBDNF gene encoded in p16THCP(mBDNF-FL-434D) includes an unintended NcoI site. This was removed with using KOD SDM PCR with primers mBDNF-NcoI-SDM-F and mBDNF-NcoI-SDM-R. The amplified DNA was chemically transformed into DH5α cells and plated on LB agar plates containing Camp, and incubated overnight. Colonies were picked, cultured and their plasmids harvested. An agarose gel was used to ensure plasmids were of the correct size, and the sequence verified using primer M13-49. mBDNF was then amplified by PCR using the mBDNF-Ex-F and mBDNF-FL-His6-HindIII-Rev primers, digested at the NcoI and *HindIII* sites and spin column purified. Cultures of DH5α pET28a(+) were prepared and harvested. The plasmids were digested at their *NcoI* and

*HindIII* sites, treated with rSAP to prevent vector religation and purified by gel electrophoresis. The digested and purified to produce and purified insert and vector were ligated and chemically transformed into DH5α cells. These were grown overnight on agar plates containing kanamycin to select for successful transformation. Colonies were picked and colony PCR (GoTaq, mBDNF-Ex-FL and $His_6$-Rev) was used to select *E. coli* bearing the correct vector. These were cultured and the plasmids harvested and sequence verified using the $His_6$-Rev primer.

pET28a(+)(mBDNF-$His_6$) was chemically transformed into expression cell lines as needed.

#### 7.3.6.2.6 pET28a(+)(OmpA-mBDNF-$His_6$)

The mutated p16THCP(mBDNF-FL-434D) described in Section 7.3.6.2.5 was used as a template for PCR and mBDNF was amplified out by Pfu PCR using primers BamHI-FL-mBDNF-Fwd and mBDNF-FL-$His_6$-HindIII-Rev. This was spin column purified and digested at the *BamHI* and *HindIII* sites. Cultures of DH5α pET28a(+)(OmpA-βNGF-$His_6$) were prepared and harvested. The plasmids were digested at their *BamHI* and *HindIII* sites, treated with rSAP to prevent vector religation and purified by gel electrophoresis. The digested and purified to produce and purified insert and vector were ligated and chemically transformed into DH5α cells. These were grown overnight on agar plates containing kanamycin to select for successful transformation. Colonies were picked and colony PCR (GoTaq, βNGF-Ex-FL and $His_6$-Rev) was used to select *E. coli* bearing the correct vector. These were cultured and the plasmids harvested and sequence verified using the $His_6$-Rev primer.

pET28a(+)(mBDNF-$His_6$) was chemically transformed into expression cell lines as needed.

# Chapter 8: Appendices

## 8.1 Bacterial Strains and Plasmids

*SNS118*, *DH5α, DH5αPir+* and pTHCP16, were kindly provided by Benkovic, S at Pennsylvania State University. pARCBD*Npu* was developed in-house from pARCBD also provided by Benkovic, S at Pennsylvania State University. pAH68 and pAH69 were obtained from the Coli Generic Stock Centre, Yale University. pEX-A2 was purchased from Eurofins MWG.

***Table 20: E. coli cell lines used in this research.***

| E. coli Strain | Genotype |
|---|---|
| BL21 DE3 | F– ompT gal dcm lon hsdSB(rB–mB–) λ(DE3 [lacI lacUV5-T7p07 ind1 sam7 nin5]) [malB+]K-12(λS) |
| DH5α | F– Φ80lacZΔM15 Δ(lacZYA-argF) U169 recA1 endA1 hsdR17 (rK–, mK+) phoA supE44 λ– thi-1 gyrA96 relA1 |
| DH5αPir+ | F– endA1 glnV44 thi-1 recA relA1 gyrA96 deoR nupG purB20 φ80dlacZΔM15Δ(lacZYA-argF)U169, hsdR17(rK–mK+), λ– |
| K12 ER2738 | F´proA+B+ lacIq Δ(lacZ)M15 zzf::Tn10(TetR)/ fhuA2 glnV Δ(lac-proAB) thi-1 Δ(hsdS-mcrB)5 |
| SNS118 | F-, Δ(araD-araB)567, ΔlacZ4787(::rrnB-3), λ-, Δ(araH-araF)570(::FRT), ΔaraEp-532::FRT, φPcp13araE534, Δ(rhaD-rhaB)568, hsdR514,ΔhisB 434 434 |
| SNS126 | F-, Δ(araD-araB)567, ΔlacZ4787(::rrnB-3), λ-, Δ(araH-araF)570(::FRT), ΔaraEp-532::FRT, φPcp13araE534, Δ(rhaD-rhaB)568, hsdR514,ΔhisB 434P22 |

## 8.2 Primer Table

***Table 21: Table of ssDNA primers used in this research.***

| | |
|---|---|
| 5AF | GCATTTTTGTCCATAAGATTAGC |
| 5AR | CATGTTTGACAGCTTATCATCG |
| BD-CT-F | GTTGTTCATATGCACTCTGACCCGGCTCGTCG |
| BD-CT-434-R | AAGAAGGAGCTCTTAAGAACCGTCAACTTTGA |
| BD-BamHI-434 | GTTGTTGGATCCTCTATCTCTTCTCGTGTTAA |
| BD-Rev | TTGTTGGAGCTCTTAACGGCCACGTTT |
| BD-NdeI-434 | GTTGTTCATATGCTGGGCGGCGGCGGCTCTGG |
| BD-TrD30-F | GTTGTTGGATCCGACATGTCTGGCGGCACGGTC |
| BD-TrV38-F | GTTGTTGGATCCGTGCTGGAAAAAGTCCCTGTT |
| BD-TrV44-F | GTTGTTGGATCCGTTTCCAAAGGCCAACTGAAA |
| C-mBDNF-F | GTTCTTCATATGCATAGTGATCCGGCACGTCG |
| C-mBDNF-R | GTTCTTGGATCCTTAACGGCCACGTTTAATGG |
| M13-49 | GAGCGGATAACAATTTCACACAGG |
| P1 | GGAATCAATGCCTGAGTG |
| P2 | ACTTAACGGCTGACATGG |
| P3 | ACGAGTATCGAGATGGCA |
| P4 | GGCATCAACAGCACATTC |
| SEQ1R | AAGTTGGGTAACGCCAGGGTT |
| T7F | TAATACGACTCACTATAGGG |
| T7R | GCTAGTTATTGCTCAGCGG |

## 8.3 Protein Sequences Table

***Table 22: Protein sequences created for this research.***

| Protein Designation | Amino Acid Sequence |
|---|---|
| 434-mBDNF | MSISSRVKSKRIQLGLNQAELAQKVGTTQQSIEQLENGKTK<br>RPRFLPELASALGVSVDWLLNGTSDSNVRFVGHVEPKGKY<br>PLISMVRAGSWCEACEPYDIKVDGSHSDPARRGELSVCDSI<br>SEWVTAADKKTAVDMSGGTVTVLEKVPVSKGQLKQYFY<br>ETKCNPMGYTKEGCRGIDKRHWNSQCRTTQSYVRALTMD<br>SKKRIGWRFIRIDTSCVCTLTIKRGR* |
| 434-mBDNF-TrD30 | MSISSRVKSKRIQLGLNQAELAQKVGTTQQSIEQLENGKTK<br>RPRFLPELASALGVSVDWLLNGTSDSNVRFVGHVEPKGKY<br>PLISMVRAGSWCEACEPYDIKVDGSDMSGGTVTVLEKVPV<br>SKGQLKQYFYETKCNPMGYTKEGCRGIDKRHWNSQCRTT<br>QSYVRALTMDSKKRIGWRFIRIDTSCVCTLTIKRGR* |
| 434-mBDNF-TrV38 | MSISSRVKSKRIQLGLNQAELAQKVGTTQQSIEQLENGKTK<br>RPRFLPELASALGVSVDWLLNGTSDSNVRFVGHVEPKGKY<br>PLISMVRAGSWCEACEPYDIKVDGSVLEKVPVSKGQLKQY<br>FYETKCNPMGYTKEGCRGIDKRHWNSQCRTTQSYVRALT<br>MDSKKRIGWRFIRIDTSCVCTLTIKRGR* |
| 434-mBDNF-TrV44 | MSISSRVKSKRIQLGLNQAELAQKVGTTQQSIEQLENGKTK<br>RPRFLPELASALGVSVDWLLNGTSDSNVRFVGHVEPKGKY<br>PLISMVRAGSWCEACEPYDIKVDGSVSKGQLKQYFYETKC<br>NPMGYTKEGCRGIDKRHWNSQCRTTQSYVRALTMDSKK<br>RIGWRFIRIDTSCVCTLTIKRGR* |
| mBDNF-FL-434 | MHSDPARRGELSVCDSISEWVTAADKKTAVDMSGGTVTV<br>LEKVPVSKGQLKQYFYETKCNPMGYTKEGCRGIDKRHWN<br>SQCRTTQSYVRALTMDSKKRIGWRFIRIDTSCVCTLTIKRG<br>RGSLGGGGSGGGGSGGGGSAAASISSRVKSKRIQLGLNQA<br>ELAQKVGTTQQSIEQLENGKTKRPRFLPELASALGVSVDW<br>LLNGTSDSNVRFVGHVEPKGKYPLISMVRAGSWCEACEPY<br>DIKVDGS* |
| mBDNF-FL-434D | MHSDPARRGELSVCDSISEWVTAADKKTAVDMSGGTVTV<br>LEKVPVSKGQLKQYFYETKCNPMGYTKEGCRGIDKRHWN<br>SQCRTTQSYVRALTMDSKKRIGWRFIRIDTSCVCTLTIKRG<br>RGSLGGGGSGGGGSGGGGSAAASISSRVKSKRIQLGLNQA<br>ELAQKVGTTQQSIEQLENGKTKRPRFLPELASALGVSVDW<br>LLNGTSDSN* |
| OmpA-mβNGF-FL-His6 | MKKTAIALAVALAGFATVAQAGSKGGGGSAAASSSHPIFH<br>RGEFSVCDSVSVWVGDKTTATDIKGKEVMVLGEVNINNS<br>VFKQYFFETKCRDPNPVDSGCRGIDSKHWNSYCTTTHTFV<br>KALTMDGKQAAWRFIRIDTACVCVLSRKAVRRGSKGGGG<br>SAAAHHHHHH* |

Protein Designation | Amino Acid Sequence

| | |
|---|---|
| OmpA-mBDNF-FL-His6 | MKKTAIALAVALAGFATVAQAGSKGGGGSAAAHSDPARR<br>GELSVCDSISEWVTAADKKTAVDMSGGTVTVLEKVPVSK<br>GQLKQYFYETKCNPMGYTKEGCRGIDKRHWNSQCRTTQS<br>YVRALTMDSKKRIGWRFIRIDTSCVCTLTIKRGRGSKGGG<br>GSAAAHHHHHH* |
| His6-TCS-FLAG-FL-TrkA-D5 | MGSSHHHHHHSSGLVPRGSHMASDYKDDDDKGSKGGGG<br>SAAAVQVNVSFPASVQLHTAVEMHHWCIPFSVDGQPAPS<br>LRWLFNGSVLNETSFIFTEFLEPAANETVRHGCLRLNQPTH<br>VNNGNYTLLAANPFGQASASIMAAFMDNPFEFN* |
| His6-TCS-FLAG-FL-TrkB-D5 | MGSSHHHHHHSSGLVPRGSHMASDYKDDDDKGSKGGGG<br>SAAAVHFAPTITFLESPTSDHHWCIPFTVKGNPKPALQWFY<br>NGAILNESKYICTKIHVTNHTEYHGCLQLDNPTHMNNGDY<br>TLIAKNEYGKDEKQISAHFMGWPGID* |
| mBDNF-FL-His6 | MHSDPARRGELSVCDSISEWVTAADKKTAVDMSGGTVTV<br>LEKVPVSKGQLKQYFYETKCNPMGYTKEGCRGIDKRHWN<br>SQCRTTQSYVRALTMDSKKRIGWRFIRIDTSCVCTLTIKRG<br>RGSKGGGGSAAAHHHHHH* |
| mβNGF-FL-His6 | MSSSHPIFHRGEFSVCDSVSVWVGDKTTATDIKGKEVMVL<br>GEVNINNSVFKQYFFETKCRDPNPVDSGCRGIDSKHWNSY<br>CTTTHTFVKALTMDGKQAAWRFIRIDTACVCVLSRKAVR<br>RGSKGGGGSAAAHHHHHH* |

# Chapter 9: References


1. Fayaz, A.; Croft, P.; Langford, R. M.; Donaldson, L. J.; Jones, G. T., Prevalence of chronic pain in the UK: a systematic review and meta-analysis of population studies. *BMJ Open* **2016,** *6* (6), e010364.

2. Breivik, H.; Collett, B.; Ventafridda, V.; Cohen, R.; Gallacher, D., Survey of chronic pain in Europe: prevalence, impact on daily life, and treatment. *Eur. J. Pain* **2006,** *10* (4), 287-333.

3. Kan, S. L.; Li, Y.; Ning, G. Z.; Yuan, Z. F.; Chen, L. X.; Bi, M. C.; Sun, J. C.; Feng, S. Q., Tanezumab for Patients with Osteoarthritis of the Knee: A Meta-Analysis. *PLoS One* **2016,** *11* (6), e0157105.

4. Brown, M. T.; Murphy, F. T.; Radin, D. M.; Davignon, I.; Smith, M. D.; West, C. R., Tanezumab reduces osteoarthritic hip pain: results of a randomized, double-blind, placebo-controlled phase III trial. *Arthritis Rheum.* **2013,** *65* (7), 1795-803.

5. Maniadakis, N.; Gray, A., The economic burden of back pain in the UK. *Pain* **2000,** *84* (1), 95-103.

6. Phillips, C. J., The Cost and Burden of Chronic Pain. *Rev Pain* **2009,** *3* (1), 2-5.

7. Young, A.; Dixey, J.; Kulinskaya, E.; Cox, N.; Davies, P.; Devlin, J.; Emery, P.; Gough, A.; James, D.; Prouse, P.; Williams, P.; Winfield, J., Which patients stop working because of rheumatoid arthritis? Results of five years' follow up in 732 patients from the Early RA Study (ERAS). *Ann. Rheum. Dis.* **2002,** *61* (4), 335.

8. Mardy, S.; Miura, Y.; Endo, F.; Matsuda, I.; Indo, Y., Congenital insensitivity to pain with anhidrosis (CIPA): effect of TRKA (NTRK1) missense mutations on autophosphorylation of the receptor tyrosine kinase for nerve growth factor. *Hum. Mol. Genet.* **2001,** *10* (3), 179-88.

9. Udayashankar, C.; Oudeacoumar, P.; Nath, A. K., Congenital insensitivity to pain and anhidrosis: a case report from South India. *Indian J. Dermatol.* **2012,** *57* (6), 503.

10. Safari, A.; Khaledi, A. A.; Vojdani, M., Congenital Insensitivity to Pain with Anhidrosis (CIPA): A Case Report. *Iran Red Crescent Med J* **2011,** *13* (2), 134-8.

11. Merighi, A.; Salio, C.; Ghirri, A.; Lossi, L.; Ferrini, F.; Betelli, C.; Bardoni, R., BDNF as a pain modulator. *Prog. Neurobiol.* **2008,** *85* (3), 297-317.

12. Pezet, S.; McMahon, S. B., Neurotrophins: mediators and modulators of pain. *Annu. Rev. Neurosci.* **2006,** *29*, 507-38.

13. Melemedjian, O. K.; Tillu, D. V.; Asiedu, M. N.; Mandell, E. K.; Moy, J. K.; Blute, V. M.; Taylor, C. J.; Ghosh, S.; Price, T. J., BDNF regulates atypical PKC at spinal synapses to initiate and maintain a centralized chronic pain state. *Mol. Pain* **2013,** *9*, 12.

14. Coull, J. A.; Beggs, S.; Boudreau, D.; Boivin, D.; Tsuda, M.; Inoue, K.; Gravel, C.; Salter, M. W.; De Koninck, Y., BDNF from microglia causes the shift in neuronal anion gradient underlying neuropathic pain. *Nature* **2005,** *438* (7070), 1017-21.

15. Kerr, B. J.; Bradbury, E. J.; Bennett, D. L.; Trivedi, P. M.; Dassan, P.; French, J.; Shelton, D. B.; McMahon, S. B.; Thompson, S. W., Brain-derived neurotrophic factor modulates nociceptive sensory inputs and NMDA-evoked responses in the rat spinal cord. *J. Neurosci.* **1999,** *19* (12), 5138-48.

16. Matayoshi, S.; Jiang, N.; Katafuchi, T.; Koga, K.; Furue, H.; Yasaka, T.; Nakatsuka, T.; Zhou, X. F.; Kawasaki, Y.; Tanaka, N.; Yoshimura, M., Actions of brain-derived neurotrophic factor on spinal nociceptive transmission during inflammation in the rat. *J. Physiol.* **2005,** *569* (Pt 2), 685-95.

17. Ghilardi, J. R.; Freeman, K. T.; Jimenez-Andrade, J. M.; Mantyh, W. G.; Bloom, A. P.; Bouhana, K. S.; Trollinger, D.; Winkler, J.; Lee, P.; Andrews, S. W.; Kuskowski, M. A.; Mantyh, P. W., Sustained blockade of neurotrophin receptors TrkA, TrkB and TrkC reduces non-malignant skeletal pain but not the maintenance of sensory and sympathetic nerve fibers. *Bone* **2011,** *48* (2), 389-98.

18. La Porte, S. L.; Eigenbrot, C.; Ultsch, M.; Ho, W. H.; Foletti, D.; Forgie, A.; Lindquist, K. C.; Shelton, D. L.; Pons, J., Generation of a high-fidelity antibody

against nerve growth factor using library scanning mutagenesis and validation with structures of the initial and optimized Fab-antigen complexes. *MAbs* **2014,** *6* (4), 1059-68.

19. Katz, N.; Borenstein, D. G.; Birbara, C.; Bramson, C.; Nemeth, M. A.; Smith, M. D.; Brown, M. T., Efficacy and safety of tanezumab in the treatment of chronic low back pain. *Pain* **2011,** *152* (10), 2248-58.

20. Lipinski, C. A.; Lombardo, F.; Dominy, B. W.; Feeney, P. J., Experimental and computational approaches to estimate solubility and permeability in drug discovery and development settings. *Adv Drug Deliv Rev* **2001,** *46* (1-3), 3-26.

21. Dubin, A. E.; Patapoutian, A., Nociceptors: the sensors of the pain pathway. *J. Clin. Invest.* **2010,** *120* (11), 3760-72.

22. Zeng, Y.; Liu, Y.; Wu, M.; Liu, J.; Hu, Q., Activation of TrkB by 7,8-dihydroxyflavone prevents fear memory defects and facilitates amygdalar synaptic plasticity in aging. *J. Alzheimers Dis.* **2012,** *31* (4), 765-78.

23. Jang, S. W.; Liu, X.; Chan, C. B.; France, S. A.; Sayeed, I.; Tang, W.; Lin, X.; Xiao, G.; Andero, R.; Chang, Q.; Ressler, K. J.; Ye, K., Deoxygedunin, a natural product with potent neurotrophic activity in mice. *PLoS One* **2010,** *5* (7), e11528.

24. Zuccato, C.; Ciammola, A.; Rigamonti, D.; Leavitt, B. R.; Goffredo, D.; Conti, L.; MacDonald, M. E.; Friedlander, R. M.; Silani, V.; Hayden, M. R.; Timmusk, T.; Sipione, S.; Cattaneo, E., Loss of huntingtin-mediated BDNF gene transcription in Huntington's disease. *Science* **2001,** *293* (5529), 493-8.

25. Ivanov, A. D.; Tukhbatova, G. R.; Salozhin, S. V.; Markevich, V. A., βNGF but not BDNF overexpression protects hippocampal LTP from beta-amyloid-induced impairment. *Neuroscience* **2015,** *289*, 114-22.

26. Johnston, A. L.; Lun, X.; Rahn, J. J.; Liacini, A.; Wang, L.; Hamilton, M. G.; Parney, I. F.; Hempstead, B. L.; Robbins, S. M.; Forsyth, P. A.; Senger, D. L., The p75 neurotrophin receptor is a central regulator of glioma invasion. *PLoS Biol.* **2007,** *5* (8), e212.

27. Wang, X.; Cui, M.; Wang, L.; Chen, X.; Xin, P., Inhibition of neurotrophin receptor p75 intramembran proteolysis by gamma-secretase inhibitor reduces medulloblastoma spinal metastasis. *Biochem. Biophys. Res. Commun.* **2010,** *403* (3-4), 264-9.

28. Kawamura, N.; Kawamura, K.; Manabe, M.; Tanaka, T., Inhibition of brain-derived neurotrophic factor/tyrosine kinase B signaling suppresses choriocarcinoma cell growth. *Endocrinology* **2010,** *151* (7), 3006-14.

29. Kawamura, K.; Kawamura, N.; Okamoto, N.; Manabe, M., Suppression of choriocarcinoma invasion and metastasis following blockade of BDNF/TrkB signaling. *Cancer Med* **2013,** *2* (6), 849-61.

30. Patani, N.; Jiang, W. G.; Mokbel, K., Brain-derived neurotrophic factor expression predicts adverse pathological & clinical outcomes in human breast cancer. *Cancer Cell Int.* **2011,** *11* (1), 23.

31. Vanhecke, E.; Adriaenssens, E.; Verbeke, S.; Meignan, S.; Germain, E.; Berteaux, N.; Nurcombe, V.; Le Bourhis, X.; Hondermarck, H., Brain-derived neurotrophic factor and neurotrophin-4/5 are expressed in breast cancer and can be targeted to inhibit tumor cell survival. *Clin. Cancer Res.* **2011,** *17* (7), 1741-52.

32. Yang, X.; Martin, T. A.; Jiang, W. G., Biological influence of brain-derived neurotrophic factor on breast cancer cells. *Int. J. Oncol.* **2012,** *41* (4), 1541-6.

33. Boyd, J. G.; Gordon, T., The neurotrophin receptors, trkB and p75, differentially regulate motor axonal regeneration. *J. Neurobiol.* **2001,** *49* (4), 314-25.

34. Wong, J., *Neurotrophin Signaling and Alzheimer's Disease Neurodegeneration − Focus on BDNF/TrkB Signaling*. InTech: 2013.

35. Ferrer, I.; Marin, C.; Rey, M. J.; Ribalta, T.; Goutan, E.; Blanco, R.; Tolosa, E.; Marti, E., BDNF and full-length and truncated TrkB expression in Alzheimer disease. Implications in therapeutic strategies. *J. Neuropathol. Exp. Neurol.* **1999,** *58* (7), 729-39.

36. Connor, B.; Young, D.; Lawlor, P.; Gai, W.; Waldvogel, H.; Faull, R. L.; Dragunow, M., Trk receptor alterations in Alzheimer's disease. *Brain Res. Mol. Brain Res.* **1996,** *42* (1), 1-17.

37. Dorsey, S. G.; Renn, C. L.; Carim-Todd, L.; Barrick, C. A.; Bambrick, L.; Krueger, B. K.; Ward, C. W.; Tessarollo, L., In vivo restoration of physiological levels of truncated TrkB.T1 receptor rescues neuronal cell death in a trisomic mouse model. *Neuron* **2006,** *51* (1), 21-8.

38. Troca-Marin, J. A.; Alves-Sampaio, A.; Montesinos, M. L., An increase in basal BDNF provokes hyperactivation of the Akt-mammalian target of rapamycin pathway and deregulation of local dendritic translation in a mouse model of Down's syndrome. *J. Neurosci.* **2011,** *31* (26), 9445-55.

39. Binder, D. K.; Routbort, M. J.; Ryan, T. E.; Yancopoulos, G. D.; McNamara, J. O., Selective inhibition of kindling development by intraventricular administration of TrkB receptor body. *J. Neurosci.* **1999,** *19* (4), 1424-36.

40. He, X. P.; Kotloski, R.; Nef, S.; Luikart, B. W.; Parada, L. F.; McNamara, J. O., Conditional deletion of TrkB but not BDNF prevents epileptogenesis in the kindling model. *Neuron* **2004,** *43* (1), 31-42.

41. Gines, S.; Paoletti, P.; Alberch, J., Impaired TrkB-mediated ERK1/2 activation in huntington disease knock-in striatal cells involves reduced p52/p46 Shc expression. *J. Biol. Chem.* **2010,** *285* (28), 21537-48.

42. Baydyuk, M.; Nguyen, M. T.; Xu, B., Chronic deprivation of TrkB signaling leads to selective late-onset nigrostriatal dopaminergic degeneration. *Exp. Neurol.* **2011,** *228* (1), 118-25.

43. Howells, D. W.; Porritt, M. J.; Wong, J. Y.; Batchelor, P. E.; Kalnins, R.; Hughes, A. J.; Donnan, G. A., Reduced BDNF mRNA expression in the Parkinson's disease substantia nigra. *Exp. Neurol.* **2000,** *166* (1), 127-35.

44. Cazorla, M.; Premont, J.; Mann, A.; Girard, N.; Kellendonk, C.; Rognan, D., Identification of a low-molecular weight TrkB antagonist with anxiolytic and antidepressant activity in mice. *J. Clin. Invest.* **2011,** *121* (5), 1846-57.

45. Montag, C.; Basten, U.; Stelzel, C.; Fiebach, C. J.; Reuter, M., The BDNF Val66Met polymorphism and anxiety: support for animal knock-in studies from a genetic association study in humans. *Psychiatry Res.* **2010,** *179* (1), 86-90.

46. Ribases, M.; Gratacos, M.; Fernandez-Aranda, F.; Bellodi, L.; Boni, C.; Anderluh, M.; Cavallini, M. C.; Cellini, E.; Di Bella, D.; Erzegovesi, S.; Foulon, C.; Gabrovsek, M.; Gorwood, P.; Hebebrand, J.; Hinney, A.; Holliday, J.; Hu, X.; Karwautz, A.; Kipman, A.; Komel, R.; Nacmias, B.; Remschmidt, H.; Ricca, V.; Sorbi, S.; Wagner, G.; Treasure, J.; Collier, D. A.; Estivill, X., Association of BDNF with anorexia, bulimia and age of onset of weight loss in six European populations. *Hum. Mol. Genet.* **2004,** *13* (12), 1205-12.

47. Lessmann, V.; Gottmann, K.; Malcangio, M., Neurotrophin secretion: current facts and future prospects. *Prog. Neurobiol.* **2003,** *69* (5), 341-74.

48. Longo, F. M.; Massa, S. M., Small-molecule modulation of neurotrophin receptors: a strategy for the treatment of neurological disease. *Nat. Rev. Drug Discov.* **2013,** *12* (7), 507-25.

49. Wiesmann, C.; Ultsch, M. H.; Bass, S. H.; de Vos, A. M., Crystal structure of nerve growth factor in complex with the ligand-binding domain of the TrkA receptor. *Nature* **1999,** *401* (6749), 184-8.

50. Robinson, R. C.; Radziejewski, C.; Stuart, D. I.; Jones, E. Y., Structure of the brain-derived neurotrophic factor/neurotrophin 3 heterodimer. *Biochemistry* **1995,** *34* (13), 4139-46.

51. Robinson, R. C.; Radziejewski, C.; Spraggon, G.; Greenwald, J.; Kostura, M. R.; Burtnick, L. D.; Stuart, D. I.; Choe, S.; Jones, E. Y., The structures of the neurotrophin 4 homodimer and the brain-derived neurotrophic factor/neurotrophin 4 heterodimer reveal a common Trk-binding site. *Protein Sci.* **1999,** *8* (12), 2589-97.

52. Gong, Y.; Cao, P.; Yu, H. J.; Jiang, T., Crystal structure of the neurotrophin-3 and p75NTR symmetrical complex. *Nature* **2008,** *454* (7205), 789-93.

53. Borsani, G.; Pizzuti, A.; Rugarli, E. I.; Falini, A.; Silani, V.; Sidoli, A.; Scarlato, G.; Baralle, F. E., cDNA sequence of human beta-NGF. *Nucleic Acids Res.* **1990,** *18* (13), 4020.

54. Jones, K. R.; Reichardt, L. F., Molecular cloning of a human gene that is a member of the nerve growth factor family. *Proc. Natl. Acad. Sci. U. S. A.* **1990,** *87* (20), 8060-4.

55. Berkemeier, L. R.; Winslow, J. W.; Kaplan, D. R.; Nikolics, K.; Goeddel, D. V.; Rosenthal, A., Neurotrophin-5: a novel neurotrophic factor that activates trk and trkB. *Neuron* **1991,** *7* (5), 857-66.

56. Arakawa, T.; Haniu, M.; Narhi, L. O.; Miller, J. A.; Talvenheimo, J.; Philo, J. S.; Chute, H. T.; Matheson, C.; Carnahan, J.; Louis, J. C.; et al., Formation of heterodimers from three neurotrophins, nerve growth factor, neurotrophin-3, and brain-derived neurotrophic factor. *J. Biol. Chem.* **1994,** *269* (45), 27833-9.

57. Lin, L. F.; Doherty, D. H.; Lile, J. D.; Bektesh, S.; Collins, F., GDNF: a glial cell line-derived neurotrophic factor for midbrain dopaminergic neurons. *Science* **1993,** *260* (5111), 1130-2.

58. Lam, A.; Fuller, F.; Miller, J.; Kloss, J.; Manthorpe, M.; Varon, S.; Cordell, B., Sequence and structural organization of the human gene encoding ciliary neurotrophic factor. *Gene* **1991,** *102* (2), 271-6.

59. Parkash, V.; Goldman, A., Comparison of GFL-GFRalpha complexes: further evidence relating GFL bend angle to RET signalling. *Acta Crystallogr. Sect. F Struct. Biol. Cryst. Commun.* **2009,** *65* (Pt 6), 551-8.

60. Silvian, L.; Jin, P.; Carmillo, P.; Boriack-Sjodin, P. A.; Pelletier, C.; Rushe, M.; Gong, B.; Sah, D.; Pepinsky, B.; Rossomando, A., Artemin crystal structure reveals insights into heparan sulfate binding. *Biochemistry* **2006,** *45* (22), 6801-12.

61. McDonald, N. Q.; Panayotatos, N.; Hendrickson, W. A., Crystal structure of dimeric human ciliary neurotrophic factor determined by MAD phasing. *EMBO J.* **1995,** *14* (12), 2689-99.

62. Mizui, T.; Ishikawa, Y.; Kumanogoh, H.; Kojima, M., Neurobiological actions by three distinct subtypes of brain-derived neurotrophic factor: Multi-ligand model of growth factor signaling. *Pharmacol. Res.* **2016,** *105*, 93-8.

63. Halban, P. A.; Irminger, J. C., Sorting and processing of secretory proteins. *Biochem. J* **1994,** *299 ( Pt 1)*, 1-18.

64. Khatib, A. M.; Siegfried, G.; Chretien, M.; Metrakos, P.; Seidah, N. G., Proprotein convertases in tumor progression and malignancy: novel targets in cancer therapy. *Am. J. Pathol.* **2002,** *160* (6), 1921-35.

65. Pang, P. T.; Teng, H. K.; Zaitsev, E.; Woo, N. T.; Sakata, K.; Zhen, S.; Teng, K. K.; Yung, W. H.; Hempstead, B. L.; Lu, B., Cleavage of proBDNF by tPA/plasmin is essential for long-term hippocampal plasticity. *Science* **2004,** *306* (5695), 487-91.

66. Nagappan, G.; Zaitsev, E.; Senatorov, V. V., Jr.; Yang, J.; Hempstead, B. L.; Lu, B., Control of extracellular cleavage of ProBDNF by high frequency neuronal activity. *Proc. Natl. Acad. Sci. U. S. A.* **2009,** *106* (4), 1267-72.

67. Bradshaw, R. A.; Pundavela, J.; Biarc, J.; Chalkley, R. J.; Burlingame, A. L.; Hondermarck, H., βNGF and ProNGF: Regulation of neuronal and neoplastic responses through receptor signaling. *Adv Biol Regul* **2015,** *58*, 16-27.

68. Casaccia-Bonnefil, P.; Carter, B. D.; Dobrowsky, R. T.; Chao, M. V., Death of oligodendrocytes mediated by the interaction of nerve growth factor with its receptor p75. *Nature* **1996,** *383* (6602), 716-9.

69. Vaegter, C. B.; Jansen, P.; Fjorback, A. W.; Glerup, S.; Skeldal, S.; Kjolby, M.; Richner, M.; Erdmann, B.; Nyengaard, J. R.; Tessarollo, L.; Lewin, G. R.; Willnow, T. E.; Chao, M. V.; Nykjaer, A., Sortilin associates with Trk receptors to enhance anterograde transport and neurotrophin signaling. *Nat. Neurosci.* **2011,** *14* (1), 54-61.

70. Teng, H. K.; Teng, K. K.; Lee, R.; Wright, S.; Tevar, S.; Almeida, R. D.; Kermani, P.; Torkin, R.; Chen, Z. Y.; Lee, F. S.; Kraemer, R. T.; Nykjaer, A.; Hempstead, B.

L., ProBDNF induces neuronal apoptosis via activation of a receptor complex of p75NTR and sortilin. *J. Neurosci.* **2005,** *25* (22), 5455-63.

71. Koshimizu, H.; Hazama, S.; Hara, T.; Ogura, A.; Kojima, M., Distinct signaling pathways of precursor BDNF and mature BDNF in cultured cerebellar granule neurons. *Neurosci. Lett.* **2010,** *473* (3), 229-32.

72. Egashira, Y.; Tanaka, T.; Soni, P.; Sakuragi, S.; Tominaga-Yoshino, K.; Ogura, A., Involvement of the p75(NTR) signaling pathway in persistent synaptic suppression coupled with synapse elimination following repeated long-term depression induction. *J. Neurosci. Res.* **2010,** *88* (16), 3433-46.

73. Woo, N. H.; Teng, H. K.; Siao, C. J.; Chiaruttini, C.; Pang, P. T.; Milner, T. A.; Hempstead, B. L.; Lu, B., Activation of p75NTR by proBDNF facilitates hippocampal long-term depression. *Nat. Neurosci.* **2005,** *8* (8), 1069-77.

74. Jeanneteau, F.; Deinhardt, K.; Miyoshi, G.; Bennett, A. M.; Chao, M. V., The MAP kinase phosphatase MKP-1 regulates BDNF-induced axon branching. *Nat. Neurosci.* **2010,** *13* (11), 1373-9.

75. Roux, P. P.; Bhakar, A. L.; Kennedy, T. E.; Barker, P. A., The p75 neurotrophin receptor activates Akt (protein kinase B) through a phosphatidylinositol 3-kinase-dependent pathway. *J. Biol. Chem.* **2001,** *276* (25), 23097-104.

76. Le Moan, N.; Houslay, D. M.; Christian, F.; Houslay, M. D.; Akassoglou, K., Oxygen-dependent cleavage of the p75 neurotrophin receptor triggers stabilization of HIF-1alpha. *Mol. Cell* **2011,** *44* (3), 476-90.

77. Forsyth, P. A.; Krishna, N.; Lawn, S.; Valadez, J. G.; Qu, X.; Fenstermacher, D. A.; Fournier, M.; Potthast, L.; Chinnaiyan, P.; Gibney, G. T.; Zeinieh, M.; Barker, P. A.; Carter, B. D.; Cooper, M. K.; Kenchappa, R. S., p75 neurotrophin receptor cleavage by alpha- and gamma-secretases is required for neurotrophin-mediated proliferation of brain tumor-initiating cells. *J. Biol. Chem.* **2014,** *289* (12), 8067-85.

78. Yamashita, T.; Tucker, K. L.; Barde, Y. A., Neurotrophin binding to the p75 receptor modulates Rho activity and axonal outgrowth. *Neuron* **1999,** *24* (3), 585-93.

79. Sachs, B. D.; Baillie, G. S.; McCall, J. R.; Passino, M. A.; Schachtrup, C.; Wallace, D. A.; Dunlop, A. J.; MacKenzie, K. F.; Klussmann, E.; Lynch, M. J.; Sikorski, S. L.; Nuriel, T.; Tsigelny, I.; Zhang, J.; Houslay, M. D.; Chao, M. V.; Akassoglou, K., p75 neurotrophin receptor regulates tissue fibrosis through inhibition of plasminogen activation via a PDE4/cAMP/PKA pathway. *J. Cell Biol.* **2007,** *177* (6), 1119-32.

80. Bonni, A.; Brunet, A.; West, A. E.; Datta, S. R.; Takasu, M. A.; Greenberg, M. E., Cell survival promoted by the Ras-MAPK signaling pathway by transcription-dependent and -independent mechanisms. *Science* **1999,** *286* (5443), 1358-62.

81. Volonte, C.; Angelastro, J. M.; Greene, L. A., Association of protein kinases ERK1 and ERK2 with p75 nerve growth factor receptors. *J. Biol. Chem.* **1993,** *268* (28), 21410-5.

82. Alonso, M.; Medina, J. H.; Pozzo-Miller, L., ERK1/2 activation is necessary for BDNF to increase dendritic spine density in hippocampal CA1 pyramidal neurons. *Learn. Mem.* **2004,** *11* (2), 172-8.

83. Medina, D. L.; Sciarretta, C.; Calella, A. M.; Von Bohlen Und Halbach, O.; Unsicker, K.; Minichiello, L., TrkB regulates neocortex formation through the Shc/PLCgamma-mediated control of neuronal migration. *EMBO J.* **2004,** *23* (19), 3803-14.

84. Numakawa, T.; Kumamaru, E.; Adachi, N.; Yagasaki, Y.; Izumi, A.; Kunugi, H., Glucocorticoid receptor interaction with TrkB promotes BDNF-triggered PLC-gamma signaling for glutamate release via a glutamate transporter. *Proc. Natl. Acad. Sci. U. S. A.* **2009,** *106* (2), 647-52.

85. Caldeira, M. V.; Melo, C. V.; Pereira, D. B.; Carvalho, R.; Correia, S. S.; Backos, D. S.; Carvalho, A. L.; Esteban, J. A.; Duarte, C. B., Brain-derived neurotrophic factor regulates the expression and synaptic delivery of alpha-amino-3-hydroxy-5-methyl-4-isoxazole propionic acid receptor subunits in hippocampal neurons. *J. Biol. Chem.* **2007,** *282* (17), 12619-28.

86. Caldeira, M. V.; Melo, C. V.; Pereira, D. B.; Carvalho, R. F.; Carvalho, A. L.; Duarte, C. B., BDNF regulates the expression and traffic of NMDA receptors in cultured hippocampal neurons. *Mol. Cell. Neurosci.* **2007,** *35* (2), 208-19.

87. Eide, F. F.; Vining, E. R.; Eide, B. L.; Zang, K.; Wang, X. Y.; Reichardt, L. F., Naturally occurring truncated trkB receptors have dominant inhibitory effects on brain-derived neurotrophic factor signaling. *J. Neurosci.* **1996,** *16* (10), 3123-9.

88. Volosin, M.; Trotter, C.; Cragnolini, A.; Kenchappa, R. S.; Light, M.; Hempstead, B. L.; Carter, B. D.; Friedman, W. J., Induction of proneurotrophins and activation of p75NTR-mediated apoptosis via neurotrophin receptor-interacting factor in hippocampal neurons after seizures. *J. Neurosci.* **2008,** *28* (39), 9870-9.

89. Com, E.; Lagadec, C.; Page, A.; El Yazidi-Belkoura, I.; Slomianny, C.; Spencer, A.; Hammache, D.; Rudkin, B. B.; Hondermarck, H., Nerve growth factor receptor TrkA signaling in breast cancer cells involves Ku70 to prevent apoptosis. *Mol. Cell. Proteomics* **2007,** *6* (11), 1842-54.

90. Lagadec, C.; Romon, R.; Tastet, C.; Meignan, S.; Com, E.; Page, A.; Bidaux, G.; Hondermarck, H.; Le Bourhis, X., Ku86 is important for TrkA overexpression-induced breast cancer cell invasion. *Proteomics Clin. Appl.* **2010,** *4* (6-7), 580-90.

91. Sofroniew, M. V.; Howe, C. L.; Mobley, W. C., Nerve growth factor signaling, neuroprotection, and neural repair. *Annu. Rev. Neurosci.* **2001,** *24*, 1217-81.

92. Schramm, A.; Schulte, J. H.; Astrahantseff, K.; Apostolov, O.; Limpt, V.; Sieverts, H.; Kuhfittig-Kulle, S.; Pfeiffer, P.; Versteeg, R.; Eggert, A., Biological effects of TrkA and TrkB receptor signaling in neuroblastoma. *Cancer Lett.* **2005,** *228* (1-2), 143-53.

93. Sobottka, B.; Reinhardt, D.; Brockhaus, M.; Jacobsen, H.; Metzger, F., ProNGF inhibits βNGF-mediated TrkA activation in PC12 cells. *J. Neurochem.* **2008,** *107* (5), 1294-303.

94. Schor, N. F., The p75 neurotrophin receptor in human development and disease. *Prog. Neurobiol.* **2005,** *77* (3), 201-14.

95. Negrini, S.; D'Alessandro, R.; Meldolesi, J., βNGF signaling in PC12 cells: the cooperation of p75(NTR) with TrkA is needed for the activation of both mTORC2 and the PI3K signalling cascade. *Biol Open* **2013,** *2* (8), 855-66.

96. Poduslo, J. F.; Curran, G. L., Permeability at the blood-brain and blood-nerve barriers of the neurotrophic factors: βNGF, CNTF, NT-3, BDNF. *Mol. Brain Res.* **1996,** *36* (2), 280-286.

97. Lu, B.; Nagappan, G.; Guan, X.; Nathan, P. J.; Wren, P., BDNF-based synaptic repair as a disease-modifying strategy for neurodegenerative diseases. *Nat. Rev. Neurosci.* **2013,** *14* (6), 401-16.

98. Sanga, P.; Polverejan, E.; Wang, S.; Kelly, K. M.; Thipphawong, J., Efficacy, Safety, and Tolerability of Fulranumab as an Adjunctive Therapy in Patients With Inadequately Controlled, Moderate-to-Severe Chronic Low Back Pain: A Randomized, Double-blind, Placebo-controlled, Dose-ranging, Dose-loading Phase II Study. *Clin. Ther.* **2016,** *38* (6), 1435-50.

99. Tiseo, P. J.; Ren, H.; Mellis, S., Fasinumab (REGN475), an antinerve growth factor monoclonal antibody, for the treatment of acute sciatic pain: results of a proof-of-concept study. *J. Pain Res.* **2014,** *7*, 523-30.

100. Chang, D. S.; Hsu, E.; Hottinger, D. G.; Cohen, S. P., Anti-nerve growth factor in pain management: current evidence. *J. Pain Res.* **2016,** *9*, 373-83.

101. Koren, E.; De Groot, A. S.; Jawa, V.; Beck, K. D.; Boone, T.; Rivera, D.; Li, L.; Mytych, D.; Koscec, M.; Weeraratne, D.; Swanson, S.; Martin, W., Clinical validation of the "in silico" prediction of immunogenicity of a human recombinant therapeutic protein. *Clin. Immunol.* **2007,** *124* (1), 26-32.

102. Suntharalingam, G.; Perry, M. R.; Ward, S.; Brett, S. J.; Castello-Cortes, A.; Brunner, M. D.; Panoskaltsis, N., Cytokine storm in a phase 1 trial of the anti-CD28 monoclonal antibody TGN1412. *N. Engl. J. Med.* **2006,** *355* (10), 1018-28.

103. Owolabi, J. B.; Rizkalla, G.; Tehim, A.; Ross, G. M.; Riopelle, R. J.; Kamboj, R.; Ossipov, M.; Bian, D.; Wegert, S.; Porreca, F.; Lee, D. K., Characterization of

antiallodynic actions of ALE-0540, a novel nerve growth factor receptor antagonist, in the rat. *J. Pharmacol. Exp. Ther.* **1999,** *289* (3), 1271-6.

104. Jang, S. W.; Liu, X.; Chan, C. B.; Weinshenker, D.; Hall, R. A.; Xiao, G.; Ye, K., Amitriptyline is a TrkA and TrkB receptor agonist that promotes TrkA/TrkB heterodimerization and has potent neurotrophic activity. *Chem. Biol.* **2009,** *16* (6), 644-56.

105. Zage, P. E.; Graham, T. C.; Zeng, L.; Fang, W.; Pien, C.; Thress, K.; Omer, C.; Brown, J. L.; Zweidler-McKay, P. A., The selective Trk inhibitor AZ623 inhibits brain-derived neurotrophic factor-mediated neuroblastoma cell proliferation and signaling and is synergistic with topotecan. *Cancer* **2011,** *117* (6), 1321-91.

106. Thress, K.; Macintyre, T.; Wang, H.; Whitston, D.; Liu, Z. Y.; Hoffmann, E.; Wang, T.; Brown, J. L.; Webster, K.; Omer, C.; Zage, P. E.; Zeng, L.; Zweidler-McKay, P. A., Identification and preclinical characterization of AZ-23, a novel, selective, and orally bioavailable inhibitor of the Trk kinase pathway. *Mol. Cancer Ther.* **2009,** *8* (7), 1818-27.

107. Constandil, L.; Goich, M.; Hernandez, A.; Bourgeais, L.; Cazorla, M.; Hamon, M.; Villanueva, L.; Pelissier, T., Cyclotraxin-B, a new TrkB antagonist, and glial blockade by propentofylline, equally prevent and reverse cold allodynia induced by BDNF or partial infraorbital nerve constriction in mice. *J. Pain* **2012,** *13* (6), 579-89.

108. Cazorla, M.; Jouvenceau, A.; Rose, C.; Guilloux, J. P.; Pilon, C.; Dranovsky, A.; Premont, J., Cyclotraxin-B, the first highly potent and selective TrkB inhibitor, has anxiolytic properties in mice. *PLoS One* **2010,** *5* (3), e9777.

109. Iyer, R.; Evans, A. E.; Qi, X.; Ho, R.; Minturn, J. E.; Zhao, H.; Balamuth, N.; Maris, J. M.; Brodeur, G. M., Lestaurtinib enhances the antitumor efficacy of chemotherapy in murine xenograft models of neuroblastoma. *Clin. Cancer Res.* **2010,** *16* (5), 1478-85.

110. Shabbir, M.; Stuart, R., Lestaurtinib, a multitargeted tyrosine kinase inhibitor: from bench to bedside. *Expert Opin Investig Drugs* **2010,** *19* (3), 427-36.

111. Simmons, D. A.; Belichenko, N. P.; Yang, T.; Condon, C.; Monbureau, M.; Shamloo, M.; Jing, D.; Massa, S. M.; Longo, F. M., A small molecule TrkB ligand reduces motor impairment and neuropathology in R6/2 and BACHD mouse models of Huntington's disease. *J. Neurosci.* **2013,** *33* (48), 18712-27.

112. Massa, S. M.; Yang, T.; Xie, Y.; Shi, J.; Bilgen, M.; Joyce, J. N.; Nehama, D.; Rajadas, J.; Longo, F. M., Small molecule BDNF mimetics activate TrkB signaling and prevent neuronal degeneration in rodents. *J. Clin. Invest.* **2010,** *120* (5), 1774-85.

113. Kajiya, M.; Takeshita, K.; Kittaka, M.; Matsuda, S.; Ouhara, K.; Takeda, K.; Takata, T.; Kitagawa, M.; Fujita, T.; Shiba, H.; Kurihara, H., BDNF mimetic compound LM22A-4 regulates cementoblast differentiation via the TrkB-ERK/Akt signaling cascade. *Int. Immunopharmacol.* **2014,** *19* (2), 245-52.

114. Covaceuszach, S.; Cattaneo, A.; Lamba, D., Neutralization of βNGF-TrkA receptor interaction by the novel antagonistic anti-TrkA monoclonal antibody MNAC13: a structural insight. *Proteins* **2005,** *58* (3), 717-27.

115. Ugolini, G.; Marinelli, S.; Covaceuszach, S.; Cattaneo, A.; Pavone, F., The function neutralizing anti-TrkA antibody MNAC13 reduces inflammatory and neuropathic pain. *Proc. Natl. Acad. Sci. U. S. A.* **2007,** *104* (8), 2985-90.

116. Eibl, J. K.; Chapelsky, S. A.; Ross, G. M., Multipotent neurotrophin antagonist targets brain-derived neurotrophic factor and nerve growth factor. *J. Pharmacol. Exp. Ther.* **2010,** *332* (2), 446-54.

117. Eibl, J. K.; Strasser, B. C.; Ross, G. M., Identification of novel pyrazoloquinazolinecarboxilate analogues to inhibit nerve growth factor in vitro. *Eur. J. Pharmacol.* **2013,** *708* (1-3), 30-7.

118. Aoki, C.; Wu, K.; Elste, A.; Len, G.; Lin, S.; McAuliffe, G.; Black, I. B., Localization of brain-derived neurotrophic factor and TrkB receptors to postsynaptic densities of adult rat cerebral cortex. *J. Neurosci. Res.* **2000,** *59* (3), 454-63.

119. Conner, J. M.; Lauterborn, J. C.; Yan, Q.; Gall, C. M.; Varon, S., Distribution of brain-derived neurotrophic factor (BDNF) protein and mRNA in the normal adult rat CNS: evidence for anterograde axonal transport. *J. Neurosci.* **1997,** *17* (7), 2295-313.

120. Horswill, A. R.; Savinov, S. N.; Benkovic, S. J., A systematic method for identifying small-molecule modulators of protein-protein interactions. *Proc. Natl. Acad. Sci. U. S. A.* **2004,** *101* (44), 15591-6.

121. Gavenonis, J.; Sheneman, B. A.; Siegert, T. R.; Eshelman, M. R.; Kritzer, J. A., Comprehensive analysis of loops at protein-protein interfaces for macrocycle design. *Nat. Chem. Biol.* **2014,** *10* (9), 716-22.

122. Fields, S.; Song, O.-k., A novel genetic system to detect protein–protein interactions. *Nature* **1989,** *340* (6230), 245-246.

123. Sato, T.; Hanada, M.; Bodrug, S.; Irie, S.; Iwama, N.; Boise, L. H.; Thompson, C. B.; Golemis, E.; Fong, L.; Wang, H. G., Interactions among members of the Bcl-2 protein family analyzed with a yeast two-hybrid system. *Proc. Natl. Acad. Sci. U. S. A.* **1994,** *91* (20), 9238-9242.

124. Hu, J. C.; O'Shea, E. K.; Kim, P. S.; Sauer, R. T., Sequence requirements for coiled-coils: analysis with lambda repressor-GCN4 leucine zipper fusions. *Science* **1990,** *250* (4986), 1400-3.

125. Dove, S. L.; Joung, J. K.; Hochschild, A., Activation of prokaryotic transcription through arbitrary protein-protein contacts. *Nature* **1997,** *386* (6625), 627-30.

126. Rodgers, D. W.; Harrison, S. C., The complex between phage 434 repressor DNA-binding domain and operator site OR3: structural differences between consensus and non-consensus half-sites. *Structure* **1993,** *1* (4), 227-40.

127. Miranda, E.; Forafonov, F.; Tavassoli, A., Deciphering interactions used by the influenza virus NS1 protein to silence the host antiviral sensor protein RIG-I using a bacterial reverse two-hybrid system. *Mol. Biosyst.* **2011,** *7* (4), 1042-5.

128. Male, A. L.; Forafonov, F.; Cuda, F.; Zhang, G.; Zheng, S.; Oyston, P. C. F.; Chen, P. R.; Williamson, E. D.; Tavassoli, A., Targeting Bacillus anthracis toxicity with a

genetically selected inhibitor of the PA/CMG2 protein-protein interaction. *Sci. Rep.* **2017,** *7* (1), 3104.

129. Struhl, K.; Davis, R. W., Production of a functional eukaryotic enzyme in Escherichia coli: cloning and expression of the yeast structural gene for imidazole-glycerolphosphate dehydratase (his3). *Proc. Natl. Acad. Sci. U. S. A.* **1977,** *74* (12), 5255-9.

130. Vakulenko, S.; Kalman, M.; Horvath, B.; Simoncsits, A., The nucleotide sequence of an aminoglycoside 3'-phosphotransferase gene from E. coli. *Nucleic Acids Res.* **1987,** *15* (19), 8111.

131. Lederberg, J., The beta-d-galactosidase of Escherichia coli, strain K-12. *J. Bacteriol.* **1950,** *60* (4), 381-92.

132. Miller, J. H., *Experiments in molecular genetics*. Cold Spring Harbour Laboratory: Cold Spring Harbour, NY, 1972.

133. Grote, A.; Hiller, K.; Scheer, M.; Munch, R.; Nortemann, B.; Hempel, D. C.; Jahn, D., JCat: a novel tool to adapt codon usage of a target gene to its potential expression host. *Nucleic Acids Res.* **2005,** *33* (Web Server issue), W526-31.

134. de Boer, H. A.; Comstock, L. J.; Vasser, M., The tac promoter: a functional hybrid derived from the trp and lac promoters. *Proc. Natl. Acad. Sci. U. S. A.* **1983,** *80* (1), 21-5.

135. Haldimann, A.; Wanner, B. L., Conditional-replication, integration, excision, and retrieval plasmid-host systems for gene structure-function studies of bacteria. *J. Bacteriol.* **2001,** *183* (21), 6384-93.

136. Phillips, G. J., New cloning vectors with temperature-sensitive replication. *Plasmid* **1999,** *41* (1), 78-81.

137. Villaverde, A.; Benito, A.; Viaplana, E.; Cubarsi, R., Fine regulation of cI857-controlled gene expression in continuous culture of recombinant Escherichia coli by temperature. *Appl. Environ. Microbiol.* **1993,** *59* (10), 3485-7.

138. Birts, C. N.; Nijjar, S. K.; Mardle, C. A.; Hoakwie, F.; Duriez, P. J.; Blaydes, J. P.; Tavassoli, A., A cyclic peptide inhibitor of C-terminal binding protein dimerization links metabolism with mitotic fidelity in breast cancer cells. *Chemical Science* **2013,** *4* (8), 3046.

139. Malakar, P.; Venkatesh, K. V., Effect of substrate and IPTG concentrations on the burden to growth of Escherichia coli on glycerol due to the expression of Lac proteins. *Appl. Microbiol. Biotechnol.* **2012,** *93* (6), 2543-9.

140. Miranda, E.; Nordgren, I. K.; Male, A. L.; Lawrence, C. E.; Hoakwie, F.; Cuda, F.; Court, W.; Fox, K. R.; Townsend, P. A.; Packham, G. K.; Eccles, S. A.; Tavassoli, A., A cyclic peptide inhibitor of HIF-1 heterodimerization that inhibits hypoxia signaling in cancer cells. *J. Am. Chem. Soc.* **2013,** *135* (28), 10418-25.

141. Arai, R.; Ueda, H.; Kitayama, A.; Kamiya, N.; Nagamune, T., Design of the linkers which effectively separate domains of a bifunctional fusion protein. *Protein Eng. Des. Sel.* **2001,** *14* (8), 529-532.

142. McCabe, B. C.; Pawlowski, D. R.; Koudelka, G. B., The bacteriophage 434 repressor dimer preferentially undergoes autoproteolysis by an intramolecular mechanism. *J. Bacteriol.* **2005,** *187* (16), 5624-30.

143. Kurokawa, Y.; Yanagi, H.; Yura, T., Overproduction of bacterial protein disulfide isomerase (DsbC) and its modulator (DsbD) markedly enhances periplasmic production of human nerve growth factor in Escherichia coli. *J. Biol. Chem.* **2001,** *276* (17), 14393-9.

144. Kurokawa, Y.; Yanagi, H.; Yura, T., Overexpression of protein disulfide isomerase DsbC stabilizes multiple-disulfide-bonded recombinant protein produced and transported to the periplasm in Escherichia coli. *Appl. Environ. Microbiol.* **2000,** *66* (9), 3960-5.

145. Hoshino, K.; Eda, A.; Kurokawa, Y.; Shimizu, N., Production of brain-derived neurotrophic factor in Escherichia coli by coexpression of Dsb proteins. *Biosci. Biotechnol. Biochem.* **2002,** *66* (2), 344-50.

146. Guan, M.; Wang, J.; Yang, L.; Zhao, Z.; Lu, K.; Zhao, L.; Xiao, J.; Li, Z.; Shi, Z., Targeting osteosarcoma vasculature with peptide obtained by phage display. *Contemp Oncol (Pozn)* **2014,** *18* (3), 165-70.

147. Yang, S. G.; Wang, S. W.; Zhao, M.; Zhang, R.; Zhou, W. W.; Li, Y. N.; Su, Y. J.; Zhang, H.; Yu, X. L.; Liu, R. T., A peptide binding to the beta-site of APP improves spatial memory and attenuates Abeta burden in Alzheimer's disease transgenic mice. *PLoS One* **2012,** *7* (11), e48540.

148. Rodi, D. J.; Janes, R. W.; Sanganee, H. J.; Holton, R. A.; Wallace, B. A.; Makowski, L., Screening of a library of phage-displayed peptides identifies human bcl-2 as a taxol-binding protein. *J. Mol. Biol.* **1999,** *285* (1), 197-203.

149. Sethi, A.; Delatte, J.; Foil, L.; Husseneder, C., Protozoacidal Trojan-Horse: use of a ligand-lytic peptide for selective destruction of symbiotic protozoa within termite guts. *PLoS One* **2014,** *9* (9), e106199.

150. Zhong, Y.; Cai, J.; Zhang, C.; Xing, X.; Qin, E.; He, J.; Mao, P.; Cheng, J.; Liu, K.; Xu, D.; Song, H., Mimotopes selected with neutralizing antibodies against multiple subtypes of influenza A. *Virol J.* **2011,** *8*, 542.

151. Sharma, A.; Saha, A.; Bhattacharjee, S.; Majumdar, S.; Das Gupta, S. K., Specific and randomly derived immunoactive peptide mimotopes of mycobacterial antigens. *Clin. Vaccine Immunol.* **2006,** *13* (10), 1143-54.

152. Van Nieuwenhove, L.; Buscher, P.; Balharbi, F.; Humbert, M.; Dieltjens, T.; Guisez, Y.; Lejon, V., Identification of mimotopes with diagnostic potential for Trypanosoma brucei gambiense variant surface glycoproteins using human antibody fractions. *PLoS Negl. Trop. Dis.* **2012,** *6* (6), e1682.

153. Li, Y.; Ning, Y.; Wang, Y.; Peng, D.; Jiang, Y.; Zhang, L.; Long, M.; Luo, J.; Li, M., Mimotopes selected with a neutralizing antibody against urease B from Helicobacter pylori induce enzyme inhibitory antibodies in mice upon vaccination. *BMC Biotechnol.* **2010,** *10*, 84.

154. Chikaev, A. N.; Bakulina, A. Y.; Burdick, R. C.; Karpenko, L. I.; Pathak, V. K.; Ilyichev, A. A., Selection of peptide mimics of HIV-1 epitope recognized by neutralizing antibody VRC01. *PLoS One* **2015,** *10* (3), e0120847.

155. Costa, L. E.; Goulart, L. R.; Pereira, N. C.; Lima, M. I.; Duarte, M. C.; Martins, V. T.; Lage, P. S.; Menezes-Souza, D.; Ribeiro, T. G.; Melo, M. N.; Fernandes, A. P.; Soto, M.; Tavares, C. A.; Chavez-Fumagalli, M. A.; Coelho, E. A., Mimotope-based vaccines of Leishmania infantum antigens and their protective efficacy against visceral leishmaniasis. *PLoS One* **2014,** *9* (10), e110014.

156. Feliciano, N. D.; Ribeiro Vda, S.; Santos Fde, A.; Fujimura, P. T.; Gonzaga, H. T.; Goulart, L. R.; Costa-Cruz, J. M., Bacteriophage-fused peptides for serodiagnosis of human strongyloidiasis. *PLoS Negl. Trop. Dis.* **2014,** *8* (5), e2792.

157. Kanki, S.; Jaalouk, D. E.; Lee, S.; Yu, A. Y.; Gannon, J.; Lee, R. T., Identification of targeting peptides for ischemic myocardium by in vivo phage display. *J. Mol. Cell. Cardiol.* **2011,** *50* (5), 841-8.

158. O'Neil, K. T.; Hoess, R. H.; Jackson, S. A.; Ramachandran, N. S.; Mousa, S. A.; DeGrado, W. F., Identification of novel peptide antagonists for GPIIb/IIIa from a conformationally constrained phage peptide library. *Proteins* **1992,** *14* (4), 509-15.

159. McConnell, S. J.; Kendall, M. L.; Reilly, T. M.; Hoess, R. H., Constrained peptide libraries as a tool for finding mimotopes. *Gene* **1994,** *151* (1-2), 115-8.

160. Lam, K. S.; Salmon, S. E.; Hersh, E. M.; Hruby, V. J.; Kazmierski, W. M.; Knapp, R. J., A new type of synthetic peptide library for identifying ligand-binding activity. *Nature* **1991,** *354* (6348), 82-4.

161. Sievers, F.; Wilm, A.; Dineen, D.; Gibson, T. J.; Karplus, K.; Li, W.; Lopez, R.; McWilliam, H.; Remmert, M.; Söding, J.; Thompson, J. D.; Higgins, D. G., Fast, scalable generation of high-quality protein multiple sequence alignments using Clustal Omega. *Mol. Syst. Biol.* **2011,** *7* (1).

162. Goujon, M.; McWilliam, H.; Li, W.; Valentin, F.; Squizzato, S.; Paern, J.; Lopez, R., A new bioinformatics analysis tools framework at EMBL-EBI. *Nucleic Acids Res.* **2010,** *38* (Web Server issue), W695-9.

163. Vodnik, M.; Zager, U.; Strukelj, B.; Lunder, M., Phage display: selecting straws instead of a needle from a haystack. *Molecules* **2011,** *16* (1), 790-817.

164. Huynh, K.; Partch, C. L., Analysis of protein stability and ligand interactions by thermal shift assay. *Curr Protoc Protein Sci* **2015,** *79*, 28 9 1-14.

165. Josephy, P. D.; Eling, T.; Mason, R. P., The horseradish peroxidase-catalyzed oxidation of 3,5,3',5'-tetramethylbenzidine. Free radical and charge-transfer complex intermediates. *J. Biol. Chem.* **1982,** *257* (7), 3669-75.

166. Dennis, M. S.; Zhang, M.; Meng, Y. G.; Kadkhodayan, M.; Kirchhofer, D.; Combs, D.; Damico, L. A., Albumin binding as a general strategy for improving the pharmacokinetics of proteins. *J. Biol. Chem.* **2002,** *277* (38), 35035-43.

167. Matochko, W. L.; Cory Li, S.; Tang, S. K.; Derda, R., Prospective identification of parasitic sequences in phage display screens. *Nucleic Acids Res.* **2014,** *42* (3), 1784-98.

168. Rodi, D. J.; Soares, A. S.; Makowski, L., Quantitative assessment of peptide sequence diversity in M13 combinatorial peptide phage display libraries. *J. Mol. Biol.* **2002,** *322* (5), 1039-52.

169. Lea, W. A.; Simeonov, A., Fluorescence polarization assays in small molecule screening. *Expert Opin Drug Discov* **2011,** *6* (1), 17-32.

170. Banfield, M. J.; Naylor, R. L.; Robertson, A. G.; Allen, S. J.; Dawbarn, D.; Brady, R. L., Specificity in Trk receptor:neurotrophin interactions: the crystal structure of TrkB-d5 in complex with neurotrophin-4/5. *Structure* **2001,** *9* (12), 1191-9.

171. Sharma, S. K.; Evans, D. B.; Vosters, A. F.; McQuade, T. J.; Tarpley, W. G., Metal affinity chromatography of recombinant HIV-1 reverse transcriptase containing a human renin cleavable metal binding domain. *Biotechnol. Appl. Biochem.* **1991,** *14* (1), 69-81.

172. Hochuli, E.; Bannwarth, W.; Dobeli, H.; Gentz, R.; Stuber, D., Genetic Approach to Facilitate Purification of Recombinant Proteins with a Novel Metal Chelate Adsorbent. *Nat Biotech* **1988,** *6* (11), 1321-1325.

173. Porath, J., Immobilized metal ion affinity chromatography. *Protein Expr. Purif.* **1992,** *3* (4), 263-81.

174. Takagi, T.; Doolittle, R. F., Amino acid sequence studies on factor XIII and the peptide released during its activation by thrombin. *Biochemistry* **1974,** *13* (4), 750-6.

175. Hopp, T. P.; Prickett, K. S.; Price, V. L.; Libby, R. T.; March, C. J.; Pat Cerretti, D.; Urdal, D. L.; Conlon, P. J., A Short Polypeptide Marker Sequence Useful for Recombinant Protein Identification and Purification. *Nat Biotech* **1988,** *6* (10), 1204-1210.

176. Indo, Y.; Mardy, S.; Tsuruta, M.; Karim, M. A.; Matsuda, I., Structure and organization of the human TRKA gene encoding a high affinity receptor for nerve growth factor. *Jpn. J. Hum. Genet.* **1997,** *42* (2), 343-51.

177. Ultsch, M. H.; Wiesmann, C.; Simmons, L. C.; Henrich, J.; Yang, M.; Reilly, D.; Bass, S. H.; de Vos, A. M., Crystal structures of the neurotrophin-binding domain of TrkA, TrkB and TrkC. *J. Mol. Biol.* **1999,** *290* (1), 149-59.

178. Shelton, D. L.; Sutherland, J.; Gripp, J.; Camerato, T.; Armanini, M. P.; Phillips, H. S.; Carroll, K.; Spencer, S. D.; Levinson, A. D., Human trks: molecular cloning, tissue distribution, and expression of extracellular domain immunoadhesins. *J. Neurosci.* **1995,** *15* (1 Pt 2), 477-91.

179. Palmer, I.; Wingfield, P. T., Preparation and extraction of insoluble (inclusion-body) proteins from Escherichia coli. *Curr Protoc Protein Sci* **2012,** *Chapter 6*, Unit6 3.

180. Wingfield, P. T.; Palmer, I.; Liang, S. M., Folding and Purification of Insoluble (Inclusion Body) Proteins from Escherichia coli. *Curr Protoc Protein Sci* **2014,** *78*, 6 5 1-30.

181. Greenfield, N. J., Using circular dichroism collected as a function of temperature to determine the thermodynamics of protein unfolding and binding interactions. *Nat. Protoc.* **2006,** *1* (6), 2527-35.

182. Pelham, H. R., Evidence that luminal ER proteins are sorted from secreted proteins in a post-ER compartment. *The EMBO Journal* **1988,** *7* (4), 913-918.

183. Lyles, M. M.; Gilbert, H. F., Catalysis of the oxidative folding of ribonuclease A by protein disulfide isomerase: dependence of the rate on the composition of the redox buffer. *Biochemistry* **1991,** *30* (3), 613-9.

184. Mezghrani, A.; Fassio, A.; Benham, A.; Simmen, T.; Braakman, I.; Sitia, R., Manipulation of oxidative protein folding and PDI redox state in mammalian cells. *EMBO J.* **2001,** *20* (22), 6288-96.

185. Hammond, C.; Helenius, A., Quality control in the secretory pathway: retention of a misfolded viral membrane glycoprotein involves cycling between the ER, intermediate compartment, and Golgi apparatus. *J. Cell Biol.* **1994,** *126* (1), 41-52.

186. Sjostrom, M.; Wold, S.; Wieslander, A.; Rilfors, L., Signal peptide amino acid sequences in Escherichia coli contain information related to final protein localization. A multivariate data analysis. *EMBO J.* **1987,** *6* (3), 823-31.

187. Movva, N. R.; Nakamura, K.; Inouye, M., Amino acid sequence of the signal peptide of ompA protein, a major outer membrane protein of Escherichia coli. *J. Biol. Chem.* **1980,** *255* (1), 27-9.

188. Yoon, S.; Kim, S.; Kim, J., Secretory Production of Recombinant Proteins in Escherichia coli. *Recent Patents on Biotechnology* **2010,** *4* (1), 23-29.

189. Duong, F.; Wickner, W., Distinct catalytic roles of the SecYE, SecG and SecDFyajC subunits of preprotein translocase holoenzyme. *EMBO J.* **1997,** *16* (10), 2756-68.

190. Natale, P.; Bruser, T.; Driessen, A. J., Sec- and Tat-mediated protein secretion across the bacterial cytoplasmic membrane--distinct translocases and mechanisms. *Biochim. Biophys. Acta* **2008,** *1778* (9), 1735-56.

191. Pogliano, J. A.; Beckwith, J., SecD and SecF facilitate protein export in Escherichia coli. *EMBO J.* **1994,** *13* (3), 554-61.

192. Bader, M.; Muse, W.; Ballou, D. P.; Gassner, C.; Bardwell, J. C. A., Oxidative Protein Folding Is Driven by the Electron Transport System. *Cell* **1999,** *98* (2), 217-227.

193. Lobstein, J.; Emrich, C. A.; Jeans, C.; Faulkner, M.; Riggs, P.; Berkmen, M., SHuffle, a novel Escherichia coli protein expression strain capable of correctly folding disulfide bonded proteins in its cytoplasm. *Microb Cell Fact* **2012,** *11*, 56.

194. Ullrich, A.; Gray, A.; Berman, C.; Dull, T. J., Human beta-nerve growth factor gene sequence highly homologous to that of mouse. *Nature* **1983,** *303* (5920), 821-5.

195. Losen, M.; Frolich, B.; Pohl, M.; Buchs, J., Effect of oxygen limitation and medium composition on Escherichia coli fermentation in shake-flask cultures. *Biotechnol. Prog.* **2004,** *20* (4), 1062-8.

196. Unden, G.; Becker, S.; Bongaerts, J.; Holighaus, G.; Schirawski, J.; Six, S., O2-sensing and O2-dependent gene regulation in facultatively anaerobic bacteria. *Arch. Microbiol.* **1995,** *164* (2), 81-90.

197. Baldwin, R. L., Temperature dependence of the hydrophobic interaction in protein folding. *Proc. Natl. Acad. Sci. U. S. A.* **1986,** *83* (21), 8069-72.

198. Sezonov, G.; Joseleau-Petit, D.; D'Ari, R., Escherichia coli physiology in Luria-Bertani broth. *J. Bacteriol.* **2007,** *189* (23), 8746-9.

199. Danquah, M. K.; Forde, G. M., Growth medium selection and its economic impact on plasmid DNA production. *J. Biosci. Bioeng.* **2007,** *104* (6), 490-7.

200. Costa, S.; Almeida, A.; Castro, A.; Domingues, L., Fusion tags for protein solubility, purification and immunogenicity in Escherichia coli: the novel Fh8 system. *Front. Microbiol.* **2014,** *5*, 63.

201. Routledge, S. J., Beyond de-foaming: the effects of antifoams on bioprocess productivity. *Comput Struct Biotechnol J* **2012,** *3*, e201210014.

202. Studier, F. W., Protein production by auto-induction in high density shaking cultures. *Protein Expr. Purif.* **2005,** *41* (1), 207-34.

203. Martin-Zanca, D.; Oskam, R.; Mitra, G.; Copeland, T.; Barbacid, M., Molecular and biochemical characterization of the human trk proto-oncogene. *Mol. Cell. Biol.* **1989,** *9* (1), 24-33.

204. Derda, R.; Tang, S. K.; Li, S. C.; Ng, S.; Matochko, W.; Jafari, M. R., Diversity of phage-displayed libraries of peptides during panning and amplification. *Molecules* **2011,** *16* (2), 1776-803.

205. Merrifield, R. B., Solid Phase Peptide Synthesis. I. The Synthesis of a Tetrapeptide. *JACS* **1963,** *85* (14), 2149-2154.

206. Konig, W.; Geiger, R., [A new method for synthesis of peptides: activation of the carboxyl group with dicyclohexylcarbodiimide using 1-hydroxybenzotriazoles as additives]. *Chem. Ber.* **1970,** *103* (3), 788-98.

207. Kaiser, E.; Colescott, R. L.; Bossinger, C. D.; Cook, P. I., Color test for detection of free terminal amino groups in the solid-phase synthesis of peptides. *Anal. Biochem.* **1970,** *34* (2), 595-8.

208. Troll, W.; Cannan, R. K., A modified photometric ninhydrin method for the analysis of amino and imino acids. *J. Biol. Chem.* **1953,** *200* (2), 803-11.

209. King, D. S.; Fields, C. G.; Fields, G. B., A cleavage method which minimizes side reactions following Fmoc solid phase peptide synthesis. *Int. J. Pept. Protein Res.* **2009,** *36* (3), 255-266.

210. Erchegyi, J.; Hoeger, C. A.; Low, W.; Hoyer, D.; Waser, B.; Eltschinger, V.; Schaer, J. C.; Cescato, R.; Reubi, J. C.; Rivier, J. E., Somatostatin receptor 1 selective analogues: 2. N(alpha)-Methylated scan. *J. Med. Chem.* **2005,** *48* (2), 507-14.

211. Han, Y.; Albericio, F.; Barany, G., Occurrence and Minimization of Cysteine Racemization during Stepwise Solid-Phase Peptide Synthesis1,2. *The Journal of Organic Chemistry* **1997,** *62* (13), 4307-4312.

212. Al-Warhi, T. I.; Al-Hazimi, H. M. A.; El-Faham, A., Recent development in peptide coupling reagents. *Journal of Saudi Chemical Society* **2012,** *16* (2), 97-116.

213. Seidel, S. A.; Dijkman, P. M.; Lea, W. A.; van den Bogaart, G.; Jerabek-Willemsen, M.; Lazic, A.; Joseph, J. S.; Srinivasan, P.; Baaske, P.; Simeonov, A.; Katritch, I.; Melo, F. A.; Ladbury, J. E.; Schreiber, G.; Watts, A.; Braun, D.; Duhr, S., Microscale thermophoresis quantifies biomolecular interactions under previously challenging conditions. *Methods* **2013,** *59* (3), 301-15.

214. Jerabek-Willemsen, M.; Wienken, C. J.; Braun, D.; Baaske, P.; Duhr, S., Molecular interaction studies using microscale thermophoresis. *Assay Drug Dev. Technol.* **2011,** *9* (4), 342-53.

215. Iwasaki, Y.; Ishikawa, M.; Okada, N.; Koizumi, S., Induction of a distinct morphology and signal transduction in TrkB/PC12 cells by nerve growth factor and brain-derived neurotrophic factor. *J. Neurochem.* **1997,** *68* (3), 927-34.